THE UNIVERSITY
of EDINBURGH

COMPUTATIONAL MODELLING OF SEPARATION PROCESSES FOR GREEN CONTINUOUS PHARMACEUTICAL MANUFACTURING

Samir Diab

Doctor of Philosophy Thesis

University of Edinburgh

2020

Declaration

I declare that this thesis was composed by myself and that the work contained herein is my own, except where explicitly stated otherwise in the text

(*Samir Diab*)

Acknowledgements

I thank the following persons and entities, without whom this would not have been possible.

Dr. Dimitrios I. Gerogiorgis for his guidance, support and motivation for the entire duration of the project and beyond. His rigour, detail and tenacity that he has instilled in me have been instrumental in making this project a success and our interactions have made for an excellent and enjoyable learning experience.

Dr. Andrew J. Alexander and Prof. James D. Litster for their thorough and detailed critical review of this thesis and for examining my *viva voce*.

Prof. Lev Sarkisov for his ongoing support and advice since my undergraduate studies.

Prof. D. Tyler McQuade and Prof. B. Frank Gupton for their support and motivation during my time in Richmond (VA, USA).

The Engineering and Physical Sciences Research Council (EPSRC, Doctoral Training Partnership PhD Fellowship), the Royal Society of Edinburgh (John Moyes Lessells Travel Scholarship) and the Society of Chemical Industry (Richardson Bursary) for their financial support.

My friends and family.

Abstract

The pharmaceutical industry has traditionally implemented batch manufacturing for the production of a wide range of products due to its mature technological development and ability for recall of products where necessary. However, several demonstrations of Continuous Pharmaceutical Manufacturing (CPM) in the past two decades have drawn significant attention from academia, industry and regulatory bodies due to its potential for smaller equipment, enhanced efficiencies, access to difficult or hazardous process conditions with greater ease and safety and reduced costs and waste. While continuous processing is not new in other manufacturing sectors, its application to pharmaceutical production has only drawn significant attention in recent years due to the numerous demonstrations of continuous flow syntheses of complex molecules and functional groups inherent of Active Pharmaceutical Ingredients (APIs), which is the foundation of any end-to-end CPM plant. The literature to date has predominantly focussed on design and optimisation of flow synthesis routes; however, the development of efficient continuous separation processes is a major bottleneck to CPM and are often challenging and materially intensive unit operations. The design of effective continuous separation processes for societally important APIs amenable to continuous production is essential for CPM success. Mathematical modelling is a viable and useful tool in the elucidation of promising designs prior to pilot plant studies that can allow rapid screening of multiple candidate configurations and can circumvent expensive and laborious experimental campaigns. Moreover, they allow optimisation of process design configurations to maximise their operational and economic benefits. This PhD thesis aims to elucidate cost-optimal upstream CPM plant and continuous separation process designs for a range of APIs. Steady-state process models for upstream CPM plants for different APIs are constructed, using published data for reaction rate law elucidation and kinetic parameter estimation, activity coefficient and group contribution models for non-ideal multicomponent mixture phase equilibria prediction and pharmaceutical process costing methodologies. The constructed models are then used for process simulation, design and optimisation of CPM plants, using Nonlinear Programming (NLP) for individual case-based process optimisation and Mixed Integer Nonlinear Programming (MINLP) for CPM process synthesis to optimality. The systematic frameworks and methods used in this work can be expanded to other APIs amenable to CPM with similar processes. This work highlights the immense value in systematic and rigorous model-based simulation and optimisation campaigns for CPM process development.

Lay Summary

This PhD thesis involves modelling and optimisation for the design of Continuous Pharmaceutical Manufacturing (CPM) processes. The pharmaceutical industry has traditionally relied on batch processing methods; however, technical and economic drivers are pushing the industry towards implementing leaner methods, including continuous processing. The plethora of continuous flow chemistry demonstrations in the past two decades, including routes towards pharmaceutical and biopharmaceutically-active molecules, have sparked significant developments in CPM research, particularly in the demonstration of continuous flow syntheses of Active Pharmaceutical Ingredients (APIs). However, the number of demonstrated continuous synthetic routes is disproportionately larger than the number of suitable continuous separation processes, which are essential prior to downstream processing and formulation of the final Drug Product. Separations are often material- and energy-intensive and are thus challenging to implement in end-to-end CPM campaigns. Effective and efficient design of continuous separation processes is paramount for successful CPM implementation. Mathematical modelling and optimisation can be used to this end in order to screen for promising process designs while circumventing costly and laborious experimental studies. This PhD thesis implements mathematical modelling, simulation and optimisation for the design and process synthesis of economically viable upstream CPM plants, including continuous synthesis and separations, namely Liquid-Liquid Extraction (LLE) and crystallisation processes. The case studies considered in this thesis are based on published demonstrations of continuous flow syntheses for diphenhydramine, rufinamide, warfarin, nevirapine and atropine and continuous cooling crystallisation processes for cyclosporine, paracetamol, aliskiren and melitracen, all of which are societally important APIs with different pharmaceutical applications. Reaction rate law elucidation and kinetic parameter estimation from published reaction data for these APIs are implemented for flow reactor design. Process simulation and optimisation are implemented for various upstream CPM plants and crystallisation cascades to gain insight into the design and operation that yield promising economic outcomes. Following this, the formulation of Mixed Integer Nonlinear Programs for process synthesis is implemented for the first time for the design of a LLE cascade as part of an upstream CPM plant as well as a crystalliser cascade with solids recycle. Valuable insight into CPM separation design have been gained from this work and the described modelling and optimisation frameworks can be extended to other APIs amenable to CPM via similar processing routes and will be of paramount importance in the transition towards lean pharmaceutical manufacturing.

Contents

List of Figures

List of Tables

PART I

INTRODUCTION & MOTIVATION

Chapter 1

Introduction

This chapter provides some background on the current state of the pharmaceutical industry as impetus for the motivation for this PhD thesis. Historical trends and the current state of Research and Development (R&D) in the pharmaceutical industry are first discussed, followed by the emergence of Continuous Pharmaceutical Manufacturing (CPM) over the past two decades as an alternative to the currently predominant batch processing paradigm and then Process Systems Engineering (PSE) applications related to CPM development.

1.1 Pharmaceutical Industry Research and Development

Batch processing has been the traditional manufacturing method used by the pharmaceutical industry due to established regulatory protocol for such a mature technology. Advantages offered by batch methods include high precision product quality control, specific batch recall and versatile equipment usage; thus, batch manufacturing methods currently dominate the pharmaceutical industry.[1] However, batch processing has several drawbacks such as poor heat transfer and mixing efficiencies (potentially leading to unacceptable quality of product and difficulties in scaleup), large inventories of material (incurring large plant footprints and capital expenditures), high volumes of waste and intensive labour requirements.[2]

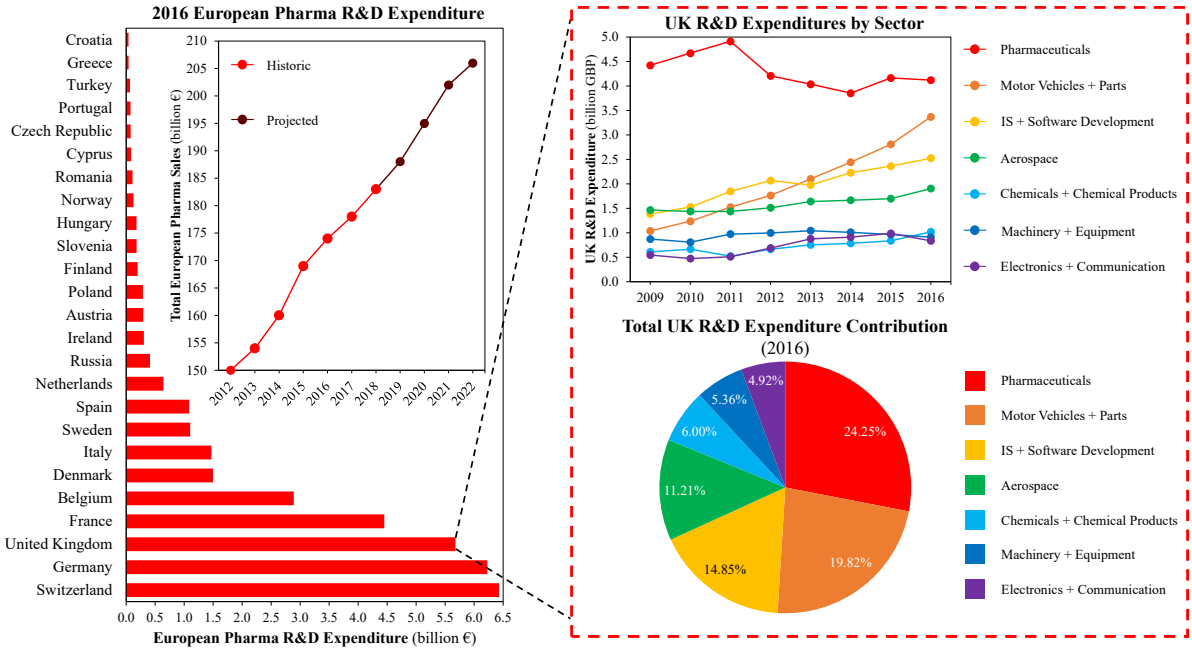

Figure 1: European pharma R&D expenditures and total sales and UK pharmaceutical manufacturing R&D trends by sector.[3–5]

In the past, production costs in the pharmaceutical industry have been considered low enough such that reductions have been unnecessary. However, Research and Development (R&D) costs for the pharmaceutical industry have been rapidly increasing over previous decades, with the pharmaceutical industry having the highest R&D expenditures of all industrial sectors[6] (Figs. 1 and 2). Capitalised costs of drug product commercialisation have also been historically increasing.[7]

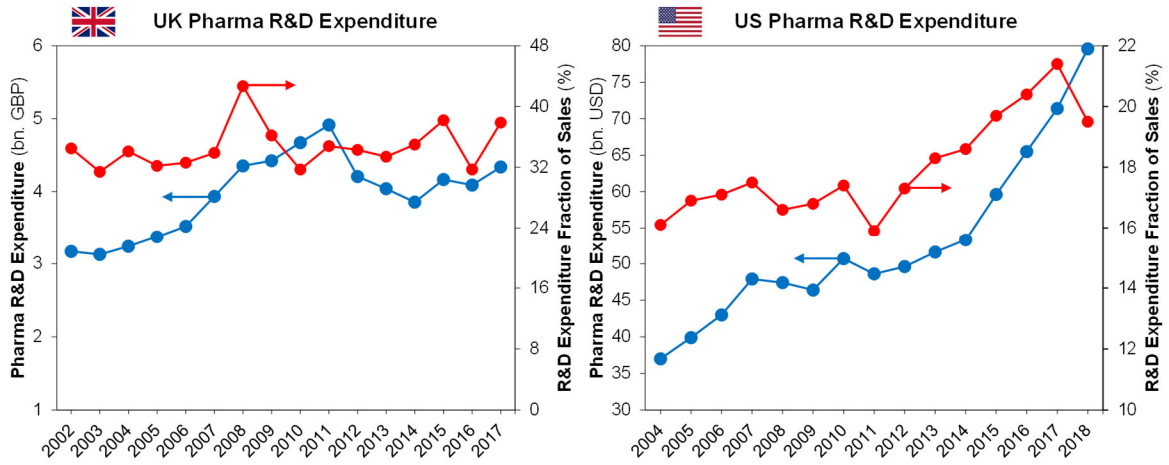

Figure 2: Historically increasing pharmaceutical R&D costs in the UK and US.[4]

When the duration of clinical trials of potential drugs and product approval is accounted for, pharmaceutical products lose approximately half of their patent life by the time they have reached the market. This leads to significant profit losses for pharmaceutical firms and increasing competition from generics manufacturers (Fig. 3), presenting a threat to firm profitability.

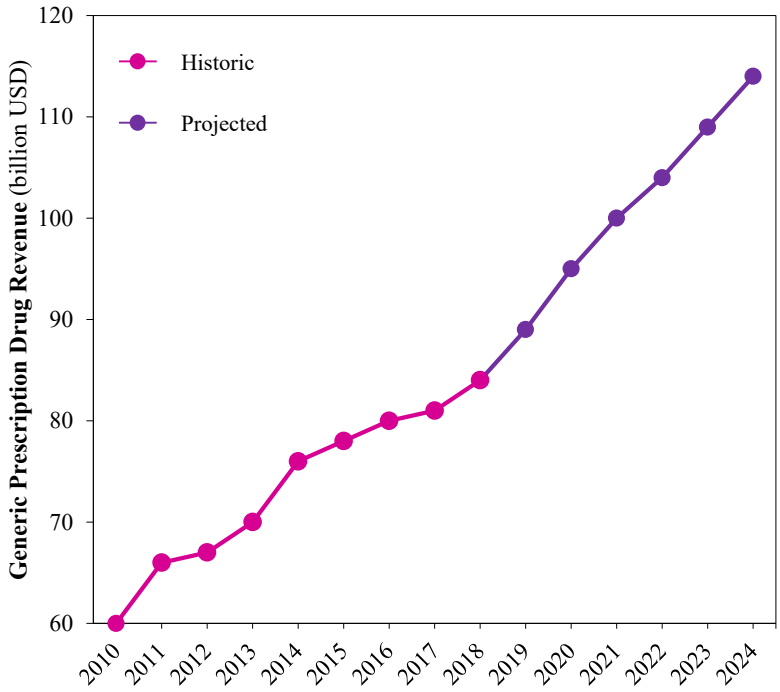

Figure 3: Increasing global generics prescription drug revenues.[8]

Manufacturing contributes approximately 30% of overall costs for pharmaceutical enterprises.[9] The performance of pharmaceutical enterprises will be significantly improved by investigation and development of innovative manufacturing technologies in order to improve process efficiencies. These improvements can allow significant cost savings in order to maintain profitability and sustainability in pharmaceutical firms.

The pharmaceutical industry produces a wide variety of products whose Active Pharmaceutical Ingredients (APIs) often have complex molecular structures, requiring multistep syntheses[10] and whose products have stringent product purities set by regulatory bodies.[11] Such requirements lead to materially-intensive manufacturing processes, which can be wasteful and have low operational asset efficiencies.[12,13]

1.2 Continuous Pharmaceutical Manufacturing

Continuous Pharmaceutical Manufacturing (CPM) has the potential to provide technological innovation, allowing several advantages over batch processing, including lower capital and operating costs,[14] reduced solvent requirements and waste handling,[15] increased process efficiency[16] and reduced plant footprints.[17] The demonstration of a continuous flow synthetic route is the foundation of any CPM process; in the past decade, there have been many demonstrations of flow syntheses for various APIs and their intermediates, which have been summarised in recent literature reviews.[10,18–21] Mixing patterns in flow reactors are much better understood than those in agitated batch vessels and the time for process development of flow reactors is significantly reduced in comparison. Implementing continuous flow synthesis often allows the application of microscale equipment (depending on the target plant capacity), featuring tubular flow reactors with inner diameters on the millimetre scale. Microreactors benefit from enhanced mixing, mass and heat transfer, safer operation, and reduced footprint.[22]

Recent ventures highlight the beginning of the transition from batch to continuous manufacturing of pharmaceutical compounds. In the past two decades, there have been many demonstrations of API production processes which have benefited by changing to a continuous manufacturing paradigm. Table 1 provides a summary of certain APIs whose manufacturing processes have been converted from batch to continuous mode to various extents. Whilst Table 1 does not provide a comprehensive review of demonstrated CPM of APIs (detailed reviews are available in the literature[10,23,24]), it is clear that the transition of manufacturing paradigm from batch to continuous processing remains predominantly in the R&D stages (lab-scale and pilot plant capacity) with only two CPM processes at production level.

Table 1: API manufacturing processes converted from batch to continuous mode.

API	Application	Level of Development				Benefits of Converting to Continuous Mode			API Capacity (kg yr^{-1})	Company / Institution	Ref.
		Labscale Demonstration			Production Level	Process Chemistry	Ease / Safety of Operation	CapEx / OpEx			
		Synth.	Purification	Formulation / Tableting							
Aliskiren Hemifurate	Hypertension	✓	✓	✓	Pilot	✓	✓	—	360.00	Novartis-MIT CCM, USA	(25)
Amitriptyline	Antidepressant	✓	✓	X	Lab	—	✓	—	4.24	University of Hanover, Germany	(26)
Amoxicillin	Antibiotic	✓	✓	✓	Production	✓	—	✓	Unavailable	GSK	(27)
Artemisinin	Antimalarial	✓	X	X	Lab	—	✓	✓	66.64	MPI for Colloids and Interfaces, Germany	(28)
AZD6906	Reflux inhibitor	✓	X	X	Pilot	—	✓	—	Unavailable	AstraZeneca	(29)
Darunavir	HIV drug	✓	✓	✓	Production	✓	—	✓	Unavailable	Janssen	(30,31)
Diphenhydramine	Antihistamine	✓	✓	X	Lab	—	✓	—	19.36	MIT	(32)
		✓	✓	✓	Lab	✓	✓	✓	18.72	MIT	(33)
Fanetizole	Anti-inflammatory	✓	X	X	Lab	—	—	—	79.68	University of Cambridge, UK	(34)
Fluoxetine	Antidepressant	✓	X	X	Lab	✓	✓	—	11.84	Eli Lilly	(35)
		✓	✓	✓	Lab	✓	✓	✓	7.36	MIT	(33)
6-Hydroxybuspirone	Psychotropic agent	✓	X	X	Lab	—	✓	—	1,166.64	Bristol-Myers Squibb	(36)
Ibuprofen	Anti-inflammatory	✓	X	X	Lab	—	✓	—	4.32	Florida State University, USA	(37)
		✓	✓	X	Lab	✓	✓	✓	64.72	MIT	(38)
Imatinib	Leukaemia	✓	X	X	Lab	✓	—	—	0.01	University of Cambridge, UK	(39)
Rufinamide	Antiepileptic	✓	✓	X	Lab	✓	✓	—	1.76	MIT	(40)
Tamoxifen	Breast cancer	✓	X	X	Lab	✓	—	—	432.00	University of Cambridge, UK	(41)
Telmisartan	Hypertension	✓	X	X	Lab	—	—	✓	0.48	Virginia Commonwealth University, USA	(42)
Vitamin D3	Liver failure	✓	X	X	Lab	✓	✓	✓	Unavailable	Tokyo Institute of Technology, Japan	(43)

There is a stagnancy inhibiting wide-spread adoption of CPM due to investments in batchwise infrastructures and limited technological expertise in continuous pharmaceutical processes in comparison to current techniques.[44] Significant financial investments in existing batch-operated plants make such a drastic change in production paradigm an unfavourable prospect.[45] Process feasibility and viability studies must be conducted before significant time and financial investments for experimental and pilot plant studies are made.

Ultimately, a process should only be implemented in continuous mode if it shows potential and benefits over existing processes. The numerous demonstrations of continuous flow syntheses of APIs[19] and other pharmaceutically relevant compounds pave the way for the development of subsequent continuous unit operations, including recent demonstrations of end-to-end CPM campaigns.[33] However, limited demonstrations of continuous separations in CPM plants impede its widespread adoption in industry, presenting a bottleneck to realising the full benefits of continuous mode.

1.3 Process Systems Engineering in Pharmaceutical Manufacturing

Recently, there has been significant interest in Process Systems Engineering (PSE)-driven efforts for pharmaceutical process design. The philosophy of PSE is a knowledge-based approach towards effective solutions for process design; the multipurpose, complex nature of pharmaceutical processes renders it suitable for such methods.[2] A PSE approach to CPM process design has shown significant promise in recent research contributions. Data-driven methods may be appropriate to gain insight into correlations between in- and outputs of processes when time limitations are such that mechanistic model development is not possible.[46] A knowledge/mechanistic approach is more appropriate for design and development, where models can be re-parameterisation for different systems.[47] Theoretical modelling also allows rapid screening of novel CPM processes for the production of candidate APIs, whilst circumventing experimental costs and labour requirements.[48] Process models have been implemented to demonstrate CPM technoeconomic feasibility and viability for various APIs.[49–51]

Mathematical optimisation can be used to establish optimal design configurations.[48,52] Theoretical methods have been previously implemented towards optimal pharmaceutical plantwide designs,[53] analysis of synthetic pathways[54,55] and life-cycle assessments.[56,57] Modelling and optimisation have also been implemented in the design of separation processes in pharmaceutical manufacturing, such as Liquid-Liquid Extraction (LLE),[58–60] crystallisation[61–67] and chromatographic methods.[68] Identification of optimal plantwide designs is essential,[69] particularly end-to-end designs encompassing synthesis and purification/separation, which will further aid process development.[70]

Chapter 2

Project Motivation

This chapter discusses the motivation for this PhD project. First, separation process design and its challenges for integration into upstream CPM plants is discussed with a focus on literature demonstrations of key separation unit operations in pharmaceutical processes, and modelling and optimisation demonstration in the literature implemented thus far. Identification of APIs which have been demonstrated as amenable to CPM in the literature, their societal importance and their market value are described as case studies for this work. The chapter is then concluded with the PhD thesis objectives and structure.

2.1 Challenges of Continuous Separation Process Design

Despite the numerous demonstrations of continuous flow syntheses[21] towards APIs, including end-to-end production campaigns,[33] only certain synthetic routes benefit from continuous operation[71] and the lack of demonstrated continuous purification and separation methods integrated in CPM plants is an important obstacle to overcome.[52] Establishing promising APIs for CPM application and screening for those with the highest likelihood of success is imperative for the elucidation of potential process configurations and successful CPM implementation.[48]

Various efforts in modelling and simulation in pursuit of continuous pharmaceutical separation process development have been demonstrated in recent years. Mathematical optimisation can be used to identify optimal process designs for pharmaceutical manufacturing campaigns;[72] plantwide modelling and optimisation with a focus on optimal continuous separation process design towards total cost minimisation have been previously implemented for various APIs.[73–77] Elucidating optimal CPM designs will aid process development.

A variety of different separation processes are implemented in pharmaceutical manufacturing processes, including (but not limited to) Liquid-Liquid Extraction (LLE), membrane purification/separation, distillation, crystallisation and chromatographic separations. Modelling and optimisation have been implemented in the design of continuous chromatographic methods[68] and membrane separations[78] for pharmaceutical manufacturing.

This PhD thesis focusses on the design of continuous LLE and crystallisation processes, both of which are very commonly implemented purification and separation processes essential to pharmaceutical production.

2.1.1 Continuous Liquid-Liquid Extraction

The aim of Liquid-Liquid Extraction (LLE) is to purify a multicomponent mixture by addition of a solvent which induces the splitting of the mixture into multiple phases, between which solutes partition; the objective is to partition undesired solute components (e.g., impurities) into one phase while the desired solute (e.g., product API) preferentially partitions into the other. Purification via LLE is typically implemented in pharmaceutical processes prior to crystallisation to ensure as few undesirable impurities as possible are incorporated into crystalline products. The design of continuous LLE processes is an important aspect of end-to-end CPM plant development.

The majority of LLE process demonstrations are still done in batch, even following a continuous flow synthesis precedent. That said, there have been a few experimental, as well as theoretical, studies on the design of continuous LLE processes for pharmaceutical manufacturing. Drageset and Bjørsvik (2016) performed an in-line continuous LLE for purification of a reactor product mixture prior to further downstream processing, allowing for input material reduction compared to the batch purification process.[58] Monbaliu et al. (2016) also implemented a continuous LLE process as part of an end-to-end CPM process for lidocaine hydrochloride (a local anaesthetic) from synthesis to aqueous formulation.[59] Jolliffe and Gerogiorgis (2017) performed a conceptual study for the technoeconomic optimisation for the purification of ibuprofen from the product stream of a demonstrated continuous flow synthesis, comparing hexane and toluene as LLE solvents.[73]

Implementation of combined experimental and modelling approaches towards integrated LLE design in the literature for pharmaceutical purifications and separations demonstrate the utility of theoretical methods in establishing optimal design and operating parameters.[58–60]

2.1.2 Continuous Crystallisation Processes

A significant portion of pharmaceutical products are sold as solids (tablets, dispersions, gels or topical treatments), and thus crystallisation is an essential unit operation in drug product manufacturing. The aim of crystallisation is to form a solid product of the desired compound with minimal impurity and/or solvent incorporation into the crystal structure while also attaining the desired polymorph, suitable mean crystal size and size distribution properties, all of which affect subsequent downstream process unit operations and the bioavailability of the drug in the patient.

The driving force for crystallisation is supersaturation, the condition in which the concentration of solute in the liquid phase (i.e., the mother liquor) is higher than its solubility concentration. Supersaturation can be generated by a number of different methods, depending on the

thermodynamics of the system, the most commonly implemented of which are: cooling (where solubility is strongly temperature-dependent), antisolvent addition (where addition of another solvent alters the solute solubility in the mixture) and evaporative crystallisation (where solvent removal increases the solute concentration in the mother liquor above its solubility).

Traditional batch crystallisation techniques have been widely studied and are generally well-understood, but batch variability leads to deviations from strict product specifications regarding crystal product quality attributes, which leads to significant quantities of waste.[79] Continuous crystallisation has received attention for its potential to increase flexibility, efficiency and quality.[80] Continuous crystallisation operates under steady-state conditions, allowing higher reproducibility and better control of important crystal properties, such as the purity and the size distribution, which directly affect the bioavailability of the product; however, as continuous processes do not discharge at equilibrium, they tend to achieve lower yields than batch crystallisations.[79] Systematic investigation of continuous crystallisation processes for pharmaceutical manufacturing is required for their implementation as part of integrated CPM plants.

Continuous crystalliser designs applicable for the pharmaceutical industry are categorised as Plug Flow Crystallisers (PFCs), Continuous Oscillatory Baffled Crystallisers (COBCs) or Mixed Suspension-Mixed Product Removal (MSMPR) crystallisers. PFCs are suited to systems with fast crystal growth and short residence times and can attain narrow crystal size distributions,[81] but fouling and clogging in narrow tube diameters is an important issue.[82] COBCs are another emerging design, which enhance heat and mass transfer, but have issues handling high solid loadings.[83] Various experimental and modelling studies have been conducted for estimation of crystallisation kinetics, proof-of-concept demonstrations, design and optimisation.[65,84–88]

MSMPR crystallisers are idealised stirred tank designs better suited for systems with slower crystallisation kinetics and can easily be adapted from existing jacketed agitated vessels for continuous applications. The MSMPR crystalliser is a widely studied continuous crystalliser design due to its simple operation, low maintenance requirements, avoidance of rapid fouling typical of continuous solids processes and tubular crystalliser designs,[89] and ease of adaptation from existing batch stirred tanks.[80] Recent work using MSMPRs for crystallisation kinetic parameter estimation,[90–93] comparison of operating strategies, process configurations and control,[61,66,67,94–103] novel crystallisation techniques,[63,104–106] specialised separations[107–113] and polymorph selectivity[114,115] have significantly developed their implementation, with some designs integrated into end-to-end CPM plants.[25,116] However, continuous crystalliser designs operate at steady-state and thus do not reach equilibrium, leading to potentially lower yields compared to batch processes; establishing

technically feasible and economically viable operating parameters for continuous designs is essential for the successful transition from batch to continuous crystallisation methods. A variety of experimental and theoretical studies have already investigated the design, simulation and optimisation of steady-state and dynamic operations of MSMPR crystallisers for various pharmaceutically relevant compounds.[117] Rapid screening of candidate flowsheet configurations of MSMPR cascades for different APIs can facilitate process development towards end-to-end CPM.[118] Experimental studies are often coupled with process modelling and simulation methodologies to construct predictive models to screen various process conditions and configurations whilst circumventing excessive time requirements and costs.[48]

The majority of continuous crystallisation studies in the literature to date have been focussed on design and optimisation for attainment of optimised process efficiency (i.e., high yield) and crystal product quality (purity, mean size, size distribution, target polymorph), which are very valuable regarding the importance of crystalline quality and purity in pharmaceutical products. This work approaches crystallisation process design and optimisation from a technoeconomic perspective.

2.1.3 Nonlinear Programming for Process Optimisation

A Nonlinear Programming (NLP) problem is defined as follows. For the objective function, f, of decision variables, $\boldsymbol{x} = x_1, \dots, x_n$, with inequality constraints, $\boldsymbol{g} = g_1, \dots, g_m$, equality constraints, $\boldsymbol{h} = h_1, \dots, h_p$, the nonlinear minimisation problem is defined by Eqs. 1–4, where non-negativity constraints can be defined within $\boldsymbol{g}$ and the problem can be defined as a maximisation problem by minimising $-f(\boldsymbol{x})$; $\boldsymbol{x}$ may also have lower ($\boldsymbol{x}_{\mathbf{LB}}$) and upper ($\boldsymbol{x}_{\mathbf{UB}}$) bounds, which may reflect feasibility constraints on an operating variable or limits of the range of applicability of a model to a range of variable values.

$$\min f(x_1, \dots, x_n) \tag{1}$$

s.t.

$$\begin{aligned} g_1(x_1, \dots, x_n) &\leq b_1 \\ &\vdots \quad\;\; \vdots \\ g_m(x_1, \dots, x_n) &\leq b_m \end{aligned} \tag{2}$$

$$\begin{aligned} h_1(x_1, \dots, x_n) &= c_1 \\ &\vdots \quad\;\; \vdots \\ h_p(x_1, \dots, x_n) &= c_p \end{aligned} \tag{3}$$

$$\boldsymbol{x}_{\mathbf{LB}} \leq \boldsymbol{x} \leq \boldsymbol{x}_{\mathbf{UB}} \tag{4}$$

The formulation of NLP problems for pharmaceutical process optimisation is used in various instances in the literature. Jolliffe and Gerogiorgis (2017) performed technoeconomic optimisation

via NLP for the design of a continuous LLE vessel as part of an upstream CPM plant for ibuprofen, wherein plant total costs were minimised subject to limitations on LLE solvent usage (corresponding to the limits of biphasic mixture formation for different continuous separation operating temperatures and candidate LLE solvents, hexane and toluene) and feasible vessel volumes.[73] The same authors also performed NLP optimisation for total cost minimisation of an upstream CPM plant for artemisinin with an antisolvent cooling crystallisation with constraints on antisolvent usage and crystallisation operating temperature, comparing different candidate antisolvents, numbers of implemented crystallisation vessels and assumption of fixed or variable crystalliser size.[74] Li et al. (2017) used NLP optimisation for MSMPR cascade design for the continuous cooling crystallisation of cyclosporine, wherein they compared two different objective functions: (1) maximise yield subject to purity constraints, (2) maximise purity subject to yield constraints. Increasing the number of stages in the NLP problem instance allowed the yield to approach close to the attained batch crystallisation equilibrium value.[63] Wang and Lakerveld (2017) used NLP to optimise a MSMPR cascade for the crystallisation of paracetamol from ethanol by cooling with membrane separations incorporated; the different problem instances considered were (1) maximise product crystal size subject to a fixed cascade residence time and impurity limit, (2) minimise the difference in temperature between different crystallisers to reduce cooling duty requirements of the cascade.[78]

2.1.4 Mixed Integer Nonlinear Programming for Optimal Process Synthesis

A Mixed Integer Nonlinear Programming (MINLP) problem is defined as follows. Similarly to the definition of a NLP problem (see Eqs. 1–4), the minimisation of an objective function is as follows, with decision variables, $\boldsymbol{x}$, some of which may be integer (x_i) and some binary (x_j).

$$\min f(\boldsymbol{x}) \tag{5}$$

s.t.

$$\boldsymbol{g}(\boldsymbol{x}) \leq \boldsymbol{b} \tag{6}$$

$$\boldsymbol{h}(\boldsymbol{x}) = \boldsymbol{c} \tag{7}$$

$$\boldsymbol{x}_{\mathbf{LB}} \leq \boldsymbol{x} \leq \boldsymbol{x}_{\mathbf{UB}} \tag{8}$$

$$x_i \in \mathbb{Z} \tag{9}$$

$$x_j \in \{0,1\} \tag{10}$$

MINLP has been implemented in a variety of applications including scheduling, asset management, power systems and process synthesis in engineering applications. Mixed integer problems are implemented for optimisation cases involving both continuous and discrete (binary or integer) decision variables, as opposed to pure NLP problems, which only have continuous decision

variables. MINLP optimisation is particularly useful for process synthesis because the number of individual problem instances that are required for comparison via simulation or NLP rapidly increases with increasing problem complexity (i.e., increasing number of unit operations, possible stream allocation etc.). Formulation and solution of MINLP optimisation problems for various separation processes have been demonstrated in the literature for reactor and synthesis network design as well as for separation process design;[119] Table 2 lists a comprehensive review of demonstrated MINLP applications for non-pharmaceutical separation process design and synthesis, including numerous examples of traditional and hybrid distillation and membrane separation processes, adsorption design and scheduling, dynamic optimisation of Simulated Moving Bed (SMB) chromatography processes. Despite the wide utility of MINLP for process synthesis, there are no applications of such methods for process synthesis and design of separation unit operations for pharmaceutical manufacturing. MINLP methods can be used for process synthesis of LLE and crystalliser cascade configurations to establish designs and flowsheet configurations that attain optimal process performances.

2.2 Market Analysis and Process Flowsheets

Identification of promising candidate APIs for CPM application as well as modelling and optimisation is essential. The experimental demonstration of a continuous flow synthetic route for upstream CPM plant design or a continuous separation cascade is required prior to model construction. Additionally, consideration of processes for APIs which are both societally important and are of economic impact in the pharmaceutical industry are key priorities in the identification of suitable APIs for CPM implementation. This sub-section discusses key APIs in the literature for which continuous manufacturing pathways have been demonstrated (on scales of lab-production or higher), their societal importance and economic impact. Continuous flow chemistry, process flowsheets and objectives from a process modelling and optimisation standpoint are discussed therein.

2.2.1 Plantwide Upstream Continuous Manufacturing

The following APIs have been identified for upstream CPM plant modelling and optimisation.

2.2.1.1 Diphenhydramine

A promising candidate API for CPM is diphenhydramine, an antihistamine with hypnotic and antidepressant applications.[144] Diphenhydramine hydrochloride is the API in the popular brand formulations such as Benadryl® and Zzzquil®. Diphenhydramine is used in many non-prescription drugs with high revenues in both the UK and US (see Fig. 4).

Table 2: Review of demonstrated MINLP optimisation applications in separation process synthesis and design.

No.	Problem	Objective	Continuous Variables		Integer Variables		Literature Reference
			Description	No.	Description	No.	
1	Process synthesis of CSTR and distillation network	Minimise cost / Maximise profit	Reactor flowrates + product compositions + volumes, Operation time	1,050	Existence of units + interconnections	36	120 (Kokossis and Floudas, 1991)
2	Pressure Swing Adsorption (PSA) scheduling	Minimise cost	Bed cycle time	18	Existence of units + interconnections	1–4	121 (Smith and Westerberg, 1991)
3	Multicomponent distillation design with multiple product streams and heat integration	Minimise cost	Column pressures, Component recoveries	12–27	Column sequence + interconnection, Heat Exchange Network (HEN) design	68–135	122 (Aggarwal and Floudas, 1992)
4	Distillation sequencing with heat integration	Minimise cost / Maximise profit	Column pressures + reflux ratio + no. trays + diameter	16	Column sequence + interconnection, HEN design	19	123 (Paules and Floudas, 1992
5	Distillation design with multiple feeds	Minimise duty Minimise reflux	Column pressures + reflux ratio + no. trays	588–1,621	Feedpoint locations	56–174	124 (Viswanathan and Grossmann, 1993)
6	Distillation sequencing with heat integration	Minimise cost	No. trays	18	Column sequence + number	1,093	125 (Novak et al., 1996)
7	Process synthesis of ethane extraction plant	Maximise profit	Compressors rotational speed, Cold tank pressure + temperature, Demethaniser pressure, Bottoms flowrate	5	Existence of unit operations	5	126 (Diaz et al., 1996)
8	Ethanol dehydration-extraction process synthesis	Minimise energy usage	Column pressure + temperature, Solvent flowrate, Reflux ratio	4	Existence of unit operations	4	127 (Diaz, Gros and Brignole, 2000)
10	Process synthesis of solvent extraction for chromium ion recovery from waste water	Minimise cost	Organic phase flowrate Product concentration	2	No. compressors + interconnections	15	128 (Alonso, Lassahn and Gruhn, 2001)
11	Dynamic optimisation of chromatographic separation of molasses from water	Maximise profit	Feed flowrates	8	Recycle options	14	129,130 (Emet and Westerlund, 2003, 2004)
12	Olefin separation process synthesis	Minimise cost	Various operating parameters	18,624	Existence of unit operations + interconnections	5,851	131 (Lee et al., 2003)
13	Distillation + membrane hybrid separation process synthesis	Minimise annual costs	Reflux ratio + vapour boilup rate	2,000–3,000	No. column trays	≤ 250	132 (Kookos, 2003)

14	Brackish water electrodialysis process synthesis	Minimise cost	Stream flowrates + concentrations, Stack voltages, Pumping duties	19	No. stages and cell pairs	2	133 (Tsiakis and Papageorgiou, 2005)
15	Process synthesis for cryogenic air separation	Minimise cost	Stream flowrates + pressures, Product specifications	11	Existence of unit operations + interconnection	46	134 (Sirdeshpande et al., 2005)
16	Process synthesis for retrofitted mass exchange networks	Minimise cost	Stream flowrates + compositions	203	Existence of unit operations and connections	48	135 (Chen and Hung, 2005)
18	Bioethanol distillation process synthesis	Minimise cost	Feed flowrate, reflux ratio, boilup rate	4,412	Feedpoint locations, ionic liquid feed flowrate, no. trays	44	136 (Chávez-Islas et al., 2011)
19	Water regeneration network synthesis	Minimise cost	Stream flowrates + concentrations, Pressures	926	Unit interconnections	432	137 (Khor et al., 2011)
20	Design of reverse osmosis systems	Minimise cost	Stream flowrates + concentrations, Pressures	246	Unit interconnections	21	138 (Lu, Liao and Hu, 2012)
21	Reverse osmosis for dilute bioethanol purification	Minimise cost	Operating pressures	1,879	Existence of unit operation, Feedpoint location, Recycle options	120	139 (Kanchanalai et al., 2013)
22	Process synthesis for gas drying via adsorption	Minimise cost	Bed length + diameter + regeneration temperature, Gas flowrate, Cycle times	6	No. beds undergoing adsorption / regeneration	2	140 (Al Wahedi et al., 2016)
23	Selection of zeolites for simulated moving bed (SMB) chromatography	Maximise profit	Stream velocities, Switching time, Column length	45,788	Zeolite selection	96	141 (Farque Hasan et al., 2017)
24	Design of dividing wall column (DWC) for ethanol dehydration	Minimise cost	Reflux ratios and boilup rates	4	No. trays, Feed locations	5	142 (Franke, 2017)
25	Process synthesis of membrane cascade for gas mixture separation	Minimise cost	Operating pressures, Stream flowrates, Membrane areas	703	Existence of unit operation	39	143 (Aliaga-Vicente, Caballero and Fernández-Torres, 2017)

The considered continuous flow synthesis of diphenhydramine has been demonstrated via two methods: in reaction solvent and as a neat mixture (without solvent).[32] The CPM route features in-line purification and crystallisation, full-atom economy and flow of molten ammonium salts. The benefits of using neat mixtures in microreactors are well documented in the literature.[145–148]

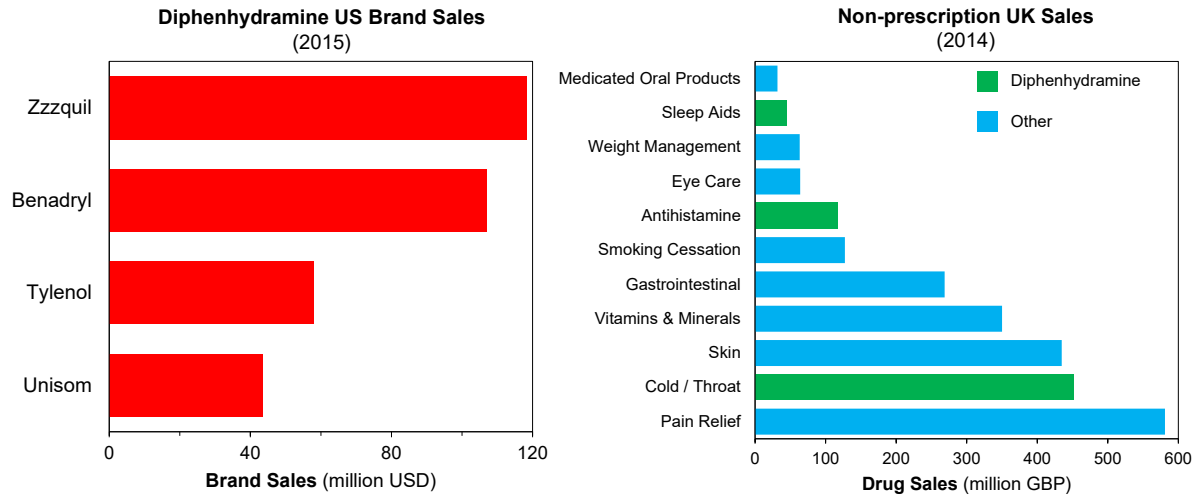

Figure 4: Diphenhydramine brand sales in the US and non-prescription sales in the UK.[149]

The considered continuous flow synthesis of diphenhydramine was described by Snead and Jamison (2013).[32] The CPM route involves the etherification of chlorodiphenylmethane (CDPM) and dimethylaminoethanol (DMAE) to form the API hydrochloride salt. The synthesis reaction is carried out via two methods: (1) in carrier solvent, *N*-methyl-2-pyrrolidone (NMP), CPMa, and (2) as a neat mixture, CPMb (Fig. 5).

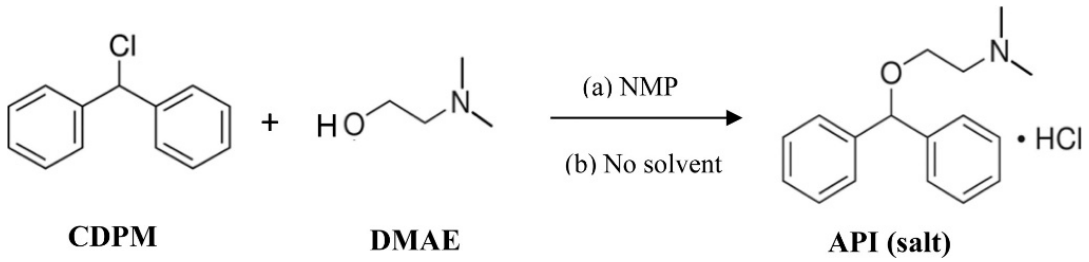

Figure 5: Continuous flow synthesis of diphenhydramine hydrochloride.[32] (a) Reaction in carrier solvent (NMP) at 180 °C, CPMa; (b) Reaction without carrier solvent ("neat") at 175 °C, CPMb.

The developed flowsheets for both syntheses are shown in Fig. 6. Reagents and carrier solvent flow into Plug Flow Reactor (PFR) R-101. Aqueous NaOH solution is then pumped into the reactor effluent to neutralise the API salt, after heating to the reaction temperature in heat exchanger (HX)-101. The neutralised effluent is then purified to obtain a product containing the API, following heating to the required separation temperature in HX-102.

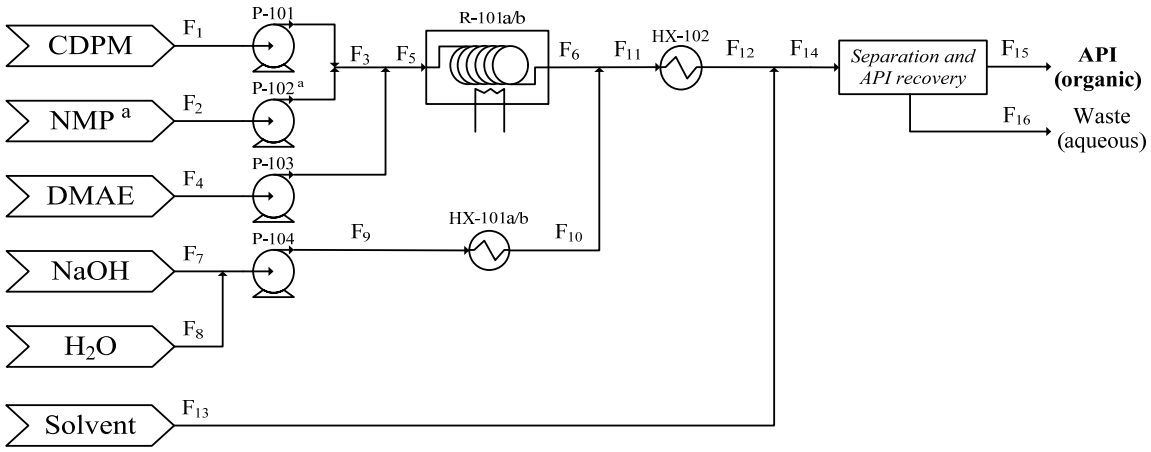

Figure 6: Developed continuous flowsheet for synthesis of diphenhydramine. (a) Process using carrier solvent (CPMa), (b) Process without carrier solvent (CPMb). "F" denotes stream numbers.

2.2.1.2 Rufinamide

Active Pharmaceutical Ingredients (APIs) containing 1,2,3-triazole rings are known to have a wide range of applications including antifungal,[150] anti-HIV,[151] anti-cancer,[152] antibacterial[153] and tuberculosis treatments,[154] amongst others. Synthetic routes towards molecules containing 1,2,3-triazole cores require generation of organoazide intermediates which pose significant operational hazards due to their high propensity for detonation.[155] Such reactions in flow can potentially be too hazardous in batch mode due to the accumulation and required isolation of organoazide intermediates between batch unit operations. Continuous operation of such reactions have the potential to circumvent these hazards by immediately reacting these intermediates in flow.[156]

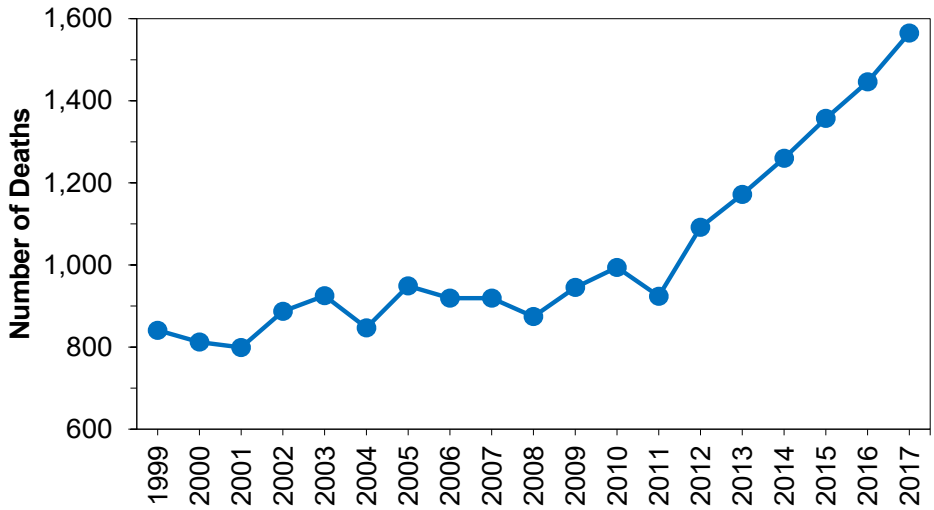

Figure 7: Historical number of cases of death by epilepsy in the US.[157]

An important advantage of continuous operation is the ability to access process conditions (e.g., high pressure and temperature) that would be otherwise too hazardous to operate in batch mode;[158] this is due to the improved heat and mass transfer characteristics inherent of the smaller equipment dimensions required for continuous operation compared to batch vessels.[17,159] Operating hazardous reactions is also inherently safer in continuous mode due to the limitation of the hazard to a smaller footprint compared to equivalent setups in batch mode.

Rufinamide is an anticonvulsant API developed for the treatment of Lennox-Gastaut syndrome (i.e., childhood onset epilepsy), present in formulations such as Banzel or Inovelon. Cases of death by epilepsy have been historically increasing (Fig. 7) and thus efficient manufacturing of antiepileptic APIs is important. Rufinamide contains a 1,2,3-triazole ring whose synthesis requires the generation of organoazide intermediates. Various synthetic routes towards rufinamide have been demonstrated in recent years[40,160–163] with life cycle assessments also elucidating process benefits of various manufacturing routes.[57] One of these demonstrations implements a continuous flow synthesis featuring three PFRs whilst avoiding the accumulation or holdup of hazardous organoazide intermediates.[40]

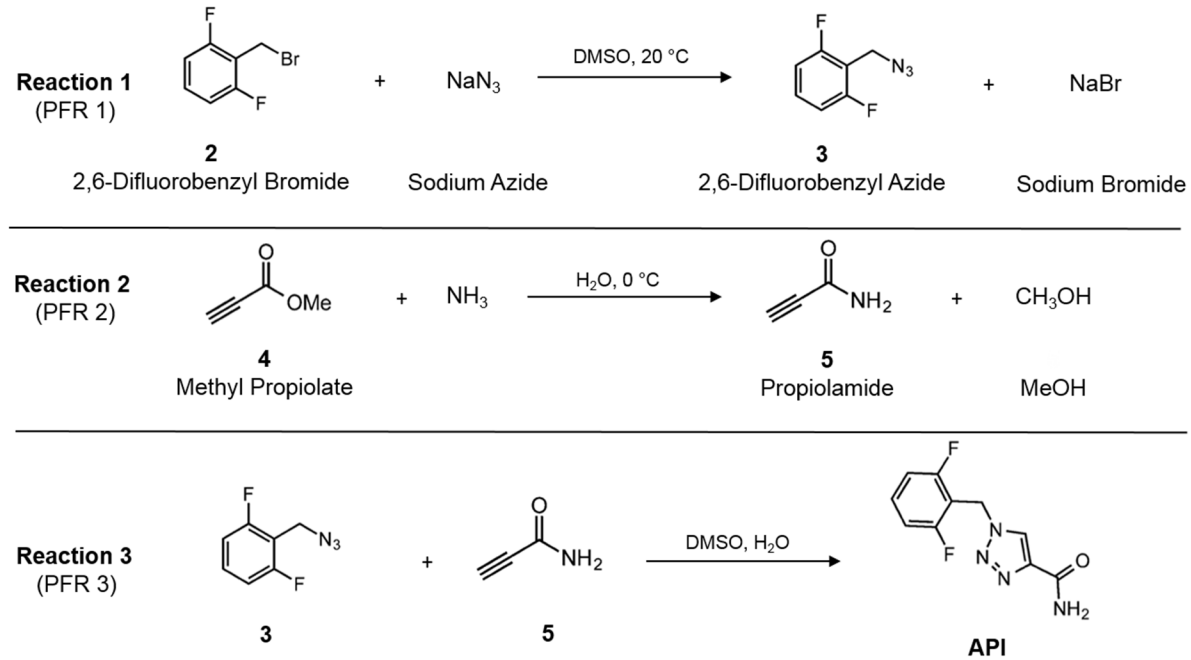

Figure 8: Reaction scheme for the continuous flow synthesis of rufinamide.[40]

The process model and flowsheet developed here is based on the continuous flow synthesis of rufinamide in a series of PFRs demonstrated by Zhang et al. (2014).[40] The reaction scheme for the CPM of rufinamide is shown in Fig. 8 and the developed CPM flowsheet in Fig. 9. The first reaction is a S_N2 substitution of 2,6-difluorobenzyl bromide (**2**) by sodium azide (NaN_3) at 20 °C, forming the intermediate 2,6-difluorobenzyl azide (**3**) and sodium bromide (NaBr) as a by-product.

Both reagents use dimethyl sulfoxide (DMSO) as a carrier solvent. The second reaction features a mixture of neat methyl propiolate (**4**) and aqueous ammonium hydroxide reacting at 0 °C to form intermediate propiolamide (**5**), condensing methanol (MeOH) as a by-product. Intermediates **3** and **5** mix at a T-junction and enter PFR-3 to synthesise the API.[40]

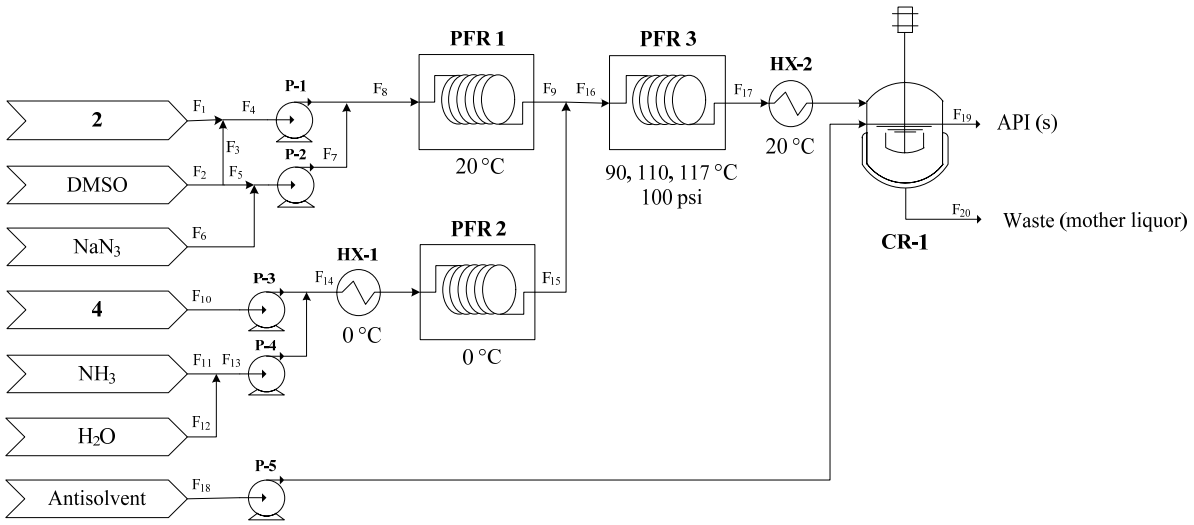

Figure 9: Conceptual flowsheet for upstream CPM of rufinamide.[40]

The original publication also reports the formation of an API regioisomer in PFR-3, which is not considered due to the lack of available kinetic data for this reaction.[40] A back pressure of 100 psi is required to regulate NH_3 gas generation.[40] The effluent of PFR-3 then undergoes antisolvent crystallisation where rufinamide is crystallised and removed as a solid product.

2.2.1.3 Warfarin

(*S*)-Warfarin is an anticoagulant API commonly used for the treatment of deep vein thrombosis and pulmonary embolism.[164] Prescription rates of cardiovascular treatments and global anticoagulant medications have both been historically increasing (see Fig.10).[165] The continuous flow synthesis of (*S*)-warfarin features a single reaction and subsequent Liquid-Liquid Extraction (LLE) process.[166] Comparison of different conceptual separation process alternatives is essential for establishing cost-effective, materially efficient designs for upstream CPM configurations. Screening of candidate continuous LLE configurations for this API has yet to be conducted; modelling, simulation and optimisation of continuous separation processes can be used for rapid design space investigation to elucidate technically feasible and economically viable processes.

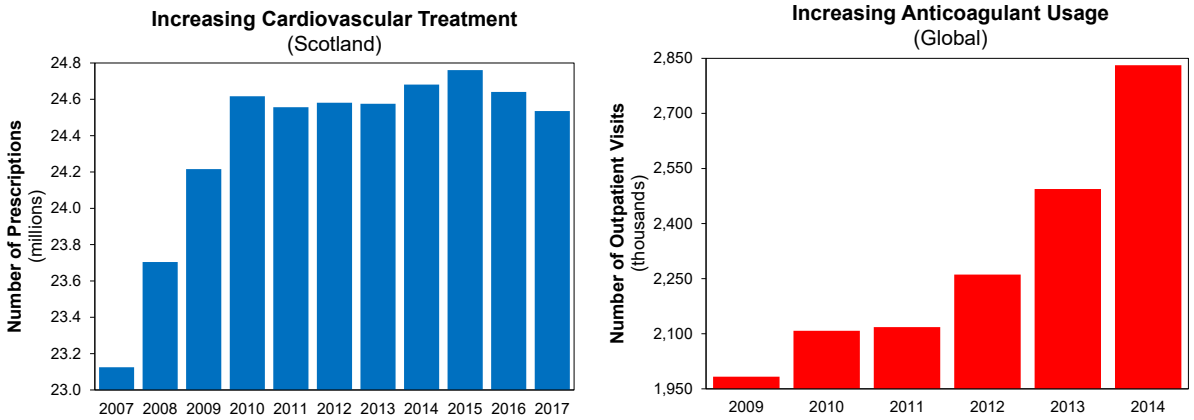

Figure 10: Increasing prescriptions of cardiovascular treatments and global anticoagulant usage.[165]

Here, steady-state process modelling and nonlinear optimisation (via NLP) is implemented for the upstream CPM of warfarin, including continuous flow synthesis and LLE. Flowsheet development based upon the published continuous synthetic route and a conceptual continuous LLE process are presented, comparing various separation solvents. Thermodynamic models for liquid-liquid phase composition and API solubility prediction in non-ideal, multicomponent mixtures for LLE design are described. Nonlinear optimisation problem formulation for total cost minimisation is subsequently presented. Minimum total costs, optimal API recoveries and material efficiencies for different process configurations are compared to establish promising LLE solvents.

The flowsheet for the CPM of (*S*)-warfarin (API) is shown in Fig. 11. The continuous flow synthesis of the API features the nucleophilic addition of 4-hydroxy-coumarin with benzalacetone in the presence of trifluoroacetic acid (TFA) and a chiral amine catalyst at 75 °C in 1,4-dioxane, with a reported conversion of 61%. Aqueous HCl is added to the reactor effluent before entering the LLE unit. Upon addition of the candidate LLE solvent, the process forms an organic (product) phase containing recovered API and an aqueous (waste) phase, between which API partitions.

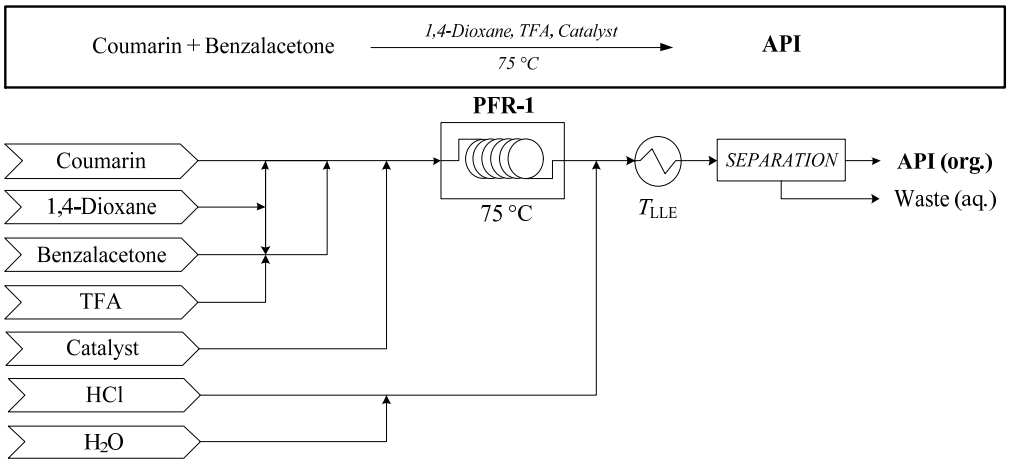

Figure 11: Process flowsheet for the continuous flow synthesis of (*S*)-warfarin[166] and subsequent continuous Liquid-Liquid Extraction (LLE).

2.2.1.4 Nevirapine

Affordability and accessibility of essential medicines remains a pressing issue for the treatment of diseases prevalent in developing countries. The treatment of the HIV continues to be one of the most prominent global health challenges; the prevalence of HIV has been historically increasing worldwide, with low- and middle-income countries being those most affected (Fig. 12). The development of efficient, cost-effective manufacturing routes towards drugs for HIV treatment is paramount to ensure global, affordable access to such medicines.[167]

The utility of CPM platforms for the development of APIs for the treatment of HIV and other societally important diseases has been demonstrated in the literature;[19,20] Table 3 lists various HIV APIs whose syntheses have benefited by implementing semi-continuous/continuous methods. The design of continuous separation processes for integration into upstream CPM is essential to realise the benefits of end-to-end continuous manufacturing for HIV API production.

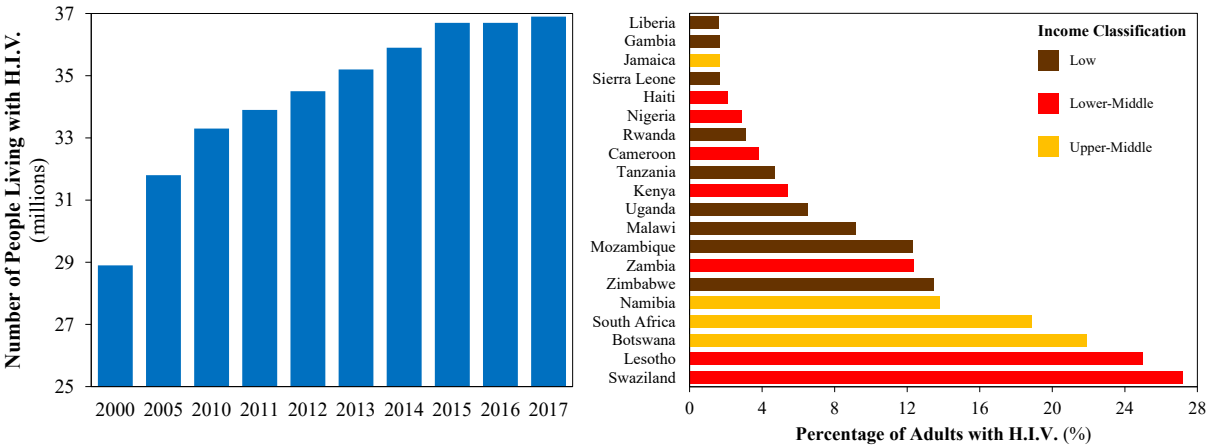

Figure 12: Increasing worldwide HIV prevalence[168] + top 20 countries with the highest rates.[169]

Nevirapine is a widely-prescribed API for HIV-1 treatment on the WHO List of Essential Medicines, whose continuous flow synthesis from two advanced starting materials was recently demonstrated with subsequent purification and batch crystallisation for final API separation.[170] The economic viability of different process alternatives for the API is yet to be systematically investigated and is essential to ensure cost optimal designs. Systematic comparison of process alternatives is essential to further aid the development of leaner manufacturing routes towards this societally important HIV API.

Various commercial routes towards nevirapine have been demonstrated in the literature with varying complexities and material intensities.[174] The recent demonstration of the continuous flow synthesis of nevirapine uses advanced starting materials (made prior to the flow synthesis in batch),

2-chloro-3-amino-4-picoline (CAPIC) and MeCAN (methyl-2-(cyclopropylamino)nicotinate).[170] The syntheses of CAPIC and MeCAN are summarised in Fig. 13.

Table 3: Demonstrated continuous/semi-continuous flow syntheses of HIV APIs.

API	Year	Continuous/Semi-Continuous	Processing Benefits	Ref.
Efavirenz	2013	Semi-continuous	Improved API yield Reduced process time Reduced number of unit ops.	171
Darunavir	2015	Continuous	End-to-end continuous process at production scale	30,31
Lamivudine	2017	Semi-continuous	Improved API yield Reduced process time	172
Nevirapine	2017	Continuous	Improved material efficiency Reduced number of unit ops.	170
Dolutegravir	2018	Continuous	Reduced process time	173

Fig. 13a illustrates the published batchwise synthesis of CAPIC. Acetone and malononitrile react in toluene (PhMe) in the presence of basic Al_2O_3 to form ylidene, followed by filtration of Al_2O_3 from the reaction mixture. Dimethyl formamide-dimethyl-sulfate (DMF-DMS) and acetic anhydride (Ac_2O) and triethylamine (TEA) are then added to the filtrate under N_2 to form enamine (**5**). Hydrogen chloride (HCl) gas is then bubbled into the reaction mixture and heated. The mixture is then concentrated by evaporating solvent and water followed by filtration of product 2-chloro-4-methylnicotinonitrile (CYCIC). Sulfuric acid (H_2SO_4) is then added to the solid CYCIC and reacted at high temperature followed by the addition of water. Aqueous NaOH is added until pH = 11. The resulting suspension is then filtered for product 2-chloro-4-methylnicotinamide (COMAD). A mixture of COMAD, water and sodium hypobromite (NaOBr) is made at 0 °C. Water is then added and the mixture is heated to 80 °C and stirred. After cooling, PhMe is added to form a biphasic mixture; the organic layer is washed with water and concentrated under vacuum to remove solvent. Hexanes are then added to precipitate CAPIC.

Fig. 13b illustrates the published batchwise synthesis of MeCAN. 2-chloronicotinonitrile, cyclopropylamine (CPA), TEA, water and isopropyl alcohol (IPA) are added at 140 °C and pressurised to 10 psi to form an intermediate. The mixture is stirred and then cooled to 60 °C. Potassium hydroxide (KOH) is then added to the reaction mixture and stirred. Concentrated HCl is added to change pH to 6 and cooled to 10 °C to precipitate 2-(cyclopropylamino)nicotinic acid (2-CAN), which is then vacuum filtered. 2-CAN is then dissolved in PhMe under N_2, adding thionyl chloride ($SOCl_2$). The reaction mixture is cooled to 0 °C followed by H_2O addition and pH adjustment to 9 with NaOH (aq.), forming a biphasic mixture. The aqueous layer is washed with toluene (PhMe) and the combined organic layers washed with H_2O and dried with Mg_2SO_4, followed by filtration and concentrated under vacuum to yield MeCAN.

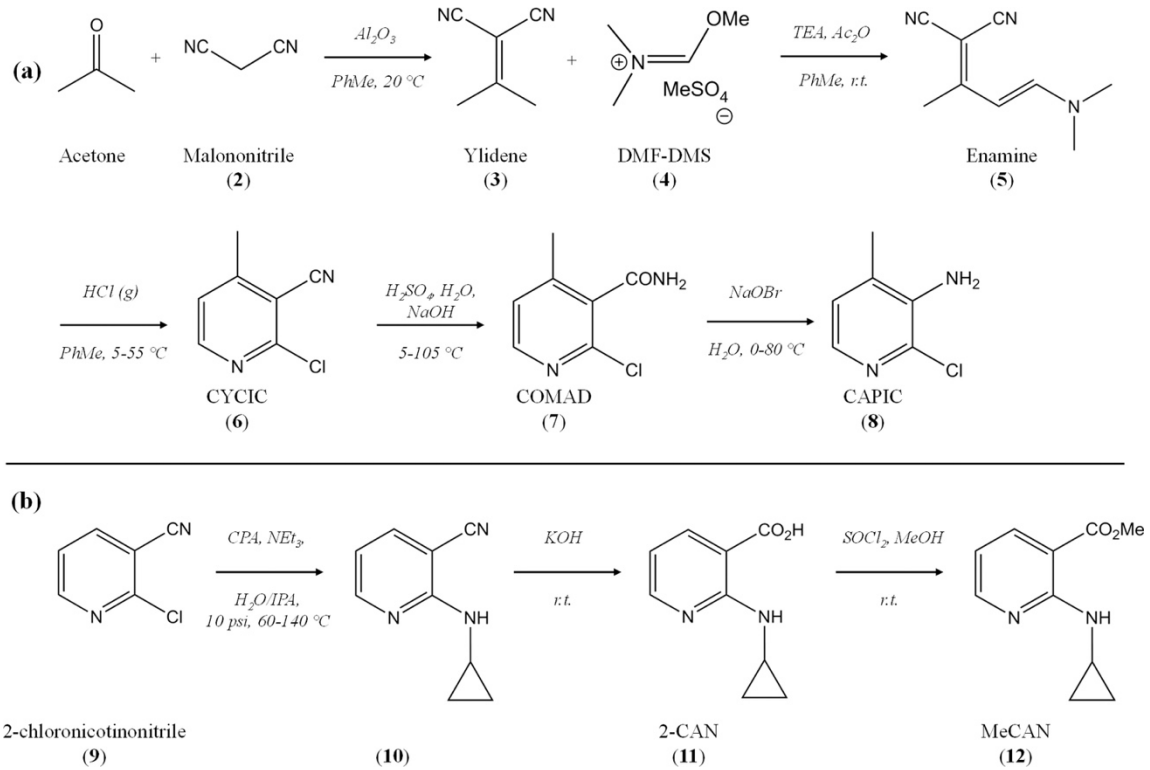

Figure 13: Published batchwise syntheses of (a) CAPIC and (b) MeCAN.[170]

The published continuous synthetic route for nevirapine from CAPIC and MeCAN is shown in Fig. 14. Starting materials CAPIC and MeCAN (in diglyme carrier solvent) are used to form intermediate *N*-(2-chloro-4-methylpyridin-3-yl)-2-(cyclopropylamino)nicotinamide (CYCLOR) in the presence of NaH, which then forms nevirapine (API). The CPM process in this work is based upon this demonstrated continuous flow synthesis, whose process modelling and simulation are further developed in later sub-sections.

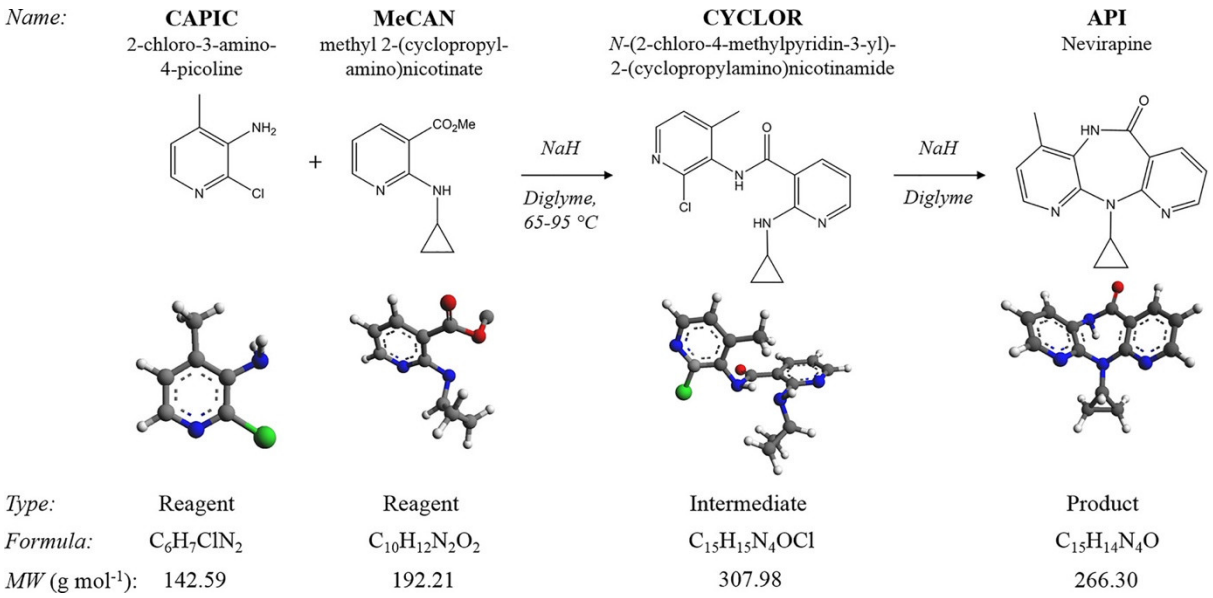

Figure 14: Nevirapine continuous synthesis from CAPIC and MeCAN.[170]

Fig. 15 shows the process flowsheet for nevirapine CPM based on the published continuous flow synthesis. The first reactor, R-101, is a thin-film reactor operated at 95 °C; reaction between CAPIC and NaH in diglyme at 95 °C forms the sodium salt of CAPIC (CAPIC-Na) with evolution of H_2 gas and an estimated 100% conversion of CAPIC. The mixture containing CAPIC-Na is added to a continuous stirred tank (R-102, 65 °C) with neat MeCAN with 82.5% conversion of CAPIC-Na to CYCLOR (+ sodium methoxide, $NaCH_3O$) reported. Finally, CYCLOR undergoes ring closure in the presence of a packed bed of NaH (R-103) to form nevirapine (API). The subsequent crystallisation can be performed in batch or continuous mode.

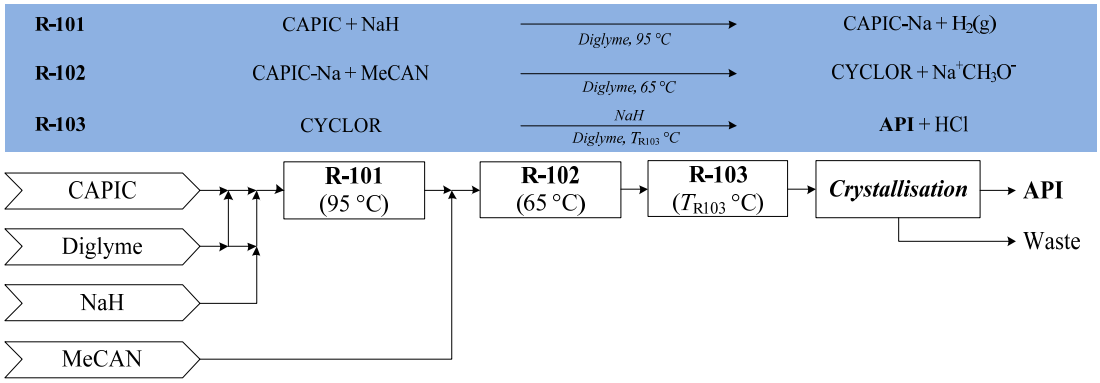

Figure 15: Process flowsheet for the CPM of nevirapine.

The flowsheet for the conceptual crystallisation process considered in this work following the continuous flow synthesis is shown in Fig. 16. The effluent of R-103 is fed to a stirred tank where aqueous HCl is added; the API is more soluble at lower pH in aqueous solutions. Activated carbon (AC) is then added to adsorb organic impurities prior to their subsequent removal via filtration.[170] Nevirapine is then crystallised from solution by decreasing the API solubility by increasing pH by addition of aqueous NaOH. The crystallisation following the continuous flow synthesis can be either implemented in batch or continuous mode.

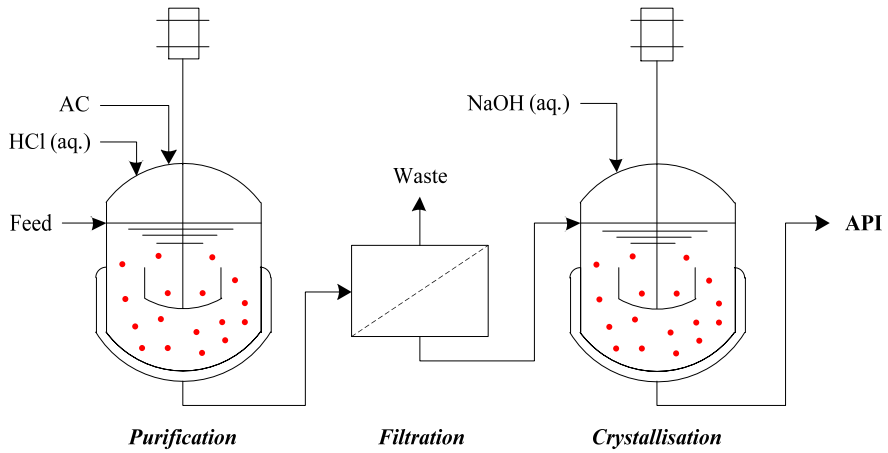

Figure 16: Crystallisation of nevirapine operated in batch (BX) or continuous (CPM) mode.

2.2.1.5 Atropine

Atropine is a WHO essential medicine, primarily used for the treatment of the effects of nerve agents and poisons, often being the most readily available patient treatment in warzones where chemical warfare is used.[175] Atropine is also used to induce cycloplegia and mydriasis for ophthalmic treatments, for the treatment of bradycardia and to inhibit salivary and mucus glands during medical procedures.[176] The continuous flow synthesis of atropine was recently demonstrated, featuring two PFRs followed by a purification via LLE;[177] the study showed an improved material efficiency over previous demonstrations.[178] Systematic comparative evaluation of process alternatives for operational feasibility and economic viability for atropine CPM has yet to be conducted and can elucidate designs of improved economic viability.

The reaction scheme for the continuous flow synthesis of atropine[177] is shown in Fig. 17. Reaction 1 features the esterification of tropine (in dimethylformamide, DMF) and neat phenylacetyl chloride at 100 °C to form tropine ester HCl, the free form of which is formed by the addition of sodium hydroxide (NaOH (aq.)). Reaction 1 attains a reported conversion of 99% of tropine to tropine ester HCl at 100 °C in a residence time of $\tau_{PFR\text{-}1}$ = 3.5 min in the literature. Reaction 2a is the aldol addition of formaldehyde (CH_2O) to tropine ester at 100 °C under basic conditions to form API (a mixture of the D- and L-isomers), attaining a reported conversion of 78%. An undesired elimination of API to apoatropine via condensation is also reported (reaction 2b).[177]

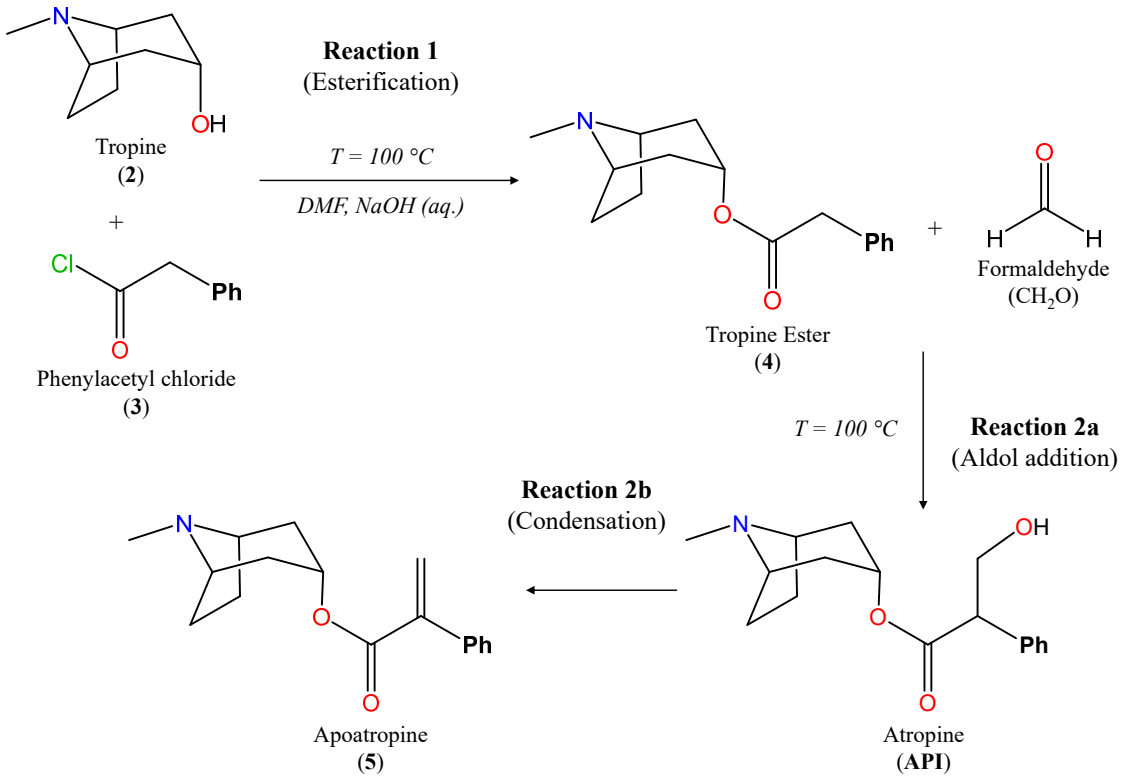

Figure 17: Reaction scheme for the continuous flow synthesis of atropine.[177]

The process flowsheet for the CPM of atropine is shown in Fig. 18. Reaction 1 occurs in PFR-1 while reactions 2a and b occur in PFR-2. Reaction conditions are as reported in the literature.[7] The reaction mixture is neutralised with HCl (aq.).[177] A subsequent API purification via LLE follows, discussed further in later sections.

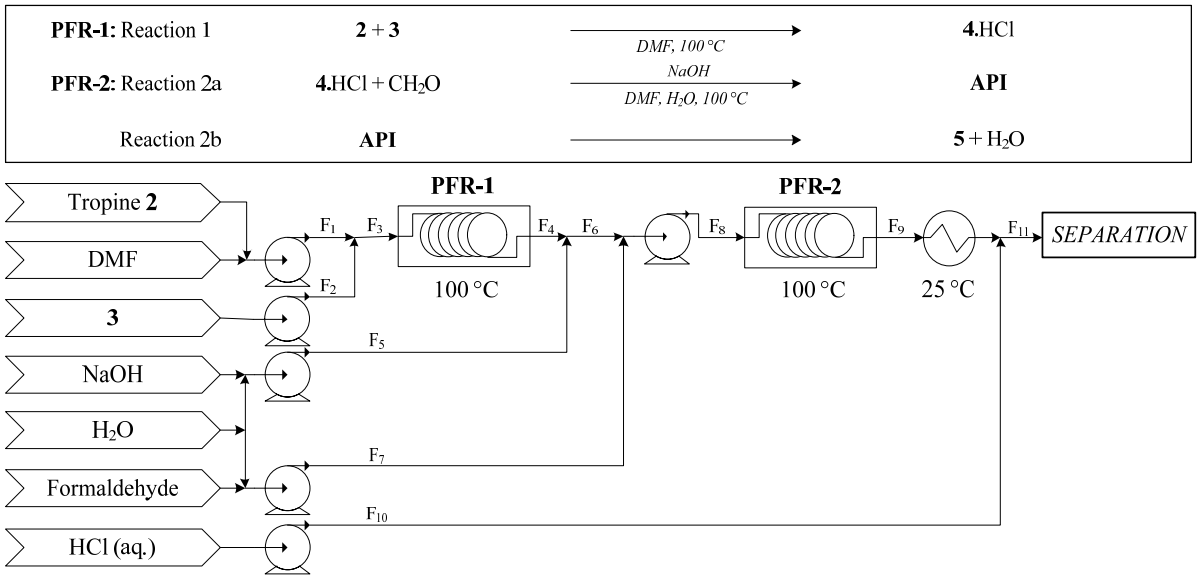

Figure 18: Process flowsheet for atropine CPM.

2.2.2 Mixed Suspension, Mixed Product Removal Crystalliser Cascades

The continuous cooling crystallisation of the following APIs has been considered in this work.

2.2.2.1 Cyclosporine, Paracetamol and Aliskiren

Several pharmaceutical compounds have been investigated for their MSMPR crystallisation in the literature, including cyclosporine, an immunosuppressant with applications for skin ailment treatment (namely psoriasis) and rheumatoid arthritis; paracetamol, the popular analgaesic + antipyretic; and aliskiren hemifumarate, a renin inhibitor for the treatment of primary hypertension. Historic and predicted revenues for prescription hypertensive[179] and non-prescription analgesics and skin treatment medicines[149] (Fig. 19) and their multiple formulation types (Table 4) illustrate the societal and economic importance of these APIs in the pharmaceutical industry. The optimal design of continuous crystallisation processes for their integration into CPM campaigns is paramount.

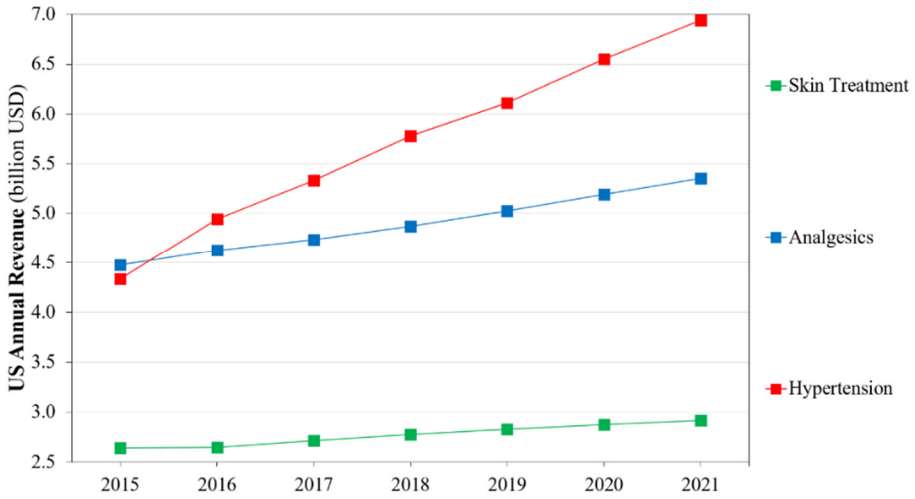

Figure 19: Historic and predicted US revenues for prescription hypertension (aliskiren) and non-prescription analgesic and skin treatment drug classes.[149,179]

The process investigated here is the continuous MSMPR cooling crystallisations of cyclosporine, paracetamol and aliskiren (hemifumarate). The process flowsheet for a cascade of MSMPR crystallisers in series for continuous crystallisation based on experimental demonstrations[63,91,92] is shown in Fig. 20. A mother liquor stream containing dissolved API enters the first crystalliser, whose product slurry is the feed stream to the subsequent crystalliser in the cascade. Crystallisation occurs by cooling only, without the need for an antisolvent to generate supersaturation. Experimental setups for the MSMPR crystallisation of cyclosporine, paracetamol and aliskiren have shown that configurations with no recycle are efficient in terms of both yield and purity.[107] For all three APIs, a series of MSMPR crystallisers without recycle are considered.

Table 4: Brands and formulations of cyclosporine, paracetamol and aliskiren.

API	Application	Brand Name	Prescription?	Patented?	Formulation
Cyclosporine	Immunosuppressant	Sandimmune®	✓	✓	Oral capsule Oral solution Intravenous solution
		Cicloral®	✓	X	Oral capsule
		Deximune®	✓	X	Oral capsule
	Psoriasis	Neoral®	✓	✓	Oral capsule Oral solution
	Rheumatoid arthritis	Neoral®	✓	✓	Oral capsule Oral solution
	Keratoconjunctivitis	Restasis®	✓	✓	Ophthalmic emulsion
Paracetamol[a]	Analgaesic	Tylenol®	X	X	Oral tablet
		Calpol®	X	X	Oral suspension
		Panadol®	X	X	Oral tablet
Aliskiren	Hypertension	Tekturna®	✓	✓	Oral tablet
		Rasilez®	✓	✓	Oral tablet

Cyclosporine is crystallised by cooling from a mother liquor solvent of acetone;[63] paracetamol is crystallised from a 4:1 mixture (volume basis) of isopropanol:water;[91] aliskiren hemifumarate is crystallised from a 1:1 mixture of ethyl acetate:ethanol (mass basis).[92] The experimental demonstration of aliskiren hemifumarate crystallisation describes a reactive crystallisation step performed at 20 °C prior to cooling crystallisation, which is assumed to have already been performed prior to the process considered here.

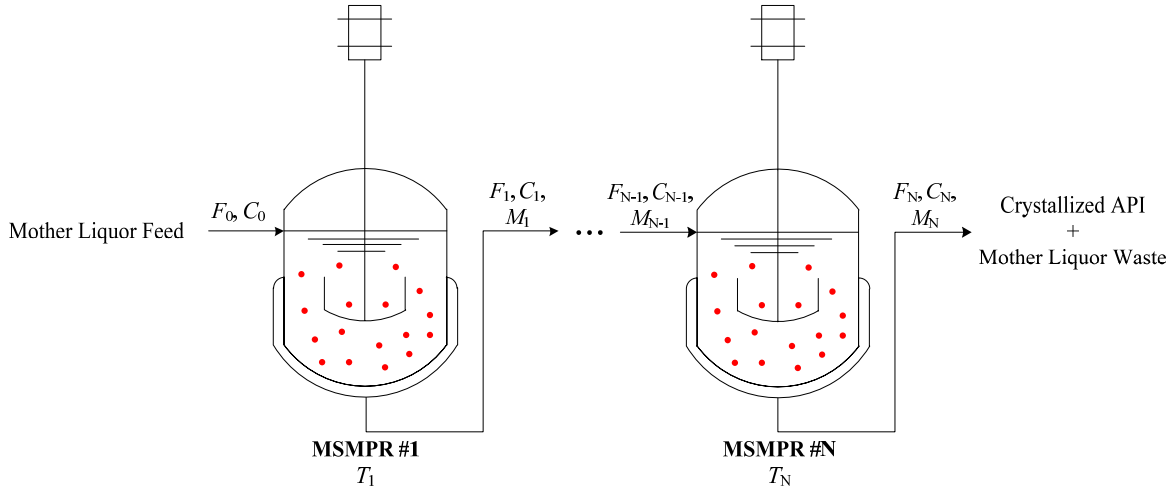

Figure 20: Process flowsheet of a cascade of continuous MSMPR crystallisers. F = flowrate, C = solute concentration in liquid phase, M = slurry density, T = crystalliser operating temperature.

2.2.2.2 Melitracen

Melitracen is a tricyclic antidepressant API available as single drug preparations and also in combinative therapies.[180] The number of US citizens affected by depression and of defined daily doses of antidepressants distributed in the UK have been historically increasing (Fig. 21). The continuous crystallisation of the API in MSMPR crystallisers was recently demonstrated,[181] facilitating its process modelling and optimisation. Existing work investigates the effects of different MSMPR design and operating parameters on crystal size for a maximum of two MSMPRs, showing significant variation in process performance and crystal product attributes when varying the number of implemented crystallisers. Investigating the effect of longer cascades and recycle options can further improve crystallisation yields in MSMPR design.[99] Economic considerations are equally important as meeting specific product attribute targets when designing crystallisation processes, especially when the effect of production scale is considered.[69,118,182]

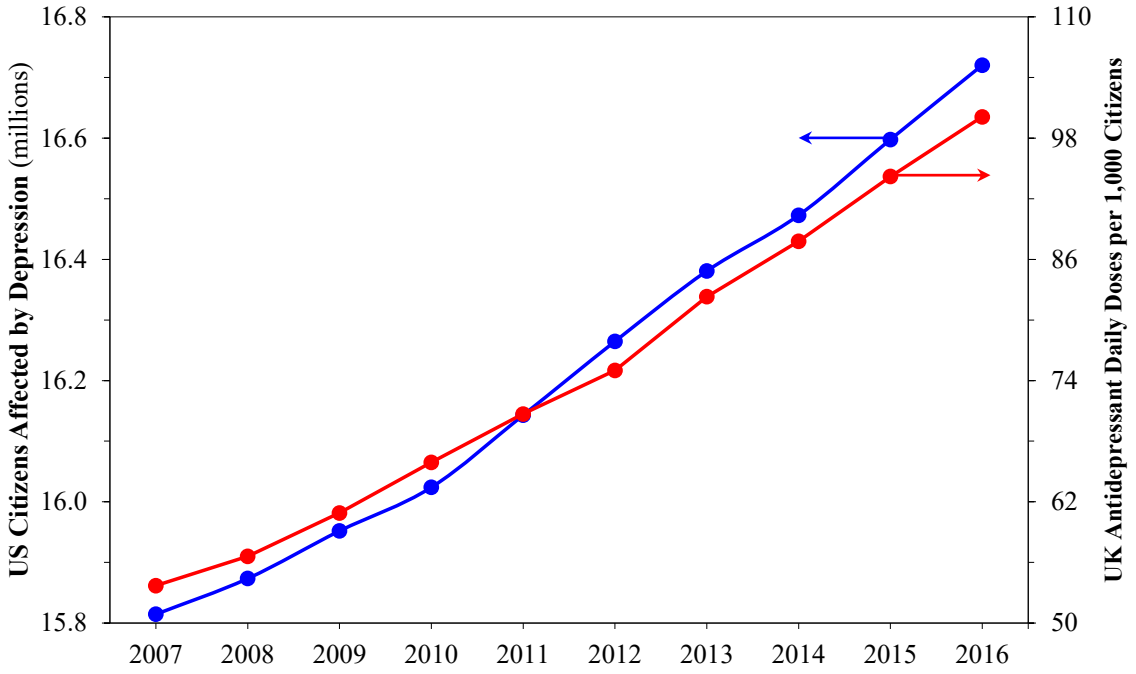

Figure 21: Historical trends in number of US citizens affected by depression (2016 US population = 323.4 million) and number of defined daily dosages administered per 1,000 UK inhabitants (2016 UK population = 65.38 million).[183,184]

2.3 Thesis Aims & Objectives

It is clear from the literature review provided and by consideration of the different APIs, their processes and societal and economic impacts, that continuous separation design is fairly limited in comparison to the number of continuous flow synthesis demonstrations, presenting a significant bottleneck in the development of end-to-end CPM processes. Steady-state modelling and optimisation of candidate CPM processes for these APIs allows rapid screening for promising plant designs. From this discussion, the following objectives were pursued for this thesis. All calculations for the case studies presented are performed in MATLAB.

2.3.1 Upstream Process Design and Simulation

Diphenhydramine: The aim of this work is to produce a process model to simulate the upstream processing (synthesis and purification stages) for CPM of diphenhydramine based upon the published continuous flow synthesis. This will involve establishing kinetic expressions of the chemical reactions of API synthesis in solvent and in a neat mixture. Relevant physical property estimations are subsequently made where necessary for subsequent unit operation design. Plug Flow Reactor (PFR) design is next conducted with the calculation of required reactor lengths for appropriate inner diameters and their required heating duties. The design of a continuous purification stage uses experimental solubility and equilibrium data as well as theoretical (group

contribution) methods, with a comparison of extraction performances and material efficiencies of different design options. An economic evaluation of the entire process shall then demonstrate the cost savings and improvements in material efficiency which can be realised by continuous separation train relative to the batch alternative, as well as the improvements realised by neat synthesis relative to the synthesis in carrier solvent. Finally, a critical discussion of the design methods will examine the technoeconomic viability of implementation of diphenhydramine CPM.

Rufinamide: This work develops a steady-state process model for the simulation of the CPM of rufinamide based on the demonstrated continuous flow synthesis in the literature. Reaction kinetic parameter regression, mass balance calculation and reactor sizing are conducted for the upstream CPM of rufinamide. Batch and continuous crystallisation processes following the continuous flow synthetic route are also modelled, implementing API solubility modelling in multicomponent process mixtures to systematically compare different separation options. Subsequent economic analyses elucidate cost savings benefits when implementing continuous crystallisation of the API vs. the batch method. A critical discussion of the results, process modelling methodologies and design methods are then provided to examine the technoeconomic feasibility and viability of the CPM of rufinamide.

2.3.2 Technoeconomic Optimisation for Reactors and Separators

Warfarin: This work describes the steady-state process modelling and technoeconomic optimisation for the upstream CPM of (*S*)-warfarin, implementing reactor design and LLE solvent comparison for purification. Reported reaction conversions and computed LLE efficiencies allow mass balance calculation and total cost minimisation via NLP to establish promising LLE solvents. The nonlinear optimisation problem is formulated for total cost minimisation. Liquid-liquid phase equilibria, API phase compositions and solubilities for LLE design are implemented via surrogate polynomials based on extensive UNIFAC modelling; API recovery rates are calculated via detailed mass transfer correlations. The methodology used here screens optimum process configurations to inform the design of upstream CPM of (*S*)-warfarin.

Nevirapine: This work conducts a systematic comparative evaluation of CPM process alternatives for nevirapine based upon the published synthetic routes via steady-state process modelling and optimisation. A conceptual continuous crystallisation process is considered for comparison to the demonstrated batch crystallisation process. Arrhenius parameter estimation from experimental kinetic data allows flow reactor design for the continuous synthesis of nevirapine. Crystallisation process design utilises an established API solubility model. A constrained NLP problem for total cost minimisation of different design alternatives is then formulated. Optimal total cost

components, plant material efficiencies and corresponding operating parameters are presented for different process configurations for comparative evaluation to establish promising designs.

Cyclosporine, Paracetamol, Aliskiren: This work conducts total cost minimisation via NLP of different MSMPR cascades for cyclosporine, paracetamol and aliskiren hemifumarate. First, we describe the continuous crystallisation process implemented for all three APIs. Subsequently, we describe the process model, costing methodology and the constrained nonlinear optimisation problem formulation for total cost minimisation. We then present minimal total cost components for all APIs for varying numbers of crystallisers and different plant API capacities with corresponding optimal design parameters of the implemented crystallisers.

2.3.3 Process Synthesis for Technoeconomic Optimisation

Atropine: This work implements steady-state process modelling and MINLP optimisation for total cost minimisation of the upstream CPM of atropine, considering the possibility for multiple LLE stages and fresh solvent addition to intermediate tanks in the separation cascade. The considered superstructure for the conceptual continuous LLE process with varying solvent feedpoint locations is then presented along with the MINLP problem formulation for plant total cost minimisation. Optimisation solutions for candidate LLE solvents and varying numbers of LLE tanks are compared, considering cost optimal LLE design configurations, vessel volumes and solvent amounts, attained API recoveries, process material efficiencies and total cost components. Comparative evaluation of optimisation results establishes promising LLE solvent choices and design configurations for atropine CPM process development.

Melitracen: This work implements MINLP optimisation of MSMPR cascades for continuous melitracen crystallisation to screen for cost optimal flowsheet configurations. The MINLP superstructure for MSMPR cascades considers varying crystalliser volumes, extent of recycle, concentration of recycle streams and their allocation to different MSMPR vessels. The MINLP optimisation problem is solved for different plant capacity assumptions and numbers of implemented crystallisers. Optimal total cost components (with sensitivity analysis on different economic parameters), flowsheet configurations and crystallisation yields and crystal product average sizes are compared for different problem instances.

2.3.4 Thesis Structure

This PhD thesis examines several different API case studies with different process flowsheets and different extents of modelling, simulation and optimisation methodological approach applied to each. The remainder of the main sections of this thesis will be structured as follows: Part II

presents process modelling and simulation for design of upstream CPM (reaction + separation) plants for diphenhydramine and rufinamide; Part III implements economic optimisation via Nonlinear Programming (NLP) for the upstream CPM of warfarin and nevirapine and for MSMPR cascade design for the continuous cooling crystallisation of cyclosporine, paracetamol and aliskiren. Part IV will describe process synthesis via MINLP optimisation for the upstream CPM of atropine and for the MSMPR cascade design for melitracen continuous cooling crystallisation. Part V will then summarise the original research contributions made in this work and the conclusions of this PhD thesis.

PART II

PLANTWIDE PROCESS DESIGN, SIMULATION & ECONOMIC EVALUATION

Chapter 3

Diphenhydramine

This chapter describes the steady-state process modelling and simulation for technoeconomic evaluation and design for the CPM of diphenhydramine based on the published continuous flow synthesis, developing a conceptual continuous LLE process for reaction effluent purification, based upon the flowsheet presented in Chapter 2 (Fig. 6).

The results presented in this chapter have also been published in the literature (Diab and Gerogiorgis, *Org. Process Res. Dev.* **2017**, *21*(7), 924–946); details can be found in Appendix B.

3.1 Kinetic Parameter Estimation

The original publication provides data for the CPMa synthesis (in NMP) at 180 °C for residence times of 5, 10 and 20 min. For the neat synthetic route (CPMb), data is provided at a reaction temperature of 175 °C for residence times of 16 and 32 min. In both routes, an equimolar mixture of CDPM and DMAE are used.[32] By considering different functions of reactant concentrations (representing zero-, first- and second-order reactions) vs. residence time, coefficients of determination have been calculated to estimate reaction orders and rate constants for each reaction. The kinetic parameter estimations for both CPMa and b are shown in Fig. 22.

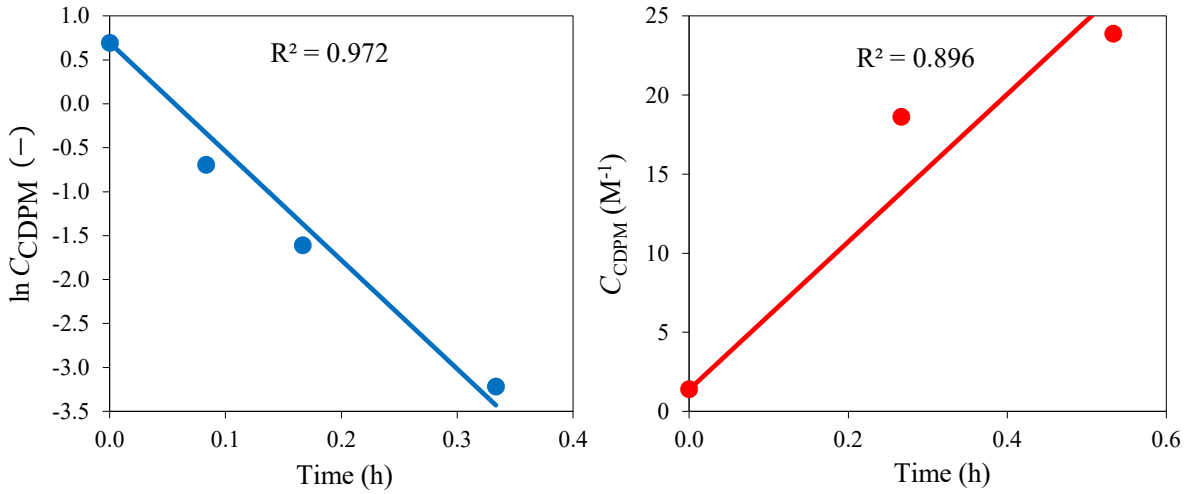

Figure 22: Diphenhydramine flow synthesis kinetic parameter estimation from experimental data.[32] (a) Synthesis in carrier solvent (NMP), CPMa (b) Synthesis in neat mixture (no carrier solvent), CPMb.

A first-order reaction in CDPM is found to be the most plausible case for CPMa (R^2 = 0.972) compared to zero- (R^2 = 0.438) and second- (R^2 = 0.111) order reactions. It is possible that resonance stabilisation of the intermediate carbocation by the two phenyl groups on CDPM (see Fig. 5, Chapter 2.2.1.1) causes it to control the reaction rate more than CDPM. It is also possible that the steric hindrance of the aromatic groups on CDPM render it less mobile in solution than DMAE; thus, the concentration of CDPM affects the rate of reaction the most, hence it is first-order in CDPM. It was estimated that the first-order rate constant for CPMa is k_1 = 12.36 hr^{-1}.

For CPMb, a second-order reaction (first-order in CDPM, first-order in DMAE) is most plausible (R^2 = 0.896) compared to zero- (R^2 = 0.716) and first- (R^2 = 0.778) order reactions. The second-order rate constant has been estimated to be k_2 = 46.44 L mol^{-1} hr^{-1}

3.2 Estimation of Thermophysical Properties

Material properties of all components are required for process design. This section discusses estimation methods used where published pure component data has been unavailable. All published and estimated component properties, including candidate solvents for LLE are provided in Table 5. Note that although theoretical methods are employed for prediction of thermophysical properties of some species in Table 5, there are published experimental values available in the literature in some cases; the methods employed in Chapters 3.2.1–3.2.3 can have significant errors for less common compounds.

3.2.1 Standard Enthalpy of Formation

Enthalpies of formation ($\Delta^0 H_f$) of components involved in solvent and neat syntheses (i.e., CDPM, DMAE and API) are required for calculation of the reactor heating duties. Where values have been unavailable in the literature, an estimation method has been used (Eq. 11).[187]

$$\Delta^0 H_f - h_{f0} = \sum_i N_i h_{1i} + \sum_j M_j h_{2j} \tag{11}$$

Here, h_{1i} refers to a contribution of primary functional groups on the molecule, whilst h_{2j} refers to secondary functional group contributions, weighted by the number of occurrences of each functional group (N_i and M_j respectively); h_{f0} has a constant value of 10.835 kJ mol^{-1}.[187] Calculated values of $\Delta^0 H_f$ required for reactor heating duties are shown in Table 5.

Table 5: Diphenhydramine CPM component physical properties.

	Component	CAS #	MW (g mol^{-1})	Density (g cm^{-3})	M.P. (^{o}C)	B.P. (^{o}C)	β (10^3 K^{-1})	C_p (J mol^{-1} K^{-1})	$\Delta^0 H_f$ (kJ mol^{-1})
Process Material	CDPM	90-99-3	202.68	1.14	16.0	140.0	1.111[185]	42.37[186]	88.37[187]
	DMAE	108-01-0	89.14	0.89	−59.0	134.1	1.090[185]	26.66[186]	−79.19[187]
	NMP	872-50-4	99.13	1.03	−24.0	203.0	0.838[188]	167.36[189]	n.r.
	API	58-73-1	5.36	1.20	162.0	343.7	1.111[185]	59.47[186]	−60.84[187]
	NaOH	1310-73-2	40.00	2.13	318.0	1,388.0	n.r.	59.45[190]	n.r.
	H_2O	7732-18-5	18.02	1.00	0.0	100.0	n.r.	75.37	n.r.
LLE Solvents	nHex	110-54-3	86.18	0.65	−95.0	68.0	n.r.	194.77	n.r.
	nHep	142-82-5	100.21	0.68	−90.6	98.4	n.r.	226.64	n.r.
	CyHex	110-82-7	84.16	0.78	6.5	80.7	n.r.	156.00	n.r.
	MeCyHex	108-87-2	98.19	0.77	−126.3	101.0	n.r.	184.50	n.r.
	DCM	75-09-2	84.93	1.33	−96.7	39.6	n.r.	102.30	n.r.
	TCM	67-66-3	119.37	1.49	−63.5	61.2	n.r.	125.34	n.r.
	Et_2O	60-29-7	74.12	1.11	−116.3	34.6	n.r.	172.50	n.r.

nHex = *n*-Hexane; nHep = *n*-Heptane; CyHex = Cyclohexane; MeCyHex = Methylcyclohexane; DCM = Dichloromethane; TCM = Trichloromethane (Chloroform); Et_2O = Diethyl ether. Values of C_P and $\Delta^0 H_f$ for LLE solvent components taken from PubChem[191] and NIST Webbook.[192]

3.2.2 Constant Pressure Heat Capacity

Specific heat capacities at constant pressure (C_P) as a function of temperature (T) for relevant components are required for heat transfer design. Where published values are unavailable, the following group contribution method has been used (Eq. 12).[186] Here, a_k, b_k, c_k and d_k are constants associated with functional group k, whilst n_k is the occurrence of each group on the molecule. Calculated values of C_P required for PFR duties are shown in Table 5.

$$C_p = \sum_k n_k a_k + \sum_k n_k b_k T + \sum_k n_k c_k T^2 + \sum_k n_k d_k T^3 \tag{12}$$

3.2.3 Enthalpy of Fusion

The total phase change entropy is approximated as the entropy of fusion ($\Delta_0^{T_{fus}} S_{pc}$) and is estimated using Eqs. 13 and 14 for aliphatic and benzenoid aromatic hydrocarbons:

$$\Delta_0^{T_{fus}} S_{pc} = \sum_k n_k G_k + n_{CH2} C_{CH2} G_{CH2} \tag{13}$$

$$C_{CH2}=\begin{cases}1.31, & n_{CH_2} \geq \sum_k n_k,\ k \neq CH_2 \\ 1.00, & \text{otherwise}\end{cases} \tag{14}$$

G_k represents the contribution of group k to the total phase change entropy. Group coefficients n_k, G_k and C_k are used for multiple occurrences of group k on a molecule. The calculation requires tabulated values for G_k and C_k from the literature.[193]

The enthalpy of fusion (ΔH_{fus}) can then be calculated from the entropy of fusion and solute melting point (T_{fus}) as follows.

$$\Delta H_{fus} \cong \Delta_0^{T_{fus}} S_{ps} T_{fus} \tag{15}$$

3.2.4 Reaction Enthalpy

Isothermal operation is assumed for all unit operations, i.e., constant temperatures are maintained by provision of sufficient heat transfer requirements. Enthalpies of reaction (ΔH_{rxn}) have been calculated using Hess' Law (Eq. 16), considering the sum of enthalpy changes in cooling the reactants from the reactor temperature (T) to T^0 = 298 K, the standard reaction enthalpy and the enthalpy associated with heating the products from standard to reaction temperature.

$$\Delta H_{rxn} = \sum C_{p_{reagents}}(T^0 - T) + \Delta H^0_{rxn} + \sum C_{p_{products}}(T - T^0) \tag{16}$$

The standard reaction enthalpy ($\Delta^0 H_{rxn}$) is calculated as the difference between the sums of enthalpies of formation of products and reagents (Eq. 17).

$$\Delta H^0_{rxn} = \sum \Delta H^0_{f\,products} - \sum \Delta H^0_{f\,reagents} \tag{17}$$

3.3 Reactor Design

It has been assumed that reaction mixtures in the PFRs are homogeneous. In the PFRs, radial and axial concentration and temperature gradients have been assumed negligible, i.e., perfect mixing and sufficient heating is provided by appropriate reactor design and completely submerging the reactor in heat transfer media with adequate circulation. The required residence time required to produce Q_{API} = 100 kg API yr^{-1} has been calculated using the PFR design equation (Eq. 18). Here, τ = PFR residence time, $C_{A,0}$, X_A and r_A = initial concentration, conversion and rate of reaction of limiting reagent A (in both cases, A = CDPM), respectively, and X_f is the final conversion.

$$\tau_j = C_{A,0} \int_0^{X_f} \frac{dX_A}{-r_A} \tag{18}$$

The estimation of PFR residence times requires values of X_f. The published data indicates a maximum conversion of 98% is possible for CPMa, whilst 95% conversion is attainable for CPMb.[32] A summary of the assumptions made for PFR design is provided in Table 6.

Table 6: Diphenhydramine kinetic parameter estimation results as a basis for reactor design.

Synthesis	**CPMa**	**CPMb**
Reaction Order	1	2
Rate Law	$-r_{CDPM} = k_1 C_{CDPM}$	$-r_{CDPM} = k_2 C_{CDPM} C_{DMAE}$
Reaction Temperature (°C)	180	175
Conversion, X_A (%)	98	95
Rate Constant, k_i (units)	12.36 (hr^{-1})	46.44 (L mol^{-1} hr^{-1})
Coefficient of Determination (R^2)	0.972	0.896

Design of all unit operations requires a plantwide mass balance. The following assumptions have been made for mass balance calculations of all component streams:

- The process' production scale is Q_{API} = 100 kg API yr^{-1}. The specified Q_{API} is met by altering a scaling factor such that the difference between the attained API production and QAPI is minimised; this is performed in MATLAB using the solver '*fminsearch'*.
- Chemical reaction only occurs within the reactor, not in any previous or subsequent units or their connecting lines.
- No reaction occurs between unreacted reagents and subsequent chemicals introduced in the process.
- Reaction mixtures are modelled as homogeneous and ideal solutions.
- Temperature changes throughout the process cause no phase transitions or precipitation of salts.

Pure component densities (ρ) at elevated reaction temperatures are required for calculation of mixture densities and volumetric throughputs. Coefficients of isothermal expansion (β) have been found in the literature or estimated where unavailable in order to calculate component density as a function of temperature according to Eq. 19. Values of β are in Table 5.

$$\rho(T) = \frac{\rho(T_0)}{1 + \beta(T - T_0)} \tag{19}$$

Molar balances across each reactor are calculated via Eq. 20.

$$F_i^j = F_{A,0}^j\left(\Theta_i^j + \nu_i^j X_A^j\right) \tag{20}$$

Here, F_i^j is the molar flowrate of component *i* exiting reactor *j*, $F_{A,0}^j$ is the inlet molar flowrate of limiting reagent A in reactor *j*, Θ_i^j is the molar ratio of component *i* to limiting reagent A in reactor *j* and ν_i^j is the stoichiometric coefficient of component *i* in reactor *j*. Molar flowrates are converted to mass flowrates using the component Molecular Weights (MWs) listed in Table 5.

Fig. 23 illustrates component mass flowrates of key streams from the process flowsheet (see Fig. 6). It can be seen for both syntheses that the API formed constitutes a significant portion of the total stream; hence a large amount of neutralising agent (NaOH) is required for both syntheses to ensure the API is not present as a salt. Approximately the same amounts of NaOH (aq.) solution are added to both PFR effluents as the same amount of API salt is being neutralised in each case. The difference in extraction solvent added between CPMa & b are associated with differences in extraction efficiency of different LLE solvents, as well as the inefficiency of the Zefluor membrane required for CPMb (see Chapter 3.4).

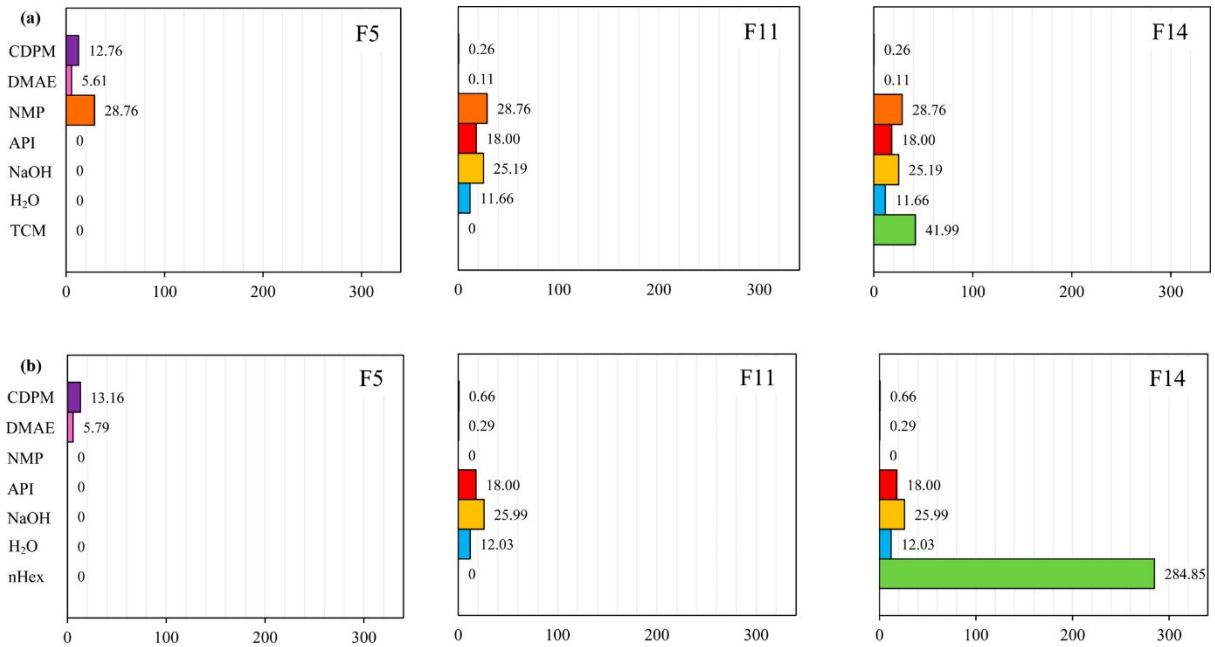

Figure 23: Component mass flowrates of key streams in the diphenhydramine CPM process (g hr^{-1}) (a) with carrier solvent (NMP), CPMa (b) as a neat mixture, CPMb.

Reactor volumes (V_j) are calculated from the required residence time and the volumetric throughput (Q_j) required to attain the specified plant capacity (Q_{API}).

$$V_j = \tau_j Q_j \tag{21}$$

Table 7 shows the computed PFR sizes for both CPMa and b. The reactor volumes obtained for both syntheses are small for the target capacity, which demonstrates the benefit of reduced equipment sizes offered by CPM. The significant difference in reactor volume between CPMa and b is due to differences in reaction mixture volumetric flowrate as the latter lacks carrier solvent.

Reactor internal diameters, d_{PFR} = {2.5, 5.0, 10.0, 15.0} mm have been considered to calculate resulting reactor lengths, L_{PFR}, corresponding to the required volumes; these diameters are comparable with those in the literature, chosen to ensure radial temperature and concentration gradients are negligible.[148] The inner diameter of the reactor is an important tuning parameter for the resulting reactor length and fouling and reactor clogging issues where solid handling is required. It is particularly important to maintain a constant reactor temperature in the neat synthesis to ensure clogging does not occur. Such issues require the need for rigorous process control to ensure high reactor performance.

Table 7: PFR design results for diphenhydramine CPM.

CPM Route	**Temperature**	**Mass Flow**	**Molar Flow**	X_A	V	d_{PFR}	L_{PFR}
	(°C)	(g hr^{-1})	(mol hr^{-1})	(%)	(mL)	(mm)	(mm)
Solvent (CPMa)	180	47.13	0.42	98	18.45	2.5	3759
						5.0	940
						10.0	235
						15.0	104
Neat (CPMb)	175	18.94	0.13	95	3.22	2.5	656
						5.0	164
						10.0	41
						15.0	18

The original paper describing the continuous flow synthesis of diphenhydramine also describes two side reactions: the formation of benzhydrol by nucleophilic substitution of CDPM, and the self-etherification of benzhydrol to form dibenzhydryl ether.[32] The work did not provide enough information to estimate kinetic parameters of these side reactions, so the model described here only accounts for the synthesis reaction. In order to obtain more accurate reactor sizes, data on these side reactions must be found in order to obtain accurate reaction kinetics.

Calculated reaction enthalpies at the reaction temperature for both CPM routes are shown in Table 8. The heating requirement of each reactor is considered as the sum of feed heating from standard to reaction temperature and heating of the endothermic reaction. The duty for CPMb is significantly lower than for CPMa due to the lower throughput, however both are of the same order of magnitude. As a result of the significantly lower reactor volume, the specific duties for the PFR for CPMb are higher than for CPMa. The magnitudes of both duties are considerable for

the reactor size and plant capacity; this is due to the elevated reaction temperatures of both synthesis routes. In the original CPM publication, there is not enough data available to determine the temperature dependence of the reaction rate constants, so analysis into the effect of temperature on conversion and heat transfer design could not be evaluated. It is also assumed that these temperatures are sufficient to keep the reaction mixtures fluid enough such that reactor clogging does not occur.[32] These calculations consider the power requirements of the reactors only, and do not include pumping, losses, LLE solvent and crystallisation heating/cooling requirements, or power for analysis and control. It is important to consider heat integration of the full process for the detailed design of CPM plants.

Table 8: Heat transfer requirements of PFRs for diphenhydramine CPM.

CPM	Reaction	ΔH_{rxn} (T_{rxn}) (kJ mol^{-1})	T_{rxn} (°C)	Flow (mol hr^{-1})	ID (mm)	L (mm)	Specific Duty (W cm^{-1})	Power (W)
CPMa	Endothermic	32.02	180	0.42	2.5	3759	0.021	7.934
					5.0	940	0.084	
					10.0	235	0.338	
					15.0	104	0.763	
CPMb	Endothermic	32.07	175	0.13	2.5	656	0.023	1.530
					5.0	164	0.093	
					10.0	41	0.373	
					15.0	18	0.850	

3.4 Phase Equilibria Prediction

3.4.1 Solid-Liquid Equilibrium

Estimation of API solubility in carrier and extraction solvents is required where published data is unavailable for accurate design of API purification. The UNIFAC method has been used.[194,195] This model assumes negligible difference in heat capacity between API at T and T_{fus}, which is commonly done in the chemical engineering literature.[196,197] The solid solubility of component i in mixture (x_i^{sat}) is calculated as follows.[198] Here, ΔH_{fus} is calculated as per Chapter 3.2.3.

$$a_i^s = x_i^{sat}\gamma_i^{sat} = \exp\left(\frac{\Delta H_{fus}}{R}\left(\frac{1}{T_{fus}} - \frac{1}{T}\right)\right) \tag{22}$$

The activity coefficient (γ_i) at saturation is calculated by Eqs. 23–34. Iteration is required to calculate the solubility of solute i, as the activity coefficient is a function of composition. The UNIFAC activity coefficient is the sum of a combinatorial (describing shape and volume effects of functional groups) and residual component (describing their energetic interactions). The

combinatorial component (γ_i^c) is calculated via the UNIQUAC model. ϕ_i and θ_i are molar weighted segment and area fractional components respectively. L_i is a compound parameter defined by parameters r_i, q_i and z (= 10). r_i and q_i are calculated from contributions of volume and surface area parameters for each functional group (R_k and Q_k, respectively) weighted by their occurrence on each a molecule (ν_k^i).

$$\ln \gamma_i = \ln \gamma_i^c + \ln \gamma_i^r \tag{23}$$

$$\ln \gamma_i^c = \ln \frac{\phi_i}{x_i} + \frac{z}{2} q_i \ln \frac{\theta_i}{\phi_i} + L_i - \frac{\phi_i}{x_i} \sum_j x_j L_j \tag{24}$$

$$\phi_i = \frac{x_i r_i}{\sum_j x_j r_j} \tag{25}$$

$$\theta_i = \frac{x_i q_i}{\sum_j x_j q_j} \tag{26}$$

$$L_i = \frac{z}{2}(r_i - q_i) - (r_i - 1) \tag{27}$$

$$r_i = \sum_k \nu_k^i R_k \tag{28}$$

$$q_i = \sum_k \nu_k^i Q_k \tag{29}$$

The residual component (γ_i^r) of the activity coefficient is calculated by Eq. 30. Γ_k and Γ_k^i are residual group activity coefficients of group k in the multicomponent mixture and in a reference solution of pure substance i, respectively. θ_m is the summation of the area fraction of group m over all different groups. x_m is the mole fraction of group m. ψ_{mn} represents the interaction between different functional groups in solution, and is calculated using an Arrhenius-type expression. Tabulated values of R and Q are required for calculation of the UNIFAC activity coefficient of molecule i, and are available in the literature.[198,199]

$$\ln \gamma_i^r = \sum_k \nu_k^i \left[\ln \Gamma_k - \ln \Gamma_k^i \right] \tag{30}$$

$$\ln \Gamma_k = Q_k \left[1 - \ln \sum_m \theta_m \psi_{mk} - \sum_m \frac{\theta_m \psi_{km}}{\sum_n \theta_m \psi_{nm}} \right] \tag{31}$$

$$\theta_m = \frac{Q_m x_m}{\sum_n Q_n x_n} \tag{32}$$

$$x_m = \frac{\sum_j v_m^j x_j}{\sum_j \sum_n v_n^j x_j} \tag{33}$$

$$\psi_{mn} = \exp\left[-\frac{U_{mn} - U_{nm}}{RT} \right] \tag{34}$$

3.4.2 Liquid-Liquid Equilibrium

Ternary mixture phase composition prediction is required for LLE modelling. The condition for liquid-liquid phase equilibria for phases 1 and 2 and solvent mixture component *i* is described by Eq. 35.[199]

$$x_{i,1}\gamma_{i,1} = x_{i,2}\gamma_{i,2} \tag{35}$$

Activity coefficients can be estimated via the UNIFAC or NRTL models; estimation via the UNIFAC model are as per Eqs. 23–34.

The NRTL activity coefficient model for a multicomponent system is described by Eq. 36.[200] Here, α_{ij} is the non-randomness parameter between components *i* and *j*. The dimensionless interaction parameter, τ_{ij}, gives the temperature dependence of the model. a_{ij} is the interaction between components *i* and *j*, which can be found in the literature[201] and *R* is the universal gas constant.

$$\ln \gamma_i = \frac{\sum_{j=1}^n x_j \tau_{ji} G_{ji}}{\sum_{k=1}^n x_k G_{ki}} + \sum_{j=1}^n \frac{x_k G_{ij}}{\sum_{k=1}^n x_k G_{kj}} \left(\tau_{ij} - \frac{\sum_{m=1}^n x_m \tau_{mj} G_{mj}}{\sum_{k=1}^n x_k G_{kj}} \right) \tag{36}$$

$$G_{ij} = \exp\left(-\alpha_{ij} \tau_{ij} \right) \tag{37}$$

$$\tau_{ij} = \frac{a_{ij}}{RT} \tag{38}$$

Table 9: Initial list of candidate solvents for diphenhydramine CPM LLE application.

Class of Solvent	LLE Solvent	Liquid-Liquid Equilibria			Solubility Data		Classification		Liquid-liquid equilibrium data	Consider for application?
		UNIFAC	NRTL	Exp. data	UNIFAC	Exp. Data	FDA[203]	Pfizer[202]		
Alkanes	nHex	✓	✓	205	✓	✗	2	Undesirable	NRTL	✓
	nHep	✓	✗	✗	✓	✗	3	Preferred	UNIFAC	✓
	CyHex	✓	✓	✗	✓	✗	2	Useable	NRTL	✓
	MeCyHex	✓	✗	✗	✓	✗	2	Useable	UNIFAC	✓
Chloroalkanes	DCM	✗	✗	205	✓	✗	2	Undesirable	Experimental data	✓
	TCM	✗	✗	205	✓	✗	2	Undesirable	Experimental data	✓
Alcohols	MeOH	✗	✗	✗	✓	205	2	Preferred	Lack of data	X
	EtOH	✗	✗	✗	✓	205	3	Preferred	Lack of data	X
	1-PrOH	✗	✗	✗	✓	✗	3	Preferred	Lack of data	X
	1-BuOH	✗	✗	✗	✓	✗	3	Preferred	Lack of data	X
	iBuOH	✗	✗	205	✓	✗	–	Preferred	Single phase	X
	1-PnOH	✗	✗	206	✓	✗	3	Useable	Single phase	X
	1-HxOH	✗	✗	206	✓	✗	–	–	Single phase	X
Carboxylic acids	AcOH	✗	✗	✗	✓	✗	3	Useable	Lack of data	X
Ketones	DMK	✗	✗	✗	✓	205	3	Preferred	Lack of data	X
	MEK	✗	✗	✗	✓	✗	3	Preferred	Lack of data	X
Esters	EtOAc	✗	✗	✗	✓	205	3	Preferred	Lack of data	X
	iPrOAc	✗	✗	✗	✓	✗	3	Preferred	Lack of data	X

nHex = n-Hexane; nHep = n-Heptane; CyHex = Cyclohexane; MeCyHex = Methylcyclohexane; DCM = Dichloromethane; TCM = Chloroform; MeOH = Methanol; EtOH = Ethanol; 1-PrOH = 1-propanol; 1-BuOH = 1-butanol; iBuOH = Isobutanol; 1-PnOH = 1-pentanol; 1-HxOH = 1-hexanol; AcOH = Acetic Acid; DMK = Acetone; MEK = Methyl ethyl ketone; EtOAc = Ethyl acetate; iPrOAc = Isopropyl acetate.

3.5 Continuous Liquid-Liquid Extraction Process Design

The product stream of both PFRs contains API in an aqueous solution after addition of NaOH (aq.). In CPMa, the PFR outlet is a binary mixture of NMP + H_2O, whilst in CPMb the solution is predominantly aqueous. In both CPMa & b, the aqueous mixture exiting R-101 is assumed to contain several dissolved solutes (unreacted CDPM and DMAE, API and NaOH). API must be extracted from this stream in order to obtain a purified product. For CPMa, this can be done by continuous Liquid-Liquid Extraction (LLE). For CPMb, addition of *n*-hexane to the aqueous stream yields a binary phase mixture which can be separated by a Zefluor membrane, as in the original CPM publication.[32] The performance of the membrane with other solvents is unknown, and thus other LLE solvent options for CPMb cannot be explored here. The emphasis in this process design case study is on technoeconomic evaluation of the impact of selection of different LLE solvent choices and less on LLE vessel design (regarding residence time + vessel volume).

3.5.1 Candidate Separation Solvent Selection

For design of LLE, equilibrium data is required for ternary systems containing NMP, water and LLE solvent (CPMa) and for the binary system of *n*-hexane and water (CPMb). An industrial solvent selection guide, classifying solvents as "preferred", "useable" or "undesirable", has been consulted for solvent selection.[202] A wide range of candidate solvents has been considered for the design of the API purification stage (Table 9). In order for a solvent to be considered suitable for application, three criteria had to be fulfilled:

- The API must exhibit preferential solubility in the candidate solvent vs. NMP + H_2O.
- The candidate solvent must form a two-phase mixture with a wide region of immiscibility. Experimental liquid-liquid equilibrium data is used where possible, with theoretical modelling employed (via UNIFAC/NRTL) where experimental data was unavailable. If there was no experimental data or required interaction parameters for the models used, the solvent could not be considered.
- The toxicity of the solvent is considered unacceptable if it is both "undesirable" in the industrial solvent selection guide[202] and a Class 1 solvent according to FDA guidelines.[203]

3.5.2 Solute Partitioning

Theoretical modelling of liquid-liquid equilibria of different ternary systems than those available in the literature has been implemented using the popular UNIFAC and NRTL models, depending on which has been able to converge for different systems. Organic and aqueous phase composition

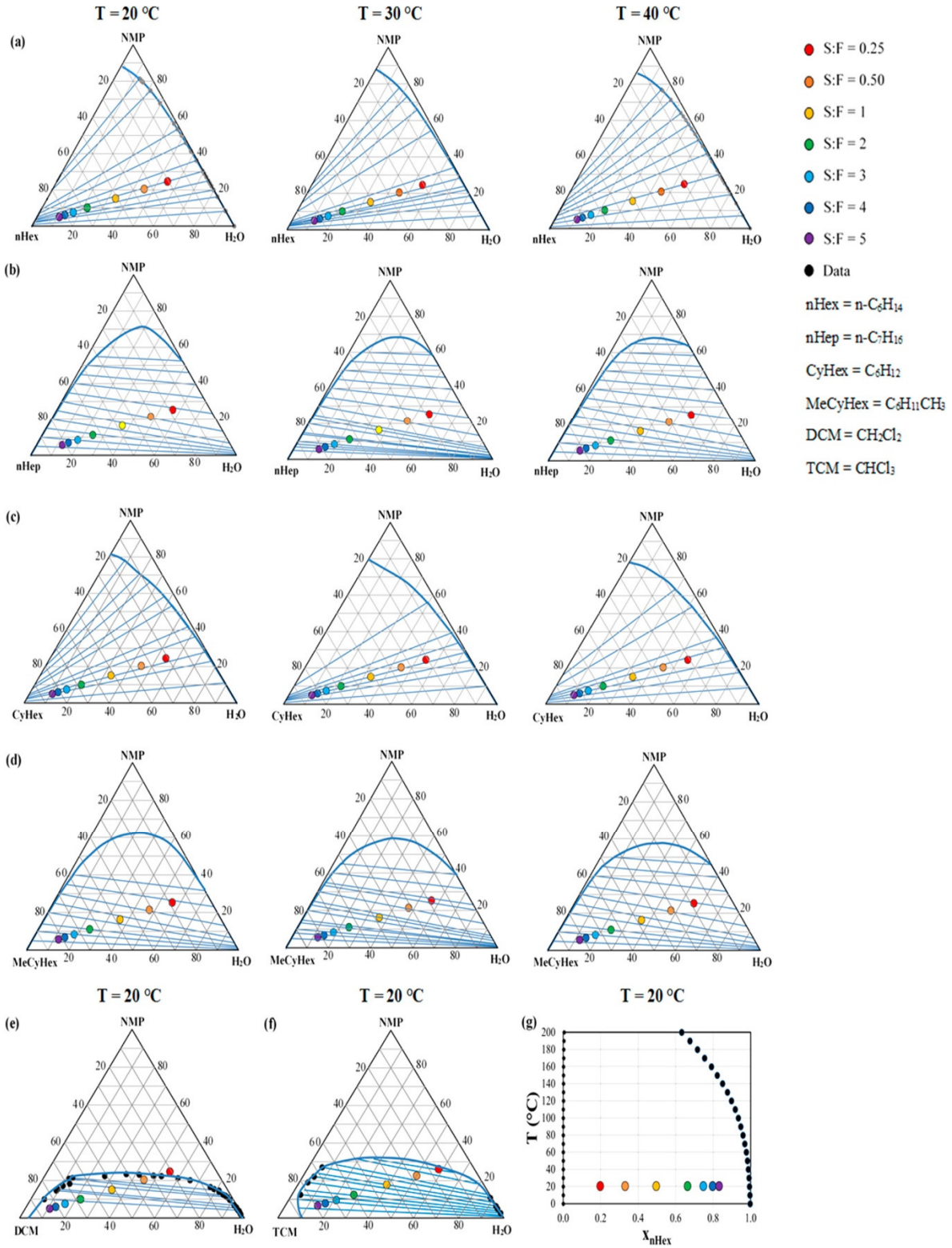

Figure 24: Liquid-liquid equilibrium phase diagrams for different candidate LLE solvents for diphenhydramine CPM. (a) – (f): Ternary systems of NMP-H_2O-Solvent, (g) Binary system of n-C_6H_{14} and H_2O for the neat process (using experimental data). S:F = LLE solvent-to-feed ratio.

are estimated via the UNIFAC/NRTL model to conduct a mass balance around the LLE process. The partition coefficient of API between the phases is assumed to be equal to the ratio of API solubilities in each phase.

Fig. 24 shows the various ternary phase diagrams obtained for the NMP-water-solvent system using theoretical methods or experimental data where appropriate (Table 9). The binary phase diagram for the *n*-hexane-water system required for CPMb has been obtained from experimental data.[204] Temperatures of 20, 30 and 40 °C have been considered for LLE design. Liquid-liquid equilibria for systems containing dichloromethane and chloroform could only be assessed at 20 °C as experimental data at other temperatures were unavailable, and these systems could not be modelled with UNIFAC or NRTL models due to the lack of required interaction parameters and non-convergence of Eqs. 23–38. For CPMb, the performance could only be examined at 20 °C as the behaviour of the membrane at higher temperatures is unknown.

3.5.3 Plantwide Recoveries and Material Efficiencies

An important design parameter in Liquid-Liquid Extraction performance is the solvent-to-feed (S:F) ratio, as it directly affects the extraction performance, the material efficiency and the operating costs associated with material usage and waste disposal. There are a wide variety of green chemistry metrics which can be used for quantitative comparison of processes.[207] The simplest, yet most intuitive of these metrics, is the Environmental (*E*)-factor, defined as the mass of waste generated per unit mass of product obtained.[208] In Eq. 39, m_{waste} = mass of waste, m_{API} = mass of recovered API, m_{bpd} = mass of byproducts, m_{ur} = mass of unreacted reagents, m_{us} = mass of unrecovered solvent and m_{uAPI} = mass of unrecovered API.

$$E = \frac{m_{waste}}{m_{API}} = \frac{m_{bpd} + m_{ur} + m_{us} + m_{uAPI}}{m_{API}} \tag{39}$$

Values of E-factor for different industrial sectors vary, with typical ranges for oil refining < 0.1, bulk chemicals manufacturing = 1–5, fine chemicals manufacturing = 5–50; in pharmaceutical manufacturing, the E-factor is typically in the range 25–200.[209,210] This is due to the complexity of typical product molecules which require multistep syntheses and intermediate separations, incurring greater volumes of waste than other processes.[211]

Another useful green chemistry metric is the Mass Productivity (*MP*), which expresses how efficiently a process uses material, including reagents as well as required neutralisation agents and extraction solvents,[207] described as follows:

$$MP = \frac{100}{E+1} \tag{40}$$

API extraction, E-factors and mass productivities have been evaluated for varying operating temperatures and LLE solvent-to-feed ratios, S:F (mass basis) for the solvents listed in Table 10.

API recoveries, E-factors and Mass Productivities have been calculated for various S:F = {0.25, 0.50, 1, 2, 3, 4, 5} on a mass basis for all candidate solvents to evaluate performance on the basis of API extraction and material efficiency. Extraction performance results for both CPMa/b are shown in Fig. 25. It can be seen that the extraction performance of all candidate solvents decreases as temperature increases. The best extractions for all solvents occur at T_{LLE} = 20 °C. It can also be seen that as S:F increases, the API extraction performance of all solvents increases, accompanied by an increase in E-factor. The increase in E-factor indicates a decrease in material efficiency of the extraction process as more solvent becomes present in the aqueous waste stream. In CPMa, both nHex and nHep achieve unacceptably low API extractions of 60.6% and 53.1%, respectively, even at T = 20 °C and a S:F = 5. These poor extraction performances are also accompanied by high E-factors of 40.31 and 48.15, respectively. CyHex and MeCyHex achieve acceptable extraction performances of 88.3% and 81.1%, respectively, both at S:F = 5, accompanied by adequate E-factors of 27.18 and 31.06, respectively. DCM and TCM both achieve very high extraction performances of 98.5 % and 98.7 %, respectively, at a low S:F = 0.5. Expectedly, the resulting E-factors attained are very good, at 3.59 and 3.43 respectively. The overall extraction performance in CPMb, which includes the inefficiency of the membrane, is unacceptably low, even at S:F = 5. This is partly due to the poor extraction performance of *n*-hexane, as described above.

Fig. 26 compares the E-factors and Mass Productivities obtained for the operating conditions considered here. Expectedly, as S:F increases, *MP* decreases due to increasing amounts of waste incurred by additional use of extraction solvent. *MP* is directly related to the E-factor, and thus the highest MP corresponds to using chloroform as an extraction solvent at T = 20 °C and S:F = 5.

The best performances of all candidate solvents for CPMa/b are summarised in Table 10. From this analysis, chloroform is the best candidate LLE solvent for CPMa due to its high extraction performance and material efficiency; however, its inherent toxicity and EHS characteristics render it unsuitable for CPM application. All of the other non-chlorinated candidate LLE solvents attain good E-factors for pharmaceutical manufacturing.[210] In order to gain a full understanding of the performance of each separation option, cost estimates as well as assessment of extraction performance and material efficiencies are required.

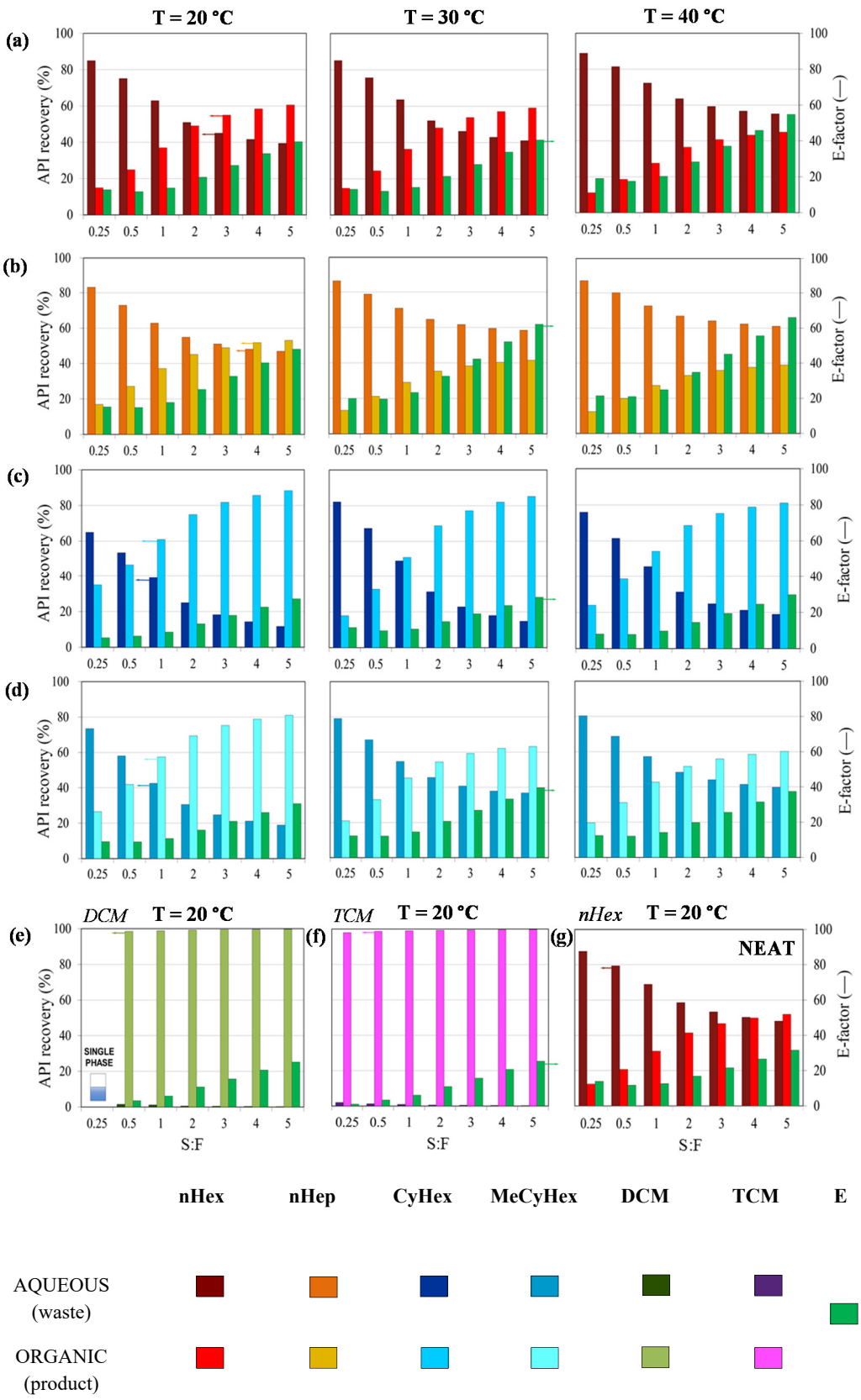

Figure 25: Performances of different diphenhydramine CPM LLE solvents and varying solvent-to-feed ratios and temperatures. *CPMa* (a) nHex (b) nHep (c) CyHex (d) MeCyHex (e) DCM (f) TCM; *CPMb* (g) nHex + membrane.

Table 10: Optimum extraction performances of all candidate diphenhydramine CPM LLE solvents.

CPM Route	Solvent	T_{LLE} (°C)	S:F (–)	API recovery (%)		*E* (–)	*MP* (%)
				Organic (product)	Aqueous (waste)		
CPMa	nHex	20	5	60.6	39.4	40.31	2.42
	nHep	20	5	53.1	46.9	48.15	2.03
	CyHex	20	5	88.3	11.7	27.18	15.91
	MeCyHex	20	5	81.1	18.9	31.06	9.44
	DCM	20	0.5	98.5	1.5	3.59	21.79
	TCM	20	0.5	98.7	1.3	3.43	48.73
CPMb	nHex	20	5	51.9	49.1	31.55	6.71

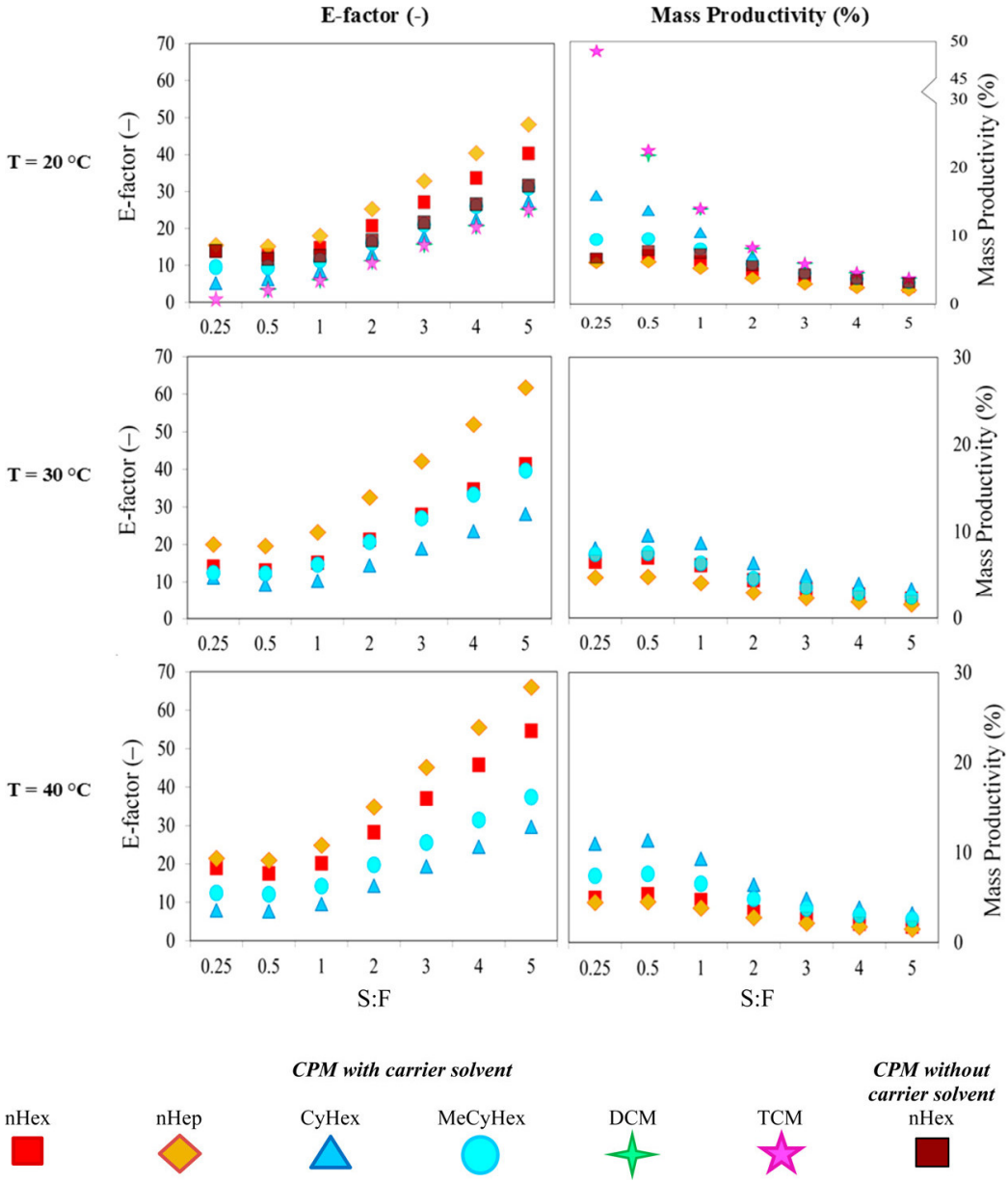

Figure 26: E-factors and mass productivities for all candidate LLE solvents at various operating conditions for diphenhydramine CPM.

3.6 Pharmaceutical Process Economic Evaluation

An approximate costing of the process is required to demonstrate the economic benefits and viability of CPM. It has been assumed that the design is constructed at an existing pharmaceutical manufacturing site with essential infrastructure already in place, operating for 8,040 hours per year. In order to demonstrate the cost savings benefits of CPM separations relative to the batch alternative (BX), an economic comparison of the two processes is made.

3.6.1 Methodology

3.6.1.1 Capital Expenditure

Where possible, vendor prices have been found for equipment of the same or similar capacity. A cost-capacity correlation has been used.[212]

$$P_2 = f P_1 \left(\frac{S_2}{S_1}\right)^n \tag{41}$$

In Eq. 41, P_j and S_j are the purchase costs and capacities, respectively, of equipment at capacity j. The exponent, n, is particular to specific equipment and ranges between 0.0–1.0. The correction factor, f, accounts for differences in equipment operation compared to the reference equipment. Where the applicable capacity range of the reference equipment has been much greater than required, the correction factor is not required (i.e., $f = 1$).[212] The cost of batch equipment of the same capacity as the continuous equipment is accounted for by applying a factor of 0.9 to the cost of the reference continuous equipment. This is due to the established status of most batch-mode technologies. Inflation of equipment prices taken from the past has been accounted for by applying Chemical Engineering Plant Cost Indices (CEPCIs). The inflation adjusted total equipment costs provides the Free-on-Board (*FOB*) cost.

To calculate the Battery Limits Installed Cost (*BLIC*), the Chilton Method[213] has been employed as follows. The cost of equipment installation is equal to 0.43 times the *FOB* cost. Additional costs incurred by process piping and instrumentation are taken as 0.3 and 0.12 times the installed equipment costs, respectively. The sum of installed, process piping and instrumentation costs gives the total physical plant cost, to which a construction factor of 0.3 is added (accounting for electricity installations, required buildings, site preparation etc.) to give the *BLIC*. The Working Capital cost is calculated as 35% and 3.5% of annual material costs for batch and continuous processes, respectively.[49] Contingency costs are taken as 20% of *BLIC*. The final *CapEx* value is taken as the sum of *BLIC* and Working Capital and Contingency (*WCC*).

The equipment requirements (reactors, heating/cooling and auxiliaries) for API synthesis for CPMa/b are the same but with different capacities. A modular plug-flow microreactor system with integrated heating is used for both reactors (R-101a/b).[214] An exponent of 1.0 is used, as suggested in the literature for PFRs.[212] The cost of heaters and coolers (HX-101a/b, HX-102) are based upon data from an appropriate vendor.[215] Solenoid metering pumps are used for pumping of reagents and solvents; costing data is taken from vendor sources of such pumps with appropriate capacities.[216]

The batch separation train (BX) for the synthesis with carrier solvent is shown in Fig. 27a. The original CPM synthesis of diphenhydramine described a threefold batchwise extraction of API with diethyl ether (Et_2O) for the synthesis with carrier solvent.[32] Thus, three LLE tanks are required (BX-T101/2/3) with intermediate pumps (BX-P101/2/3) for the batchwise extraction. Pumps are costed using the same source as those used in the API synthesis; LLE tanks are costed as closed, agitated vessels.[212]

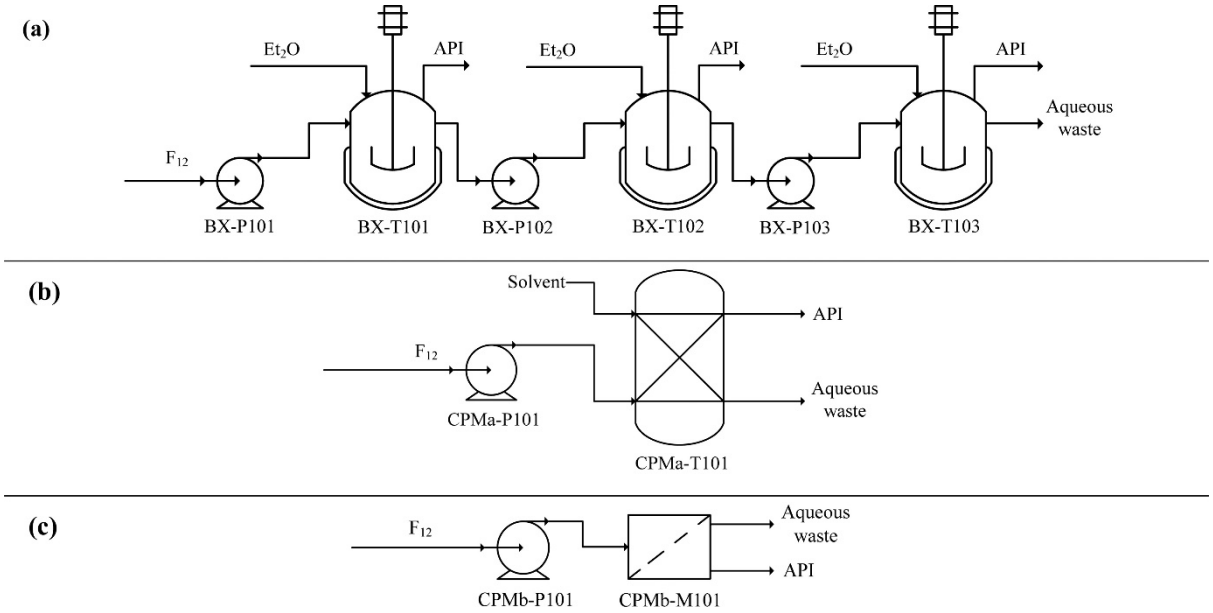

Figure 27: Different separation trains considered for diphenhydramine CPM economic analysis. (a) Batch separation train, (b) CPM separation trains for process with carrier solvent (CPMa) and without carrier solvent (CPMb).

The CPMa separation train is shown in Fig. 27b. In this work, a continuous LLE process is designed, with various solvents compared for performance in terms of API recovery and mass efficiency (E-factor). The continuous extraction unit (CPMa-T101) is costed as a mixing tank with a gravity phase separator including the required drives and pumps.[212]

The CPMb separation train is shown in Fig. 27c. The original CPM synthesis of diphenhydramine describes extraction of API from the aqueous PFR effluent with hexanes followed by membrane

separation of the biphasic mixture (CPMb-M101). Costing of the Zefluor membrane used data for a similar membrane.[217]

Table 11: Material requirements (kg yr^{-1}) for diphenhydramine CPM with different separation options.

Material	**BX**	**CPMa**						**CPMb**
		nHex	nHep	CyHex	MeCyHex	DCM	TCM	
CDPM	128	169	194	116	126	104	103	203
DMAE	56	74	85	51	55	46	45	89
NMP	288	380	437	261	284	234	233	0
NaOH	252	333	383	228	249	205	204	400
H_2O	117	154	177	106	115	95	95	185
Solvent	1,181	5,479	6,381	3,804	4,144	341	340	439

3.6.1.2 Operating Expenditure

Specific material prices have been sourced to estimate the costs associated with reagents and solvent requirements, which constitutes a significant portion of Operating Expenditure (*OpEx*) costs; material requirements for the process with different separation options are provided in Table 11; material prices are provided in Table 12. Costs of utility requirements are taken as 0.96 GBP kg^{-1} of material input. Costs of waste disposal are taken as 0.35 GBP L^{-1} solvent, which are a significant portion of the waste. These costings are taken from an economic analysis of an integrated CPM process.[49] Labour costs for CPM separations have been not included due to the small scale of this design, as well as the automated nature of CPM processes.

Table 12: Prices of materials used in diphenhydramine CPM with different separation options.

Synthesis		**LLE**	
Material	**Price** (GBP kg^{-1})	**Material**	**Price** (GBP kg^{-1})
CDPM	0.18	nHex	0.49
DMAE	0.45	nHep	0.13
NMP	1.98	CyHex	1.07
NaOH	0.25	MeCyHex	0.12
H_2O	0.60	DCM	0.12
		TCM	0.11
All prices quoted from Available Chemicals Directory[218]		Et_2O	1.59

3.6.1.3 Plantwide Total Costs

The total cost has been estimated assuming a 20-year plant lifetime and discount rate (taken as the annual discount rate, i) of 5%. This is a rather conservative estimate for the current economic climate. The total cost is calculated as the sum of *CapEx* and time-discounted *OpEx*.

$$Total\ Costs = CapEx + \sum_{i=1}^{20} \frac{OpEx}{(1+i)^i} \tag{42}$$

3.6.2 Comparative Economic Analysis

Material requirements have been increased to account for the calculated inefficiencies of different unit operation designs. A comparison of different separation scenarios for both CPMa and b is shown in Fig. 28. Total cost savings are achieved for all continuous separations (CPMa/b) relative to the process with a batch separation (BX). This is due to the significant CapEx savings available by significant reductions in separation equipment requirements relative to the batch separation. The greatest total cost savings are attainable by implementing CPMb; this is due to the reduced material requirements which give CapEx savings from the reduction in equipment size in the absence of carrier solvent. In CPMa, the greatest CapEx savings are available with chloroform as LLE solvent. This is also due to the reduced material requirements compared to separations implementing other LLE solvents, accessible by the high extraction efficiency of both dichloromethane and chloroform. However, neither chlorinated solvent options can be considered acceptable due to their EHS characteristics.

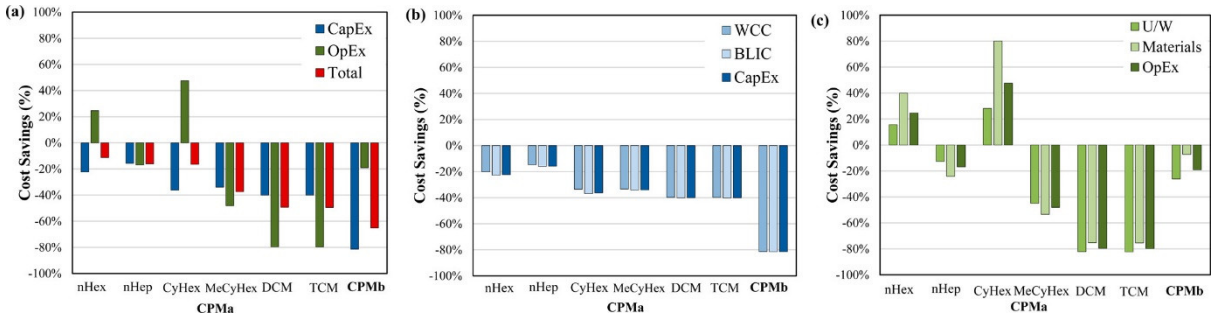

Figure 28: Diphenhydramine CPM cost savings elements of different separation options relative to the batch separation. (a) Total cost savings, (b) CapEx savings, and (c) OpEx savings.

The greatest *OpEx* savings are available by using chloroform as LLE solvent in CPMa. This is due to the high extraction performance (i.e., material efficiency) and the low material cost compared to other solvents. Indeed, the *OpEx* savings available with chloroform in CPMa are even greater than for CPMb due to its low cost compared to nHex as well as the poor extraction performance

of CPMb. *OpEx* savings are unavailable with nHex and CyHex in CPMa, due to the higher material costs of these solvents.

3.7 Discussion

By determination of kinetic parameters from published experimental data, reactor volumes of 18.45 mL and 3.22 mL have been calculated for CPMa and b, respectively. The obtained reactor volumes demonstrate the benefit of small equipment requirements available via CPM. Group contribution methods have been used for material property estimation. Such estimations have been required in order to calculate of reactor heating duties, which showed that considerable heating is required for both CPMa and b due to the elevated reactor operating temperatures.

Activity coefficient models have been required for calculation of API solubility in different solvents and for calculation of liquid-liquid equilibria. Original thermodynamic studies are necessary for the provision of experimental ternary equilibrium data which would enable comparisons, corroboration and further validation of the model-based process simulation results and the technoeconomic conclusions presented. Several candidate solvents for continuous Liquid-Liquid Extraction of API from the aqueous PFR effluent into an organic product phase have been considered based upon their propensity to form a multiphase mixture, favourable solubility of API in the candidate LLE solvent compared to the carrier solvent, and their inherent toxicity according to an industrial solvent selection guide and FDA guidelines. From an initial list of solvents (limited by available experimental data, convergence of UNIFAC/NRTL models and EHS criteria), *n*-hexane, *n*-heptane, cyclohexane, methylcyclohexane, dichloromethane and chloroform have been compared as promising candidates for application. The evaluated solvents cover a wide range of toxicities and extraction performances. From a solely technical viewpoint, the best LLE solvent in terms of process performance and material efficiency (E-factor) is chloroform, demonstrating an impressively high API extraction of 98.7%, which secures a low E-factor of 3.43; this material efficiency is very good for pharmaceutical processes, which are typically very wasteful. This solvent also promises the greatest total cost savings (49.5%) and reduction in E-factor relative to the batch separation (E = 3.43 compared to E = 10.21 for batch) of all separation cases for CPMa. Nevertheless, the known and extremely high toxicity of this solvent prohibits any recommendation for CPM consideration, because the subsequent solvent exchange (required for downstream processing and final product formulation) would be extremely costly, and any remnant traces would be catastrophic to product as well as patients.

Prediction of phase equilibria of non-ideal multicomponent mixtures for which experimental data is not available for corroboration, necessitating methods such as UNIFAC + NRTL models. The

accuracy of these models for less common mixtures can be poor, which must be considered when interpreting the presented results. Activity coefficient models are best used for highlighting promising process options, but not for high accuracy design.

Methylcyclohexane is the next strongest performer among all candidate LLE solvents considered; it also presents remarkably advantageous characteristics (E = 31.06, which is low for pharmaceutical manufacturing; total cost savings of 37.3%) and its lower toxicity renders it significantly more acceptable for CPM implementation. Indeed, the most environmentally friendly solvent analysed, *n*-heptane, shows the worst extraction performance and highest E-factor of all candidates considered. If greater amounts of solvent are acceptable for production-scale CPM use (i.e., S:F > 5), then greener solvents are an even more attractive option, which would though incur greater *OpEx*. This trade-off between high-performance (yet toxic) solvents and less advantageous LLE candidates (which are inherently safer due to significantly lower toxicity) is an undeniable reality underlining the importance and potential of model-based plantwide design, simulation and optimisation of CPM processes.

3.8 Chapter Conclusions

Diphenhydramine is a promising candidate for Continuous Pharmaceutical Manufacturing. Its high global demand necessitates materially and economically efficient manufacturing techniques which have been explored via process modelling in this work. By illustrating the small reactor volumes typical of the CPM process, the material efficiencies available through continuous separation trains, and the associated financial benefits, a strong case can be made for the advantages of this emerging technology.

Despite the small scale of production considered in this study, the viability of CPM of diphenhydramine is evident. The benefits of small equipment and material efficiency compared to batch processes are apparent for specific separation options. Further experimental investigation of neat CPM processes at pilot plant and production scale should be conducted (with perhaps even more efficient separations than those explored here), in order to gain further understanding of these desirable operating conditions. It is also important that downstream processing options be considered to quantify the benefits of a fully integrated CPM process over current batch techniques.

Chapter 4

Rufinamide

This chapter describes the steady-state process modelling and simulation for technoeconomic evaluation and design for the CPM of rufinamide based on the published continuous flow synthesis, developing a conceptual continuous antisolvent crystallisation process for API separation from the reactor effluent, based upon the flowsheet presented in Chapter 2 (Fig. 9).

The results presented in this chapter have also been published in the literature (Diab and Gerogiorgis, *Comput. Chem. Eng.* **2018**, *111*, 102–114); details can be found in Appendix B.

4.1 Reactor Design and Comparison of Rate Law Assumptions

Steady-state process modelling and simulation for the CPM of rufinamide assumes a plant capacity of Q_{API} = 100 kg API yr^{-1}; this is ensured via the same method as in Chapter 3. PFR design requires reaction kinetic parameter regression and mass balance calculations. The following general assumptions are made in the process modelling methodology:

1. Reactions occur in the PFRs only and not in any associated connecting lines or units.
2. The only reactions occurring in PFRs-1–3 are those shown in Fig. 9.
3. Isothermal operation of all PFRs is ensured by providing suitable heat transfer media and the selection of appropriate PFR dimensions.
4. Temperature changes and reaction/formation of components in the process cause no phase changes or affect the flow – no phase changes during the synthesis stages were observed by the authors of the experimental demonstration.[40]
5. All process mixtures prior to crystallisation are homogenous and considered ideal solutions.

Molecular weights and densities of process components are required for the conversion of stream flowrates for the purposes of reactor design, calculation of API mixture solubilities and economic analyses. Physical properties and details of all process components described above for the continuous flow synthesis of rufinamide are listed in Table 13.

Kinetic parameters are required for the design of PFRs. Reaction rate constants are calculated from experimental data and assumptions made are described in this section. The results and assumptions for kinetic parameter estimation are summarised in Tables 14 and 15.

Table 13: Rufinamide CPM process component physical properties.

Component	CAS #	MW (g mol^{-1})	ρ (g mL^{-1})	M.P. (°C)	B.P. (°C)
2	85118-00-9	207.02	1.63	53.50	184.90
DMSO	67-68-5	78.13	1.10	19.00	189.00
NaN_3	26628-22-8	65.01	1.85	275.00	300.00
3	106308-60-5	133.15	1.07	unavailable	unavailable
NaBr	7647-15-6	102.89	3.21	747.00	1390.00
4	922-67-8	84.07	0.95	unavailable	104.05
NH_3	7664-41-7	17.03	0.77	-77.73	-33.34
H_2O	7732-18-5	18.02	1.00	0.00	100.00
5	7341-96-0	69.06	1.10	59.50	134.60
MeOH	67-56-1	32.04	0.79	-97.60	64.70
API	106308-44-5	240.21	1.52	198.23	431.97

Reactions 1 and 2 (Fig. 8) are assumed to be pseudo-first-order, as they involve large organic molecules (**2** and **4** in Reactions 1 and 2, respectively) reacting with an excess of a smaller molecules (NaN_3 and NH_3 in reactions 1 and 2, respectively). Reaction 3 involves two large organic molecules, for which results considering reaction 3 as either first-order in **3**, or overall second-order (first-order in both **3** and **5**) are compared. Here, kinetic parameter estimation methods for all three reactions are described. Given a target/known conversion (see Tables 14 and 15), the first- and second-order rate constants are calculated from Eqs. 43 and 44, respectively.

$$k_{1,j} = \frac{1}{\tau_j \ln(1 - X_\mathrm{f})} \tag{43}$$

$$k_{2,j} = -\frac{1}{\tau_j C_{\mathrm{A},0}} \int_0^{X_\mathrm{f}} \frac{\mathrm{d}X_\mathrm{A}}{(1 - X_\mathrm{A})(\Theta_\mathrm{B} + \nu_\mathrm{B} X_\mathrm{A})} \tag{44}$$

$k_{i,j}$ is the i^{th} order rate constant of the reaction occurring in PFR j, Θ_B is the molar ratio of excess reagent to the limiting reagent and ν_B is the stoichiometric coefficient of excess reagent. The integral in Eq. 44 is calculated for reported attainable conversions.

In reaction 1, 1.3 equivalents of NaN_3 react with **2** to form **3**, with a reported conversion of **2** of 100% at room temperature for a residence time of 1 min.[40]The first-order rate constant of reaction 1 is estimated as $k_{1,1}$ = 9.21 min^{-1}. Reaction 2 involves 4 equivalents of NH_3 reacting with 1 equivalent of **4**; the reported conversion of **4** is 95% at 0 °C for a residence time of 5 min.[40] The first-order rate constant of reaction 2 was estimated to be $k_{1,2}$ = 0.60 min^{-1}.

Table 14: Rufinamide CPM kinetic parameter estimation results for reactions in PFRs 1 and 2.

	PFR *j*	
	1	2
Reaction	**2** + NaN_3 → **3**	**4** + NH_3 → **5** + MeOH
Reaction Order, i	1	1
Rate Law	$-r_A = k_{1,1}C_A$	$-r_A = k_{1,2}C_A$
Reactor temperature, T_j (°C)	20	0
Final conversion, X_f (%)	99.99	95
First-order rate constant, $k_{1,j}$ (min^{-1})	9.21	0.60

Fig. 29 summarises attainable API yields at varying temperatures for reaction 3 (T_3) reported for the continuous flow synthesis of rufinamide.[40] Attainable API yield decreases beyond a certain temperature due to the reported formation of an API regioisomer. A third-order polynomial has been fit to the experimental API yield-temperature data, from which the temperature corresponding to the maximum API yield is estimated; this temperature is 117 °C with a maximum API yield of 99.56%. Below T_3 = 117 °C, it is assumed that only the desired reaction occurs. First- and second-order rate constants for reaction 3 at temperatures of 90, 110 (both considered in the literature[40]) and 117 °C, are considered for which we assume that the only reaction occurring in PFR-3 is reaction 3.

In reaction 3, 1 equiv. of **3** reacts with 1.42 equiv. of **5** to form rufinamide (API). First- and second-order reaction rate constants were estimated using Eqs. 43 and 44 from attainable conversions of 83%, 98% and 99.56% at operating temperatures (T_3) of 90, 110 and 117 °C, respectively, all for residence times of 6.47 min.[40] First- and second-order reaction rate constants for reaction 3 are listed in Table 15.

The Arrhenius law (Eq. 45) describes the temperature-dependency of reaction rate constants.

$$k_{i,j}(T_j) = A\exp\left(-\frac{E_a}{RT_j}\right) \tag{45}$$

where A is the pre-exponential factor and E_a is the reaction activation energy. Values of A and E_a can be estimated from calculated first- and second-order rate constants at different temperatures in PFR-3; these values are provided in Table 15. The estimated Arrhenius parameter values are $A = 1.06\times10^6$ and $E_a = 4.58\times10^6$ J mol^{-1}. The operating temperature of PFR-3 (T_3) affects the reaction conversion, which alters the process mass balances and total costs of different process designs. We compare the effect of the operating temperature (T_3 = 90, 110 and 117 °C) and the assumed order of reaction 3 (first- and second-order) on process modelling results.

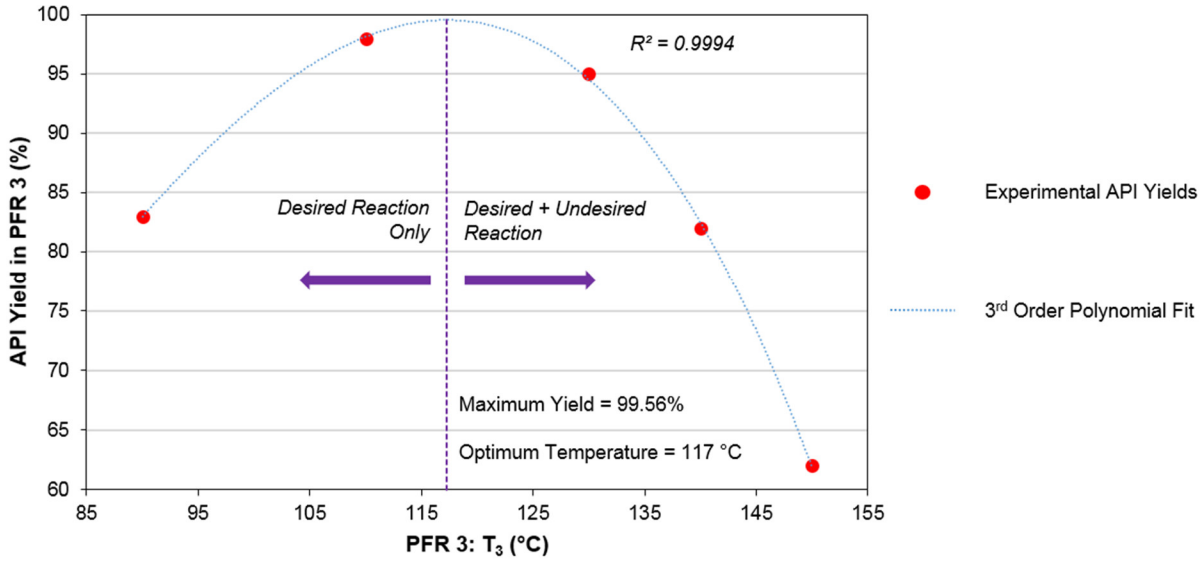

Figure 29: Rufinamide yield in PFR-3 reported by Zhang et al. (2014)[40] as a function of reaction temperature, T_3.

Reactor volumes are calculated as in Chapter 3.3. The calculated mass balances are based on the process for the continuous flow synthesis of rufinamide (API) described by Zhang et al. (2014).[40] Component mass flowrates of key flowsheet streams (see Fig. 9) for all considered operating temperatures of PFR-3 (T_3 = 90, 110 and 117 °C) are shown in Fig. 30; these streams are the feed to PFR-1 (F_8), PFR-2 (F_{14}) and PFR-3 (F_{16}) and the effluent of PFR-3 (F_{17}) prior to crystallisation.

For all CPM process variations (different considerations of the operating temperature of PFR-3), DMSO (the carrier solvent in PFR-1) contributes a significant portion of the total mass balance throughout the whole process. Reagents for reaction 1 in PFR-1 (**2** and NaN_3) are nearly negligible in streams following PFR-1 (F_{16} and F_{17} in Fig. 9) due to the high attainable conversion (99.99% assumed here). Similarly, the reagents for reaction 2 and PFR-2 (**4** and NH_3) are in trace quantities following PFR-2 due to the high conversion attained in the reactor. Due to these high conversions, there are significant quantities of desired intermediates (**3** and propiolamide) and by-products (NaBr and MeOH) in the feed to PFR-3 (F_{16} in Fig. 9). Rufinamide (API) is present in significant quantities due to the high conversions attained at all PFR-3 operating temperatures (T_3) considered and to account for subsequent crystallisation inefficiencies.

Table 15: Rufinamide reaction kinetics and Arrhenius parameter estimation results for the reaction in PFR 3.

Reaction	**3 + 5 → API**					
PFR 3: T_3 (°C)	90		110		117	
X_A (%)	83		98		99.56	
Reaction Order	1	2	1	2	1	2
Rate Law	$-r_A = k_{1,3}C_A$	$-r_A = k_{2,3}C_AC_B$	$-r_A = k_{1,3}C_A$	$-r_A = k_{2,3}C_AC_B$	$-r_A = k_{1,3}C_A$	$-r_A = k_{2,3}C_AC_B$
$C_{A,0}$ (M)	n.r.	0.248	n.r.	0.248	n.r.	0.248
$k_{i,j}$ (units)	0.27 (min^{-1})	1.34 (M^{-1} min^{-1})	0.60 (min^{-1})	3.51 (M^{-1} min^{-1})	0.79 (min^{-1})	4.85 ($M^{-1}min^{-1}$)

PFR volumes are calculated (Fig. 31) from required reaction residence times to meet reported attainable conversions and material throughputs calculated from process mass balances. Small reactor volumes are calculated for PFRs-1 and 2 for all PFR-3 operating temperatures (T_3) considered; this is due to the high attainable conversions (= 99.99% and 95% in PFRs-1 and 2, respectively) short residence times (= 1 and 5 min for PFRs-1 and 2, respectively) and low material throughputs required to meet the desired plant capacity. Computed volumes for PFR-3 for all considered operating temperatures (T_3) and both reaction order assumptions are higher due to the higher material throughput and longer residence time (= 6.47 min) required to reach the target attainable conversions compared to the previous PFRs.

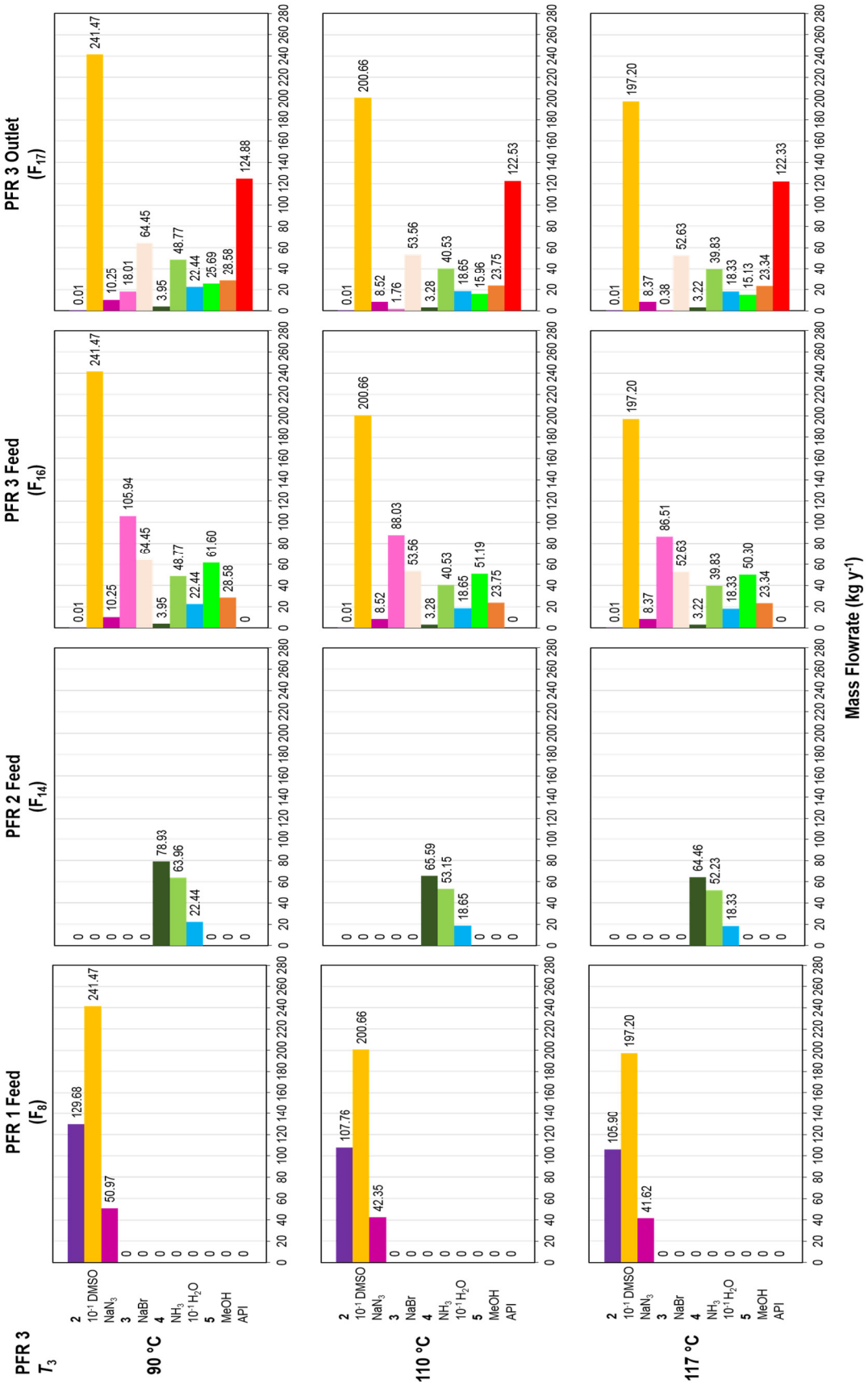

Figure 30: Process mass balances of key flowsheet streams for the CPM of rufinamide under different considerations of the operating temperature of PFR 3 (T_3).

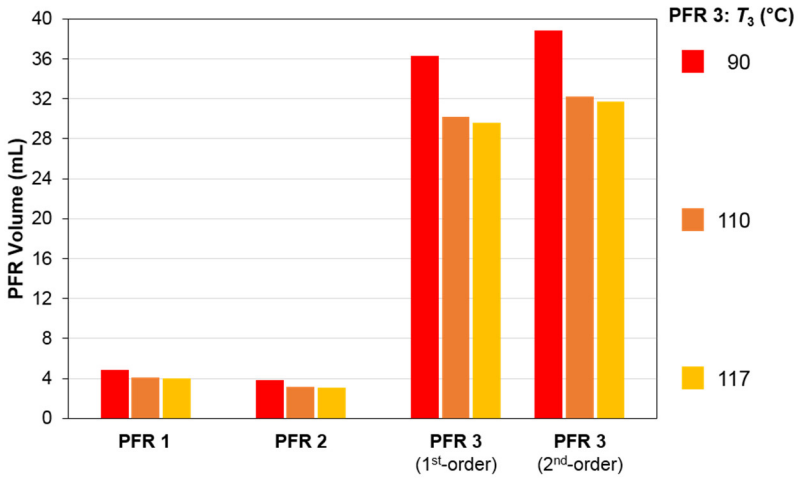

Figure 31: Rufinamide CPM PFR volumes for different assumptions of temperature and reaction order in PFR-3.

Appropriate choice of the internal diameter of PFRs (d_{PFR}) is an important design parameter for the resulting PFR length as well as ensuring negligible axial temperature and concentration gradients.[219] Here, we consider PFR inner diameters of 2.5–15.0 mm, in accordance with reported microreactor applications;[25] the flow regime corresponding to these reactor diameters was not considered as part of reactor design and analysis here, but is later integrated as part of the methodology in Chapter 8. Resulting reactor lengths for different inner diameters are shown in Fig. 32 for all PFR-3 design variations. Reactor lengths vary from very small (< 10 cm) to considerable sizes (< 750 cm). Reactors of significant length can be coiled in order to reduce the overall equipment size and maintain the benefit of small plant footprint available via continuous operation.[17,25,28]

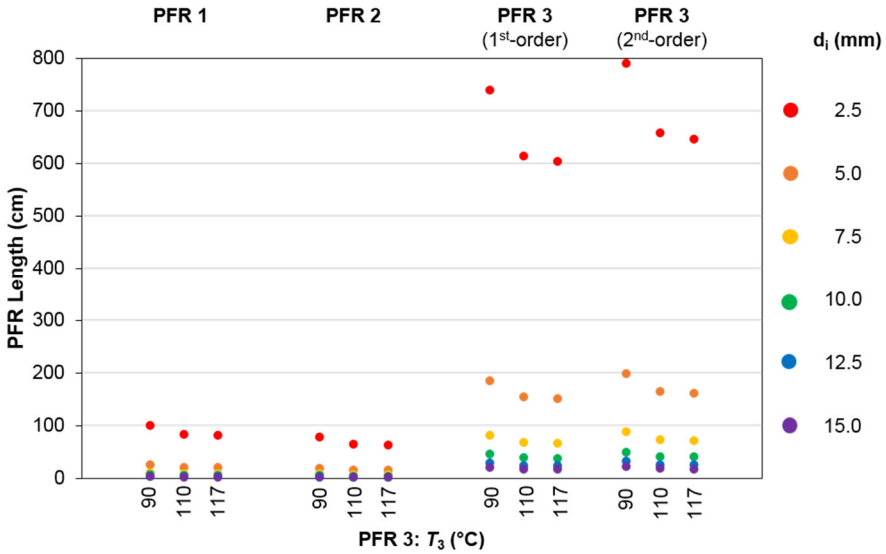

Figure 32: Rufinamide CPM PFR lengths for varying inner diameters for different assumptions of the temperature and reaction order in PFR 3.

Figs. 31 and 32 show only a small difference in PFR volumes and lengths between different considerations of first- and second-order assumptions for reaction 3. It is important to note that these results neglect the undesired side reaction forming a regioisomer of rufinamide in PFR-3, which will affect the results presented here. It has been assumed that only the desired reaction occurs in PFR-3 for the operating temperatures considered in this work. Kinetic data for this side reaction is required.

4.2 Rufinamide Aqueous Solubility Estimation

The modelling of crystallisation processes requires API solubility data in multicomponent mixtures. Very limited data for rufinamide solubilities in pure components or mixtures exist in the literature; experimental solubilities of rufinamide in pure DMSO and water at 25 °C (mole fraction solubility = 0.014) are available. Theoretical methods for drug solubility estimation in pure solvents and multicomponent mixtures can be implemented;[220] however, essential interaction parameters for rufinamide (corresponding to the triazole functionality) for even the most rigorous and established activity coefficient models are unavailable. A correlation between the octanol-water partition coefficient ($\ln K_{ow} = -0.12$) and the API molar volume ($V_m = 212.47$ cm^3 mol^{-1}) can be used to estimate the API solubility in water[221]

$$\ln C_{API}^{sat} = \chi - \omega V_m - \ln K_{OW} + \ln \eta \tag{46}$$

$$\eta = \exp\left(\frac{\Delta S}{R}\right)\left(1 - \frac{T_{cryst}}{T_{fus}}\right) \tag{47}$$

$$\frac{\Delta S}{R} \approx 6.8 \tag{48}$$

where C_{API}^{sat} is the solute solubility in water (mol m^{-3}), η is the fugacity ratio, ΔS is the entropy of fusion, χ and ω are model parameters ($\chi = 3.9 \pm 0.2$, $\omega = 0.005 \pm 0.001$).[221] K_{ow} is a function of temperature; a correlation between K_{ow} and temperature is unavailable, so all crystallisation processes are modelled at $T_{cryst} = 25$ °C. The API solubility in the mixture is calculated as the sum of mole fraction weighted API solubilities in DMSO (carrier solvent) and water (antisolvent).

4.3 Continuous Crystallisation Design

The crystallisation yield of API is calculated from the feed API mole fraction and the API mole fraction solubility at saturation

$$Y = 100\left(1 - \frac{C_{\mathrm{API}}^{\mathrm{sat}}}{C_{\mathrm{API}}^{\mathrm{feed}}}\right) \tag{49}$$

where Y is the API crystallisation yield and $C_{\mathrm{API}}^{\mathrm{feed}}$ is the API concentration in the effluent of PFR-3 fed to the crystalliser. The method was validated by reproducing the experimental batch crystallisation yield of rufinamide within 1%.

In all cases, the effluent of PFR-3 is considered a binary mixture of DMSO and water (single phase) in which all stream components (API, unreacted reagents, by-products) are considered dissolved solutes. The original continuous flow synthesis publication for rufinamide reports direct batchwise antisolvent crystallisation from the effluent of PFR-3 using water as an antisolvent at an antisolvent-to-feed ratio (AS:F, by mass) of 1.83, with a total crystallisation residence time of 75 min.[40]

Here, we compare the continuous flow synthesis of rufinamide with the demonstrated batch crystallisation route (BX) to that with a conceptual continuous crystallisation method also using water as an antisolvent (CPM). Both BX and CPM crystallisation processes are considered single-stage. For the modelling of continuous crystallisation, we consider antisolvent-to-feed ratios of 0.25–5 to investigate the effect of varying antisolvent usage. A crystalliser residence time (τ_{cryst}) = 60 min is assumed for all CPM processes and a factor of 90% is applied to consider the non-attainment of thermodynamic equilibrium in steady-state (continuous) processes. Assumptions about the continuous crystalliser residence time were made due to the lack of crystallisation kinetic parameters for higher-fidelity population balance modelling. Continuous crystalliser residence times range from the scale of minutes[222] to as long as 20 hr.[63] The considered continuous crystalliser residence time considered here for rufinamide production is optimistic; longer residence times will incur greater *CapEx* contributions and lead to lower CPM cost savings vs. the process with a batch crystallisation. It should also be noted that possible polymorphism is not considered here, which may impose further limitations of feasible regions of operation for rufinamide CPM.

Crystalliser volumes (V_{cryst}) for CPM processes are calculated from the crystalliser residence time and the total volumetric flowrate through the crystalliser (Q_{cryst}).

$$V_{\mathrm{cryst}} = \tau_{\mathrm{cryst}} Q_{\mathrm{cryst}} \tag{50}$$

4.4 Technoeconomic Analysis

4.4.1 Plantwide Yields

Calculated API mixture solubilities and attainable crystallisation yields for continuous crystallisation of rufinamide from the effluent of PFR-3 using water as an antisolvent are shown in Fig. 33. In all cases, increasing AS:F decreases the API mixture solubility and thus increases the attainable crystallisation yield. Beyond AS:F = 2, the crystallisation yield only increases incrementally, and thus the increased antisolvent usage and resulting crystalliser volumes will lead to unnecessary increases in *CapEx*, *OpEx* and poorer material efficiencies (implying greater quantities of waste). For this reason, AS:F = 2 is chosen for all subsequent economic analyses.

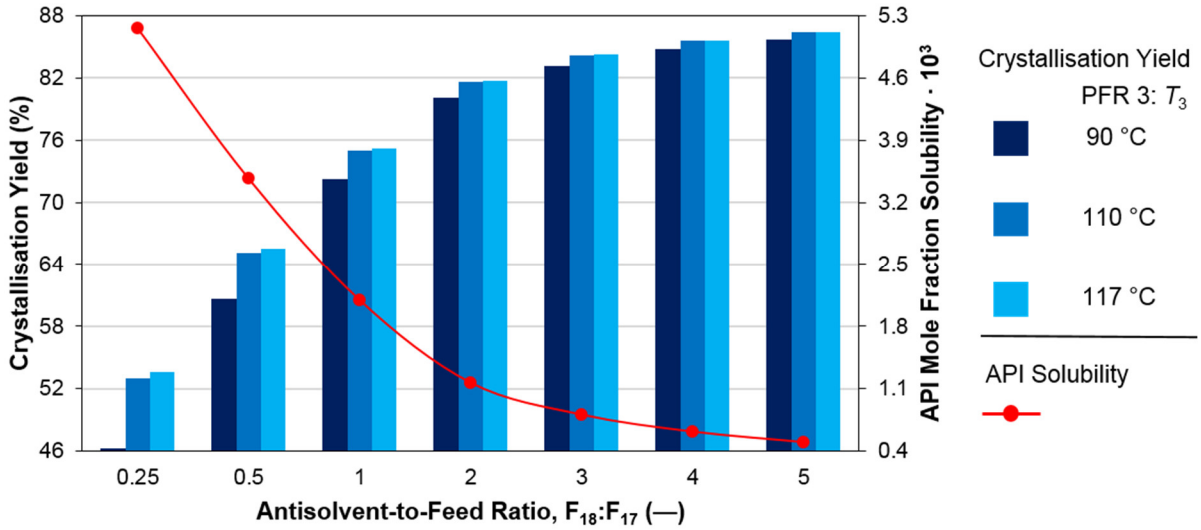

Figure 33: Rufinamide mixture solubility and attainable crystallisation yield.

4.4.2 Material Efficiencies

Process Mass Intensities ($PMI = E + 1$) and Mass Productivities (MPs) (see Chapter 3.5.4) for the batch process and varying CPM process considerations (different PFR-3 operating temperatures, T_3) are shown in Fig. 34. CPM process options consider 70% recovery of carrier- and anti-solvent following continuous crystallisation; AS:F = 1.83 for batch crystallisation[40] and AS:F = 2 for all considered continuous crystallisations. As the operating temperature in PFR-3 (T_3) increases, PMIs decrease and, correspondingly, MPs increase due to the increased plantwide API recoveries attainable as the conversion in PFR-3 increases. The PMIs attained for CPM processes are good for typical attainable values for pharmaceutical processing (see Chapter 3.5.3).[209] These results show the significant improvements in material efficiency and reduction in environmental impact available via CPM implementation from the improved green chemistry metrics shown in Fig. 34.

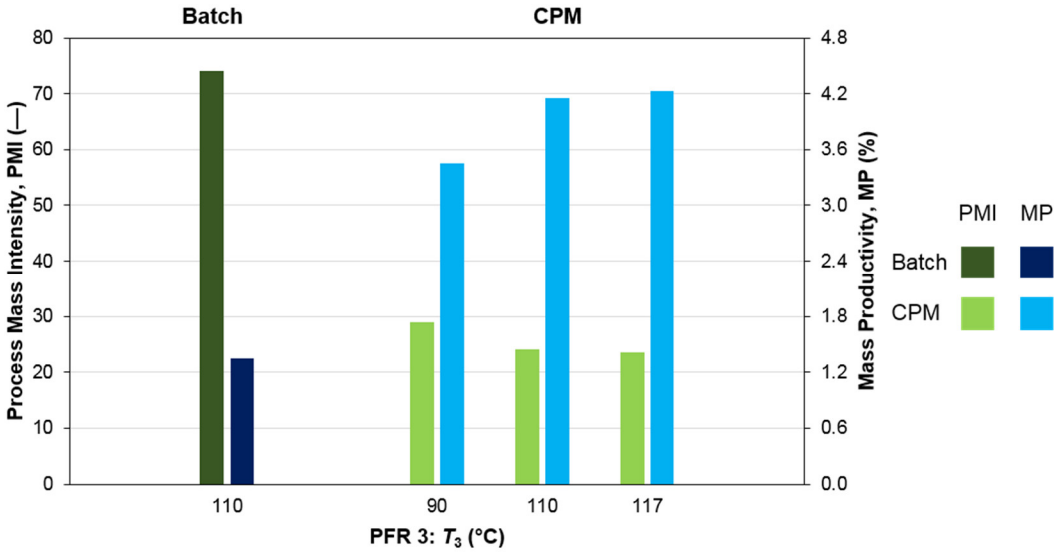

Figure 34: Process Mass Intensities (PMIs) and Mass Productivities (MPs) of the process with batch and continuous crystallisation options for different assumptions of the operating temperature of PFR 3.

4.4.3 Plantwide Total Cost Components

Total cost components are calculated as per Chapter 3.6.1. Unit capacities and material requirements are scaled to account for reaction and crystallisation inefficiencies to meet the specified plant capacity. A comparison between different total cost components for processes with a batch crystallisation process and a continuous crystallisation from the effluent of PFR-3, considering different operating temperatures of PFR-3 (T_3). Table 16 shows the calculated cost components and differences between batch and CPM process variations.

BLIC savings are only attainable for T_3 = 110 and 117 °C when a first-order reaction in PFR-3 is considered, and only for T_3 = 117 °C when a second-order reaction in PFR-3 is considered. This is due to the higher plantwide API recoveries attainable when implementing a batch crystallisation compared to the continuous crystallisation when PFR-3 is operated at lower temperatures; lower recoveries require increased material throughputs to meet the plant capacity and thus larger equipment. *WCC* costs are significantly lower for all continuous options considered due to the significantly lower solvent requirements due to the solvent recovery option considered for CPM as well as the additional labour and handling requirements of the batch process. Correspondingly, both material and Utilities and Waste (*U&W*) costs are significantly lower for all CPM options compared to the process implementing a batch crystallisation.

Table 16: Cost components (10^3 GBP) and differences between rufinamide batch and CPM processes for different operating temperatures in PFR 3 (T_3).

PFR 3 = 1st order

	Batch	CPM (AS:F = 2; SR = 70%)					
T_3 (°C)	110	90		110		117	
	Cost	Cost	Difference	Cost	Difference	Cost	Difference
BLIC	156	174	+11.5%	150	–4.0%	148	–5.3%
WCC	396	60	–84.8%	51	–87.1%	50	–87.3%
CapEx	552	234	–57.5%	201	–63.6%	198	–64.1%
10^{-1} · Materials	1,298	909	–30.0%	909	–30.0%	909	–30.0%
10^{-1} · *U&W*	1,249	874	–30.1%	874	–30.1%	874	–30.1%
10^{-1} · *OpEx*	2,547	1,783	–30.0%	1,783	–30.0%	1,783	–30.0%
Total	26,020	18,060	–30.6%	18,027	–30.7%	18,024	–30.7%

PFR 3 = 2nd order

	Batch	CPM (AS:F = 2; SR = 70%)					
T_3 (°C)	110	90		110		117	
	Cost	Cost	Difference	Cost	Difference	Cost	Difference
BLIC	163	182	+16.6%	156	+0.3%	154	–1.1%
WCC	397	62	–84.4%	53	–86.7%	52	–86.9%
CapEx	560	244	–55.8%	209	–62.1%	206	–62.7%
10^{-1} · Materials	1,298	909	–30.0%	909	–30.0%	909	–30.0%
10^{-1} · *U&W*	1,249	874	–30.1%	874	–30.1%	874	–30.1%
10^{-1} · *OpEx*	2,547	1,783	–30.0%	1,783	–30.0%	1,783	–30.0%
Total	26,028	18,069	–30.6%	18,035	–30.7%	18,032	–30.7%

CapEx, *OpEx* and total cost savings of CPM options relative to the process implementing batch crystallisation for varying PFR-3 design assumptions are shown in Fig. 35. It is shown that varying the operating temperature in PFR-3 (T_3) and different assumptions of reaction order (first- or second-order) have only a small effect on the calculated total cost components. *CapEx* savings variations across different design options are observed due to the effect of PFR-3 operating temperature (T_3) on conversion, and thus plantwide API yield, which directly affects the required material throughput and unit sizes. OpEx costs show little variation for each PFR-3 operating temperature (T_3) chosen for first- and second-order reaction assumptions (in PFR-3) due to similar mass balances. Thus, there is little variation in total cost savings for different design assumptions for PFR-3. Thus, the reaction order in PFR-3 has only a slight effect on the CPM process. Nevertheless, it is imperative to make informed decisions from detailed kinetic data to present accurate cost components for different process options.

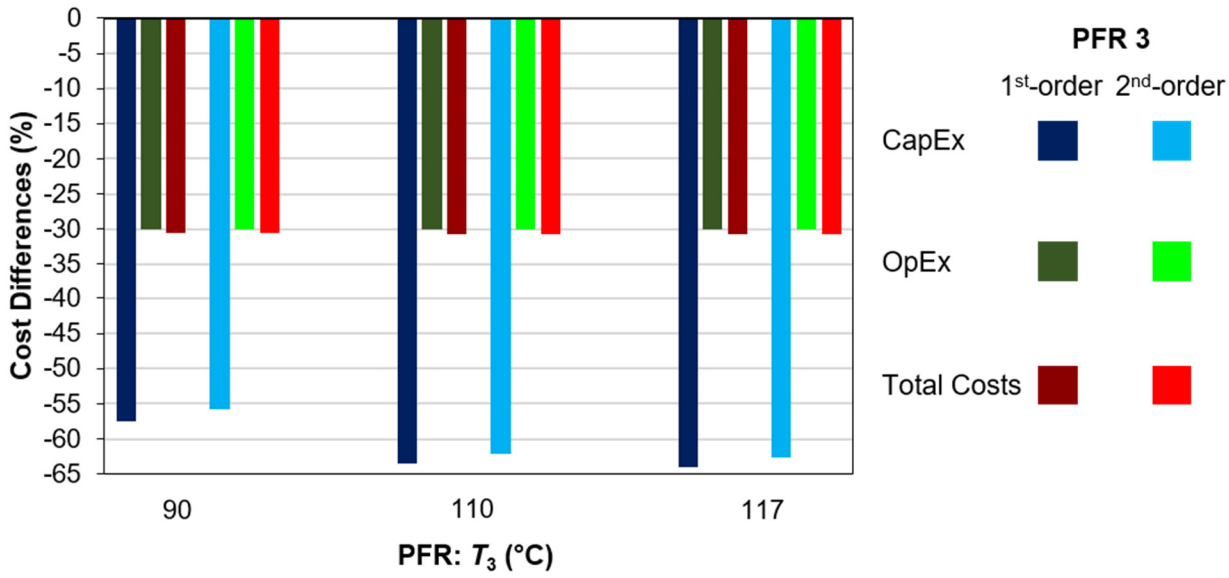

Figure 35: Rufinamide CPM cost savings of implementing a continuous crystallisation process relative to implementing a batchwise crystallisation.

4.5 Chapter Conclusions

Rufinamide is an anticonvulsant API that requires materially efficient and economically viable manufacturing methods. This study has developed a steady-state process model for the CPM of rufinamide for a plant capacity of Q_{API} = 100 kg API yr^{-1}. The model is based upon a published continuous flow synthetic route featuring three PFRs for the API synthesis which circumvents the accumulation or isolation of hazardous intermediate organoazides required for the generation of molecules containing 1,2,3-triazole rings. The demonstrated route features short residence times and high conversions towards rufinamide.

The technoeconomic evaluation conducted features kinetic parameter estimation for different assumptions of the reaction order in the final PFR, reactor sizing based on steady-state mass balance calculations and the desired API plant capacity for different operating temperatures of the final PFR, comparison of batch and continuous crystallisation routes via API solubility modelling in multicomponent mixtures and economic analyses to establish cost savings attainable when implementing a continuous crystallisation with respect to the batch crystallisation.

Small PFR volumes and lengths for the specified plant capacity are computed for all process design variations (different assumptions on the reaction order in the final PFR and its operating temperature), demonstrating a clear CPM advantage. Calculated crystallisation yields for varying extents of antisolvent usage account for non-attainment of thermodynamic equilibria typical of steady-state (continuous) operation. Environmental impacts of different process options are

compared via the PMI and MP which quantify the material efficiency of manufacturing processes; results show a significant reduction in environmental impact when implementing a continuous crystallisation method compared to the batch crystallisation (lower PMIs and higher MPs). Cost estimations follow an established methodology for batch and continuous pharmaceutical processes and show significant total cost savings when implementing a continuous crystallisation process with respect to the batch crystallisation route.

The process modelling and simulation for the CPM of rufinamide demonstrated in this work shows the importance of conducting such conceptual studies for pharmaceutical processes prior to further development and scale-up. The results demonstrate the environmental and economic benefits of continuous operation for the manufacturing of this societally important API. The potential for a scaled-up application of this process must be further developed by considering its implementation when integrated with subsequent essential downstream unit operations.

PART III

NONLINEAR PROGRAMMING FOR ECONOMIC OPTIMISATION

Chapter 5

Warfarin

This chapter describes the steady-state process modelling and technoeconomic optimisation (via NLP) for design of CPM of warfarin based on the published continuous flow synthesis, developing a conceptual continuous LLE process for reaction effluent purification, based upon the flowsheet presented in Chapter 2 (Fig. 11).

The results presented in this chapter have also been published in the literature (Diab and Gerogiorgis, *Comput. Aided Chem. Eng.* **2018**, *43*, 1643–1648); details can be found in Appendix B.

5.1 Optimisation Problem Formulation and Constraints

The aim of the optimisation is to minimise the total cost (calculated as per Chapter 3.6) objective function.

$$\min \textit{Total Cost} \tag{51}$$

s.t.

$$0 < \tau_{LLE} \tag{52}$$

$$1 < r_{LLE} < 4 \tag{53}$$

The discount rate (t = 5%) accounts for inflation and the plant lifetime = 20 years. Annual operation of 8,040 hours is considered. Optimisation decision variables are the LLE residence time (τ_{LLE}) and relative solvent feed rate (r_{LLE}). Total cost components are calculated as described in Chapter 3.6. Solvent recovery following LLE is arbitrarily chosen as 70% in accordance with similar CPM studies;[73] all material requirements are scaled to account for reaction and separation inefficiencies. The plant capacity (Q_{API} = 100 kg API yr^{-1}) is met by specifying a NLP constraint.

5.2 Reactor Design

The literature demonstration of the continuous flow synthesis of warfarin[166] describes the attained conversion of X_A = 61% for a residence time of 10 min; due to the lack of kinetic data (as a function of reaction/residence time), it is assumed that designed PFRs have this residence time and attainable conversion. Reactor (PFR) volumes and component stream flowrates are calculated as per Chapter 3.3.

5.3 Continuous Liquid-Liquid Extraction Design

5.3.1 Candidate Liquid-Liquid Extraction Process Solvents

The considered continuous LLE process for optimisation via NLP is a single stage mixer-settler. Upon addition of the candidate LLE solvent, the process forms an organic (product) phase containing recovered API and an aqueous (waste) phase, between which API partitions. Several candidate separation solvents are compared for continuous LLE: ethyl acetate (EtOAc), isopropyl acetate (iPrOAc), isobutyl acetate (iBuOAc), 1-heptanol (HepOH), 1-octanol (OcOH) and *n*-heptane (nHep). These solvents allow a wide envelope of immiscibility and are considered acceptable by an industrial solvent selection guide.[223] Ternary phase equilibria for phase composition prediction uses the UNIFAC model and API partitioning estimation are calculated as per Chapter 3.5.

5.3.2 Mass Transfer Correlations

The solute extraction factor (E_f), which is calculated from the solute molar partition coefficient (m) between the LLE solvent (S) and the feed (F). The continuous LLE efficiency, E_{LLE}, is calculated by Eq. 55.

$$E_f = \frac{mS}{F} \tag{54}$$

$$E_{LLE} = \frac{1}{\frac{Q_{LLE}}{KaV_{LLE}} + 1} \tag{55}$$

Here, K is the overall mass transfer coefficient, Q_{LLE} is the LLE volumetric throughput, a is the interfacial area between phases, and V_{LLE} is the LLE tank volume. K is calculated from continuous and dispersed phase mass transfer coefficients, k_c and k_d, respectively, which are calculated by phase Sherwood numbers, Sh_p ($p = c$ and d denote continuous and dispersed phases, respectively) via the Skelland-Moeti correlation.[224]

$$K = \frac{1}{\frac{1}{k_c} + \frac{1}{k_d}} \tag{56}$$

$$Sh_d = \frac{k_d d_{32}}{D_{API,d}} \approx 6.6 \tag{57}$$

$$Sh_c = \frac{k_c d_{32}}{D_{\mathrm{API},c}} = 1.27\times10^{-5} Sc_c^{1/3} Fr_c^{5/12} Eo^{5/4} \phi^{-1/2} Re_{\mathrm{imp}}^{2/3} \left(\frac{d_{\mathrm{imp}}}{d_{32}}\right)^2 \left(\frac{d_{32}}{d_t}\right)^{1/2} \quad (58)$$

Here, d_{32} is the Sauter mean droplet diameter, $D_{\mathrm{API},p}$ is the API molecular diffusivity in phase p, Sc_c is the continuous phase Schmidt number, Fr_c is the continuous phase Froude number, Eo is the Eotvos number, ϕ is the continuous phase volume fraction, Re_{imp} is the LLE tank impeller Reynolds' number and d_{imp} and d_t are the impeller and tank inner diameters, respectively, assuming a tank aspect ratio of 1 and a tank-to-impeller diameter ratio of 2.

$$D_{\mathrm{API},p} = \frac{k_b T_{\mathrm{LLE}}}{6\pi\mu_p r_{\mathrm{API}}} \quad (59)$$

$$Sc_c = \frac{\mu_c}{\rho_c D_{\mathrm{API},c}} \quad (60)$$

$$Fr_c = \frac{d_{\mathrm{imp}} N_{\mathrm{imp}}^2}{g} \quad (61)$$

$$Eo = \frac{\rho_d d_{32}^2 g}{\sigma} \quad (62)$$

$$Re_{\mathrm{imp}} = \frac{d_{\mathrm{imp}}^2 N_{\mathrm{imp}} \rho_m}{\mu_m} \quad (63)$$

Here, T_{LLE} is the LLE operating temperature (25 °C), μ_p and ρ_p are the phase viscosity and density, respectively, r_{API} is the API molecular radius, N_{imp} is the LLE tank impeller speed (= 6 r.p.s. in this work), g is the acceleration due to gravity, σ is the interphase surface tension, and ρ_m and μ_m are the mixture density and viscosity, respectively. Estimation of mixture densities and viscosities assume perfect mixing. The Sauter mean droplet diameter, d_{32}, depends on the Weber number, We.

$$d_{32} = \begin{cases} 0.052 d_{\mathrm{imp}} We^{-0.6} e^{4\phi} & , We < 10^3 \\ 0.390 d_{\mathrm{imp}} We^{-0.6} & , We > 10^3 \end{cases} \quad (64)$$

$$We = \frac{d_{\mathrm{imp}}^3 N_{\mathrm{imp}}^2 \rho_c}{\sigma} \quad (65)$$

$$a = \frac{6\phi}{d_{32}} \quad (66)$$

5.4 Plantwide Recoveries and E-Factors

Attainable *E*-factors (calculated as per Chapter 3.5.3) for all processes vary between 57–127; whilst these values are high in comparison to other manufacturing sectors, they are between modest and poor for pharmaceutical manufacturing processes (see Chapter 3.5.3).[225] The *E*-factor variations are directly related to corresponding API recoveries; as API recovery increases, material requirements and waste (and thus the *E*-factor) decrease. Implementing the process configuration with the lowest total costs (iBuOAc, 60 °C) attains E = 58.4, which is low in comparison to other options in this work.

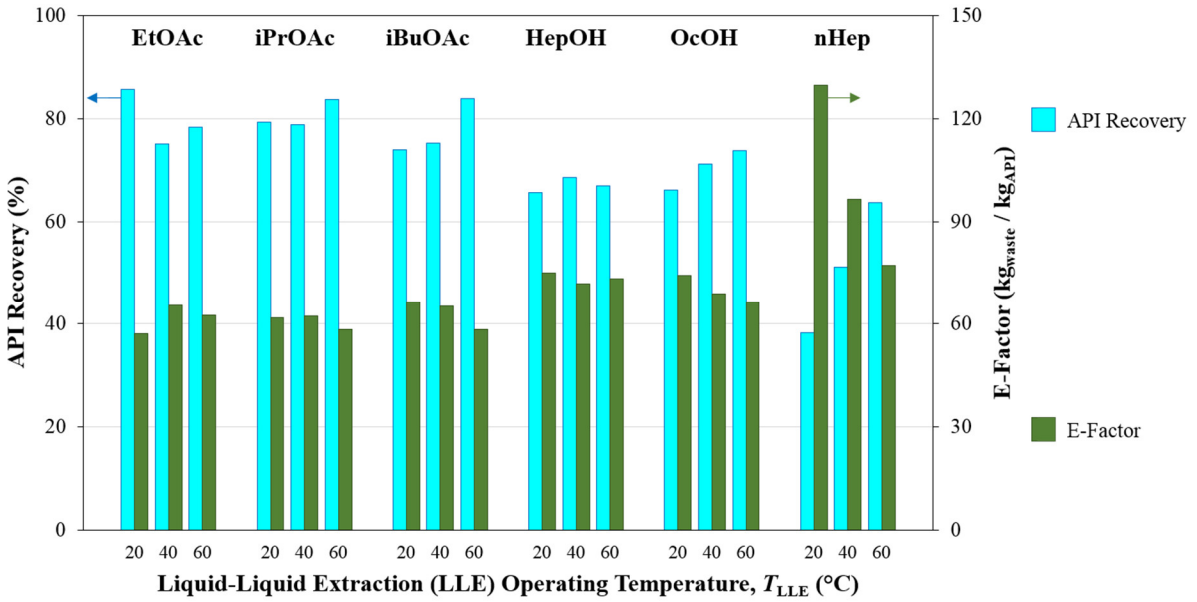

Figure 36: Warfarin CPM recoveries and E-factors corresponding to total cost minima.

5.5 Plant Total Cost Components

Minimum total costs for each LLE solvent and operating temperature are shown in Fig. 37. The LLE solvent with the lowest minimum total costs is iBuOAc (293.87×10^6 GBP, 60 °C), followed by EtOAc (299.91×10^6 GBP, 20 °C) and iPrOAc (299.93×10^6 GBP, 60 °C). These solvents perform comparably due to their similar molecular structures and polarities, inducing similar phase compositions and thus comparable API recoveries. This effect is also observed for HepOH and OcOH, which attain the next lowest total costs (339.43×10^6 GBP and 324.54×10^6 GBP, respectively) both operating at T_{LLE} = 60 °C. The poorest performance is attained using nHep (lowest cost = 350.52×10^6 GBP at T_{LLE} = 60 °C).

For most cases, increasing operating temperature leads to lower total costs due to the enhanced mass transfer (recovery) rates of API into the product phase, which requires shorter LLE tank residence times (lower *CapEx*) and material requirements (lower *OpEx*) to meet the plant capacity

of Q_{API} = 100 kg API yr^{-1}. When nHep is implemented as a separation solvent, *OpEx* is significantly higher for all LLE operating temperatures (T_{LLE} = 20, 40, 60 °C) considered, due to the low API recoveries attainable in comparison to other separation solvents considered in this work (Fig. 36). In all process configurations, the solvent feed rate (r_{LLE}) is pushed to its lower bound (= 1). The solvent feed rate and its assumed recovery following LLE directly affects materials and waste treatment costs (key *OpEx* components). The sensitivity of total cost minima to varying solvent recovery can be readily compared using the framework described here.

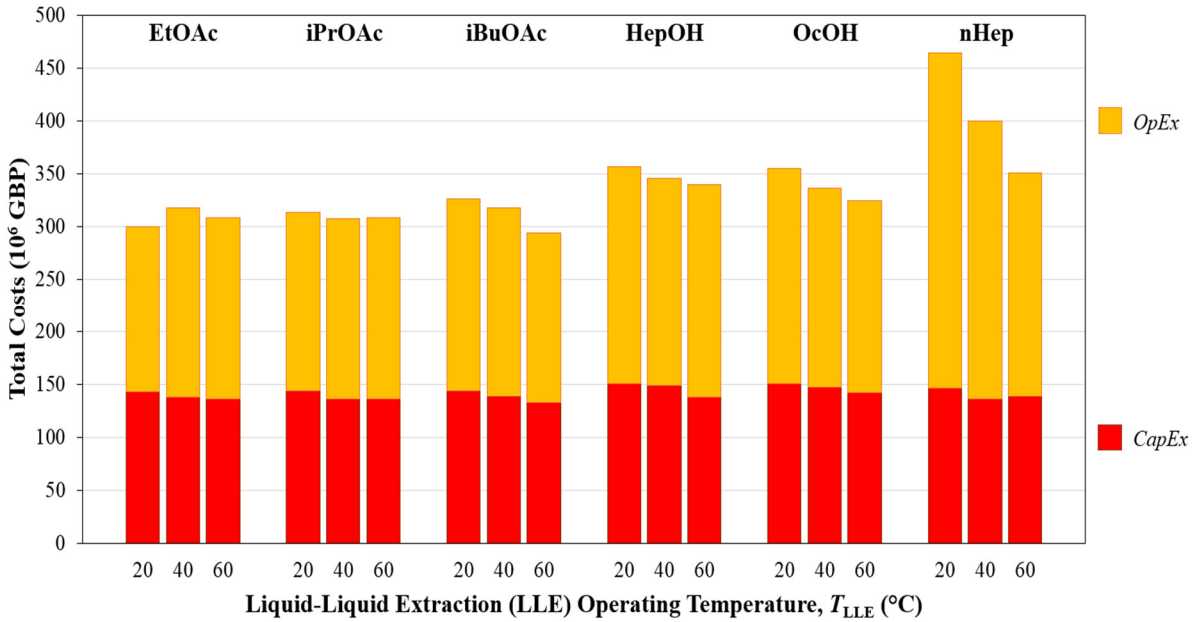

Figure 37: Minimum total costs attainable for different warfarin CPM LLE configurations.

The described framework can be used to perform sensitivity analyses with respect to economic data (e.g., varying material prices, rates of interest) and other operational assumptions (e.g., achieved solvent recovery). It also allows the investigation of the effect of plant capacity on total cost components and *E*-factors, an essential consideration during process development. Candidate separation solvents investigated for application here have been selected based upon their suitability for LLE (i.e., exhibit rapid phase splitting with the process mixture and are considered suitable with respect to detailed EHS criteria). Warfarin is available in both liquid (dispersion) and solid (tablet) formulations, and thus consideration of crystallisation and downstream processing following the upstream CPM considered in this work is important. Consideration of the effects of LLE solvent choices and resulting API recoveries and purities in the organic product phase on the requirement for additional purification prior to further processing will aid LLE solvent selection. The methodology described in this work can be implemented for other APIs requiring continuous

LLE, provided essential mass balance and thermodynamic data are available for modelling and total cost minimisation.

5.6 Chapter Conclusions

This study presents the systematic evaluation of six candidate separation solvents for the continuous Liquid-Liquid Extraction (LLE) of (*S*)-warfarin following the experimentally demonstrated continuous flow synthesis. Comparison of minimum total costs via nonlinear optimisation with LLE solvent feed rate and tank residence time as decision variables establish promising candidate LLE solvents for the CPM of (*S*)-warfarin. Isobutyl acetate (iBuOAc) emerges as a promising candidate LLE solvent, attaining the lowest minimum total costs of 293.87×10^6 GBP and a reasonable E-factor of 58.4, followed by ethyl acetate and isobutyl acetate. The considered alcohols (1-heptanol and 1-octanol) and *n*-heptane attain inferior performance (higher total costs) due to their lower maximum (theoretical) API recoveries.

The technoeconomic and environmental impact analyses presented in this work can inform the future design of CPM processes for this societally important API. Consideration of wider operating parameter sets and additional LLE solvents can be performed by adapting the existing framework, given the availability of required thermodynamic data and physical properties. Sensitivity analyses with respect to varying performance assumptions (e.g., varied attainable reaction and separation efficiencies upon scale up) and economic considerations (available solvent recovery, interest rates etc.) can be implemented within the framework and will add robustness to the presented results. Consideration of the effects of carrier and separation solvent combinations on subsequent upstream (e.g. crystallisation) and downstream (product formulation) unit operations will aid the development and successful transition of this process to end-to-end CPM.

Chapter 6

Nevirapine

This chapter describes the steady-state process modelling and technoeconomic optimisation (via NLP) for design of CPM of nevirapine based on the published continuous flow synthesis, developing a conceptual continuous pH crystallisation process for reaction effluent purification, based upon the flowsheet presented in Chapter 2 (Fig. 15).

The results presented in this chapter have also been published in the literature (Diab et al., *Org. Process Res. Dev.* **2019**, *23*(3), 320–333); details can be found in Appendix B.

6.1 Arrhenius Parameter Estimation for Reactor Design

Modelling and design of each reactor in the process flowsheet (Fig. 15) is discussed. Fixed process conditions for each reactor are summarised in Table 17.

Table 17: Summary of continuous flow reactor conditions used in nevirapine CPM.

Reactor	**Reaction**	**Temperature, T (°C)**	τ (units)	X_A (%)
R-101	CAPIC + NaH → CAPIC-Na	95	8.56 (s)	100
R-102	CAPIC-Na + MeCAN → CYCLOR	65	2 (hr)	82.5
R-103	CYCLOR → API	T_{R103}	21 (min)	$X_A^{R103} = f(T_{R103})$

Full conversion of CAPIC to CAPIC-Na (X_A^{R101} = 100%) is reported for a R-101 operating temperature of 95 °C and an estimated residence time of 8.56 s; this stoichiometric conversion in a short residence time is attained by implementing a thin-film reactor to enhance and heat and mass transfer to expedite the reaction.[170] The operating temperature of R-101 is chosen to be the same as in the published experimental demonstration; thus, the same reaction performance is assumed for modelling CAPIC-Na formation in R-101. The operating temperature, residence time and attained conversion of CAPIC-Na in R-102 are also assumed as per the published experimental demonstration.

Temperature-dependent kinetic data for API formation in R-103 is available in the literature;[170] at temperatures of 120, 140 and 165 °C, CYCLOR conversions to API of 10, 60 and 96% are attainable, respectively, each for an estimated residence time of 21 min.[10] The reactor volume is calculated as in Chapter 3.3. The limiting reagent is CYCLOR as NaH in the packed bed is in significant excess and so it is assumed that the reaction is first-order in CYCLOR. Following this

assumption, the first-order rate constant, k, at different temperatures can be estimated. This allows the regression of Arrhenius law (see Chapter 4.1) parameters for API formation in R-103, allowing the explicit modelling of CYCLOR conversion to API as a function of temperature, T. The Arrhenius plot from the available kinetic data is shown in Fig. 38 with good fit ($R^2 > 0.96$); regressed parameters are E_a = 1.565 kJ mol^{-1} and $A = 8.49\times10^{13}$, assuming the reaction is first-order in CYCLOR. Availability of a wider kinetic dataset will allow further validation of Arrhenius parameter estimation results and investigation of more complex candidate rate law expressions. Reactor volumes and process flowrates are calculated as in Chapter 3.3.

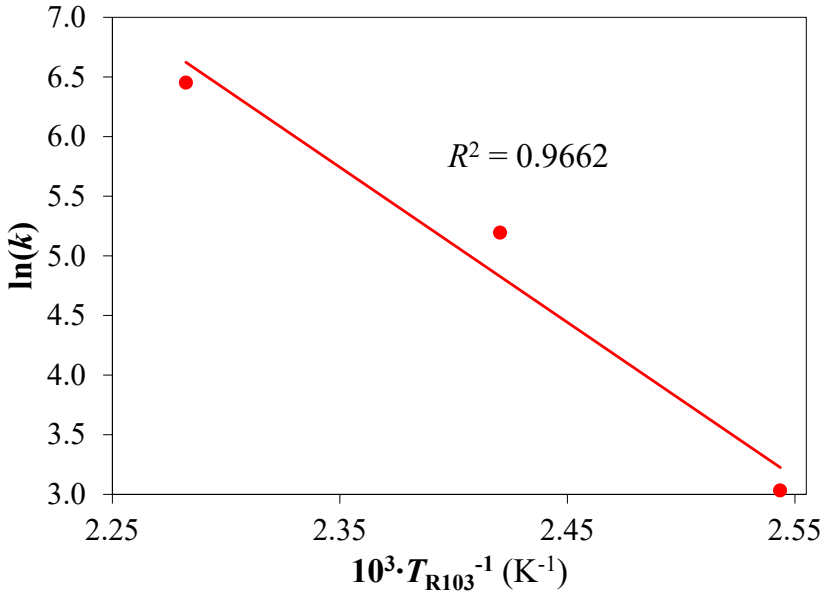

Figure 38: Arrhenius plot for ring closure in nevirapine continuous flow synthesis from CYCLOR.

6.2 Continuous Crystallisation Design

The batch crystallisation yield has a reported yield of 96% in a residence time of 1 hr operating at 25 °C and pH_{CRYST} = 7.[170] Here, we compare the conceptual steady-state continuous crystallisation to the demonstrated batch process by varying the pH of the continuous crystallisation. Table 18 summarises fixed processing conditions for both batch and continuous crystallisation process designs. The pH of the stream fed to the crystallisation process for both batch and continuous crystallisation processes is approximately 0.5 following reactor effluent purification with HCl and AC (see Chapter 2, Fig. 16).

Table 18: Summary of process conditions for nevirapine batch + continuous crystallisation process models.

	Batch (BX)	Continuous (CPM)
Temperature (°C)	25	25
Thermodynamic efficiency (%)	100	70
τ (hr)	1	0.5
Feed pH	≈ 0.5	≈ 0.5
Operating pH, pH_{CRYST}	7	Variable
Yield, Y (%)	96	$Y = f(pH_{CRYST})$

6.2.1 Nevirapine Aqueous Solubility Estimation

Crystallisation process design requires modelling of API solubility in process mixtures. The mixture prior to pH increase for API crystallisation is predominantly aqueous (solvent content >96 mol% H_2O), thus the mixture is assumed to be purely aqueous for crystallisation modelling purposes. The aqueous solubility, S_{aq}, of nevirapine in the crystallisation stage (see Fig. 38) as a function of pH is modelled by[226]

$$S_{aq} = S_0(1 + 10^{pKa-pH}) \tag{67}$$

where S_0 = 4.58×10^{-2} g L^{-1} (solubility under non-ionising conditions) and pK_a = 2.8 at 25 °C; correlation parameter values (S_0 and pK_a) are only available at 25 °C, thus additional temperatures for pH crystallisation modelling cannot be considered. The modelled aqueous API solubility as a function of pH is shown with experimental values as reported by various literature references in Fig. 39, showing good agreement with experimental values.[226–228]

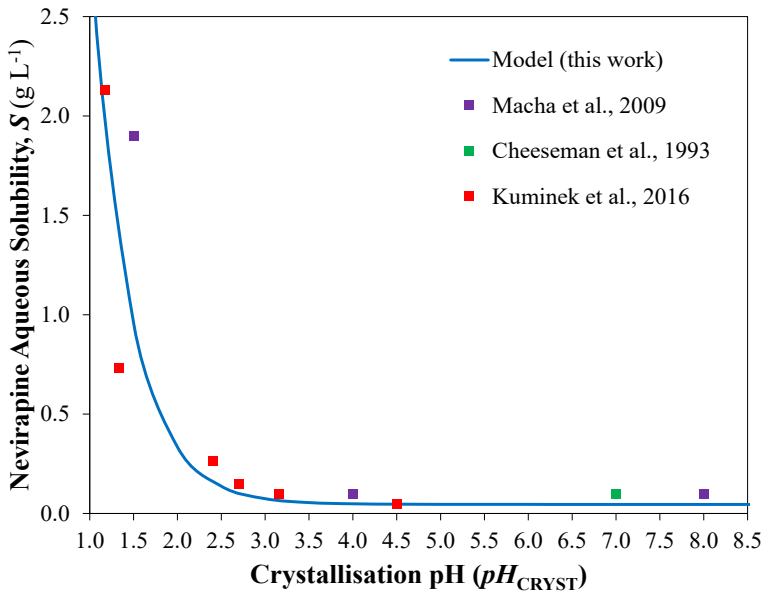

Figure 39: Aqueous API solubility model = f(pH) with experimental values.[226–228]

6.2.2 Crystallisation Yield Estimation

The crystallisation yield (Eq. 67) is estimated from the API concentration in the mother liquor, C_i, and the aqueous API solubility.

$$Y = 1 - \frac{C_i}{S_{aq}} \tag{67}$$

Both batch and continuous crystallisation processes' feed streams enter at pH ≈ 0.5. A residence time of 0.5 hr is assumed for the continuous crystallisation. The residence time for the considered continuous crystallisation of nevirapine was arbitrarily chosen due to the lack of crystallisation kinetic parameters require to enable higher-fidelity population balance modelling. The chosen value for the continuous crystallisation residence time is on the lower end of the range of typical values;[63,222] longer residence times will lead to larger crystalliser vessels which imply greater *CapEx*. This will affect the total cost component results, cost differences vs. the process with a batch crystallisation. It is assumed that the batch crystallisation attains full (100%) thermodynamic equilibrium. A conservative thermodynamic efficiency of 70% is assumed for the continuous crystallisation to account for uncertainty in the non-attainment of equilibrium and assumed residence time and the calculated yield. This will likely result in an under-prediction of continuous crystallisation yield and thus an over-estimation of total costs, which should be considered when interpreting the optimisation results presented here.

6.3 Effect of Unit Operation on Plant Efficiency

Total cost components are calculated as per Chapter 3.6. Cost response surfaces under different design assumptions were generated (presented in Fig. 40) to investigate the design space and to ensure that multiple cost minima are not present. Cost response surfaces for all design cases show a sharp peak (i.e. very high total costs) at low R-103 operating temperature T_{R103} and low crystallisation pH (pH_{CRYST}). Under these conditions, very low API recovery is attained and thus higher material requirements and unit operation capacities are required to meet the desired plant capacity (Q_{API}), resulting in high *CapEx* and *OpEx*. At higher capacity (Q_{API}), response surfaces take a similar shape but present higher total cost values due to the increased material throughput and correspondingly larger unit operation scales. Varying Solvent Recovery, SR = {0, 40, 80}% (reflecting worst-case, intermediate and lab-reported values[170]). is also shown to significantly affect the cost response surfaces due to its effect on solvent requirements, which is a major contributor to the mixture composition and thus on *OpEx* components, as well as waste.

The effect of R-103 operating temperature (T_{R103}) on total costs is significant; total costs decrease rapidly as T_{R103} increases from 120 to 165 °C. Operating temperature in R-103 significantly affects the conversion of CYCLOR to API, thus plantwide API yield is very sensitive to T_{R103}; expensive reagents, especially starting materials CAPIC (= 5 GBP kg^{-1}) and MeCAN (= 10 GBP kg^{-1}), make materials costs a major contributor to total costs and so a high API yield in R-103 (i.e., high T_{R103}) is preferred. The effect of each decision variable (T_{R103} and pH_{CRYST}) on plantwide API yield is shown in Fig. 41 to illustrate this point. The optimisation problem formulation in this work could alternatively be defined to maximise Net Present Value (*NPV*), which may yield different results. Comparison of results for a different objective function formulation could be useful, given the availability of reliable projected API and brand sales prices.

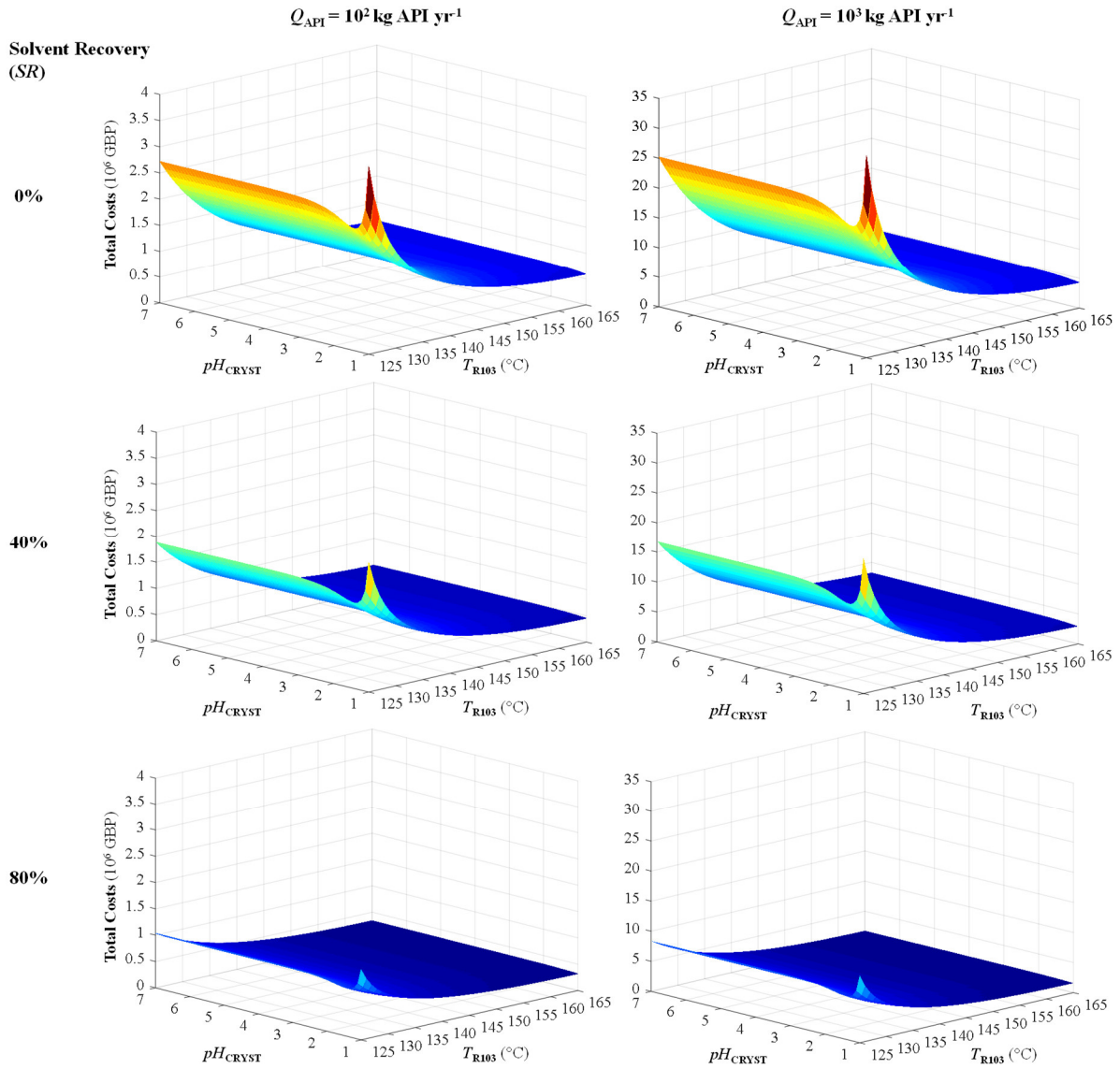

Figure 40: Total cost response surfaces for nevirapine CPM under different design assumption of plant capacity (Q_{API}) and solvent recovery (*SR*).

The effect of operating crystallisation pH (pH_{CRYST}) on total costs is also similar across different design assumptions. At the lower bound of R-103 operating temperature (T_{R103} = 120 °C), low pH (e.g., at the lower bound of pH_{CRYST} = 1) results in high total costs. At low T_{R103}, the low conversion of CYCLOR to API in R-103 means plantwide yield is already poor prior to crystallisation; low pH_{CRYST} implies lower crystallisation yield and thus higher total costs are incurred due to increased material requirements and unit operation scales needed to meet the desired plant capacity (Q_{API}). The implemented model of aqueous API solubility vs. pH shows a plateau in solubility beyond some pH value below 7. Increasing the crystallisation pH too high will result in incremental increases in API yield only which will unnecessarily increase material usage and crystallisation volumes, and thus total costs (as observed in the cost response surfaces in Fig. 40). At the upper bound of R-103 operating temperature (T_{R103} = 165 °C), the effect of crystallisation pH is not so significant. The yield of API is already high when T_{R103} is higher (due to increased conversion of CYCLOR to API in R-103) and thus the effect of higher pH in the crystallisation is not as important. This is further illustrated by the plantwide API yield response surface in Fig. 41.

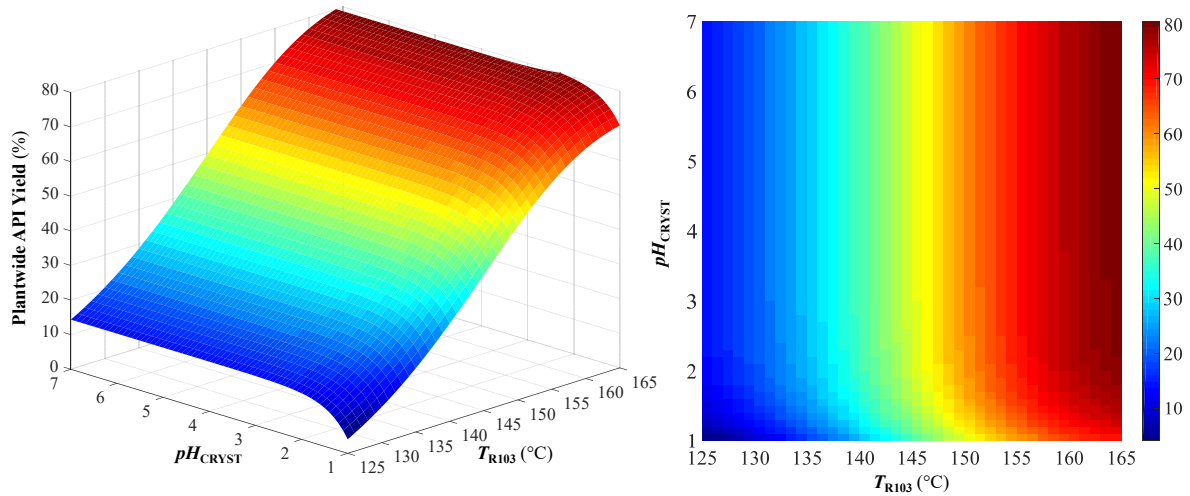

Figure 41: Response surface of plantwide nevirapine yield vs. R-103 operating temperature (T_{R103}) and crystallisation pH (pH_{CRYST}).

6.4 Optimisation for Plant Total Cost Minimisation

The objective of the NLP problem is to minimise plantwide total costs, calculated as per Chapter 3.6. The continuous decision variables are the operating temperature of R-103, T_{R103}, and crystallisation pH, pH_{CRYST}, both of which influence the final API yield by influencing R-103 conversion to API and crystallisation yield, respectively. While increasing T_{R103} enhances the conversion of CYCLOR to API, there are associated utilities costs with heating R-103, which contribute to *OpEx* and plant total costs. Similarly, while increasing pH_{CRYST}, the crystallisation pH

increases, but also incurs higher material costs as well as larger crystallisation capacities, which contribute to total costs.

$$\min \; Total\ Cost \tag{68}$$

s.t.

$$120\ °C \leq T_{R103} \leq 165\ °C \tag{69}$$

$$1 \leq pH_{CRYST} \leq 7 \tag{70}$$

Constraints on R-103 operating temperature are chosen to be the lower and upper bounds of available temperature data for Arrhenius parameter estimation (120 and 165 °C, respectively) to ensure validity of the regressed parameters for subsequent modelling and optimisation (Eq. 69). Constraints on crystallisation pH (Eq. 70) were chosen to be from $pH_{CRYST} = 1$ (close to feed mixture point, pH ≈ 0.5) and pH = 7 (the BX crystallisation pH).

The optimisation problem is solved in MATLAB using the interior-point algorithm with tolerances of 10^{-6}. Plant capacities of $Q_{API} = \{10^2, 10^3\}$ kg API yr^{-1} are investigated to represent small-/pilot-scale designs. As in Chapter 5, the plant capacity is met by specifying it as a NLP constraint. The effect of solvent recovery, *SR*, is also considered, as this has a significant effect on material consumption, and thus *OpEx*. A reported *SR* = 80% is reported in the literature;[170] the attainable *SR* may be lower and so *SR* = {0, 40}% are also considered.

The NLP problem was solved for all individual combinations of plant capacity, $Q_{API} = \{10^2, 10^3\}$ kg API yr^{-1} and assumed Solvent Recovery, *SR* = {0, 40, 80}%, i.e., six problem instances. Multiple initial values for decision variables are tested to ensure a unique optimal solution for each problem instance. Initial values of decision variable for each problem instance are R-103 temperature, $T_{R103,0}$ = {130, 145, 160} °C and crystallisation pH, $pH_{CRYST,0} = \{2, 4, 6\}$, i.e., a total of nine initial points per problem instance. Unique solutions were attained for all problem instances for different decision variable initial values. Solution times were short for all problem instances (Table 19).

Table 19: Nevirapine CPM NLP solution time for different problem instances.

Q_{API} (kg API yr^{-1})	*SR* (%)	**Solution time** (s)
10^2	0	14.5
	40	19.5
	80	7.8
10^3	0	8.7
	40	7.5
	80	7.4

The optimal values of the decision variables (T_{R103} and pH_{CRYST}) corresponding to minimum total costs under different design assumptions are shown in Fig. 42. These optima are compared to the process implementing a batch crystallisation, where T_{R103} = 165 °C and pH_{CRYST} = 7. In all of the batch and continuous crystallization design cases, the optimum T_{R103} is the upper bound (165 °C). The optimum crystallization pH varies across different *SR* assumptions. At lower *SR* (= 0%), an optimum pH of ~4 is observed for both considered capacities; *OpEx* components are significant contributors to cost, and thus, higher crystallisation yields are preferred to minimise the objective function. For higher *SR* (= 40, 80%), pH_{CRYST} is driven to the lower bound (= 1); the effect of enhancing the crystallisation yield by increasing pH_{CRYST} is not as important when a significant percentage of the solvent is recovered and T_{R103} is high. At higher capacity (Q_{API} = 10^3 kg API yr^{-1}), higher *SR* is required to allow a lower pH for minimum total cost. In industrial practice, for safety purposes it may be necessary to neutralise the mixture following crystallization and API crystal removal, but this was not considered as part of the presented analysis.

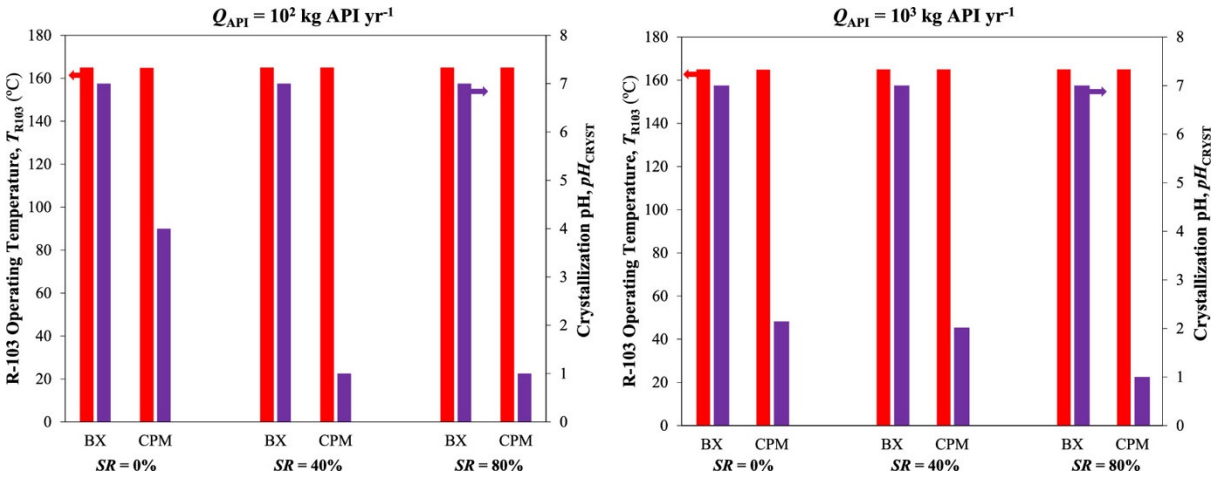

Figure 42: Optimal reactor operating temperature (TR103) and crystallisation pH (pH_{CRYST}) corresponding to the total cost minima under different design assumptions for nevirapine CPM.

Material efficiencies of different design assumptions quantified by the *E*-factor (see Chapter 3.5.4) are shown in Fig. 43. For all batch designs, *E*-factor values are very high, even for pharmaceutical processing which is renowned for having highly materially intensive manufacturing routes;[12] this is due to all batch crystallisation processes being operating at pH_{CRYST} = 7, requiring significant quantities of base to neutralise the feed mixture. In all cases, increasing solvent recovery significantly reduces *E*-factor due to the large contribution of solvent to process mixture and waste compositions. All CPM designs achieve values lower than this, but only higher solvent recoveries allow this for the process with a batch crystallisation; even so, the attained E-factors are mid-range with respect to typical pharmaceutical manufacturing processes (see Chapter 3.5.3). Elucidation of

attainable solvent recoveries at different production scales will further clarify the likely material efficiencies of different design assumptions to elucidate materially efficient CPM plant designs.

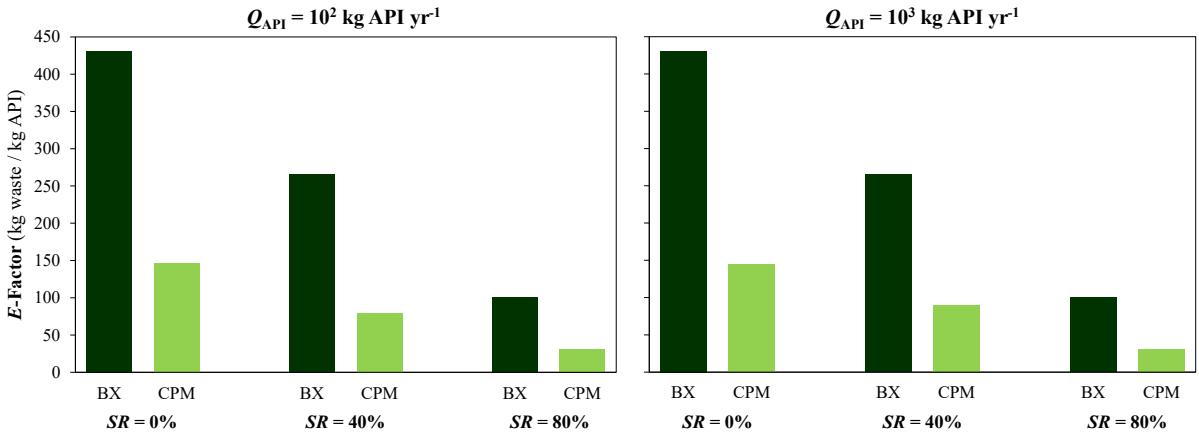

Figure 43: Environmental (*E*)-factors at cost optima for different nevirapine CPM design assumptions.

It should be noted that the wide range of conditions considered here (reactor temperature and crystallisation pH) will possibly lead to different polymorphs forming in the purification + crystallisation processes. Although the literature study upon which the considered process is based did not contain sufficient data to perform population balance modelling, nor did it investigate the attained polymorphs of the obtained nevirapine crystals,[170] the possibility of polymorphism under different process conditions should be considered in future work.

6.5 Economic Analysis

6.5.1 Plant Total Costs

Minimum total cost components for CPM compared the process with the BX crystallisation are compared in Fig. 44. Total costs at Q_{API} = 10^3 kg API yr^{-1} are higher, reflecting the increased material requirements and unit operation scales. *OpEx* components are more significant than *CapEx* in all design cases due to the expensive reagents required for the API synthesis. As solvent recovery increases, *OpEx* components decrease significantly and substantially lower total costs. Utilities and waste components are the most significantly affected by varying solvent recovery due to the large quantity of solvent in the process mixture; materials costs are less affected by varying solvent recovery as the reagents used are much more expensive than solvent components in the considered process. In all cases, CPM designs have significantly lower *OpEx* components than for BX designs due to the reduced material requirements of the crystallisation process when operating at lower pH.

For varying solvent recovery assumptions, *CapEx* components remain roughly the same, as internal process stream flowrates through each unit operation remain fairly consistent. In all cases, CPM designs have lower *CapEx* components than their BX counterparts due to the lower material throughputs of these processes. The availability of detailed crystallisation kinetic models with experimental data and model parameters can help to elucidate crystallisation process performance and unit operation design, which will likely have a significant effect on *CapEx*. The equipment cost correlation used is the most widely implemented and reliable available in the peer-reviewed literature; design capacities required for the considered plant capacities (Q_{API}) are at the lower end of the cost correlation application range, and thus purchase cost overestimation may be present. Additional uncertainty in calculated unit purchase costs is present due to the lack of cost estimation methods for specific equipment, e.g., thin film reactors; however, the cost correlation used here is the best available. Some specialised unit operations have specific cost correlations established, which may be more accurate than the general correlation used in this work. Cost correlations specific to particular unit operations should be used where possible to allow accurate prediction of *CapEx* component contributions to total costs. Furthermore, the considered processes (both BX and CPM) are considered to take advantage of being constructed at an existing pharmaceutical manufacturing site; additional costs may also be incurred if green-field construction is required.

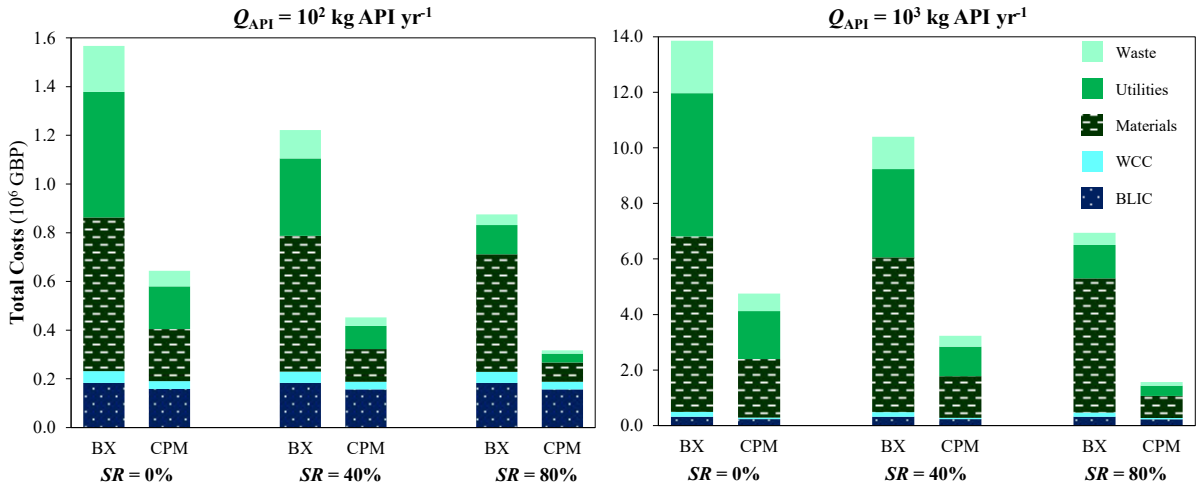

Figure 44: Total cost components for different nevirapine CPM design assumptions.

6.5.2 Nevirapine Cost of Goods: Batch vs. Continuous Manufacturing

In all cases, CPM designs are more economically viable than those implementing a BX crystallisation. The most significant savings are realised in *OpEx* components (materials, utilities and waste components, as described in the costing methodology), which allow significant total savings due to their large contribution to plant total costs. Ensuring affordable, accessible HIV

medicines is essential; HIV drug unit prices have varied widely in previous years, so quantifying attainable price per unit mass is an important consideration for HIV drug manufacturing.[229] The API Cost of Goods (*CoG*) is calculated to quantitatively compare differences in affordability of nevirapine under different design assumptions. The *CoG* is calculated as the mass of API produced during the plant lifetime (= 20 yr) divided by the total cost of constructing and operating the plant.

$$CoG = \frac{20 Q_{\mathrm{API}}}{Total\ Costs} \tag{71}$$

The resulting API *CoG* values under different design assumptions are presented in Fig. 45. For all cases, CPM designs allow lower API *CoG* than their batch (BX) alternatives due to the significant total cost savings allowed by continuous operation. Solvent recovery has a significant effect on the resulting *CoG* due to the large contribution of solvent to *OpEx* components, which dominate total costs of all design cases. While this analysis does not clarify exactly what price the API will be sold at, the estimated *CoG* values indicate that CPM implementation can allow for lower API sales prices to expand global access to this HIV drug.

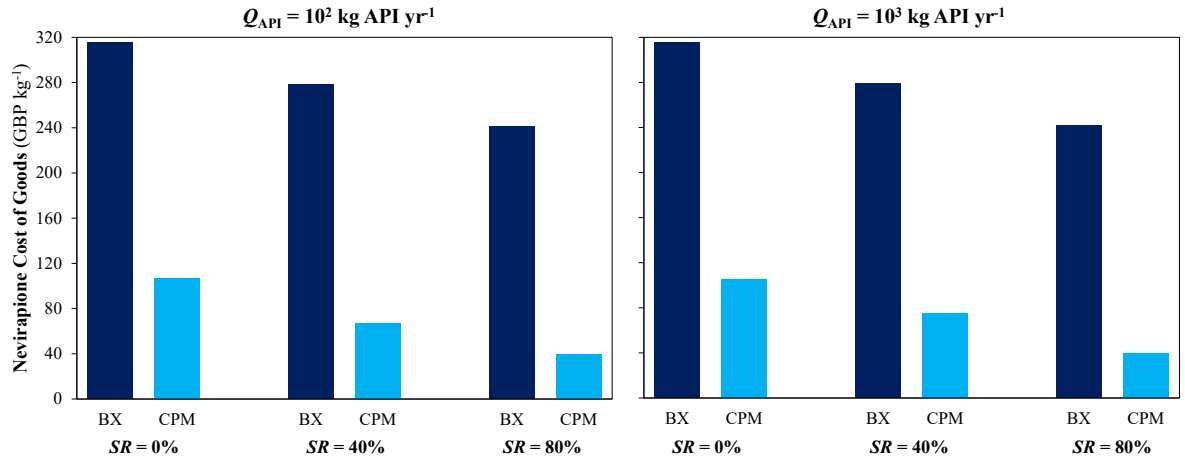

Figure 45: Estimated nevirapine cost of goods from total costs of different plant design.

6.5.3 Sensitivity Analysis: Effects of Starting Material Prices

The starting materials (CAPIC and MeCAN) for the continuous synthesis of nevirapine considered in this work are advanced compounds synthesised from multistep batch processes (see Fig. 13).[170] Consideration of key material price fluctuations is an important form of sensitivity analysis that should be implemented in modelling and economic evaluation during candidate process screening and development stages. Here, we consider the effect of increasing CAPIC and MeCAN material prices by 50% from the base case values on plant total costs, i.e. CAPIC price = [5,10] GBP kg^{-1}, MeCAN price = [10,20] GBP kg^{-1}, at discrete values of decision variables, T_{R103} = {130, 145, 160}

°C and pH_{CRYST} = {2, 4, 6} for Q_{API} = 10^2 kg API yr^{-1} and SR = 40%; observed trends are expected to be the same for alternative values of Q_{API} and SR. The effects of varying material prices for these discrete decision variable values are shown in Fig. 46. Although starting material prices do affect total plant costs in all design cases, the effect of T_{R103} is still the most sensitive parameter affecting total costs. Further process intensification for the batchwise syntheses of CAPIC and MeCAN will ensure reasonable starting material prices to ensure the economic viability of the process designs investigated here.

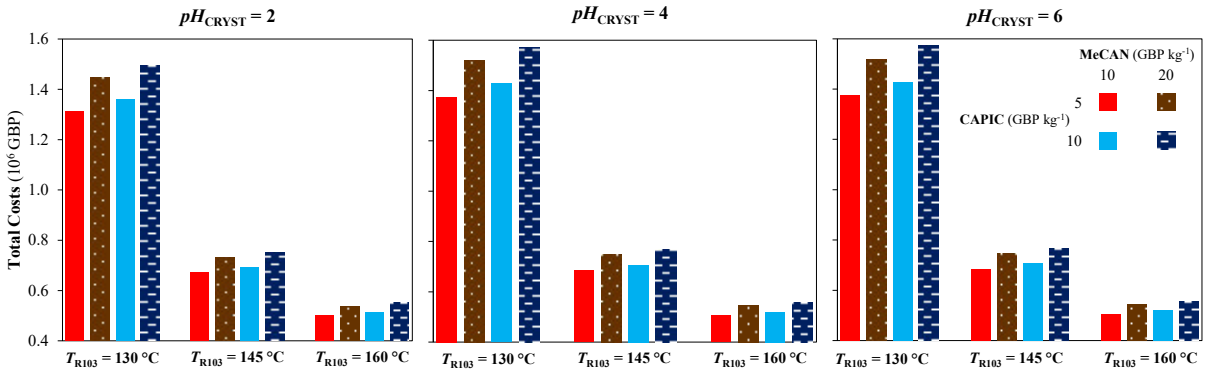

Figure 46: Effect of starting material prices and T_{R103} and pH_{CRYST} on nevirapine CPM plant total costs (Q_{API} = 10^2 kg API yr^{-1}, SR = 40%).

6.6 Chapter Conclusions

This work has formulated and solved a NLP problem for the total cost minimisation of the plantwide upstream CPM of nevirapine, a societally important API for HIV-1 treatment. Optimisation of a conceptual continuous crystallisation for the purification of the API synthesis effluent following the continuous flow synthesis under various design assumptions (plant capacity and solvent recovery) are used to quantitatively evaluate different designs for nevirapine CPM. The operating temperature of the final reactor R-103 (T_{R103}) is driven to the upper bound in all design cases to maximise API synthesis yield while crystallisation pH (pH_{CRYST}) is always lower than that of the batch crystallisation (pH = 7) for CPM designs to minimise major *OpEx* contributions to plant total costs. In all design cases, CPM designs achieve lower total cost components, improved material efficiencies and lower API *CoG* values, demonstrating the promise of CPM over batch for nevirapine production and improving global, affordable access to HIV APIs. This work also demonstrates the value of conducting technoeconomic optimisation studies towards the development of continuous processes in pursuit of economically viable end-to-end CPM plants.

Chapter 7

Cyclosporine, Paracetamol and Aliskiren

This chapter considers MSMPR cascades without recycle for continuous cooling crystallisation of cyclosporine, paracetamol and aliskiren, based upon the flowsheet in Chapter 2 (Fig. 20).

The results presented in this chapter have also been published in the literature (Diab and Gerogiorgis, *Ind. Eng. Chem. Res.* **2018**, *57*(29), 9489–9499); details can be found in Appendix B.

7.1 MSMPR Crystalliser Design

The considered cooling crystallisation MSMPR cascades have no antisolvent usage, recycle implementation or up-/downstream requirements as part of the study. We assume that fresh mother liquor feed streams contain negligible amounts of impurity that will affect the attained crystal product in these processes. Knowledge of typical crystallisation feed stream compositions in integrated CPM processes will greatly enhance the understanding of impurity distributions on optimal continuous crystallisation process designs for the APIs studied here.

The cascade consists of N = 1–3 crystallisers. We consider plant API capacities (Q_{API} = {10^2, 10^3, 10^4} kg API yr^{-1}) to investigate the effects of production scale, which can significantly affect the economic viability of CPM designs.[69] Varying design capacities considered here do not signify a range of capacities implemented for a single plant; they are considered for separate plant designs to comparatively illustrate the effect of capacity on relevant cost components and their relative contribution to total plant costs. As in Chapters 4 and 5, the plant capacity is met by specifying it as a NLP constraint. The considered plant capacities are low in comparison to typical market sizes of such societally important APIs. Continuous technologies are not yet widely implemented in pharmaceutical manufacturing, and so it is likely that a CPM process would first be implemented on smaller scales, as have been most demonstrations in the literature. Three different capacities have been compared for each API to illustrate the effect of capacity on relative cost component contributions to total costs and on cost optimal design and operating parameters. One to three implementable MSMPRs is a reasonable number of vessels and is consistent with other literature studies. Crystalliser operating temperatures are between –10 and 20 °C, and the maximum total cascade residence is 15 hr. Concentrations of dissolved API in mother liquor feed streams (C_0) vary according to experimental procedures;[63,91,92] cyclosporine, paracetamol and aliskiren feed concentrations of 25, 8.86 and 6% w/w, respectively, are assumed.

7.1.1 Solubility Estimation

Solubilities of APIs (i.e., API saturation concentrations, C_i^{sat}) as a function of temperature are required for description of crystallisation kinetics. Saturation concentrations as a function of temperature are described as temperature-dependent polynomials regressed from experimental solubility data for cyclosporine,[103,230] paracetamol,[91] and aliskiren.[92]

$$C_i^{sat} = (1.17\times10^{-4})T_i^2 + (2.00\times10^{-4})T_i + 0.05 \quad \text{for cyclosporine} \quad (72)$$

$$C_i^{sat} = (3.79\times10^{-2})T_i^2 + (3.77\times10^{-1})T_i + 0.21 \quad \text{for paracetamol} \quad (73)$$

$$C_i^{sat} = (7.60\times10^{-7})T_i^3 - (3.20\times10^{-5})T_i^2 + (5.20\times10^{-4})T_i + (4.50\times10^{-3}) \quad \text{for aliskiren} \quad (74)$$

7.1.2 Nucleation and Growth Kinetics

Crystal growth and nucleation kinetics are described by Arrhenius-type power law expressions.[231]

$$G_i = k_{g0}\exp\left(-\frac{E_{a,g}}{R(T_i + 273.15)}\right)\left(\frac{C_i}{C_i^{sat}} - 1\right)^{g_{MSMPR}} \quad (75)$$

$$B_i = k_{b0}\exp\left(-\frac{E_{a,b}}{R(T_i + 273.15)}\right)\left(\frac{C_i}{C_i^{sat}} - 1\right)^{b_{MSMPR}} M_i^{m_{MSMPR}} \quad \text{for cyclosporine}$$

$$B_i = k_{b0}\left(\frac{C_i}{C_i^{sat}} - 1\right)^{b_{MSMPR}} M_i^{m_{MSMPR}} \quad \text{for paracetamol} \quad (76)$$

$$B_i = k_{b0}\left(\frac{C_i}{C_i^{sat}} - 1\right)^{b_{MSMPR}} \quad \text{for aliskiren}$$

Here, G_i and B_i are the crystal growth and nucleation rates in MSMPR i operating at temperature T_i, respectively. C_i and C_i^{sat} are the MSMPR outlet and saturation (solubility) concentrations at T_i, respectively. M_i is the slurry density in MSMPR i. Growth kinetic parameters are k_{g0}, the growth pre-exponential factor, E_{ag}, the growth energy barrier, and g_{MSMPR}, the growth exponent. Nucleation parameters are k_{b0}, the nucleation pre-exponential factor, E_{ab}, the nucleation energy barrier, b_{MSMPR}, the nucleation exponent, and m_{MSMPR}, the slurry density exponent. The crystallisation studies from which parameters were taken did not distinguish between primary and secondary nucleation effects and thus it is assumed that both are lumped into Eq. 76; for this reason, consideration of specific agglomeration and breakage effects could not be considered here. Temperature-dependency of crystal nucleation for paracetamol and aliskiren has not been considered in the literature.[91,92] Similarly, m for aliskiren is considered equal to zero.[92] No effects of polymorphism were observed in the experimental studies from which crystallisation kinetic parameters were taken and so it is also assumed that no polymorphs are observed in this work. Crystallisation kinetic parameters from the literature for all APIs are summarised in Table 20.

7.1.3 Population Balance Equations

The general one-dimensional (i.e., linear growth is assumed) steady-state population balance model is described by a system of Ordinary Differential Equations (ODEs). For a MSMPR cascade with slurry recycle, the population balance equations are described by Eqs. 78–80. Here, n_i is the population density function of crystals between size L and L+dL. In Eq. 79, the first term represents the stream entering from the previous stage (i–1), the second term represents the recycle stream entering stage i and the last term represents the product stream leaving stage i. Eqs. 78–80 form a system of ODEs that are satisfied by the boundary conditions, n_i^0 (Eq. 80), representing the population density of nuclei.

$$G_1 V_1 \frac{\mathrm{d}n_1}{\mathrm{d}L} = R_1 n_{N+1} - F_1 n_1 \qquad i = 1 \tag{78}$$

$$G_i V_i \frac{\mathrm{d}n_i}{\mathrm{d}L} = F_{i-1} n_{i-1} + R_i n_{N+i} - F_i n_i \qquad \forall i = 2,\ldots,N \tag{79}$$

$$n_i^0 = \frac{B_i}{G_i} = n_i(L = 0) \qquad \forall i = 1,\ldots,N \tag{80}$$

The suspension density, M_i, is also calculated from the population balance via Eq. 81. Here, k_v and ρ_{API} are the volume shape factor and crystal density of API solute.

$$M_i = k_v \rho_{API} \int n_i L^3 \mathrm{d}L \tag{81}$$

Table 20: Steady-state process model parameters for continuous MSMPR crystallisation of cyclosporine, paracetamol and aliskiren.

API	Cyclosporine[63]		Paracetamol[91]		Aliskiren[92]	
	Value	Units	Value	Units	Value	Units
k_{g0}	1.13×10^{7}	m min^{-1}	2.00×10^{-2}	m min^{-1}	2.9×10^{-4}	m min^{-1}
E_{ag}/R	9.06×10^{3}	K	1.73×10^{3}	K	3.5×10^{2}	K
g_{MSMPR}	1.33	(–)	1.08	(–)	1.08	(–)
k_{b0}	4.80×10^{20}	# crystals m^{-3} min^{-1}	295	# crystals kg^{-1} s^{-1}	3.2×10^{7}	# crystals m^{-3} min^{-1}
E_{ab}/R	7.03×10^{3}	K	(–)	K	(–)	K
b_{MSMPR}	1.50	(–)	2.14	(–)	1.95	(–)
m_{MSMPR}	2/3	(–)	1.62	(–)	0	(–)
k_v	$\pi/6$	(–)	0.61	(–)	0.04	(–)

7.1.4 Mass Balances

The steady-state mass balances for each process assume no material accumulation and account for volumetric changes due to API crystallisation. The general mass balance equations are as follows.

$$F_0 C_0 + F_{N+1}\left(1 - \frac{M_{N+1}}{\rho_{\text{API}}}\right) C_N + R_1 M_{N+1} - F_1\left(1 - \frac{M_1}{\rho_{\text{API}}}\right) C_1 - F_1 M_1 = 0 \qquad i = 1 \tag{82}$$

$$F_{i-1}\left(1 - \frac{M_{i-1}}{\rho_{\text{API}}}\right) C_{i-1} + F_{i-1} M_{i-1} + R_i\left(1 - \frac{M_{N+1}}{\rho_{\text{API}}}\right) C_N + R_i M_{N+1} - F_i\left(1 - \frac{M_i}{\rho_{\text{API}}}\right) C_i - F_i M_i = 0 \qquad \forall i = 2,\ldots,N \tag{83}$$

Eq. 82 describes stage 1 in the MSMPR cascade. The first term in Eq. 82 is the dissolved API in the feed mother liquor stream to the cascade, the second and third terms are the API dissolved in the mother liquor and crystallised API in the recycle stream fed to stage 1, respectively, and the third and fourth terms are the API dissolved in the mother liquor and crystallised API leaving stage 1, respectively. For processes with no recycle (as is the case here), $R_i = 0$. Eq. 83 describes MSMPR stages $i = 2,...,N$, whose terms are similar to Eq. 82 but without the fresh feed mother liquor term ($F_0 C_0$). In both Eqs. 82 and 83, the bracketed terms describe the volume fraction of the suspension not occupied by crystallised API.

7.1.5 MSMPR Model Solution

Simultaneous solution of the MSMPR model requires iteration on the vector of C_i values, where $C_0 > C_i > C_i^{\text{sat}}$ holds for all crystallisers. Fig. 47 illustrates the workflow for the solution of the MSMPR model.[93,230] First, an initial guess is made for C_i values. The suspension densities are then estimated by solution of the mass balance equations, M_i^{mb}. Crystallisation kinetics are then computed, allowing solution of the system of ODEs describing population balances. Suspension densities calculated from the population balance equations, M_i^{pbe}, are then calculated. If the difference between M_i^{mb} and M_i^{pbe} is greater than the set tolerance ($= 10^{-6}$), another guess of C_i values are made. Upon convergence, the system of MSMPR model equations are solved.

7.2 Technoeconomic Optimisation of MSMPR Cascades

7.2.1 Optimisation Problem Definition

The objective function (Eq. 84) of the nonlinear optimisation problem is the total cost, calculated as in Chapter 3.6. The decision variables are the residence time and temperature of each crystalliser in the cascade, both of which affect the final attainable crystallisation yield, process mass balances and total costs of the cascade design. Crystallisation temperatures are constrained between –10 and 20 °C and the temperature of each crystalliser must be lower than or equal to the previous. Crystallisers of equal residence times are assumed for the problem formulation. Implementing crystallisers of equal volumes makes their purchase and acquirement from equipment suppliers/manufacturers simpler and less expensive. Additionally, the total cascade residence time is allowed a maximum of 15 hr in accordance with previous work.[230]

$$\min \textit{Total Cost} \tag{84}$$

$$-10\ ^\circ\text{C} \leq T_N \leq \ldots \leq T_1 \leq 20\ ^\circ\text{C} \tag{85}$$

$$\tau_1 = \ldots = \tau_N \tag{86}$$

$$\sum_{i=1}^{N} \tau_i \leq 15\ \text{hr} \tag{87}$$

The NLP formulation here is described to minimise total costs; if the formulations were to maximise profits or Net Present Value (*NPV*), it is possible that different residence times would be preferred. Formulating the objective function as *NPV* (for maximisation) requires the estimation of product sales revenues. While API class sales trends have been historically increasing (Fig. 19), future market sales variations of individual APIs and brands are unknown and cannot be accurately accounted for. For this reason, the objective is instead to minimise the plant total costs. Incorporation of crystal quality constraints (size properties, purity, desired polymorph) in the NLP objective function definition is not considered here, but is important for downstream production and Drug Product efficacy. Varying the objective function definition of an optimisation problem can give differing optimal design and operating parameters; comparison of optimisation results for a different objective function formulation here could be useful, given the availability of reliable projected API and brand sales prices.

The optimisation problem is solved in MATLAB using the interior-point algorithm with tolerances of 10^{-6}. The problem was solved separately for all combinations of API = {cyclosporine,

paracetamol, aliskiren}, number of implemented crystallisers, N = {1, 2, 3}, and plant capacity, $\mathcal{Q}_{\text{API}}$ = {10^2, 10^3, 10^4} kg API yr^{-1}, i.e., 9 problem instances in total.

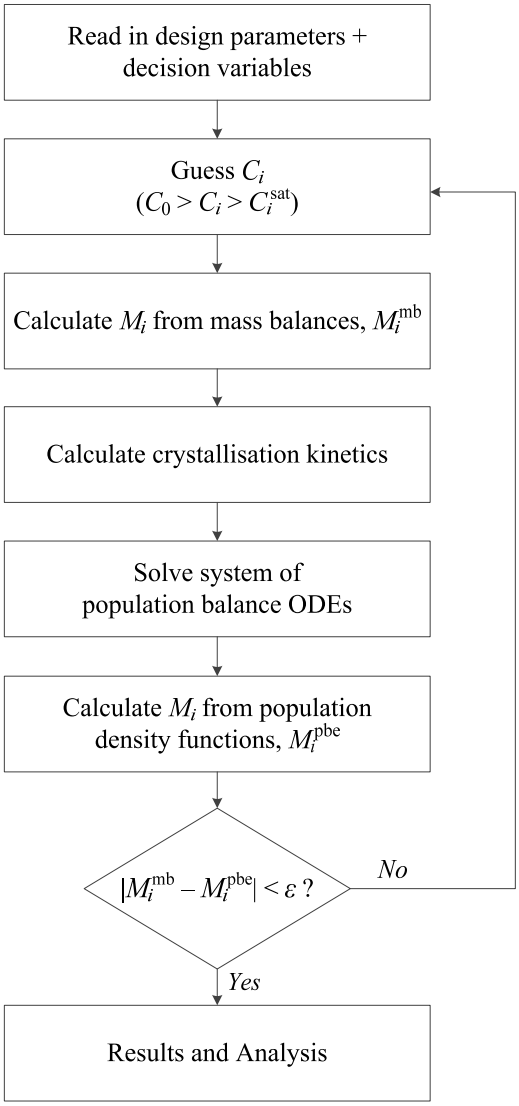

Figure 47: Solution algorithm for the MSMPR crystallisation model.

Multiple initial values for decision variables have been used to ensure a unique optimal solution for each problem instance. Different combinations of initial temperature of each crystalliser were selected based upon values evenly distributed between lower and upper permissible temperature bounds (Eq. 85). Different combinations of initial residence times were chosen such that their sum was less than the maximum allowable value (Eq. 87). The temperature and residence time of each crystalliser in series are the decision variables of the nonlinear optimisation problem; thus, the number of decision variables for configurations consisting of N crystallisers = $2N$. Table 21 shows the combinations of starting points used for varying numbers of crystallisers for each API and considered plant capacity. Each problem instance resulted in a unique solution, independent of the starting point.

Table 21: Decision variable initial values for and plant capacities for different numbers of crystallisers.

N	Decision Variable	Initial Value	No. points, $\boldsymbol{T_0} \times \boldsymbol{\tau_0}$
1	$\boldsymbol{T_0} = T_{1,0}$ (°C)	{ -5 , 0 , 5 }	9
	$\boldsymbol{\tau_0} = \tau_{1,0}$ (hr)	{ 3 , 8 , 13 }	
2	$\boldsymbol{T_0} = [T_1, T_2]_0$ (°C)	{ [-5,-5] , [0,-5] , [10,5] , [15,15] }	20
	$\boldsymbol{\tau_0} = [\tau_1, \tau_2]_0$ (hr)	{ [3,3] , [3,6] , [3,9] , [6,3] , [9,3] }	
3	$\boldsymbol{T_0} = [T_1, T_2, T_3]_0$ (°C)	{ [-5,-5,-5] , [0,-5,-5] , [5,0,0] , [10,5,5] , [15,10,10] , [15,15,15]	24
	$\boldsymbol{\tau_0} = [\tau_1, \tau_2, \tau_3]_0$ (hr)	{ [3,3,3] , [3,3,6] , [3,6,3] , [6,3,3] }	

7.2.2 Total Cost Components

Total cost minimisation via NLP optimisation was implemented for each API (cyclosporine, paracetamol and aliskiren), for a varying number of crystallisers and plant capacity. Fig. 48 shows total cost components, which illustrates the decreasing contribution of *CapEx* components to total costs. Total *CapEx* increases with plant API capacity due to the need for larger crystalliser volumes to contain higher throughputs of crystallisation magma. Total *CapEx* values are dominated by *BLIC* contributions due to the high cost of crystallisation equipment, and *WCC* contributions increase with plant capacity as it is a linear function of material requirements. Both *BLIC* and *WCC* contributions increase with the number of implemented crystallisers, despite decreasing total crystallisation volumes and material requirements. This is due to the cost of additional pumps and cooling equipment accompanying the crystalliser cascade for continuous operation.

Fig. 49 illustrates optimal process configurations (i.e., crystalliser operating temperatures and residence times corresponding to total cost minima) for each API with different numbers of crystallisers and API capacities considered. Crystalliser volumes increase with plant capacity to accommodate increased material throughputs. Increasing the number of implemented crystallisers decreases the total crystallisation volume required. MSMPR operation assumes perfectly mixed, homogeneous crystalliser magmas discharging at equilibrium, and thus the crystalliser operates at the exit concentration; implementing multiple crystallisers increases product concentrations and thus increases yields, which thus requires smaller crystallisers for a given capacity. Total residence times for aliskiren are long due to the slow crystallisation kinetics of the API (and hence its good suitability for MSMPR operation) in accordance with experimental demonstrations.[92]

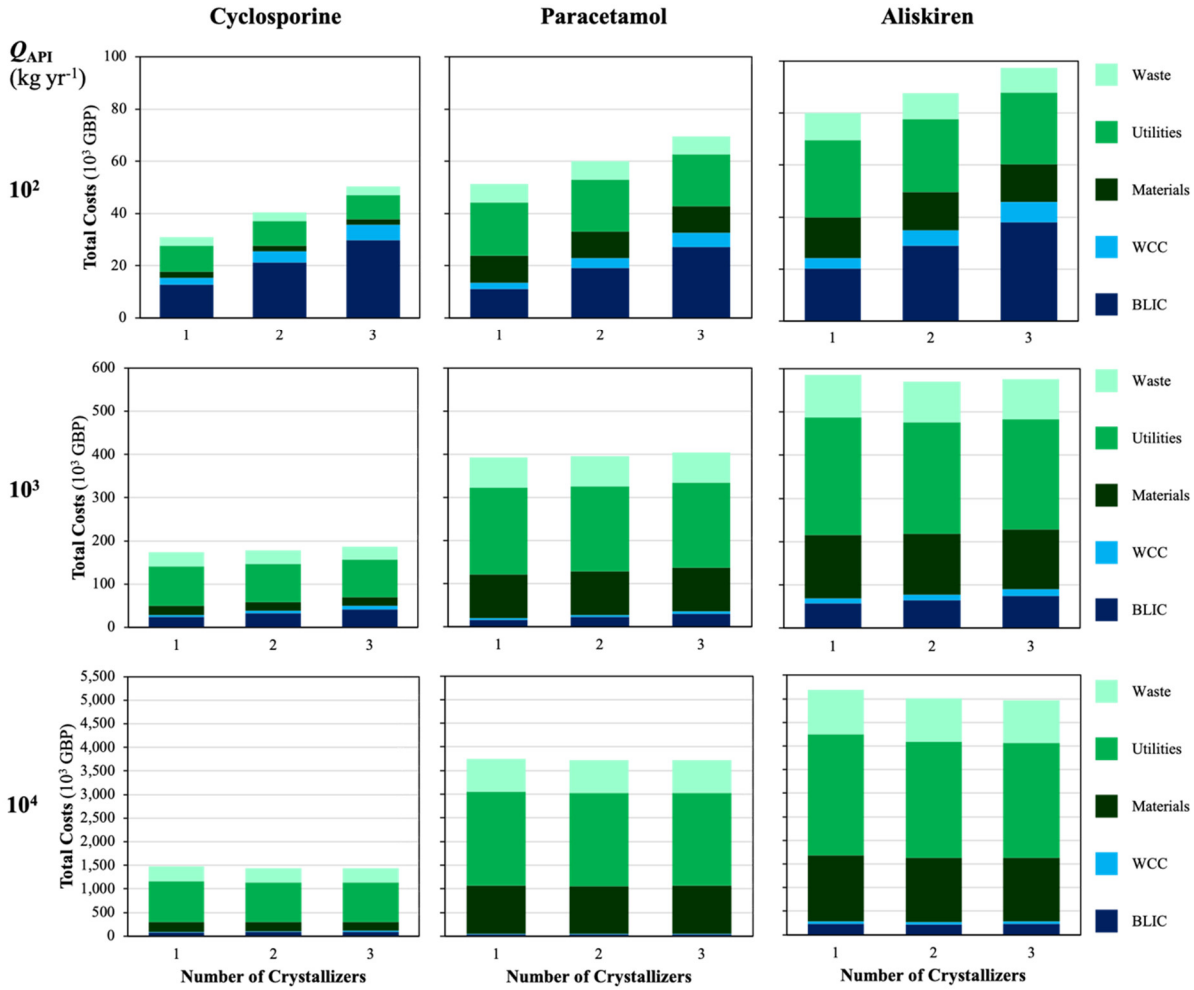

Figure 48: Minimum total cost components for cyclosporine, paracetamol and aliskiren at different plant capacities.

Crystalliser design capacities (i.e., volumes) required for the considered plant capacities are at the lower end of the cost correlation application range, and thus purchase cost overestimation may be present. Additional uncertainty in calculated crystalliser purchase costs is present due to the lack of cost estimation methods for smaller crystalliser volumes associated with lower plant capacities, e.g., cyclosporine at Q_{API} = 10^2 kg API yr^{-1}; however, the cost correlation used here is the best available in the literature.

Total *OpEx* increases with plant API capacity due to the higher required material throughputs and associated utilities and waste handling costs. Fig. 50 shows the fractional relative minimum total cost component contributions for each API at varying plant capacities for one crystalliser. At lower API capacities, *CapEx* contributions are more significant; as plant capacity increases, *OpEx* component contributions become more significant, which is further illustrated by their continuing dominance over normalised *CapEx* components as plant API capacities increase. Utilities costs

dominate *OpEx* contributions, however materials and waste handling costs become more significant with increasing plant capacity.

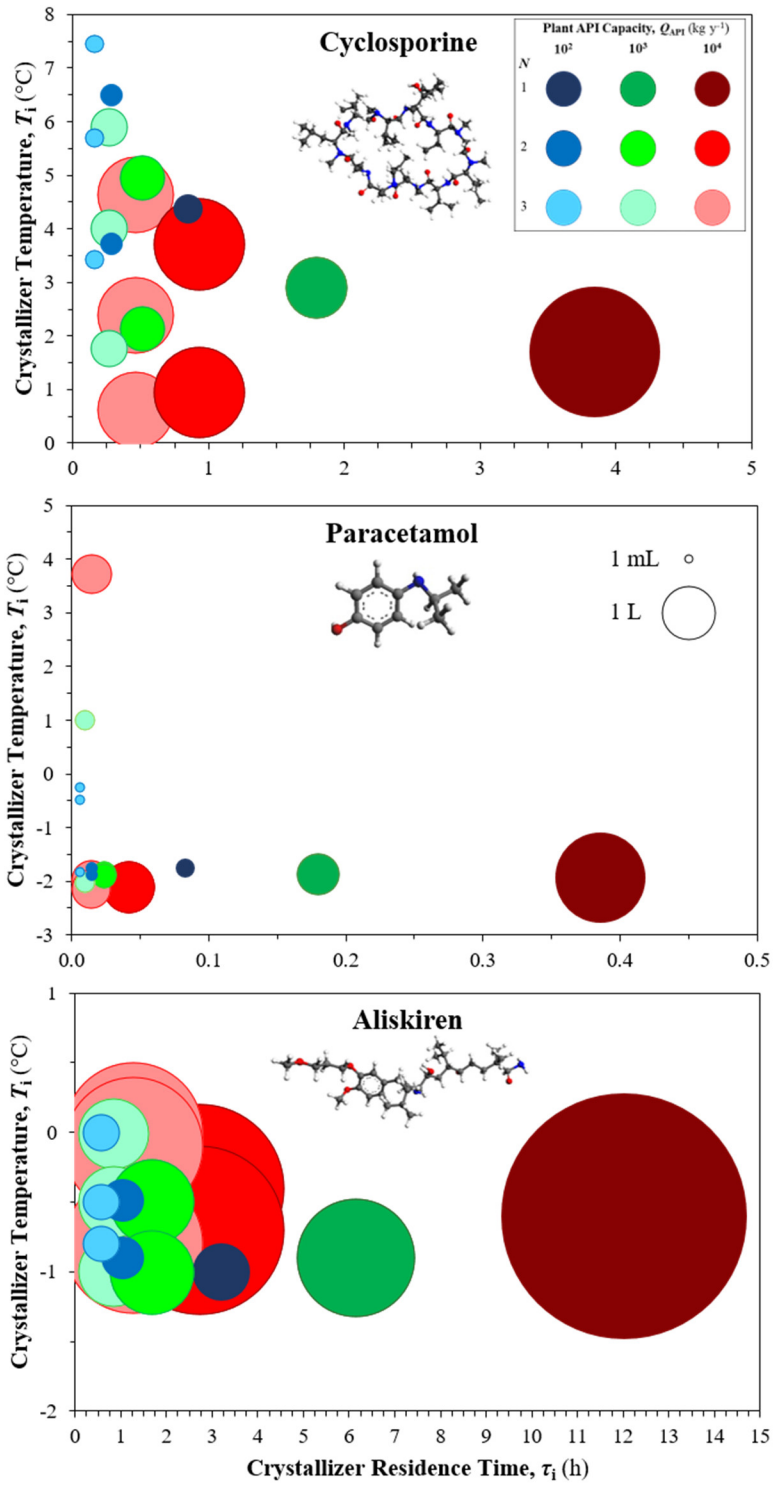

Figure 49: Crystalliser operating temperatures and residence times corresponding to total cost minima for cyclosporine, paracetamol and aliskiren; bubble diameters are proportional to crystalliser volumes. For $N > 1$, different bubbles correspond to different crystallisers at different operating temperatures ($T_1 \geq \ldots \geq T_N$).

Cyclosporine operating temperatures are above zero and decrease along the crystalliser cascade (Fig. 49), as described in the NLP constraints. Crystallisers for paracetamol and aliskiren also decrease in temperature along cascades, however, operate at lower temperatures. In both cases, as the number of implemented crystallisers is increased, operating temperatures increase and residence times decrease; additional costs associated with increased cooling duties and larger crystallisers are not considered beneficial with respect to total costs. Rigorous temperature control via high-fidelity instrumentation can ensure designs remain at their optimal design parameters. The implementation of Process Analytical Technology (PAT) is essential for the success of CPM technologies, with recent studies illustrating its importance in crystallisation applications.[232] Optimal crystalliser operating temperatures correspond to those required to attain minimum total costs of a design option; deviations from optimum design and operating parameters will lead to sub-optimal designs (i.e., higher total costs).

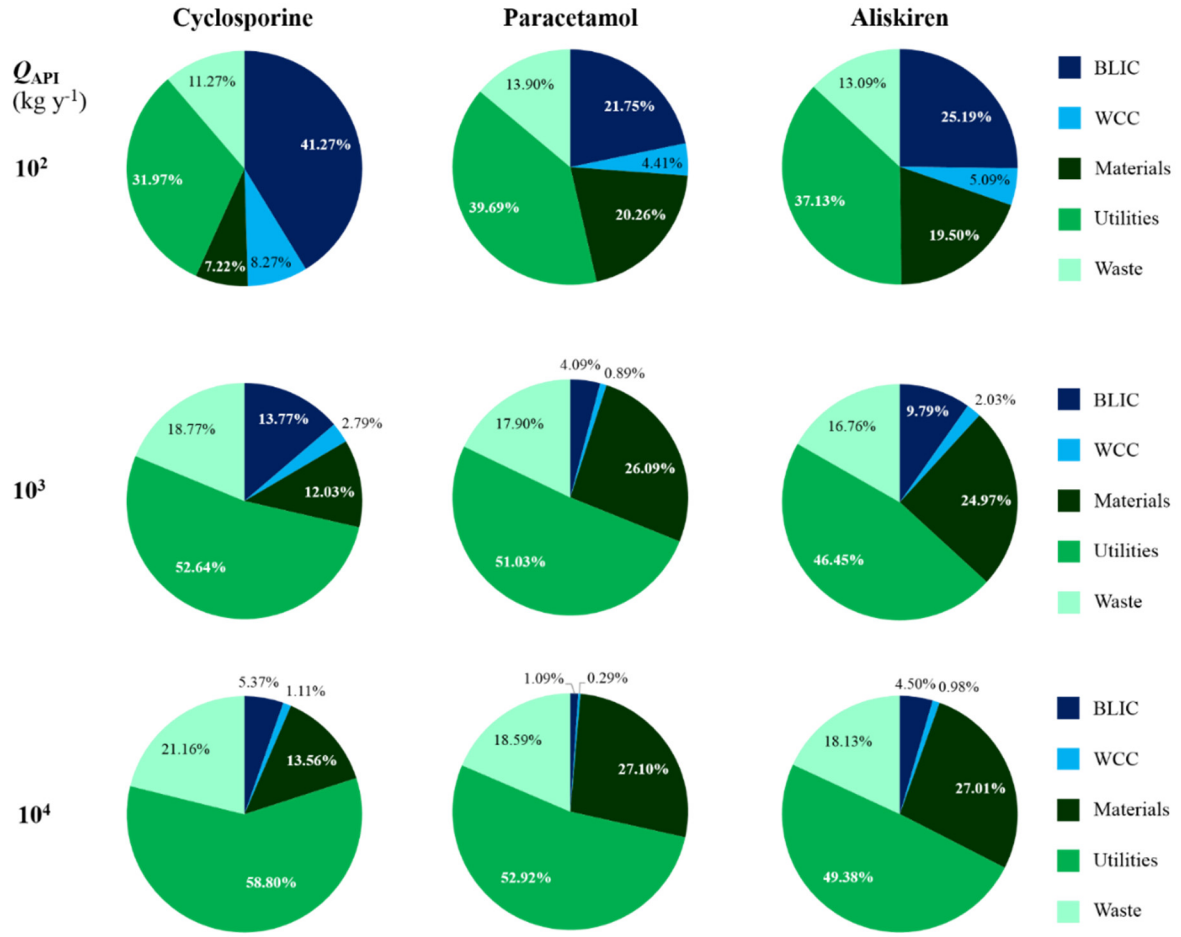

Figure 50: Component contributions towards total costs when implementing one crystalliser for cyclosporine, paracetamol and aliskiren.

Minimum total costs for cyclosporine crystallisation are attained when implementing one crystalliser only for API capacities of 10^2 and 10^3 kg API yr^{-1} (see Fig. 48). Yield improvements associated with multiple crystalliser usage are only incremental; thus, the associated additional *BLIC* costs are not beneficial. However, when the plant capacity is increased to 10^4 kg API yr^{-1}, cyclosporine crystallisation has lower total costs when two crystallisers are implemented. At higher capacities, *OpEx* components dominate total costs, and so even incremental increases in crystallisation yield and distributed cooling loads across crystallisers can bring cost savings benefits.

For plant capacities of 10^2 and 10^3 kg API yr^{-1}, paracetamol crystallisation is cost optimal when implementing one crystalliser due to incremental yield improvements attainable with multiple crystalliser implementation at these capacities. Implementing two crystallisers is optimal at a plant capacity of 10^4 kg API yr^{-1}; this is due to the greater contribution of *OpEx* towards total costs at increased capacities as well as the reduced total crystalliser volume required.

Continuous crystallisation of aliskiren at a plant capacity of 10^2 kg API yr^{-1} is cost optimal when implementing one crystalliser only; implementing two crystallisers at a capacity of 10^3 kg API yr^{-1} and three crystallisers at 10^4 kg API yr^{-1} is more cost effective. The mother liquor solvent considered here (ethyl acetate:ethanol mixture) is more expensive than solvents for cyclosporine and paracetamol, thus material costs contribute more towards the dominant *OpEx* components.

For the considered APIs and number of implementable crystallisers (N = {1, 2, 3}), multiple crystalliser usage is favoured as capacity increases. It is likely that there is some maximum number of crystallisers that allow minimum total costs for capacities beyond a certain value, however this cannot be stated with certainty from the results presented here; this can be clarified in future work. Total cost minimisation at higher capacities can be investigated in the described modelling framework and methodology.

The relative effect of varying crystallisation kinetics between the considered APIs varies with the plant capacity. For $Q_{API} = 10^2$ kg API yr^{-1}, cyclosporine *CapEx* components are significantly more dominant than at higher capacities for this API; material costs (*OpEx*) are less significant at lower capacities and thus the effect of cyclosporine's slow crystallisation kinetics on *CapEx* (requiring longer residence times and crystalliser volumes) become more significant. *CapEx* component contributions for aliskiren are greater than those for paracetamol due to its slower crystallisation kinetics. For both aliskiren and paracetamol, *OpEx* components are more significant even at $Q_{API} = 10^2$ kg API yr^{-1} as these APIs both require more expensive solvent components than cyclosporine. The current modelling methodology and framework allows different APIs, capacities

and numbers of implemented MSMPR crystallisers to be considered easily, given the availability of crystallisation kinetic parameters and API temperature-dependent solubility data.

7.3 Chapter Conclusions

This work has conducted total cost minimisation of continuous MSMPR crystalliser cascades for three societally and economically important APIs widely produced by the pharmaceutical industry: cyclosporine, paracetamol and aliskiren. Nonlinear optimisation results show that the optimal number of crystallisers attaining minimal total costs is dependent on plant capacity. For the considered APIs, implementing one crystalliser is preferred at lower capacities, whilst multiple crystalliser usage is preferred at higher plant capacities. This result is observed due to the increasing dominance of operating expenditure contributions towards total costs at increased capacities, making the benefits of implementing more crystallisers (enhanced yields, reduced utility loads) worth the increased capital expenditure of purchasing multiple crystallisation units. This work has illustrated the value of conducting technoeconomic optimisation studies such as this towards the development of continuous separations in pursuit of economically viable end-to-end CPM plants.

PART IV

PROCESS SYNTHESIS VIA MIXED-INTEGER NONLINEAR PROGRAMMING

Chapter 8

Atropine

This chapter describes the steady-state modelling and MINLP optimisation for process synthesis for CPM of atropine based on the published continuous flow synthesis, developing a conceptual continuous LLE process for reaction effluent purification, based upon the flowsheet in Chapter 2 (Fig. 18). All relevant material properties are listed in Table 22.

The results presented in this chapter have also been published in the literature (Diab et al., *Comput. Chem. Eng.* **2019**, *124*, 28–42; Diab et al., *Comput. Aided Chem. Eng.* **2019**, *46*, 211–216; Diab and Gerogiorgis, *AIChE J.* **2019**, *65*(11), e16738); details can be found in Appendix B.

Table 22: Atropine CPM component physical properties.[191,192]

Type	Component	CAS #	Formula	MW (g mol^{-1})	m.p. (°C)	b.p. (°C)	ρ (g cm^{-3})	μ (mPa s)
Reagent	Tropine	120-29-6	$C_8H_{15}NO$	141.21	64.0	233.0	1.02	–
	DMF	68-12-2	C_3H_7NO	73.09	–60.5	153.0	0.95	0.92
	Phenylacetyl chloride	103-80-0	C_8H_7ClO	154.59	–	94.5	1.17	–
	Sodium hydroxide	1310-73-2	NaOH	40.00	318.0	1,388.0	2.13	–
	Water	7732-18-5	H_2O	18.02	100.0	0.0	1.00	1.00
	Formaldehyde	50-00-0	CH_2O	30.03	–92.0	–19.0	0.82	–
	API	51-55-8	$C_{17}H_{23}NO$	289.37	118.5	–	1.21	–
	Apoatropine	207-906-7	$C_{17}H_{21}NO$	271.36	62.0	–	–	–
	Hydrogen chloride	7647-01-0	HCl	36.46	–114.2	–85.1	1.49	–
LLE	Ammonium chloride	12125-02-	NH_4Cl	53.94	338.0	520	1.52	–
	Dichloromethane, DCM	75-09-2	CH_2Cl_2	84.93	–96.7	39.6	1.33	0.43
	Diethyl ether, Et_2O	60-29-7	$C_4H_{10}O$	74.12	–116.3	34.6	0.71	0.22
	Butyl acetate, BuOAc	123-86-4	$C_6H_{12}O$	116.16	–78.0	126.1	0.88	0.69
	Toluene	108-88-3	C_7H_8	92.14	–95.0	111.0	0.87	0.59

8.1 Reaction Kinetic Parameter Estimation

Kinetic parameter estimation from available experimental reaction performance data should be implemented where possible to gain an understanding of kinetic behaviour and for PFR sizing. For the esterification reaction, the published continuous flow synthesis reports 99% conversion to tropine ester at 100 °C in a residence time of 3.5 min.[177] As time-dependent kinetic data is not

available for this reaction, this work assumes the same reported performance; given the availability of a wider dataset for this reaction, kinetic parameter estimation can be performed, which will deepen insight into its kinetic behaviour.

For the aldol addition, conversions of **5** of 67% and 78% are attained after 8 min and 24 min, respectively, at 100 °C, using 6.0. equiv. formaldehyde with 1.2 equiv. NaOH (aq.) added to the effluent of PFR-1 prior to entering PFR-2.[177] This data is used to compare candidate rate law expressions for PFR-2; by plotting different functions of reagent (tropine ester and formaldehyde) concentrations vs. time, coefficients of determination (R^2) are estimated to determine the goodness of fit of candidate rate law expressions. Zero-order, first-order in limiting reagent tropine ester and overall second-order (first-order in both tropine ester and formaldehyde) rate law expressions are considered. The integral forms of the zero-, first- and second-order rate laws are written as Eqs. 88–90, respectively; these give linear functions of reagent concentration vs. time from which reaction rate constants can be estimated.

$$C_{\mathbf{5}} = C_{\mathbf{5},0} - k_0 \tau_{\mathrm{PFR}} \tag{88}$$

$$\ln\left(\frac{C_{\mathbf{5}}}{C_{\mathbf{5},0}}\right) = -k_1 \tau_{\mathrm{PFR}} \tag{89}$$

$$\ln\left(\frac{C_{\mathbf{5},0} C_{\mathrm{CH_2O}}}{C_{\mathbf{5}} C_{\mathrm{CH_2O},0}}\right) = k_2 \left(C_{\mathrm{CH_2O},0} - C_{\mathbf{5},0}\right) \tau_{\mathrm{PFR}} \tag{90}$$

Functions of reagent concentrations vs. time representing candidate rate law expressions considered here are plotted in Fig. 51. An overall second-order (first in **5**, first in formaldehyde) rate law is the most plausible case (R^2 = 0.890), followed by a first-order rate law (R^2 = 0.670), followed by a zero-order rate law (R^2 = 0.512) of the candidate rate law expressions considered here. The second-order rate law constant for the aldol addition reaction is estimated as k_2 = 1.68 L mol^{-1} hr^{-1}. Greater availability of kinetic data for the reaction set will allow further validation of kinetic parameter estimation results, allow investigation of more complex candidate rate law expressions and allow explicit consideration of the elimination of API to apoatropine. The dataset size per regression should be as large as reasonably possible, i.e., enough to establish whether a linear relationship is present whilst considering the effects of noise. However, the required experimental effort in terms of time and labour to generate sufficiently large datasets for multiple reactions is an important consideration in kinetic data acquisition, warranting the consideration of simulation and model optimisation to aid such efforts.[54,233] From the limited published data, approximately 39.2% of API formed converts to apoatropine;[177] this is considered in mass balance and equipment sizing calculations.

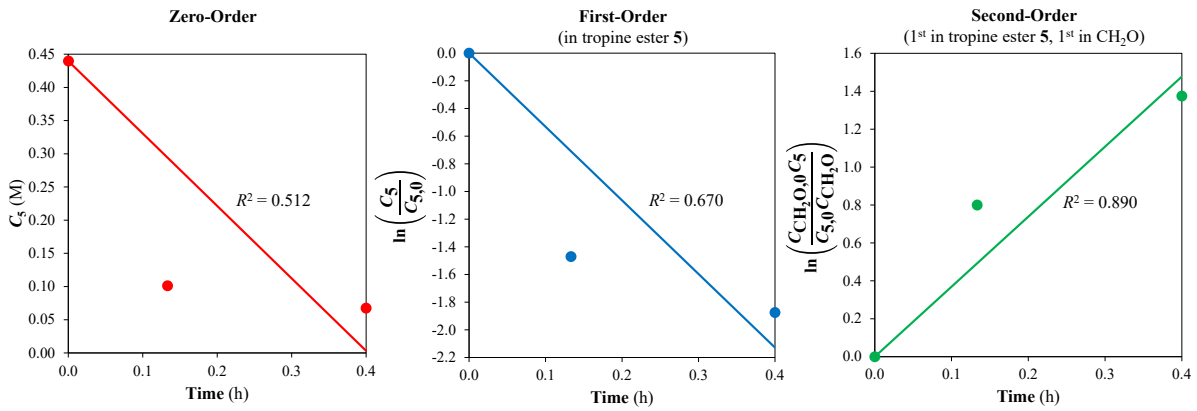

Figure 51: Comparison of goodness of fit of candidate rate law expressions for the aldol addition from experimental kinetic data for atropine CPM.

8.2 Dimensionless Number Analysis for Reactor Diameter Selection

Selecting an appropriate PFR inner diameter (d_{PFR}) is an important consideration in reactor design for continuous flow synthesis to ensure the benefits of enhanced heat and mass transfer demonstrated on lab-scale are realised at larger production scales, as well as considerations of process safety and operability of inherently hazardous reactions. Here, we calculate the required PFR diameters and the corresponding reactor lengths for different designs to ensure the assumption of homogeneity is valid and to maximise the benefits of synthesising atropine in continuous flow. Turbulent flow conditions (i.e., homogeneous velocity profile) are ensured by designing PFRs such that their diameter allows for a Reynolds number (*Re*, Eq. 91) > 4,000. The Péclet number (*Pe*, Eq. 82) describes the ratio of convective to conductive heat transfer; it is desired that $Pe \geq 1$ to ensure reactor temperature homogeneity.

$$Re_{PFR} = \frac{\rho_m u_{PFR} d_{PFR}}{\mu_m} \tag{91}$$

$$Pe_{PFR} = \frac{u_{PFR} L_{PFR} \rho_m C_{p,m}}{\lambda_m} \tag{92}$$

Here, u_{PFR} is the average fluid mixture velocity in the PFR (calculated from the volumetric flowrate, Q_{PFR}, and the cylindrical cross section), L_{PFR} is the PFR length and $C_{p,m}$ and λ_m are the mixture specific heat capacity at constant pressure and thermal conductivity, respectively. Mixture viscosities (μ_m) and densities (ρ_m) are calculated from solvent components (DMF + H_2O) at the reactor temperatures (both T = 100 °C) as solvent content is ≥ 90 mol% in both PFRs.

The Damköhler number, *Da*, describes the ratio of reaction to mixing time-scales: it is desired that $Da \leq 1$ to ensure that sufficient mixing occurs before reaction so there are negligible radial

concentration gradients at any axial position in the PFR. Here, D_i is the reagent diffusivity (Eq. 93), k_b is the Boltzmann constant, μ_m is the mixture viscosity and r_i is the component molecular radius. First-order kinetics are assumed for reaction 1 in PFR-1 and overall second-order (first-order in both limiting reagent A and excess reagent B with stoichiometric feed quantities) are considered for reaction 2a in PFR-2. The expression for *Da* depends on the rate law expression of the reaction.[71,234,235] First-order kinetics in limiting reagent A describe *Da* via Eq. 94; overall second-order (first-order in both limiting and excess reagent A and B, respectively) kinetics for stoichiometric feed quantities describe *Da* by Eqs. 95 and 96.

$$D_i = \frac{k_b T}{6\pi\mu_m r_i} \tag{93}$$

$$Da_A = -\ln(1 - X_A)\frac{d_{PFR}^2}{4\tau_{PFR} D_A} \qquad \text{for first-order kinetics in A} \tag{94}$$

$$Da_A = \frac{\Theta_B}{\Theta_B - 1}\ln\left(\frac{\Theta_B - X_A}{\Theta_B - \Theta_B X_A}\right)\frac{d_{PFR}^2}{4\tau_{PFR} D_A} \qquad \text{for first-order in both A and B (non-stoichiometric)} \tag{95}$$

$$Da_B = \frac{Da_A}{\Theta_B} \tag{96}$$

To ensure homogeneity in the reaction mixture for both PFRs, the critical diameters allowing homogeneous velocity ($Re \geq 4{,}000$), temperature ($Pe \geq 1$) and concentration ($Da \leq 1$) are calculated. The following analysis compares the critical diameters corresponding to these dimensionless number values; the smallest diameter allowing for all conditions simultaneously for each reactor is found to establish design values. Values of *Re* and *Pe* are dependent on plant volumetric throughputs, which vary between LLE design cases. Each LLE design case considered for MINLP optimisation vary the LLE solvent implemented and number of implemented LLE tanks (N). The screening of candidate LLE solvents for consideration and MINLP problem formulation are described further in later sections.

The Reynolds number as a function of PFR diameters is plotted for different design cases in Fig. 52. Critical PFR diameters corresponding to $Re = 4{,}000$ vary between design cases, as *Re* is a function of PFR volumetric throughput (Q_{PFR}), which varies between design cases (LLE solvent choice and number of implemented tanks, N), as well as the chosen diameter. A similar analysis of Péclet numbers as a function of diameter between different designs is shown in Fig. 53. Critical diameter values corresponding to $Pe = 1$ are significantly higher than for $Re = 4{,}000$.

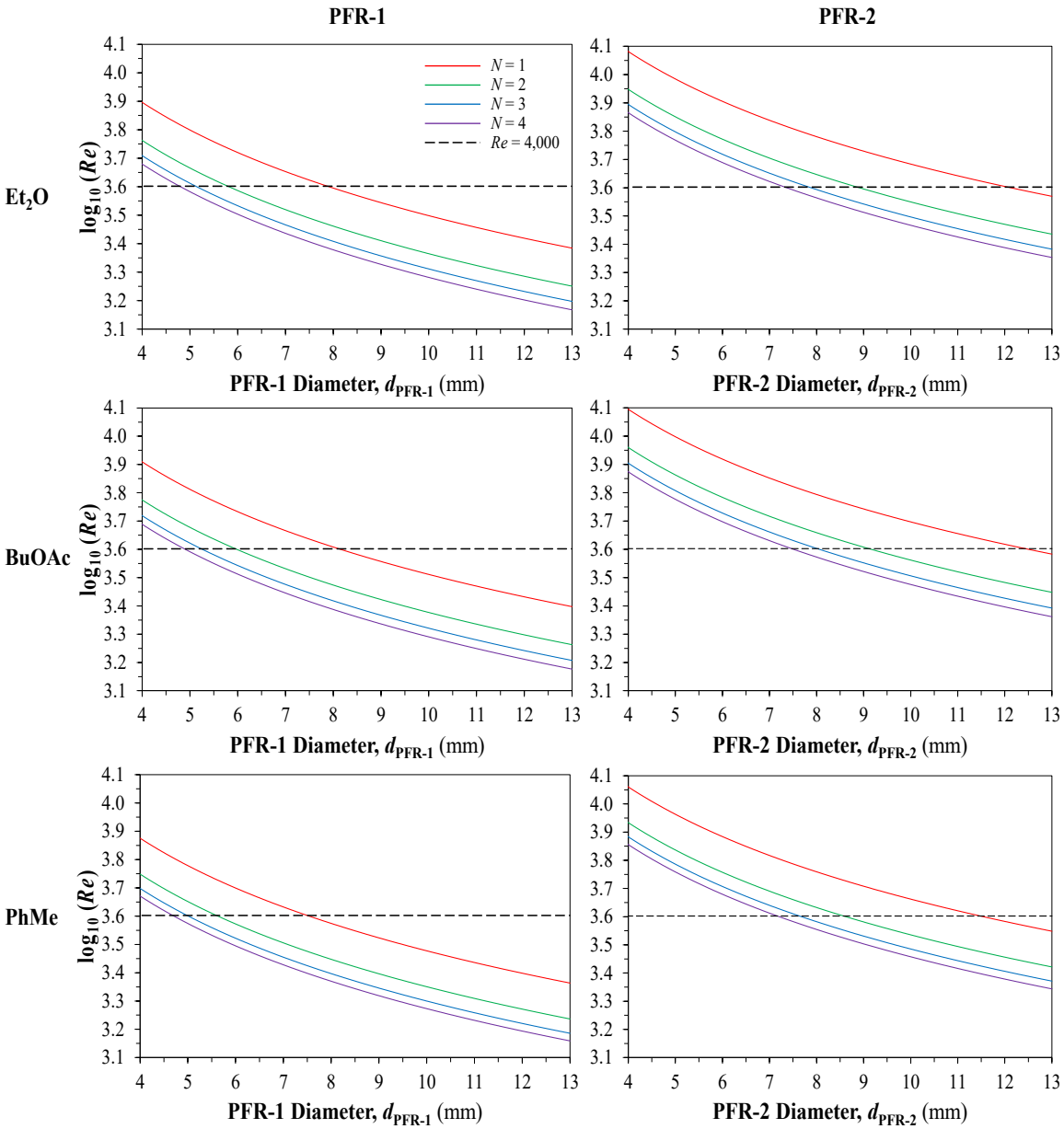

Figure 52: Reynolds number as a function of PFR-diameter for different atropine CPM design cases. LLE solvents: Et_2O = diethyl ether, BuOAc = butyl acetate. *N* = no. LLE vessels.

The Damköhler number is a function of conversion, reactor diameter and residence time. Damköhler numbers for each PFR are the same for different design cases (LLE solvent choice, number of implemented LLE vessels, *N*), as they are independent of volumetric throughput. The Damköhler number of limiting tropine in PFR-1 as well as for limiting tropine ester and excess CH_2O in PFR-2 as a function of PFR diameter is plotted in Fig. 54. The maximum allowable diameters corresponding to $Da = 1$ are much lower than for the critical *Re* and *Pe* values. Ensuring the reaction mixture is sufficiently mixed before reaction occurs is essential to maximise reaction efficiency, which is ensured by keeping $Da \leq 1$. The Damköhler number of limiting tropine ester determines the critical diameter of PFR-2, as $Da_{tropine} << Da_{CH2O}$.

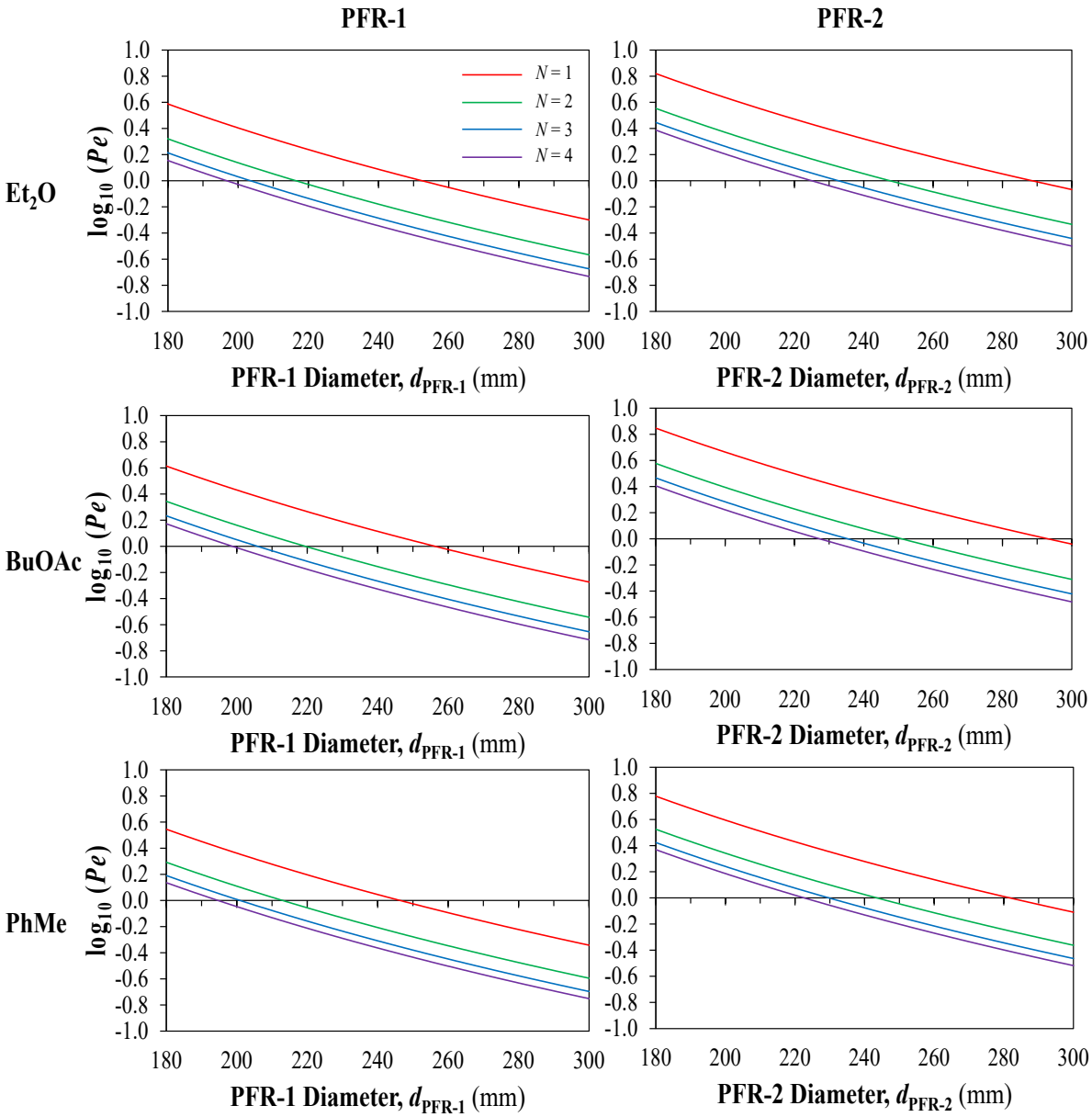

Figure 53: Péclet numbers as a function of PFR diameters for different atropine CPM design cases. LLE solvents: Et_2O = diethyl ether, BuOAc = butyl acetate. N = no. LLE tanks.

Critical diameters corresponding to different dimensionless number analyses and design cases are summarised in Table 23. In all design cases, the Damköhler number gives the lowest critical diameter, i.e. the maximum design value for each PFR diameter, to ensure the assumption of homogeneous reaction mixtures is valid and to maximise the benefits of continuous API synthesis. The maximum allowable PFR diameters are $d_{PFR\text{-}1} \leq 4.03$ mm and $d_{PFR\text{-}2} \leq 3.63$ mm. Design PFR diameters of $d_{PFR} = \{1, 2, 3\}$ mm are chosen to ensure all design values are below the critical values shown in Table 23.

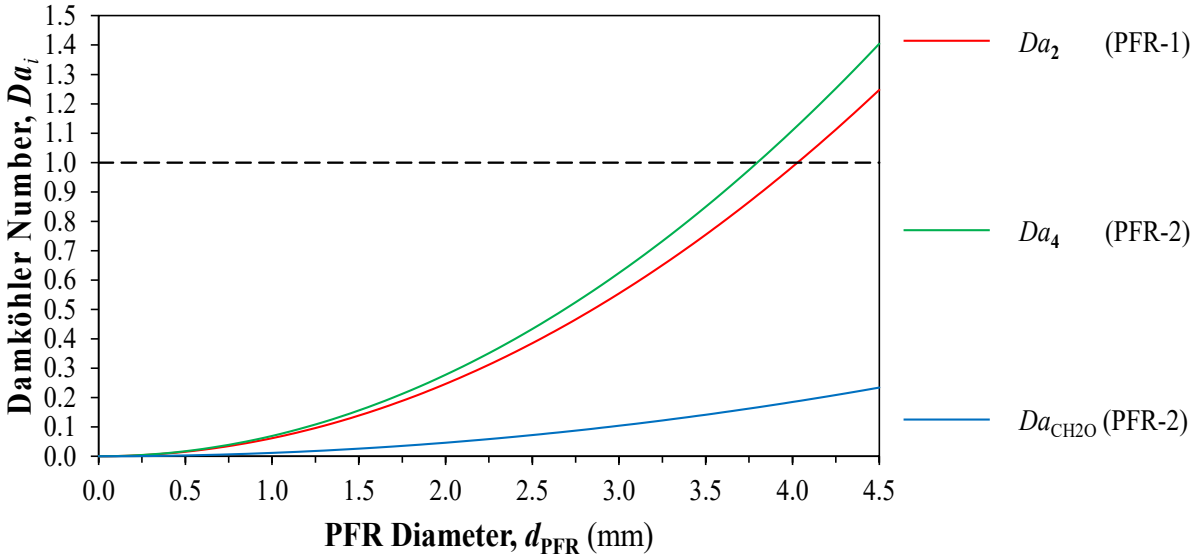

Figure 54: Damköhler number vs. PFR diameter for different atropine CPM design cases.

Table 23: Atropine CPM critical PFR diameters for dimensionless numbers corresponding to homogeneity conditions. LLE solvents: Et_2O = diethyl ether, BuOAc = butyl acetate. N = no. LLE tanks.

Et_2O				**PFR-1**				**PFR-2**
N	Re = 4,000	Pe = 1	Da = 1	$d_{PFR,MAX}$ (mm)	Re = 4,000	Pe = 1	Da = 1	$d_{PFR,MAX}$ (mm)
1	7.87	252.41	4.03		12.06	288.59	3.63	
2	5.79	216.50	4.03	4.03	8.87	247.53	3.63	3.63
3	5.12	203.52	4.03		7.84	232.68	3.63	
4	4.78	196.77	4.03		7.33	224.97	3.63	
BuOAc				**PFR-1**				**PFR-2**
N	Re = 4,000	Pe = 1	Da = 1	$d_{PFR,MAX}$ (mm)	Re = 4,000	Pe = 1	Da = 1	$d_{PFR,MAX}$ (mm)
1	8.12	256.34	4.03		12.44	293.08	3.63	
2	5.95	219.44	4.03	4.03	9.12	250.90	3.63	3.63
3	5.24	205.89	4.03		8.02	235.40	3.63	
4	4.88	198.76	4.03		7.48	227.25	3.63	
PhMe				**PFR-1**				**PFR-2**
N	Re = 4,000	Pe = 1	Da = 1	$d_{PFR,MAX}$ (mm)	Re = 4,000	Pe = 1	Da = 1	$d_{PFR,MAX}$ (mm)
1	7.50	246.39	4.03		11.49	281.70	3.63	
2	5.61	212.98	4.03	4.03	8.59	243.50	3.63	3.63
3	4.99	200.93	4.03		7.64	229.72	3.63	
4	4.68	194.70	4.03		7.18	222.60	3.63	

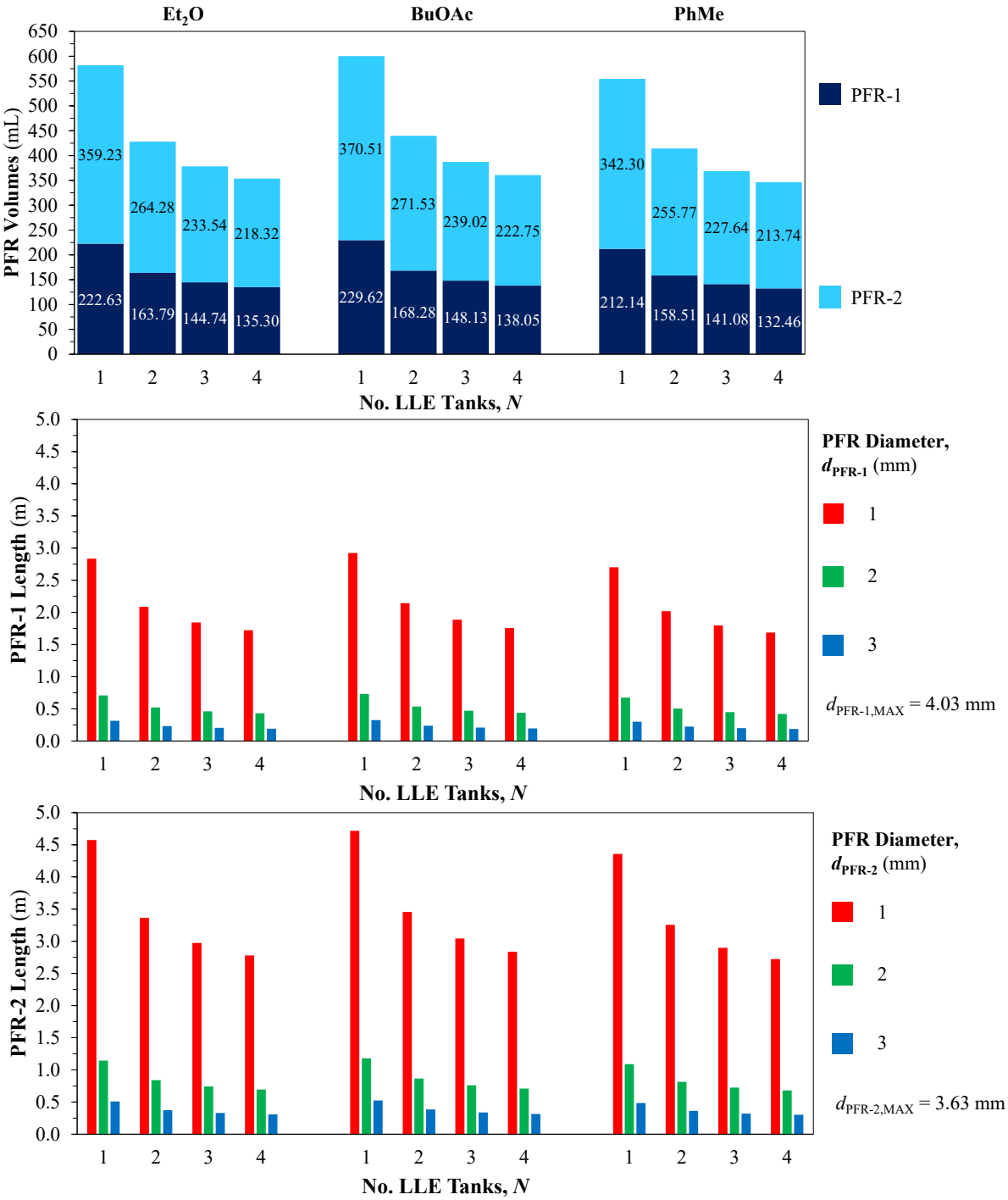

Figure 55: Computed PFR volumes and lengths for different diameters for atropine CPM.

Process flowrates and required PFR volumes are calculated as in Chapter 3.3. Fig. 55 shows computed reactor volumes for PFR-1 and 2 for different optimised MINLP problem instances of different LLE solvent and numbers of tanks (N). For all LLE solvent choices, $V_{PFR-2} > V_{PFR-1}$ due to the larger volumetric flowrate through PFR-2 due to the greater number of reagents (reactants + solvents + other) at this point in the process flowsheet (Fig. 18) as well as τ_{PFR-2} being slightly longer than τ_{PFR-1}. Increasing the number of vessels decreases the volumes of both PFRs and the

total reaction volume required for atropine continuous flow synthesis due to the corresponding increasing LLE efficiency, which in turn increases plantwide efficiency and reduces the total material throughput required to meet the desired plant API capacity ($\dot{Q}_{API}$) and thus the PFR volumes. The current modelling framework can easily consider alternate values of $\dot{Q}_{API}$ to investigate the effect of varying plant capacity on all MINLP optimisation results.

Fig. 55 also shows resulting PFR lengths for various diameter values. Design reactor diameter values of $d_{PFR} = \{1, 2, 3\}$ mm are considered, as these are safely below the critical diameter values for homogeneous reaction mixtures (Table 23). In all cases (cost optima for different problem instances), resulting reactor lengths are feasible and appropriate for the given plant capacity ($\dot{Q}_{API}$) and for the assumption of homogeneous reaction mixture implemented in this work. Although smaller diameters are preferable, the resulting PFR length is an important consideration for the equipment footprint and implemented heating media in which PFRs will be immersed. Coiling reactors can also allow for easier heat exchange and immersion in necessary heat transfer media.

Table 24: Initial list of candidate LLE solvents for atropine CPM.

Class	LLE Solvent	Notation	L-L Equilibria		Partition Coefficient	Classification		Consider
			Exptl.	UNIFAC?		FDA[203]	GSK[223]	
Alkanes	Hexane	nHex	✓	✓	X	2		X
	Heptane	nHep	✓	✓	X	3		X
Chloroalkanes	Dichloromethane	DCM	✓	✓	177	2		X
	Chloroform	TCM	✓	✓	X	2		X
Alcohols	1-Butanol	BuOH	✓	✓	X	3		X
Ketones	Methyl ethyl	MEK	✓	✓	X	3		X
Esters	Ethyl acetate	EtOAc	✓	✓	X	3		X
	Butyl acetate	BuOAc	✓	✓	177	3		✓
Aromatics	Toluene	PhMe	✓	✓	177	2		✓
Ethers	Diethyl ether	Et_2O	✓	✓	177	3	(–)	✓

8.3 Candidate Separation Solvent Screening

Appropriate solvent selection for LLE design is imperative due to its significant effect on material usage and impact on process performance. Table 24 provides an initial list of LLE solvents based on the attainability of immiscible mixtures, API partition coefficient data in the ternary system DMF + H_2O + LLE solvent and EHS classification by the FDA and a GSK solvent classification guide.[223] The FDA classes solvents as class 1 (should be avoided), 2 (should be limited) and 3 (lower risk), while the GSK guide classifies solvents as "red" (major issues), "amber" and "green"

(few issues). The chosen LLE solvent must be able to form an immiscible mixture with the incoming binary DMF + H_2O solvent mixture (all those listed in Table 24), have API partition coefficient data available and be suitable based on EHS criteria, i.e., FDA classification > 1 and "green" or "amber" based on the GSK guide. The considered LLE solvents in this work are diethyl ether (Et_2O), butyl acetate (BuOAc) and toluene (PhMe).

8.3.1 Ternary Phase Diagrams

Modelling of candidate continuous LLE designs requires liquid-liquid equilibria data for the ternary solvent system DMF + H_2O + LLE solvent. The ternary diagrams of the considered LLE solvents are shown in Fig. 56, estimated by solution of the UNIFAC model for liquid-liquid equilibria (see Chapter 3.4);[236] all options have a high propensity to form multiphase mixtures, i.e., exhibit rapid phase splitting in a wide operating region.

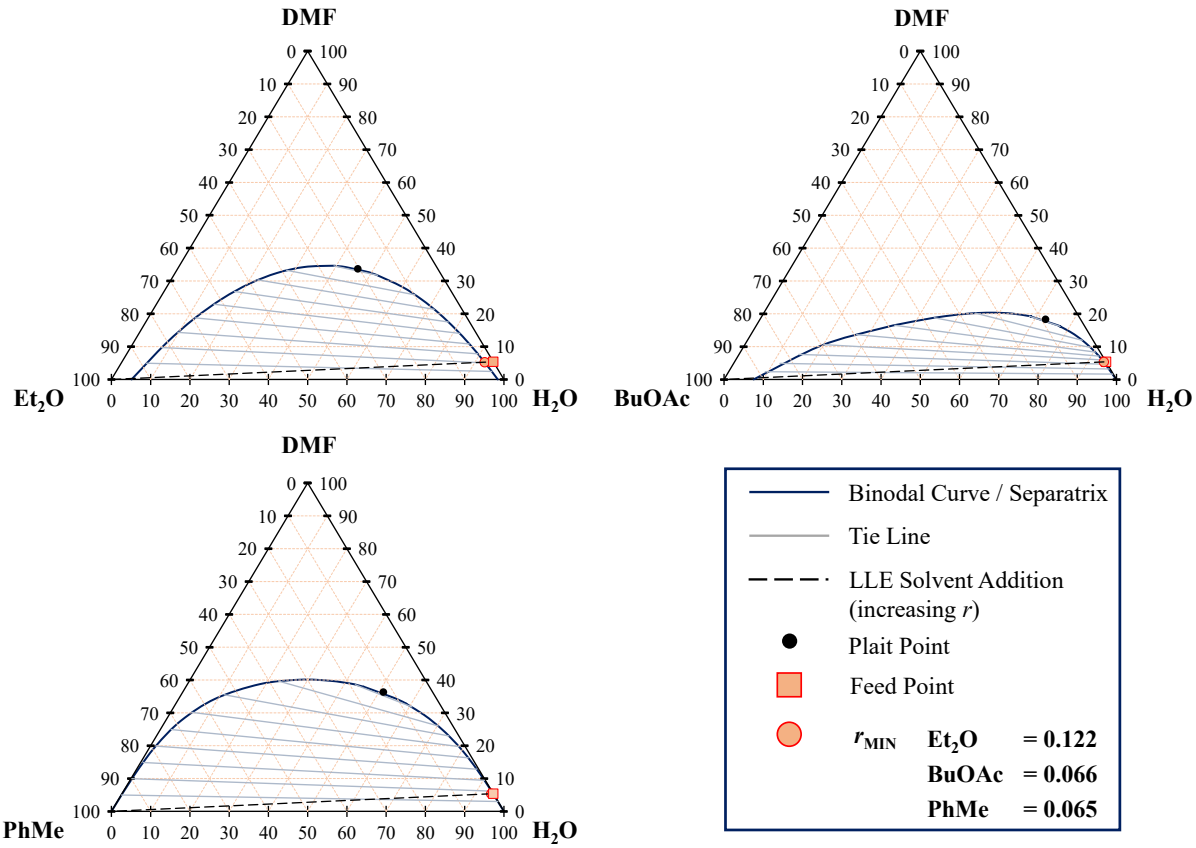

Figure 56: Ternary phase diagrams for the system DMF + H_2O + LLE solvent (Et_2O, BuOAc, PhMe) computed via the UNIFAC model (T_{LLE} = 25 °C) for atropine CPM.

Fig. 56 also shows the LLE feed point (DMF + H_2O mixture) compositions before LLE solvent (Et_2O, BuOAc, PhMe) addition and minimum r required to form an immiscible mixture = r_{MIN}, which is the point where the line of LLE solvent addition (between the DMF + H_2O feed point

and the pure LLE solvent corner on the ternary phase diagrams) intersects the binodal curve/separatrix (the boundary of compositions separating miscible and immiscible regions, estimated via UNIFAC). Values of r_{MIN} vary between different ternary systems due to the differing thermodynamic behaviour between them, e.g., the r_{MIN} value for the ternary system containing Et_2O is higher than for BuOAc and PhMe systems due to the smaller envelope of immiscibility. To remain safely within the immiscible region in the design of different LLE processes, a minimum value of $r \geq 0.20$ is chosen.

8.3.2 Modelling of Phase Compositions

Estimation of LLE phase compositions are required for calculation of phase properties (densities, viscosities, surface tensions) for continuous LLE efficiency estimation. Varying the LLE solvent-to-feed ratio (r) affects resulting phase compositions, quantities and physical properties that consequently affect LLE efficiency. Modelling of phase compositions is implemented via surrogate polynomials, expressing solvent component compositions in organic and aqueous phases as functions of r via Eq. 97, where $x_{i,p,}^{S}$ is the mole fraction of component i in phase p for the solvent system DMF + H_2O + S and α, β and γ are the quadratic polynomial coefficients. Partition coefficients of API between organic and aqueous phases for different solvent systems at T_{LLE} = 25 °C are taken from the literature.[177] Table 25 provides coefficient values for Eq. 97 for each solvent system, solvent component and phase.

$$x_{i,p}^{S} = \alpha_{i,p}^{S} r^2 + \beta_{i,p}^{S} r + \gamma_{i,p}^{S} \tag{97}$$

Table 25: Coefficients for Eq. 97 estimating ternary phase compositions of the system DMF + H_2O + LLE solvent (S) for atropine CPM based upon extensive UNIFAC modelling.

LLE Solvent (S)		**Et_2O**			**BuOAc**			**PhMe**		
Phase	**Component**	α	β	γ	α	β	γ	α	β	γ
Org.	DMF	$5.50 \cdot 10^{-3}$	$-4.66 \cdot 10^{-2}$	$1.11 \cdot 10^{-1}$	$-9.00 \cdot 10^{-4}$	$-5.10 \cdot 10^{-4}$	$7.78 \cdot 10^{-2}$	$2.90 \cdot 10^{-3}$	$-2.37 \cdot 10^{-2}$	$8.57 \cdot 10^{-2}$
	H_2O	$1.80 \cdot 10^{-3}$	$-1.70 \cdot 10^{-2}$	$9.05 \cdot 10^{-2}$	$4.40 \cdot 10^{-3}$	$-3.44 \cdot 10^{-2}$	$1.76 \cdot 10^{-1}$	$3.00 \cdot 10^{-5}$	$-2.00 \cdot 10^{-4}$	$6.00 \cdot 10^{-4}$
	S	$-7.20 \cdot 10^{-3}$	$6.36 \cdot 10^{-2}$	$7.98 \cdot 10^{-1}$	$-3.60 \cdot 10^{-3}$	$3.96 \cdot 10^{-2}$	$7.46 \cdot 10^{-1}$	$-2.90 \cdot 10^{-3}$	$2.39 \cdot 10^{-2}$	$9.14 \cdot 10^{-2}$
Aq.	DMF	$3.50 \cdot 10^{-3}$	$-3.20 \cdot 10^{-3}$	$-3.00 \cdot 10^{-4}$	$1.40 \cdot 10^{-3}$	$-1.35 \cdot 10^{-2}$	$5.14 \cdot 10^{-2}$	$9.00 \cdot 10^{-4}$	$-1.01 \cdot 10^{-2}$	$4.75 \cdot 10^{-2}$
	H_2O	$-2.79 \cdot 10^{-2}$	$2.54 \cdot 10^{-2}$	$2.50 \cdot 10^{-3}$	$-4.00 \cdot 10^{-4}$	$9.10 \cdot 10^{-3}$	$9.43 \cdot 10^{-3}$	$-1.10 \cdot 10^{-3}$	$1.11 \cdot 10^{-2}$	$9.47 \cdot 10^{-1}$
	S	$6.18 \cdot 10^{-2}$	$9.21 \cdot 10^{-1}$	$1.71 \cdot 10^{-2}$	$-1.10 \cdot 10^{-3}$	$4.40 \cdot 10^{-3}$	$5.50 \cdot 10^{-3}$	$2.00 \cdot 10^{-4}$	$-1.00 \cdot 10^{-3}$	$5.20 \cdot 10^{-3}$

8.3.3 Solute Partition Coefficients

Estimation of API and impurities partitioning between organic and aqueous phases is required for the modelling of CPM-LLE of atropine. Partition coefficients of each solute in different combinations of LLE solvent + H_2O systems at pH = 7 and T_{LLE} = 25 °C based upon extensive SPARC simulations, details of which can be found in the literature.[177] For all CPM-LLE solvent systems, operation at pH = 7 is chosen, for which published partition coefficients for each solute are provided in Table 26. It is assumed that polar components NaOH and NaCl (byproduct from neutralisation of tropine ester by NaOH) remain in the aqueous phase, whereas phenylacetyl chloride and formaldehyde are assumed to partition completely into the organic phase. Provision of partition coefficient data for those species not listed in Table 26 will allow more accurate estimation of solute component content of LLE phases required for process development of subsequent downstream unit operations.

Table 26: Partition coefficients of atropine and impurities in different solvent systems (S) at pH = 7 based upon published SPARC-derived values.[177]

Component	S = Et_2O	S = BuOAc	S = PhMe
API	0.326	0.359	0.273
Tropine	0.028	0.027	0.021
Tropine Ester	2.054	2.312	2.598
Apoatropine	2.054	3.043	3.486

Component partitioning of API and impurities are based upon partition coefficient data assuming pure organic (LLE solvent) and aqueous (water) phases.[177] Real LLE phases are not pure components, but multicomponent solvent mixtures, including DMF carrier solvent, and various solutes (API, impurities, other reagents). The presence of DMF and other components are not considered to affect the partition coefficient data used to estimate solute partitioning; consideration of these effects require partition coefficient data in multicomponent mixtures, which is not available. Investigation into the effect of additional component presence on solute partitioning will further elucidate the performance of different LLE designs.

8.4 Continuous Liquid-Liquid Extraction Cascade Superstructure

Mass transfer correlations for prediction of extraction efficiencies are as per Chapter 5.3, using the Skelland-Moeti correlation. The MINLP superstructure is illustrated in Fig. 57. The flow synthesis effluent, which is the feed to the LLE cascade, *F*, enters from the left in Fig. 57. The superstructure considers a cascade of tanks with counter-current flow of LLE solvent and the possibility for co-

current flow of fresh LLE solvent to tank k in the cascade. The continuous decision variables are the tank volume, V_{LLE}, and the LLE solvent to feed ratio, r_k; the binary decision variable, y_k (for tank k = 1,…,N–1), determines whether fresh LLE solvent is added to tank k (note that y_k is only applicable when $N \geq 2$, as co- and counter-current flow configurations are identical when $N = 1$). Fresh solvent addition is implemented for tank k if $y_k = 1$, otherwise $y_k = 0$. Note that no additional solvent is added to tank N other than that added via counter-current flow, as adding two separate streams of solvent to tank N is equivalent to adding a single counter-current fresh solvent stream. If all $y_k = 0$, a purely counter-current LLE configuration is implemented.

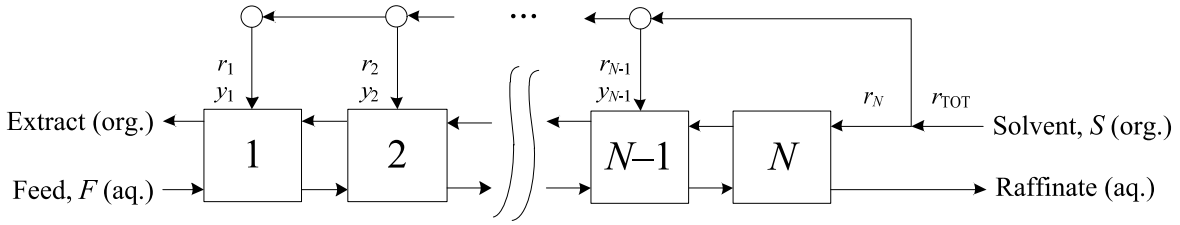

Figure 57: Continuous LLE MINLP superstructure for atropine CPM.

8.4.1 Solvent Allocation

The total amount of LLE solvent fed to the cascade and the amount in each tank must be such that the process mixture remains fully immiscible as per the UNIFAC-modelled ternary phase diagrams; this is ensured by maintaining r_k in each tank, as well as the sum of $r_k \geq 0.20$ (the lower bound of LLE solvent-to-feed ratio). The total LLE solvent present in tank k, S_k, is the amount entering via counter-current flow from subsequent tank k+1 and the fresh amount added if applicable (Eq. 98). Of the terms in brackets in Eq. 98, the first represents the fresh LLE solvent added to tanks k to N–1 and the second is the amount added to tank N entering stage k via counter-current flow.

$$S_k = \left(\sum_{k}^{N-1} y_k r_k + r_N \right) F \tag{98}$$

8.4.2 Optimisation Problem Formulation and Constraints

The objective of the MINLP optimisation problem is to minimise the total plant cost (estimated as per Chapter 3.6). The integer variable, y_k, must be binary, the summation of which is constrained to state that only tanks 1 to N–1 may have fresh LLE solvent added in co-current flow. The LLE solvent-to-feed ratios to tank k are constrained to ensure fully immiscible mixtures in each tank; a maximum $r \leq 5$ is chosen so that excessive amounts of LLE solvent are not used. The volumes of each LLE tank (V_{LLE}) are also constrained to have a minimum feasible volume of 1 L.

$$\min \textit{Total Cost} \tag{99}$$

s.t.

$$y_k \in \{0,1\} \qquad \forall k \in 1,\ldots, N\text{–}1, \text{ for } N \geq 2 \tag{100}$$

$$\sum_{k=1}^{N-1} y_k \leq N - 1 \qquad \text{for } N \geq 2 \tag{101}$$

$$0.20 \leq r_k \leq 5 \qquad \forall k \in 1,\ldots,N \tag{102}$$

$$0.20 \leq \sum_{k=1}^{N} r_k \leq 5 \tag{103}$$

$$1 \leq V_{\text{LLE},k} \qquad \forall k \in 1,\ldots,N \tag{104}$$

The MINLP superstructure describes the attribution of fresh LLE solvent in co-current mode to intermediate tanks in addition to counter- current solvent flow entering tank N (as per Fig. 57). The superstructure does not consider N or the LLE solvent choice as decision variables, with these design parameters being considered as separate optimisation problem instances, i.e., 12 problem instances in total. For each problem instance, there are $2N$ continuous decision variables ($V_{\text{LLE},k}$, r_k) and N–1 integer decision variables (y_k), i.e., a total of $3N$–1 decision variables. There are also varying numbers of linear equality constraints for different problem instances, of which there are N for V_{LLE}, $2N$+1 for r_k and the sum of r_k and one for y_k for $N \geq 2$.

Separate MINLP problem instances of LLE solvent = {Et_2O, BuOAc, PhMe} and number of LLE tanks, N = {1, 2, 3, 4} are solved. For a given combination of decision variables, process mass balances and PFR volume calculations accounting for reaction and continuous LLE inefficiencies are scaled to meet the desired plant capacity, $Q_{\text{API}} = 10^3$ kg API yr^{-1}. As in the NLP cases presented in Part 2, the plant capacity is met by specifying it as a NLP constraint. The MINLP optimisation problem is solved using the Basic Open Source Nonlinear Mixed Integer Programming (BONMIN) solver via MATLAB's OPTI Toolbox.[237] The solver uses a coin or branch and cut method for the mixed integer problem and the Interior Point Nonlinear Optimiser (IPOPT) solver for the relaxed NLP problem. A multistart routine using multiple initial guesses for each decision variable is also implemented.

8.5 Optimal Plantwide Designs

8.5.1 Liquid-Liquid Extraction Cascade Design

The MINLP optimisation results show the same continuous LLE configuration to be optimal for all LLE solvent choices and N considered, operating in mode with fresh solvent added to the first tank, as shown in Fig. 58. Purely counter-current LLE (i.e., all $y_k = 0$) is typically more economical in terms of solvent usage whereas cross-current LLE is more flexible and allows for faster dynamics; the LLE superstructure considered in this work is a combination of the two flow arrangements, allowing fresh solvent to be added to tanks in addition to the counter-current extract entering the tank. The superstructure considered here is relatively simple, but can be expanded to consider various combinations of feed splitting and solvent reflux by the consideration of additional binary variables.[238] For all cases, counter-current LLE solvent flow with fresh solvent addition co-current to the first tank in the cascade is established as optimal. The same optimal behaviour for $N > 4$ is also observed. The presented range of tank values considered (N = 1–4) is appropriate for the chosen plant capacity ($Q_{API} = 10^3$ kg API yr^{-1}) and can be readily expanded for consideration in the described modelling and optimisation framework.

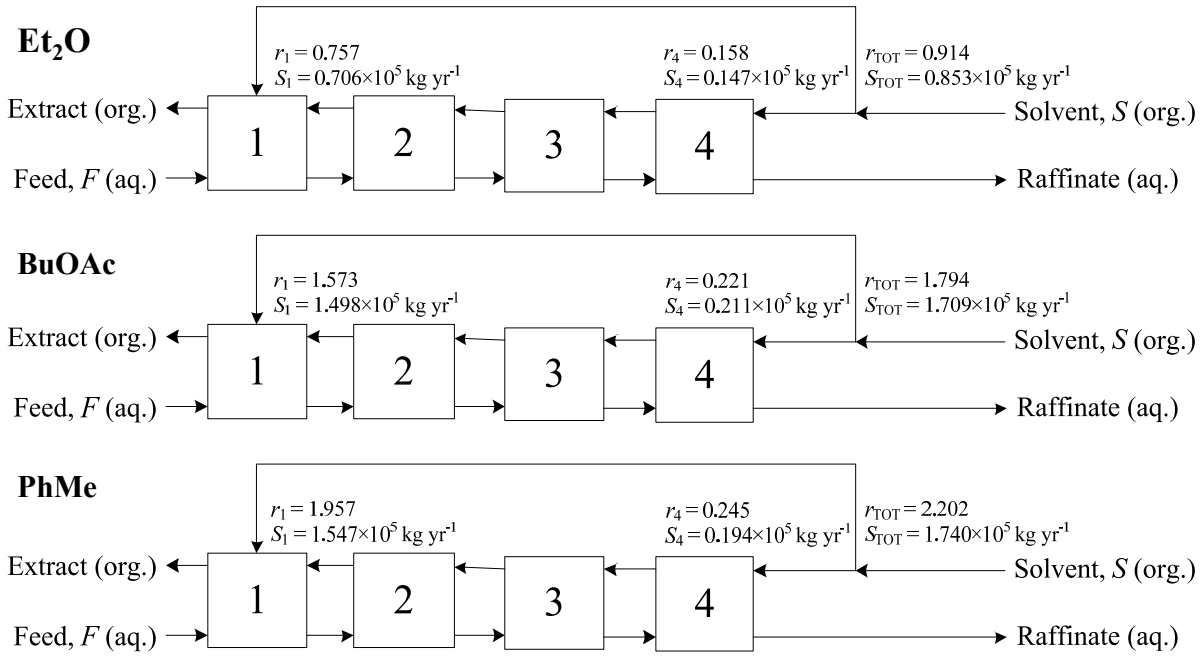

Figure 58: Optimal continuous LLE design configurations for atropine CPM ($y_2, y_3 = 0$).

Optimal LLE solvent-to-feed ratios (r_k) for each LLE solvent choice are also shown in Fig. 58. Using BuOAc as the LLE solvent choice results in the highest r_k, followed by PhMe and then Et_2O at the resulting cost minima. However, the absolute values of LLE solvent flowrates do not follow this pattern; flowrates are highest for PhMe, followed by BuOAc and then Et_2O; the actual

flowrates required depend on values of r_k determined by the MINLP solution as well as the resulting API recoveries of the design (tank number and sizes, LLE solvent choice, flowrates etc.).

Vessel volumes of LLE units corresponding to optimal designs for each LLE solvent choice are shown in Fig. 59. The total cascade volume is the largest when BuOAc is selected as the LLE solvent, followed by PhMe and then Et_2O, which have significantly smaller cascade volumes. The same trend in LLE volumes is observed as for optimal r values; this is likely due to the observed trends in value of total volumetric throughputs of the cascades, i.e., greater flowrates result in larger required tank volumes. Resulting r and V_{LLE} values affect API recoveries from the plant due to their effect on LLE efficiency and are thus important to consider in this analysis. Although individual vessel volumes decrease with increasing N, the total cascade volumes increase with this trend. Implementing multiple smaller vessels is more beneficial than a single larger tank, despite the total cascade volume being higher; the effect this trend has on *CapEx* components will be discussed in Chapter 8.5.3.

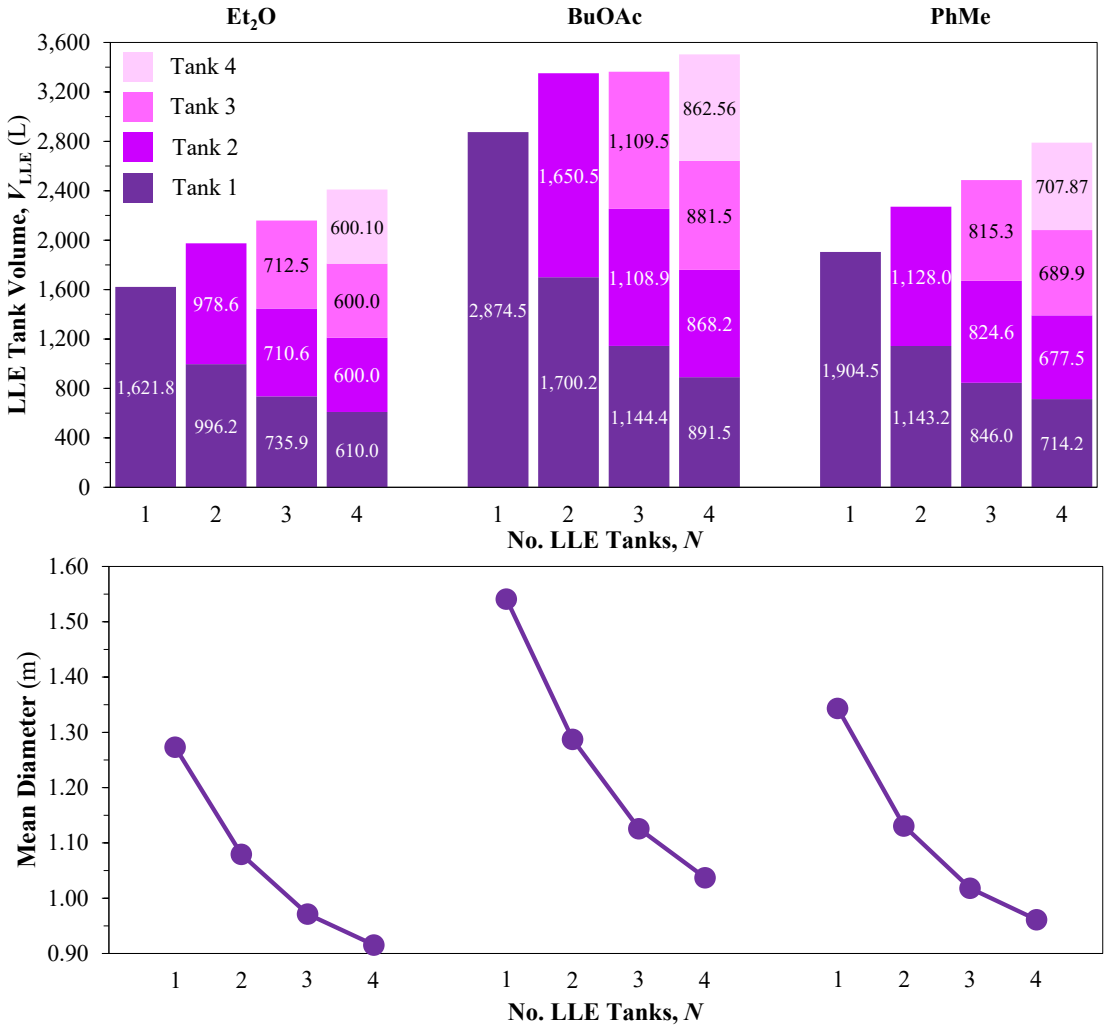

Figure 59: Atropine CPM LLE vessel volumes corresponding to optimal design configuration.

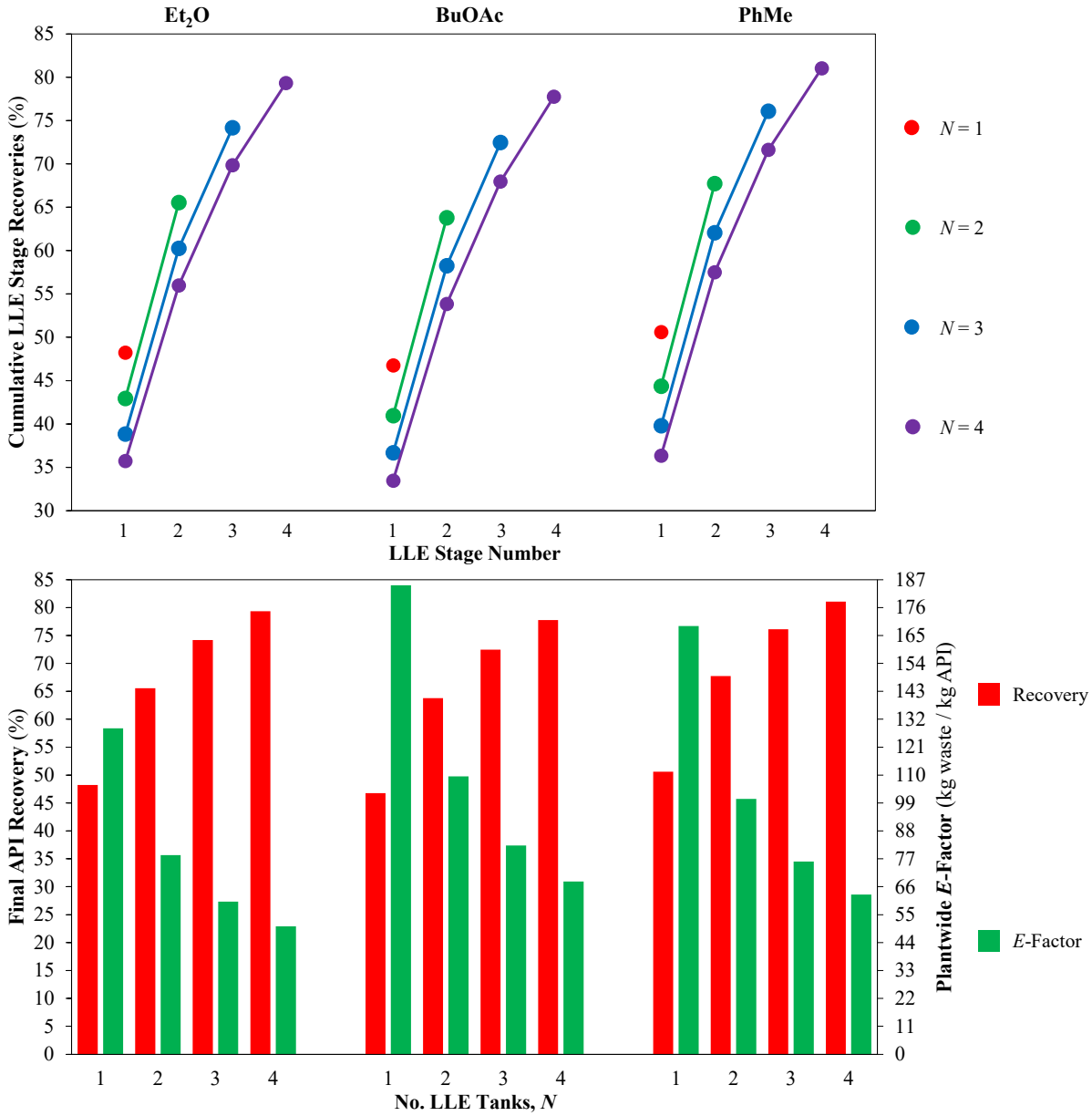

Figure 60: Atropine recoveries and *E*-factors corresponding to optimum plant designs.

Fig. 59 also shows the mean tank diameter for each tank for different LLE solvent choice and implemented N; mean values are shown for $N \geq 2$ as individual tank volumes are approximately the same when multiple tanks are implemented. Mean tank diameters decrease as N increases due to the decreasing individual tank volumes. The tank aspect ratio, as well as the ratio of tank-to-impeller diameter affects the overall mass transfer coefficient and thus the overall LLE efficiency; variation of the assumed tank design ratios can be easily varied as a form of sensitivity analysis.[51]

8.5.2 Plantwide Recoveries and Material Efficiencies

The attained recoveries (Fig. 60) at cost optimal points are similar for each N between LLE solvent choices. This result does not imply that all solvents perform similarly in general, only that the

recoveries attained at cost minima are approximately the same. This result is an indication that beyond a certain API recovery, the benefits of enhanced recovery do not outweigh the associated additional costs by, e.g., increasing LLE cascade volumes (resulting in higher *CapEx*) and/or greater LLE solvent usage. As N increases, the recovery in each individual tank decreases due to the decreasing volumes (Fig. 59), but the final API recovery increases. It is also important to note that all LLE processes are considered implemented at T_{LLE} = 25 °C, without consideration of other temperatures due to the lack of solute partition coefficient data between product phases as a function of temperature.

The attained E-factors (see Chapter 3.5.4) are quite high for all LLE solvent choices; however, such values are not uncommon in pharmaceutical manufacturing processes, which are typically very materially-intensive compared to other manufacturing sectors such as oil and gas processes, which can have E-factors as low as 0.1. Consideration of solvent reflux/recycle and/or recovery to improve the material efficiencies of these processes will likely results in lower E-factors for different LLE designs, but will inevitably increase MINLP problem complexity. Consideration of subsequent crystallisation process requirements on product streams should also be implemented for system solvent harmonisation, which aids process intensification and CPM process development. Incorporation of downstream crystallisation impurity limits could be included in the problem formulation to give additional complexity to the MINLP problem.

8.5.3 Economic Analysis

8.5.3.1 Total Cost Components

Total cost components corresponding to optimal process designs for different LLE solvent choices are shown in Fig. 61. For *CapEx* components, *BLIC* dominates over *WCC* for all process designs due to expensive equipment (particularly PFRs). For *OpEx* components, materials costs are the most significant contributor, followed by utilities and waste costs. As the number of implemented LLE tanks increases, overall *OpEx* contributions decrease due to the corresponding enhanced API recoveries with increasing N. Waste costs are modelled via an assumed cost per unit volume of waste produced from different process designs without explicit consideration of the mode of waste treatment. Consideration of specific operations and material requirements for waste treatment will increase both *CapEx* and *OpEx* components presented here, which should be considered when interpreting the results.

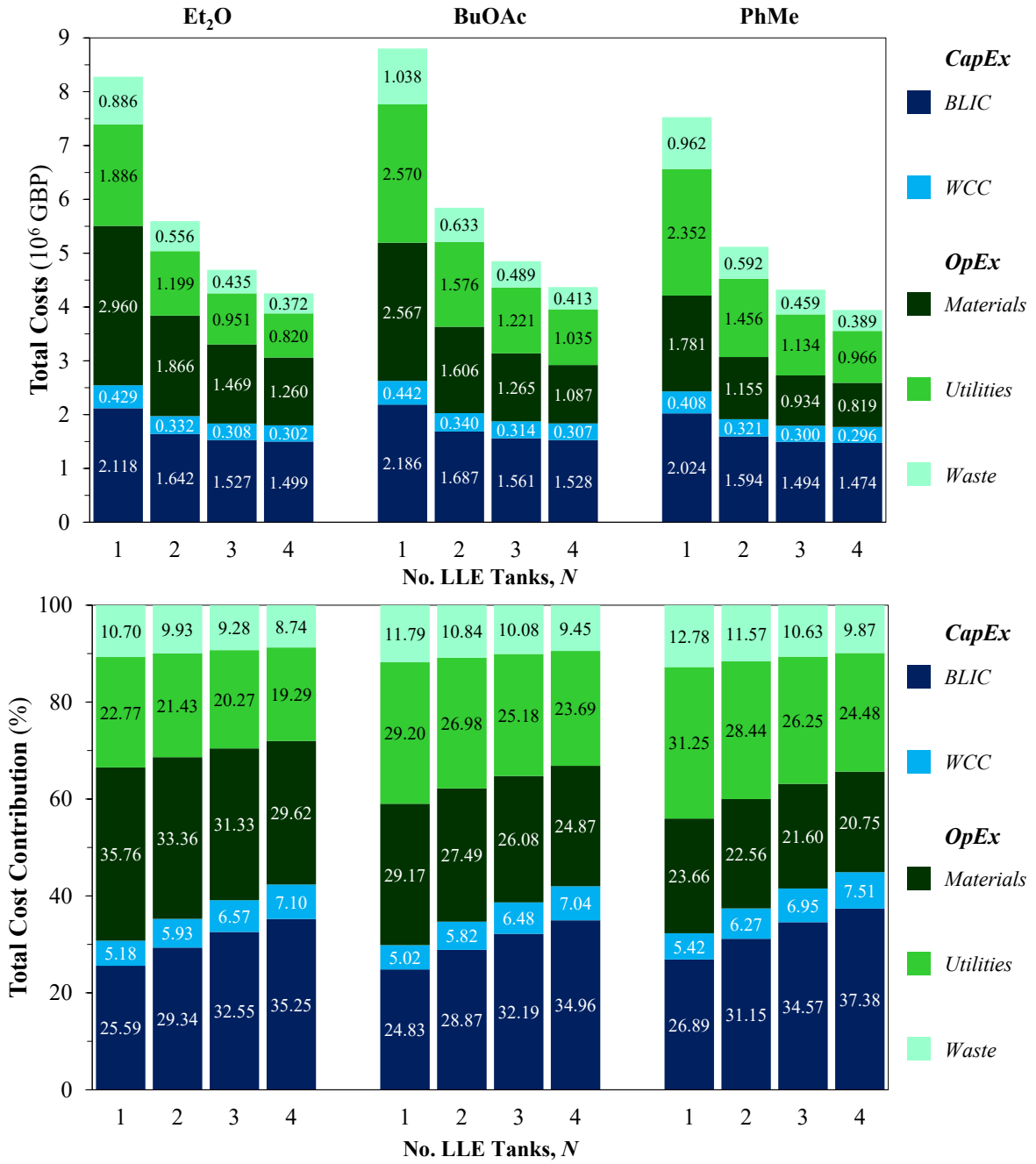

Figure 61: Total cost components and contributions of different LLE design configurations for atropine CPM.

8.5.3.2 Reactor vs. Separator Component Distribution

It was shown earlier (Fig. 59) that increasing the number of implemented tanks (*N*) results in decreased individual tank volumes but increased total cascade volumes. Despite this, the total *CapEx*, a significant portion of which is *BLIC* (containing equipment costs), still decreases with increasing *N*. The reason for this trend is related to the effect of increasing *N* on plant API recoveries and resulting PFR volumes at MINLP cost minima. Increasing *N* increases the plant API recovery (Fig. 60), which subsequently reduces the required material throughput to meet the

target plant capacity (Q_{API}) and thus PFR volumes. The reactors are significantly more expensive than LLE equipment in this work and thus the benefit of decreasing *CapEx* contributions of the PFRs is more significant than the increasing *CapEx* contributions associated with increasing *N*. This is illustrated in Fig. 62, which compares the *FOB* contributions of PFRs and LLE equipment for varying *N* for different LLE solvent choices. The *FOB* contributions of PFRs are much more significant than LLE contributions in all cases and with increasing *N*, PFR *FOB* costs decrease while LLE *FOB* costs increase. Increasing *N* also lowers *OpEx* due to the reduction of material throughput, utilities and waste (both of which are a function of material throughput in the implemented costing methodology) associated with enhanced recoveries + plantwide efficiencies.

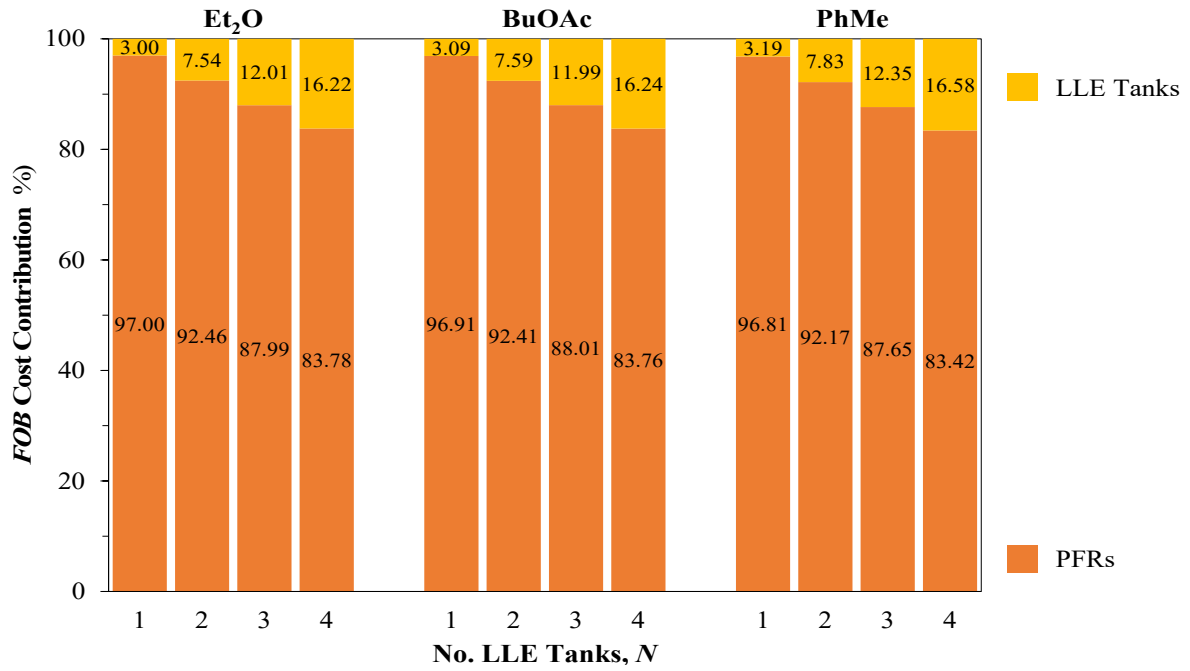

Figure 62: Free on Board (*FOB*) PFR and LLE equipment contributions for atropine CPM.

The MINLP optimisation results show PhMe is the best LLE solvent choice (Fig. 61), attaining the lowest total costs of 3.944×10^6 GBP. Further corroboration of optimisation results with experimental validation as well as solvent harmonisation with crystallisation and other downstream processes is essential for atropine CPM development. Although PhMe is shown to be more economically viable, it has less favourable EHS characteristics compared to BuOAc.[223] The current MINLP problem formulation is for minimisation of total costs; the problem may be reformulated for maximising profits or Net Present Value (*NPV*), which may yield different process design and total cost component results to those presented here for total cost minimisation. It is noted that the total cost components continue decreasing for the considered number of LLE vessels (N = 1–4); cases of $N > 4$ were not considered due to the lengthy MINLP computational times taken. It should be noted that there may be improved (i.e., lower) total cost minima for $N > 4$.

8.6 Chapter Conclusions

This work solves a novel MINLP problem for the total cost minimisation of the CPM of atropine, establishing plant designs corresponding to optimal LLE design configurations and operating parameters. The implemented process model incorporates kinetic parameter estimation from experimental data for PFR design, as well as an evaluation of dimensionless numbers (*Re*, *Pe*, *Da*) to compute maximum allowable PFR diameters to ensure homogeneous reaction mixtures (with respect to concentration, velocity and temperature gradients) to maximise the benefits of continuous processes for atropine flow synthesis. Continuous LLE modelling used ternary phase composition estimation via UNIFAC and appropriate mass transfer correlations. For all LLE solvent choices, implementing four tanks in counter-current mode with additional solvent flow to the first tank is the optimal design configuration from the considered superstructure. Toluene (PhMe) emerges as the most economically favourable LLE solvent choice with a total cost of 3.944×10^6 GBP at API recovery = 81.0% and *E*-factor = 62.9 for a plant capacity of $\dot{Q}_{\mathrm{API}} = 10^3$ kg API yr^{-1}. This work demonstrates the value of conducting technoeconomic optimisation studies towards the development of continuous processes in pursuit of economically viable end-to-end CPM and the value of MINLP methodologies for rapid screening of solvent selection and plant designs.

Chapter 9

Melitracen

This chapter describes the steady-state process modelling and MINLP optimisation for process synthesis for the MSMPR continuous cooling crystallisation of melitracen.

9.1 Continuous MSMPR Cascade Superstructure

Capellades et al. (2019) demonstrated continuous crystallisation of melitracen from ethanol via cooling in a MSMPR cascade without recycle.[181] Solids recycling in MSMPR cascades has been demonstrated in the literature, allowing for enhanced crystallisation yields.[99,230] In this work, a MSMPR cascade with solids recycle is considered; the conceptual flowsheet is shown in Fig. 63.

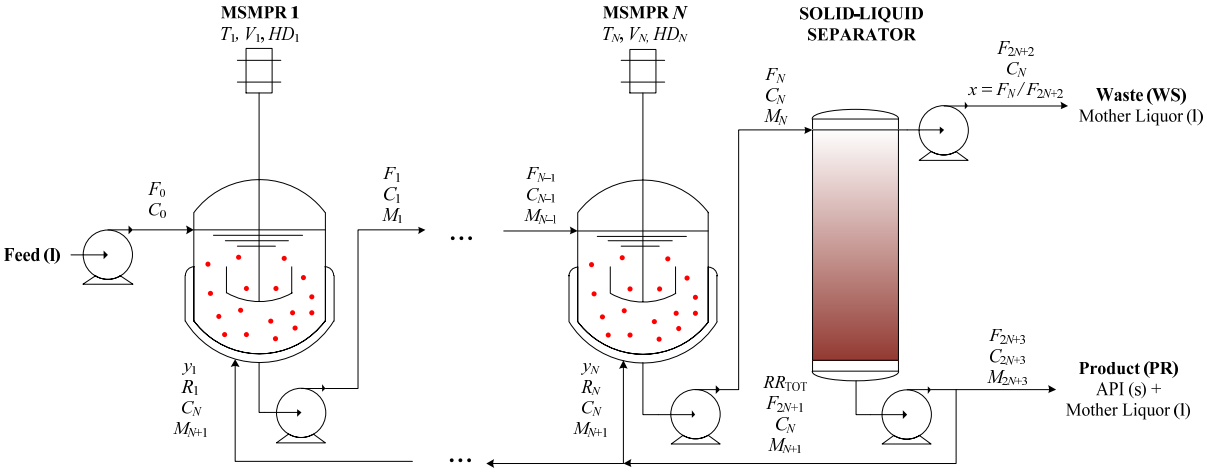

Figure 63: MSMPR cascade for continuous cooling crystallisation of melitracen with solids recycle.

A clear mother liquor feed stream enters MSMPR 1, with dissolved API solute concentration C_0 and volumetric flowrate F_0. The product stream exiting one MSMPR (F_i) is then the feed stream to the subsequent MSMPR in the cascade, consisting of N crystallisers in total. The product stream of crystalliser N (F_N) then enters a solid-liquid separator, in which clear mother liquor is removed in order to concentrate the stream suspension, which exits from the bottom of the separator, producing recycle streams R_i. The concentrated stream is the product, with some being recycled back to select crystallisers. Design and operating parameters for the process are the MSMPR temperatures (T) and volumes (V), the total recycle ratio (RR_{TOT}), the mother liquor removal ratio ($x = F_N / F_{2N+2}$) and binary variable, y_i, deciding whether to send recycle to stage i. Each MSMPR i has a holdup of crystallised API, HD_i. For each crystalliser, F_i, C_i and M_i are the volumetric flowrate of the stream leaving the stage, the equilibrium API concentration in the mother liquor

and the suspension density, respectively. All flowsheets and process designs are for plant API capacities of Q_{API} = {10^3, 10^4} kg API yr^{-1}. The steady-state process models for all flowsheet configurations describe crystallisation kinetics, population balance equations and mass balances. Simultaneous solution of these equations describes continuous crystallisation in the MSMPR crystalliser cascade.

It is assumed that the total stream of recycled material (F_{2N+1}) is equally distributed between those crystallisers to which it will be fed (i.e., those with binary variable $y_i = 1$). A mass balance equation around the gravity-driven separator gives the following,

$$R_i = \frac{y_i RR_{TOT}(1-x)}{\sum_{i=1}^{N} y_i} F_N \quad \forall i = 1,\ldots,N \tag{105}$$

where x is the clear liquor removal ratio (controlling the suspension density of the stream leaving the bottom of the solid-liquid separator, M_{N+1}), defined as F_N / F_{2N+2} and RR_{TOT} is the total recycle ratio (controlling how much material is sent back to the MSMPR cascade vs. that withdrawn as product).

The solubility concentration of API in ethanol, C^{sat}, as a function of temperature during cooling crystallisation is described by Eq. 106, taken from the literature, with $R^2 > 0.99$ vs. experimental data.[181] The published experimental data and the regressed correlation (Eq. 106) of C^{sat} vs. T are shown in Fig. 64.

$$C_i^{sat} = 15.282 \exp(0.041 T_i) \quad \forall i = 1,\ldots,N \tag{106}$$

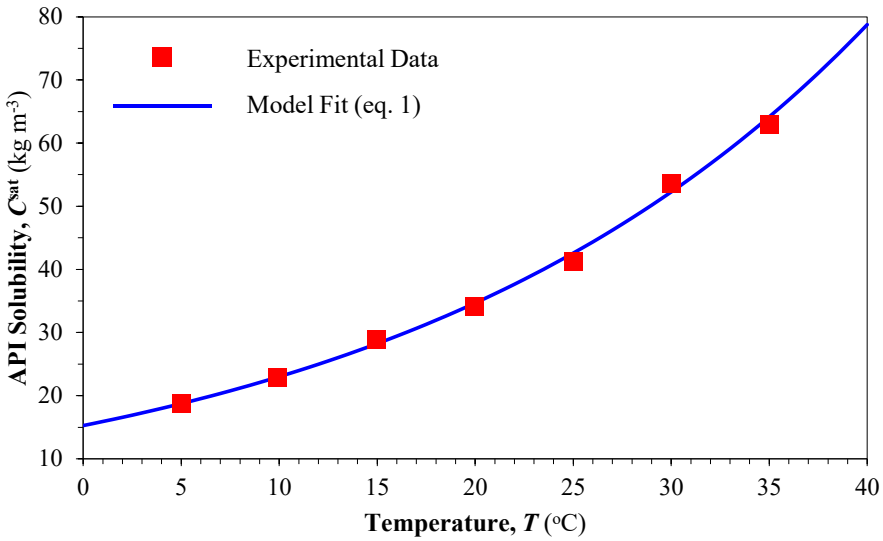

Figure 64: Melitracen solubility concentration (C^{sat}) as a function of temperature (T) (Eq. 106) in ethanol vs. experimental data ($R^2 > 0.99$).[181]

Crystal nucleation, B, and growth, G, rates are calculated as in Chapter 7.1.2, respectively. No polymorphism was described in the experimental study on MSMPR crystallisation of melitracen and so polymorphic effects are not considered in this work either. All required crystallisation kinetic parameters for melitracen are listed in Table 27.

Table 27: Kinetic parameters for MSMPR crystallisation of melitracen from ethanol.[181]

Model Equations	Parameter	Value	Units
Nucleation rate, B	k_{b0}	4.79×10^{22}	$m^{-3}\ s^{-1}$
	E_b	7.30×10^{4}	$J\ mol^{-1}$
	b_{MSMPR}	2.60	–
	m_{MSMPR}	0.56	–
Growth rate, G	k_{g0}	13.1	$m\ s^{-1}$
	E_g	5.25×10^{4}	$J\ mol^{-1}$
	g_{MSMPR}	0.87	–
Population balances	k_v	3.74	–
	ρ_{API}	1,280	$kg\ m^{-3}$

9.2 Optimisation for Maximisation of Net Present Value

The objective of the MINLP optimisation problem is to maximise the attained Net Present Value (NPV) of the crystallisation process (Eq. 107), calculated as the sum of inflation-adjusted profit from API sales minus $OpEx$ over the plant lifetime minus total $CapEx$. Annual profit is calculated from sales of API produced. The wholesale price of melitracen is taken as p_{API} = 50 GBP kg API^{-1}. The problem has $2N+2$ continuous decision variables (V_i, T_i, x, RR_{TOT}) and N binary variables (y_i). Various constraints are also imposed on the problem. Crystalliser volumes must be finite. Temperatures are bounded such that the solubility estimation is consistent with experimental results in the literature.[181] For cooling crystallisation, each MSMPR temperature must be equal to or lower than the previous and the fresh feed mother liquor is at T_0 = 60 °C, as per the experimental demonstrations.[181] The total recycle ratio (RR_{TOT}) and clear solvent removal ratio (x) are constrained to values observed in the literature.[99] Binary decision variables must be 0 or 1.

$$NPV = -CapEx + \sum_{k=1}^{20} \frac{\text{Profit} - OpEx_{\text{annual}}}{(1+t)^k} \tag{107}$$

$$\text{Profit} = p_{API} Q_{API} \tag{108}$$

$$\max NPV \tag{109}$$

s.t.

$$0 < V_i \qquad \forall i = 1,\ldots,N \tag{110}$$

$$0 \leq T_i \leq 40\ °C \qquad \forall i = 1,\ldots,N \tag{111}$$

$$T_N \leq \ldots \leq T_1 \qquad \forall i = 1,\ldots,N \tag{112}$$

$$T_0 = 60\ °C \tag{113}$$

$$0.0 \leq RR_{TOT} \leq 0.9 \tag{114}$$

$$0.0 \leq x \leq 0.5 \tag{115}$$

$$y_i = \{0,1\} \qquad \forall i = 1,\ldots,N \tag{116}$$

The MINLP optimisation problem is solved using the Basic Open Source Nonlinear Mixed Integer Programming (BONMIN) solver via MATLAB's OPTI Toolbox.[237] As in the previous NLP + MINLP cases presented, the plant capacity is met by specifying it as a NLP constraint.

9.3 Continuous Crystallisation Cascade Design

9.3.1 Crystallisation Kinetics

Crystallisation kinetics (nucleation and growth rates, *B* and *G*, respectively) for different plant capacities (Q_{API}) and number of crystallisers (*N*) are shown in Fig. 65. The system of model equations for crystallisation kinetics, mass balances and population balances are solved simultaneously to describe the MSMPR cascade behaviour (see Chapter 7.1.5). Growth rates increase along the cascade until $N = 3$ and then decrease, while nucleation rates generally continually increase and then plateau. The balance of growth and nucleation rates in a crystallisation system is important in controlling the crystallisation yield (affecting process efficiency and cost components) and product quality attributes such as Mean Crystal Size (*MCS*) and size distribution width (affecting downstream operations and drug product bioavailability).

9.3.2 Supersaturations and Mean Crystal Sizes

Resulting supersaturations and suspension densities (*M*) for different considered plant capacities (Q_{API}) and number of crystallisers (*N*) are shown in Fig. 66. The supersaturation increases gradually increases along the MSMPR cascade in all design cases with decreasing temperature. Suspension densities increase continually along the cascade in all cases as the crystallisation yield, and hence amount of solid product in suspension, increases. The chosen upper bound of the clear mother liquor removal ratio (x) in the MINLP optimisation problem definition is such that suspension densities are not so high that streams cannot be handled by peristaltic pumps.[99,181]

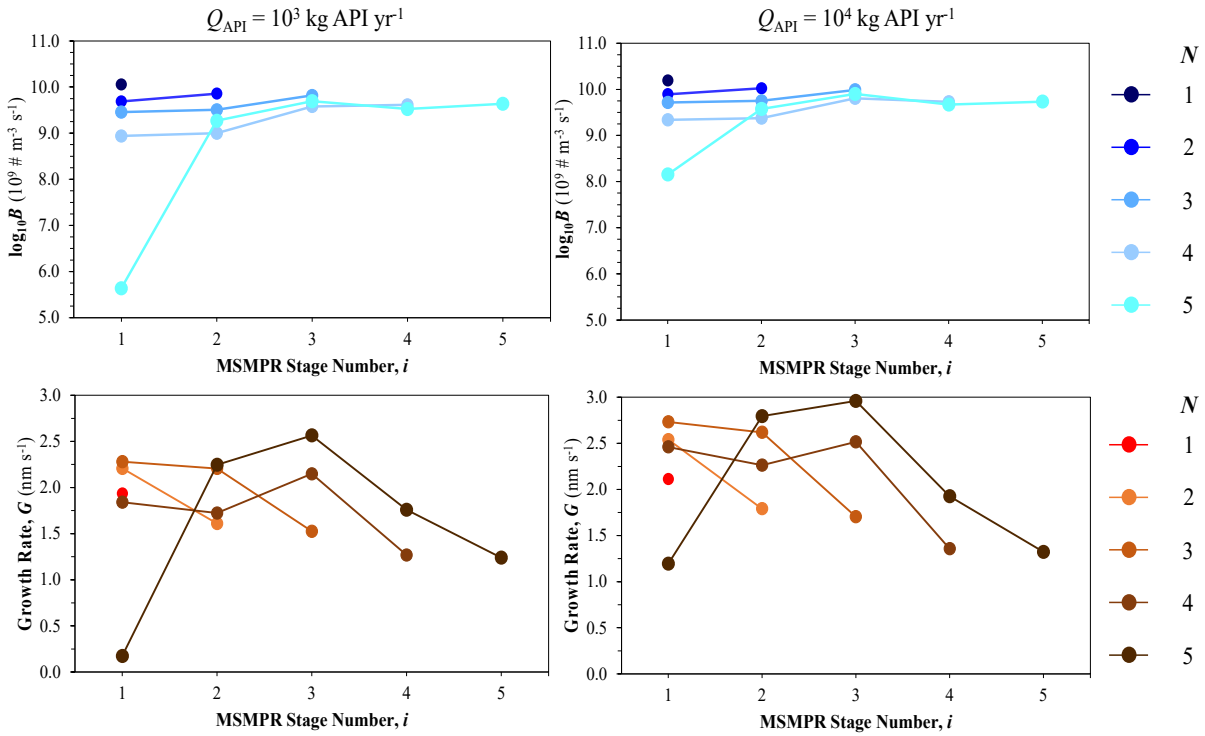

Figure 65: Optimal melitracen crystal nucleation and growth rates at both considered plant capacities (Q_{API}) at each stage (i) for different assumed numbers of crystallisers (N).

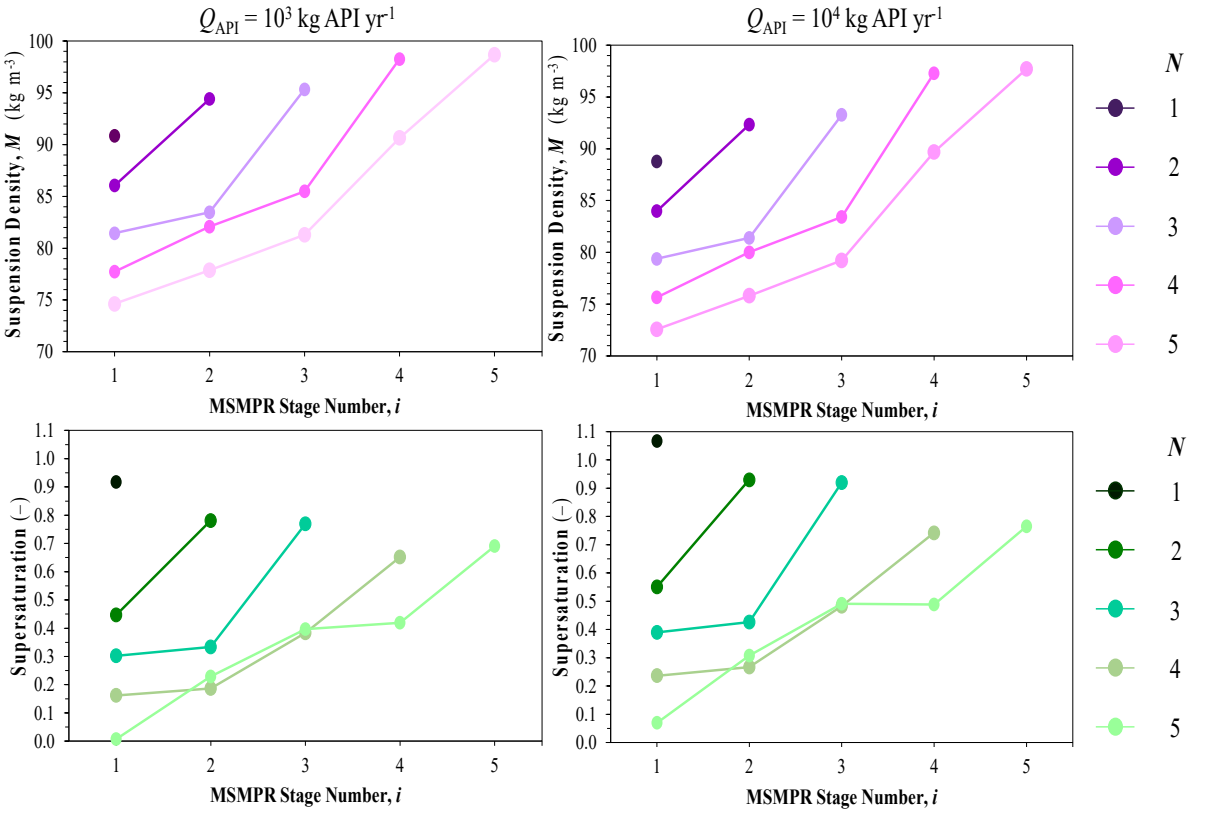

Figure 66: Optimal melitracen MSMPR suspension densities (M) and supersaturations at both considered plant capacities (Q_{API}) at each stage (i) for different numbers of crystallisers (N).

The attained final *MCS* values for different cascade designs (implemented *N*) at different considered plant capacities (Q_{API}) are shown in Fig. 67. Values of *MCS* are slightly lower for the higher considered Q_{API}; the desired *MCS* depends on the implemented downstream unit operations and drug product formulation. The attained *MCS* values here are very low and will likely lead to difficulties in solid-liquid separation unit operation and solid flowability during downstream processes. This highlights a need to incorporate crystal quality (size properties as well as purity and polymorph constraints) into the optimisation problem formulation. The published nucleation and growth kinetic parameters from the literature that are used in this work did not account for agglomeration and breakage either, which will affect the computed crystal sizes. Harmonisation of downstream operation with the considered crystallisation process, as well as upstream API synthesis as part of plantwide design problems give significant insight into process development where sufficient information for up- and downstream unit operation design is available.

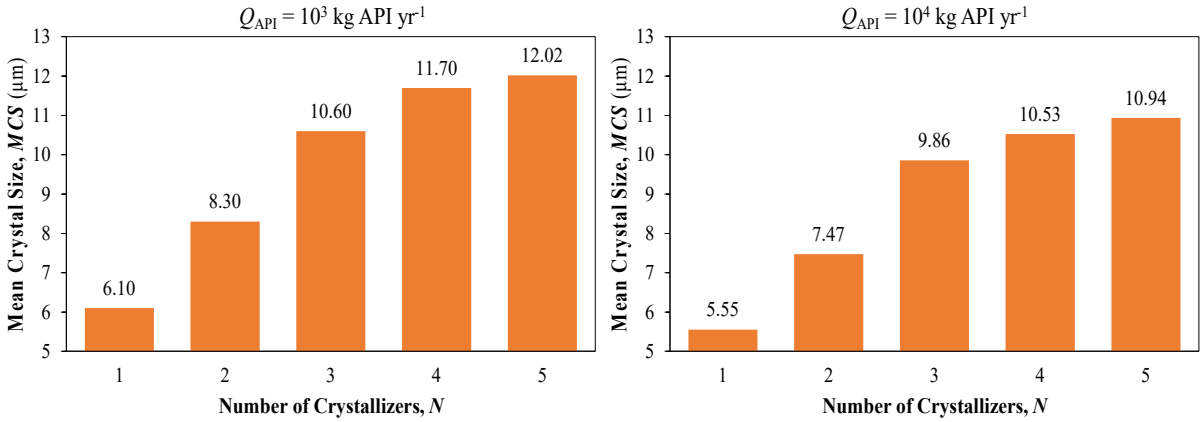

Figure 67: Final Mean Crystal Size (*MCS*) at both considered plant capacities (Q_{API}) for different assumed numbers of crystallisers (*N*).

9.3.3 Optimal Cascade Configuration Design and Operation

The optimal flowsheet configurations corresponding to MINLP optima (i.e., *NPV* maxima) are shown in Fig. 68. The optimal flowsheet configurations (for both capacities) varies for different numbers of implemented crystallisers (*N*). For $N = \{1, 2\}$, recycle streams are allocated to all crystallisers in the MSMPR cascade. However, for $N \geq 3$, not all crystallisers have recycle streams fed to them, i.e., not all $y_i = 1$ (binary decision variable in the MINLP optimisation problem). Lower capacities and effects of alternative numbers of crystallisers out with the range considered here (i.e., $N > 5$) can be easily investigated in the described MINLP optimisation framework.

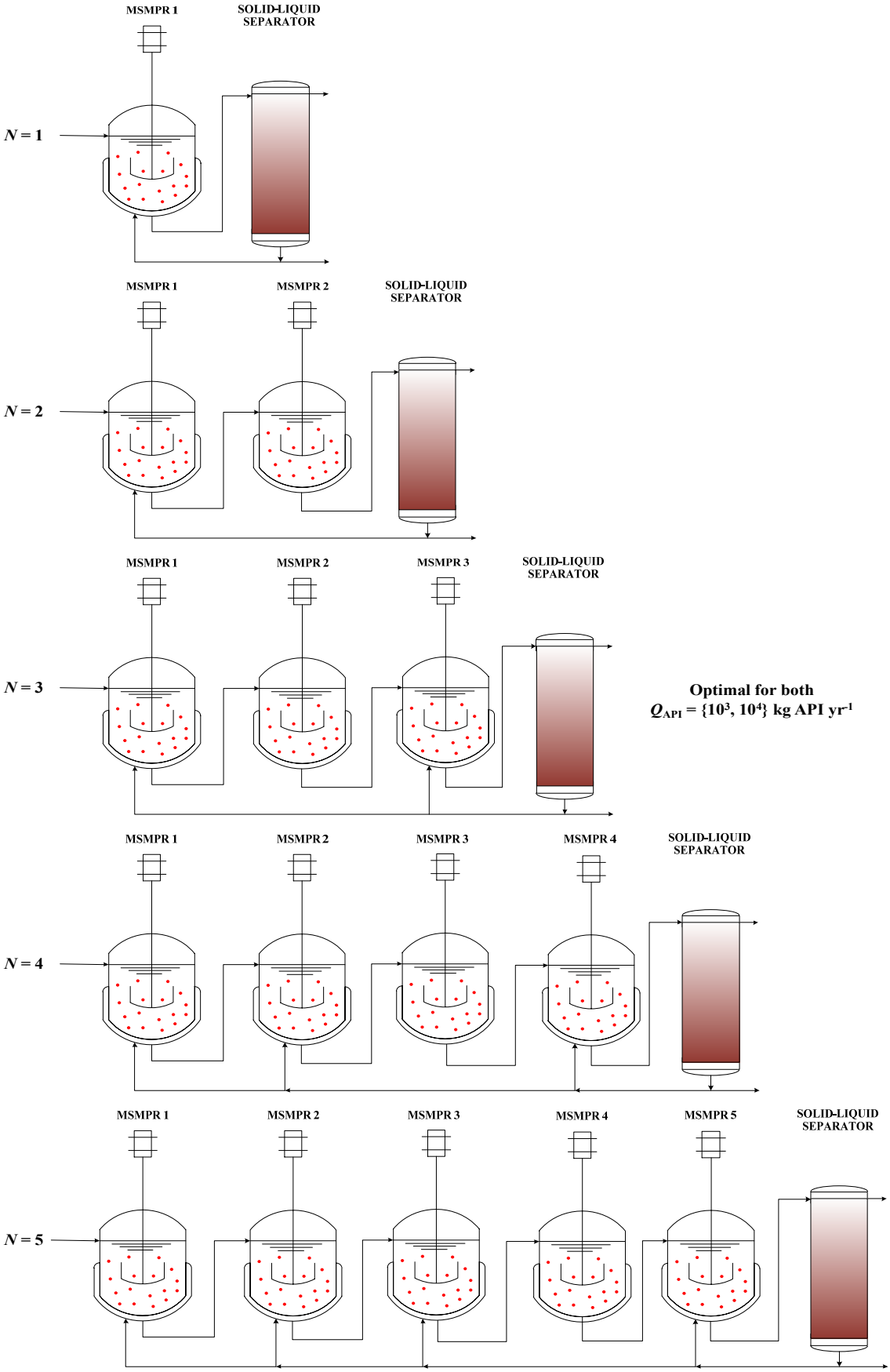

Figure 68: Optimal melitracen MSMPR cascade configurations for different numbers of crystallisers (N) at both considered plant capacities (Q_{API}).

The cost-optimal number of crystallisers is the same for both considered plant capacities (Q_{API}), N = 3, as is the allocation of recycle streams, i.e., to the first and final (third) crystallisers with the second vessel receiving no recycle; this corresponds to MINLP binary decision variables y = [1 0 1]. Varying the extent of recycle to different crystallisers has been shown to be an important decision variable in controlling the crystallisation yield in MSMPR cascades with solids recycle,[99,230] which in turn affects the productivity and costs to attain a specific desired plant capacity. Allocating solids recycle to multiple stages, as opposed to just one crystalliser, increases the extent of nucleation throughout the cascade which increases the final crystallisation yield. Were the final *MCS* or size distribution considered as objective functions or constraints in the optimisation problem, allocation and extent of solids recycle may vary, as crystal growth would be more important. Implementing multi-objective optimisation on both crystallisation yields and product quality attributes such as *MCS* and size distribution width is often implemented for dynamic optimisation of batch and continuous processes.[239]

The optimal recycle ratios (RR_{TOT}, extent of recycle) and clear mother liquor removal ratios (x, controlling concentration of recycle streams) for different considered plant capacities (Q_{API}) and numbers of crystallisers (N) are shown in Fig. 69. For both considered capacities, the optimal recycle ratios decrease from N = 1–3 and then increase, whereas the optimal clear mother liquor removal ratios decrease. Increasing RR_{TOT} and x increase the available surface area for crystallisation in each vessel, however ultimately incur greater recycle flowrates which require larger vessels (i.e., sufficient crystalliser residence time) to attain suitable yields and the desired productivity to meet the set plant capacity (Q_{API}). The decrease in the clear mother liquor removal ratio (x) with N = 1–3 indicates that the recycle streams do not need to be as concentrated (i.e., less mother liquor removed in waste stream F_{2N+2}) for N = 3 in order to be cost optimal; this also leads to less waste and enhanced material efficiency.

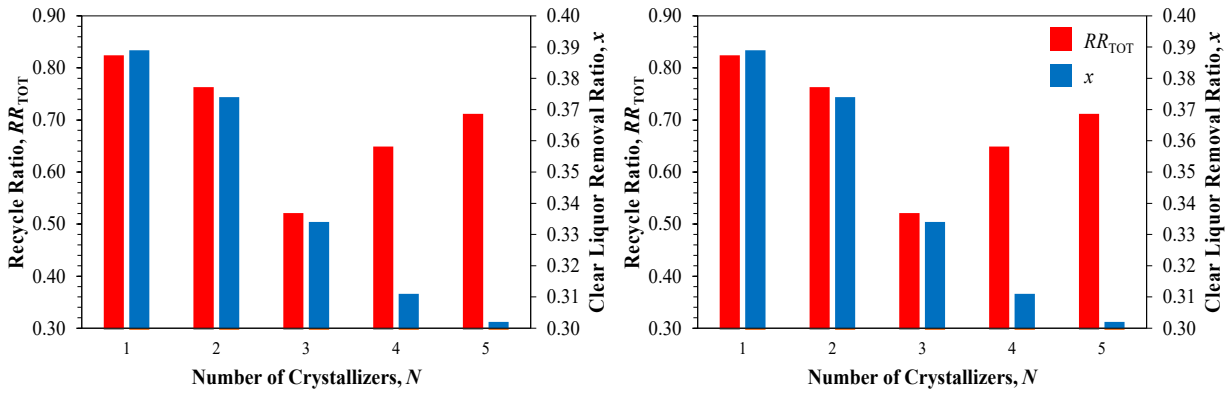

Figure 69: Optimal melitracen MSMPR cascade recycle ratios and clear mother liquor removal ratios at both considered plant capacities (Q_{API}) at each stage for different numbers of crystallisers.

The current MINLP problem formulation assumes the solids recycle stream is distributed equally between those crystallisers for which $y = 1$. Formulation of problems with unequal stream distribution between crystalliser cascade elements can allow for tighter control of crystal product quality attributes. The current MINLP problem is formulated for economic optimisation does not consider product quality attribute constraints; however, if such constraints were implemented, unequal recycle allocation may be beneficial.

Optimal crystalliser volumes (V) for different plant capacities (Q_{API}) and number of crystallisers (N) are shown in Fig. 70. As the number of implemented crystallisers increases from $N = 1$–3, total cascade volumes decrease and then increase for $N > 3$. As N increases, individual vessel volumes decrease; implementing multiple smaller volume stages is beneficial in terms of attained crystallisation yield (see Chapter 5.3, Fig. 71). Crystalliser volumes are larger for designs at the higher considered capacity, reflecting the larger volumetric throughputs to meet the higher API production requirements.

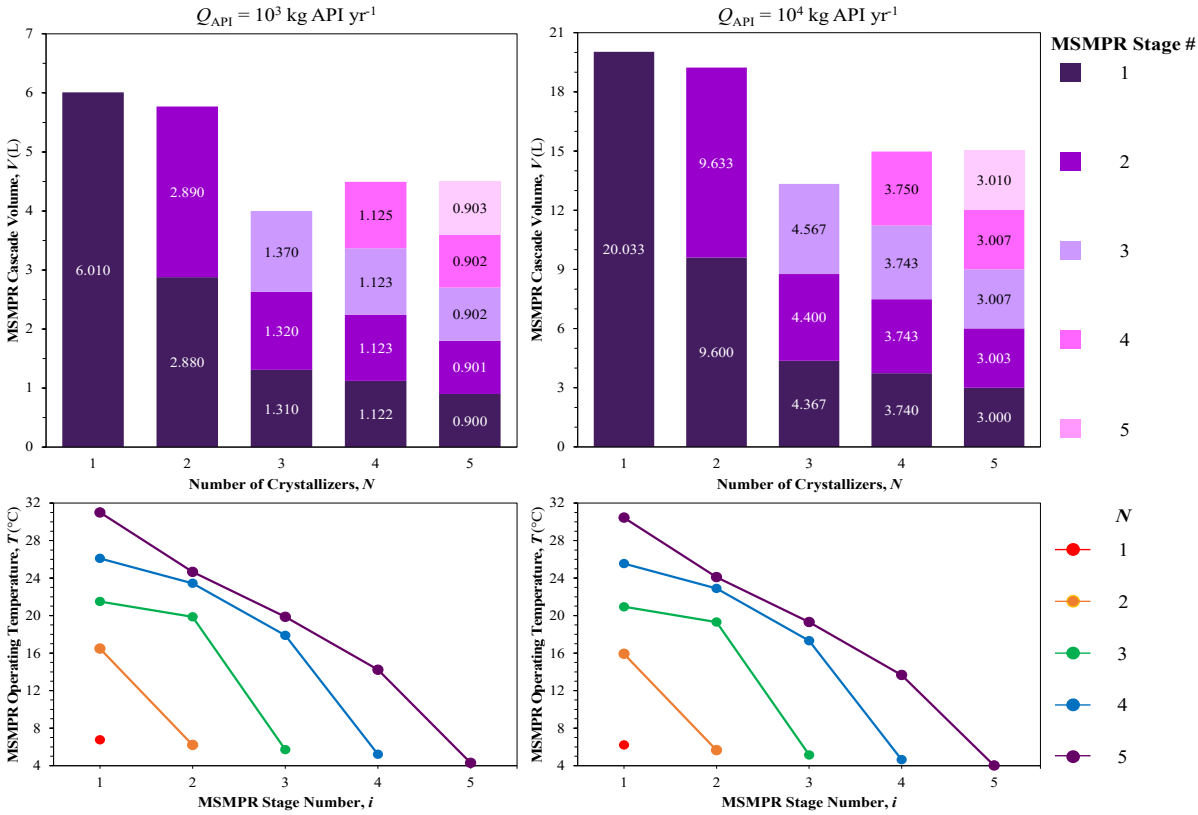

Figure 70: Optimal tank volumes (V) and melitracen MSMPR operating temperatures (T) at both considered plant capacities (Q_{API}) at each stage (i) for different numbers of crystallisers (N).

Optimal crystalliser operating temperatures (T) for different plant capacities (Q_{API}) and numbers of crystallisers (N) are also shown in Fig. 70. As N increases, individual stage temperatures are higher but the final temperature (T_N) is lower, which allows for increased crystallisation yields.[118]

Temperatures always decrease along the cascade to ensure supersaturation is generated in each crystalliser to cause more product API to crystallise from solution from the previous vessel, as imposed as one of the MINLP problem constraints. An assumption of the considered MSMPR model is that perfect mixing of the crystalliser contents is attained, such that the outlet solution concentration is the same as that throughout the MSMPR vessel. The model also assumes that heat transfer from crystalliser to cooling jacket is instant; the validity of this assumption weakens with increasing plant capacity and volumes. Consideration of heat transfer dynamics should be considered as part of further non-steady-state studies.

9.4 Attained Unit Operation Material Efficiencies

Attained crystallisation yields at each MSMPR stage for different considered plant capacities (Q_{API}) and varying total numbers of crystallisers (N) are shown in Fig. 71. Yields progressively increase along the cascade as more API is crystallised from solution. Individual stage yields are lower as N increases, but ultimately the final yield increases when N is higher; eventually the final yield plateaus for $N \geq 4$. This result indicates that beyond a certain number of crystallisers, the benefit of increasing yield associated with increasing N is no longer beneficial with respect to the NPV.

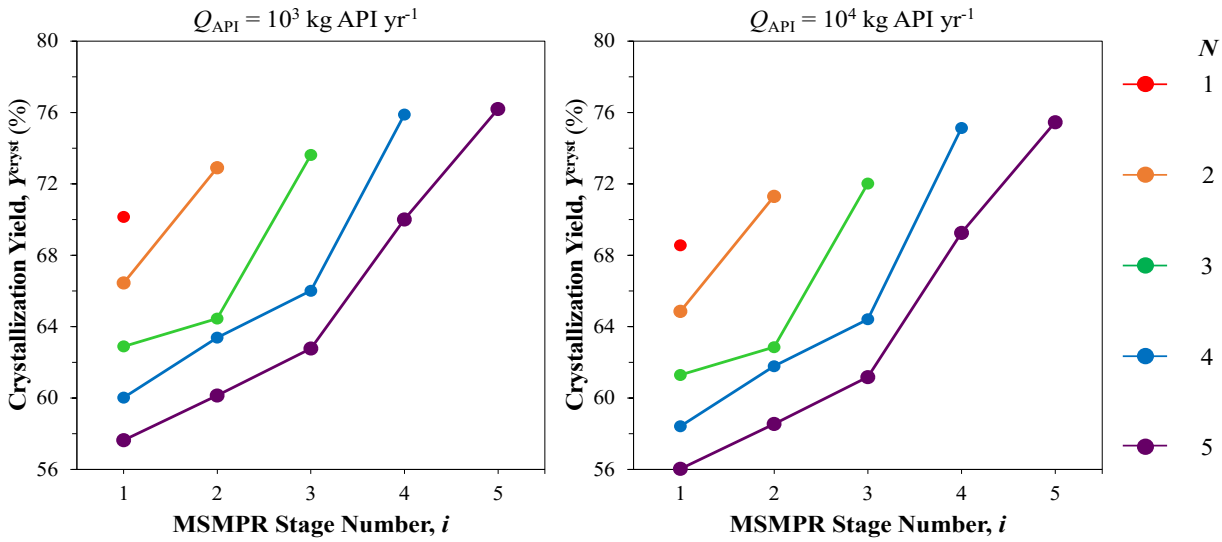

Figure 71: Optimal melitracen crystallisation yields (Y^{cryst}) at both considered plant capacities (Q_{API}) at each stage (i) for different numbers of crystallisers (N).

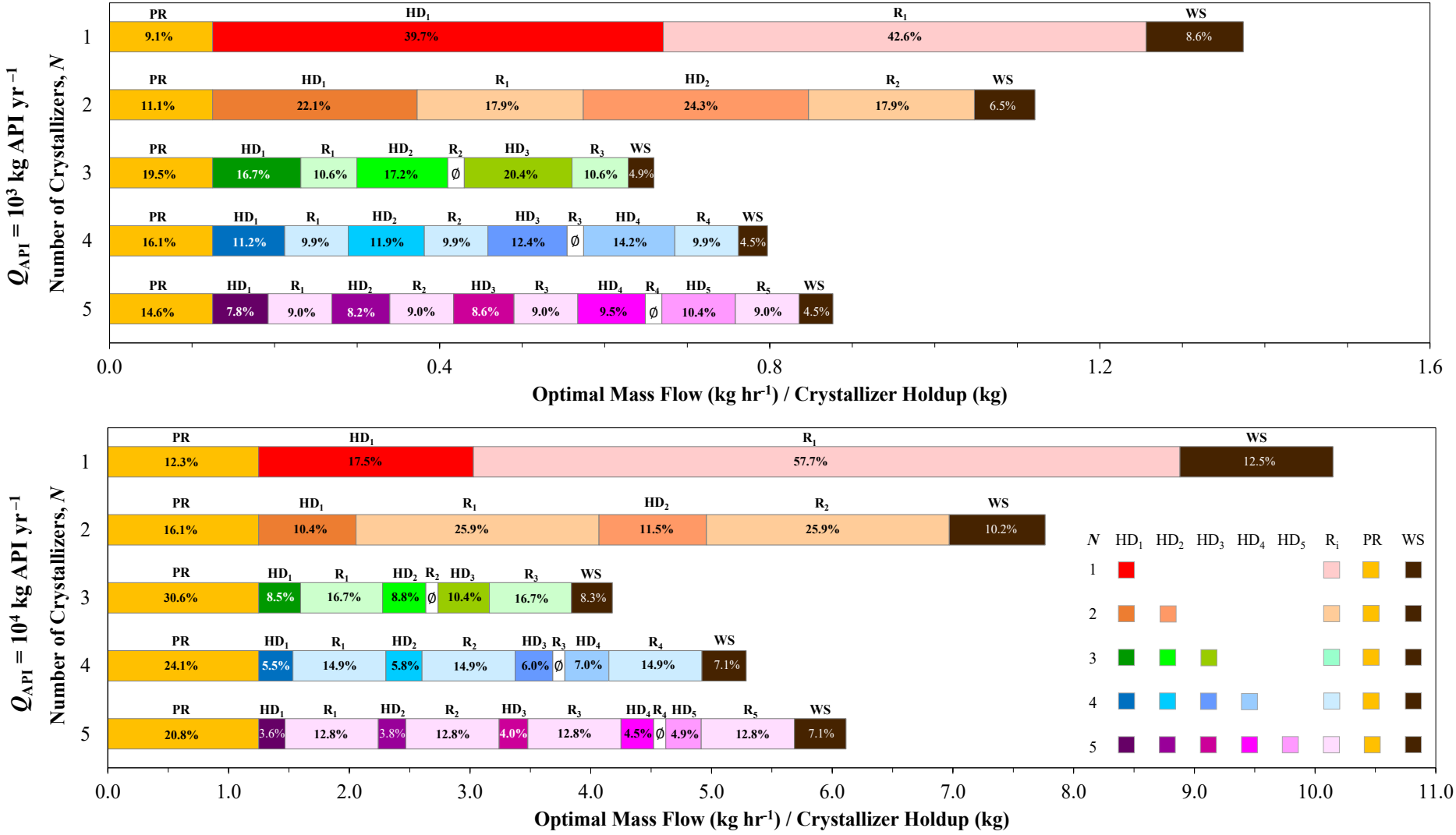

Figure 72: Optimal plantwide and MSMPR crystalliser mass holdups and flowrates of crystallised melitracen in key flowsheet streams.

Fig. 72 shows the API mass flowrates of key flowsheet streams (see Fig. 63) corresponding to *NPV* maxima found by solution of the described MINLP optimisation problem for different considered plant capacities (Q_{API}) and numbers of crystallisers (N). This analysis serves as a comparative evaluation of the amount of crystallised API withdrawn as product vs. that leaving the MSMPR cascade as waste and that within recycle streams (R_i), crystalliser holdups (HD_i) and total waste (WS). Fig. 72 shows the total material amounts for different design considerations in streams and MSMPR vessel holdups on an hourly basis as well as individual component contributions as fractions of the total amounts.

The amount of crystallised API product (PR in Fig. 72) for different numbers of crystallisers (N) is the same for different plant capacities is the same, as each design must produce its target amount of crystalline API product. Total mass quantities differ between each considered plant capacity, reflecting the different total material throughputs required. For each considered plant capacity, there are similar trends observed. As the number of crystallisers (N) increases, the values of individual mass holdups and recycle streams decrease as the crystallisation yields increase and the units become more efficient. However, the total material quantities decrease to a point (N = 3), i.e., the plant becomes more materially efficient, beyond which the total material quantities increase and the benefits of increasing N are no longer observed, reflecting results presented in previous sections. The benefits of improving material efficiency with increasing N = 1–3 is also shown by the decreasing quantities of waste; for N > 3, the benefits of reduced waste decreases with respect to N = 3 vs. N = {1, 2}.

For both considered plant capacities, for $N \geq 3$, there are recycle streams which equal zero, i.e., the MINLP optimisation has determined that no recycle be allocated to certain crystallisers (i.e., y_i = 0 for certain stages i). For the higher considered plant capacity ($Q_{API} = 10^4$ kg API yr^{-1}), relative quantities of product vs. that withheld in recycle streams and vessel holdups is higher than at the lower considered capacity ($Q_{API} = 10^3$ kg API yr^{-1}); relative quantities of waste also increase.

The current study considers only a stream of pure melitracen in solution which is to be crystallised in the MSMPR cascade. Recent studies considering the effects of impurity compounds on component solubilities and crystallisation kinetics highlight the importance of such considerations.[240] While thermal degradation of melitracen was not reported within the considered temperature range in the experimental study from which crystallisation kinetic parameters were taken,[181] expansion of this modelling framework to other APIs should take such phenomena and effects into consideration, as investigated in recent MSMPR studies.[241] Lower capacities and effects of alternative numbers of crystallisers out with the range considered here (i.e., N > 5) can be easily

investigated in the described MINLP optimisation framework; however, the number of variables, constraints and computational time will increase substantially.

9.5 Comparative Economic Evaluation of MSMPR Cascades

9.5.1 Optimal Net Present Value and Total Cost Components

Optimal Capital (*CapEx*) and Operating (*OpEx*) Expenditure components for different considered plant capacities (Q_{API}) and number of implemented crystallisers (N) at the end of the plant lifetime are shown in Fig. 73 (calculated as per Chapter 3.6). Total cost components are higher for Q_{API} = 10^4 kg API yr^{-1} than for Q_{API} = 10^3 kg API yr^{-1} in correspondence with the required larger equipment capacities and material throughputs associated with higher plant capacities. Total *CapEx* and *OpEx* components both decrease from N = 1–3 and then increase for $N \geq 3$, following the trend observed for cascade volumes (Fig. 70). This result is observed for *CapEx* components because *BLIC* is a function of equipment capacities (from *FOB* components), of which MSMPR vessels are a significant component; the *WCC* is a function of material throughput, which also follows the same decreasing then increasing trend.

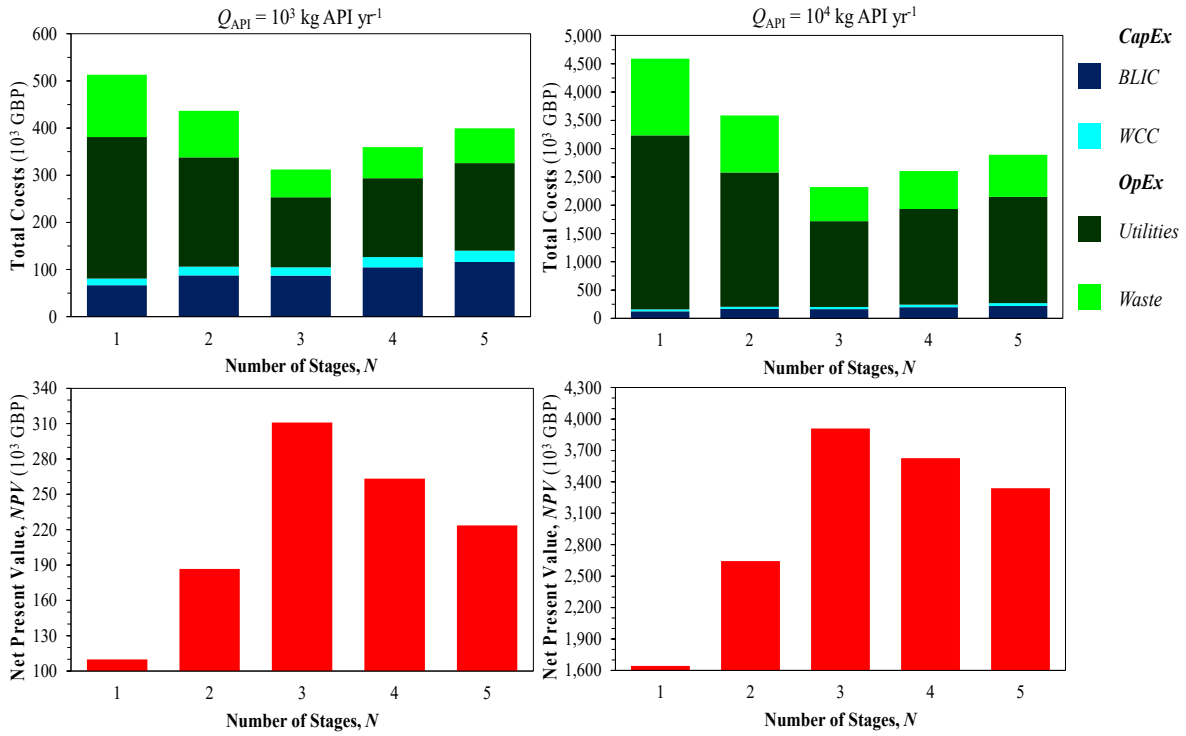

Figure 73: Optimal Capital (*CapEx*) and Operating (*OpEx*) Expenditure components and Net Present Values (*NPV*) at both considered plant capacities (Q_{API}) for different numbers of crystallisers (N) for melitracen crystallisation.

Total *CapEx* is dominated by *BLIC* due to the costs of equipment being much greater than *WCC* costs which are a function of material throughputs. Total *OpEx* is dominated by utilities components, which are associated with material handling and MSMPR cooling duties. Solvent (i.e., ethanol from the mother liquor solution) recovery from product and waste streams (i.e., F_{2N+3} and F_{2N+2} in Fig. 63, respectively) but can easily be incorporated into the existing MINLP framework.

Resulting *NPV* maxima for different plant capacities (Q_{API}) and numbers of implemented crystallisers (N) are also shown in Fig. 73. For both considered plant capacities, *NPV* maxima are attained for $N = 3$, where total cost components are their lowest due to the previously discussed trends. The optimal flowsheet configuration and crystalliser vessel design and operating parameters depend on the kinetic and thermodynamic (i.e., solubility) behaviour of the API being crystallised, the solvent in which the API is dissolved and the method of supersaturation generation; a recent study showed the importance of the solvent effect considerations on crystallisation kinetics.[242] Nevertheless, given crystallisation kinetic parameters and solubility behaviour, the current modelling framework may be expanded to other APIs amenable to cooling crystallisation in MSMPR cascades.

9.5.2 Cost Component Breakdown by Process Stream and Vessel

Fig. 74 compares a *CapEx* component breakdown per crystallisation unit vs. annualised *OpEx* components (calculated as the sum of time discounted *OpEx* over the plant lifetime and averaged per year) and annualised profits from API sales (averaged in the same way). Profits are relatively substantially higher vs. expenditures (negative cash flows) for the higher plant capacity (Q_{API}); this supports the previous discussion of the benefits of operating this MSMPR cascade at higher production capacities. The *BLIC* breakdown per unit crystalliser are approximately the same for each capacity and number of crystallisers; this is due to each of the individual vessel volumes being approximately equal in each design case (choice of LLE solvent and N for each considered Q_{API}).

9.5.3 Economic Sensitivity Analysis

Sensitivity analysis on the considered value of interest rate (t) is implemented to investigate the effect of varying economic parameters on designs. Here, we vary the interest rate for the MINLP optimised designs (which used a base case value of $t = 5\%$) for different considered plant capacities (Q_{API}) and number of crystallisers (N).

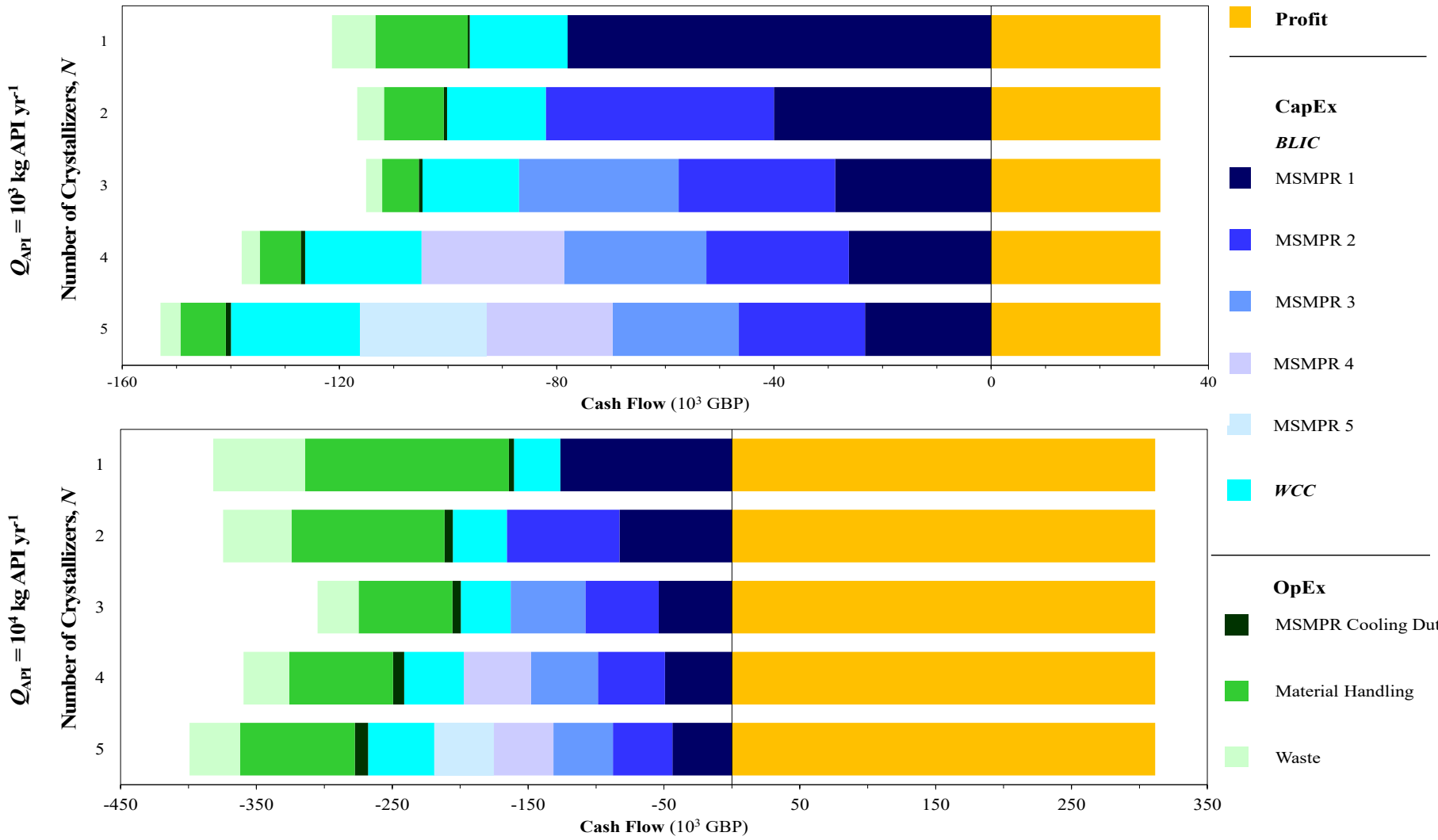

Figure 74: Annualised cost breakdown of cash flows for different considered plant capacities (Q_{API}) and numbers of crystallisers (N) for melitracen crystallisation.

Fig. 75 shows the effect of varying interest rates, t = {2, 5, 8, 10}%, on the calculated *NPV* for fixed, optimal designs established by solution of the MINLP optimisation problems for both considered plant capacities (Q_{API}). At both capacities, the assumed value of t affects the final *NPV* at the end of the plant lifetime significantly; as t increases, the *NPV* decreases due to the greater effect of inflation and thus decreasing time value of profits. The percentage difference in *NPV* by varying t at Q_{API} = 10^4 kg API yr^{-1} is less than for Q_{API} = 10^3 kg API yr^{-1}, i.e., operating at higher production capacities is more economically stable. It is important to note that this sensitivity analysis has been performed by varying t for fixed optimal plant designs from the MINLP optimisation problem solution in which t = 5% is the assumed value; it is possible that solving the MINLP optimisation problem for different values of t may result in different optimal plant configurations and crystalliser designs for the considered values of Q_{API} and N. Nevertheless, variation of the assumed interest rate t is of value to investigate the effect of economic parameters.

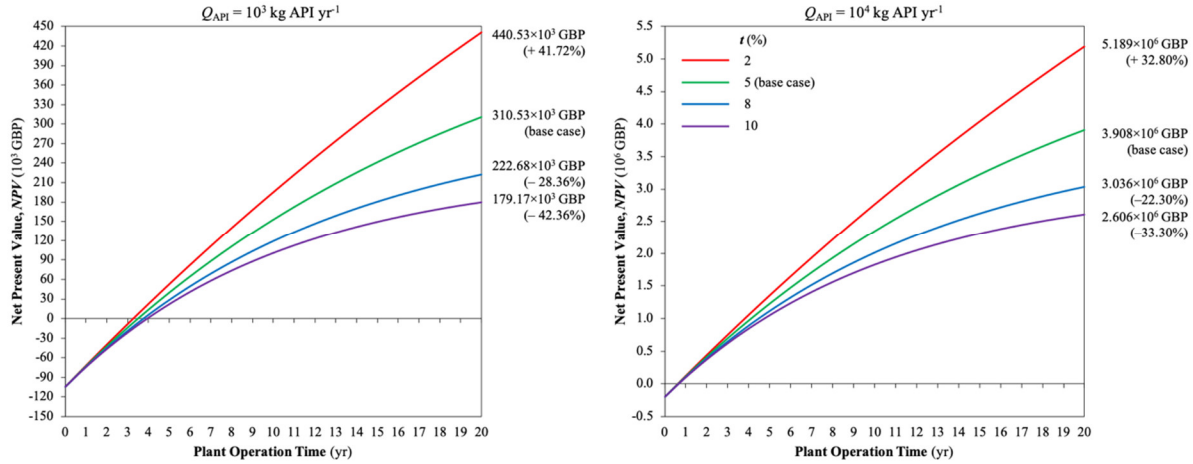

Figure 75: Net Present Value (*NPV*) vs. plant operation time for varying assumptions of interest rates for both considered plant capacities at optimal designs (N = 3) for melitracen crystallisation.

The Payback Period (*PBP*) is defined as the plant operation time taken for the total *CapEx* investment to be paid off, i.e., the time taken until *NPV* = 0. Calculated PBP for different plant capacities (Q_{API}), number of implemented crystallisers (N) and assumed interest rate (t) for optimal designs presented in previous sections are shown in Fig. 76. The calculated *PBP* values for Q_{API} = 10^4 kg API yr^{-1} are significantly less than for Q_{API} = 10^3 kg API yr^{-1}; while profits increase significantly at a higher production capacity, total cost (i.e., *CapEx* and *OpEx* components) do not increase as significantly to have such a detrimental effect on the economic performance. This result supports the idea mentioned in the previous paragraph that higher production capacities are beneficial for continuous crystallisation. However, this does not account for the negative effects of scale on mixing and heat and mass transfer efficiencies, upon which the considered MSMPR

model is based. Investigating the effect of API sales price on the presented MINLP optimisation results will also provide further insight into the sensitivity of the MSMPR cascade design to different economic parameters.

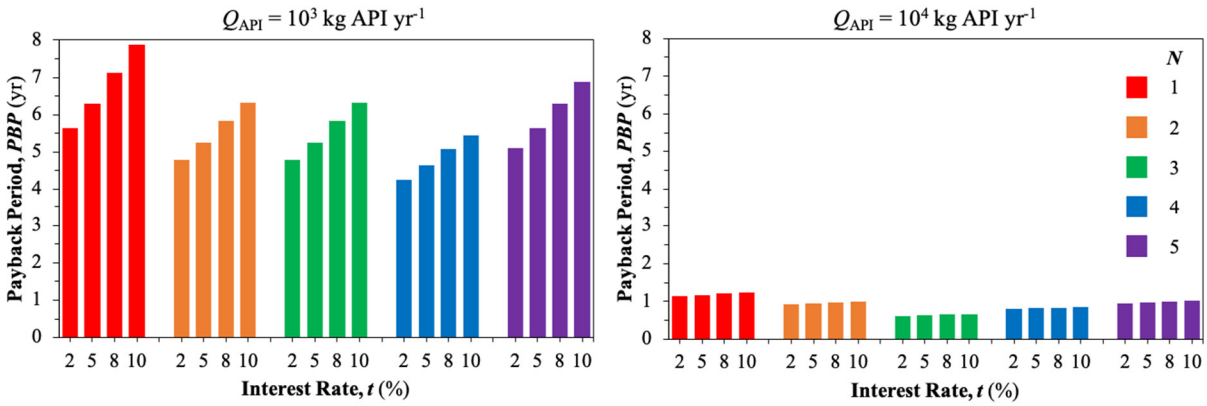

Figure 76: Payback Period (*PBP*) for varying assumptions of interest rates (base case is t = 5%) for both considered plant capacities (Q_{API}) for different numbers of implemented crystallisers (N) for melitracen crystallisation.

9.6 Chapter Conclusions

This study has constructed and solved a MINLP optimisation problem for the maximisation of the Net Present Value (*NPV*) of a cascade of continuous cooling MSMPR crystallisers for the production of melitracen, an antidepressant API. The MINLP optimisation problem considered varying numbers of crystallisers (N = 1–5) and different plant API capacities (Q_{API} = {10^3, 10^4} kg API yr^{-1}), with crystalliser vessel volumes, operating temperatures and recycle options as decision variables. Plantwide material efficiencies (i.e., crystallised API product vs. API withheld in the MSMPR cascade and lost in waste streams) increase until N = 3, beyond which the benefits of increasing the number of crystalliser vessels decreases. The cost optimal number of vessels N = 3 for both considered capacities with recycle streams allocated to the first and third crystallisers in the MSMPR cascade. The final *NPV* values were shown to be sensitive to the considered interest rate, which will fluctuate throughout the plant lifetime in practice. This study presents the first implementation of MINLP optimisation for the design of a cascade of MSMPR crystallisers and its novelty and utility lies in the rapid screening of flowsheet configurations for pharmaceutical crystallisation processes; the modelling and optimisation framework can be extended to any API or solute amenable to cooling crystallisation given the availability of growth and nucleation kinetic parameters and solubility data.

PART V

RESEARCH CONTRIBUTIONS & THESIS CONCLUSIONS

Chapter 10

Research Contributions

This thesis makes several novel research contributions, summarised herein. The most significant contributions include reaction kinetic parameter estimations for several API continuous flow syntheses, CPM process design for several APIs, the first instance of NLP optimisation for MSMPR crystallisation cascade design and the first instances of MINLP optimisation for pharmaceutical separation process synthesis, namely LLE and MSMPR cascades.

10.1 API Continuous Flow Synthesis Reaction Kinetic Analysis

This work performs reaction rate law elucidation and kinetic parameter estimation for several societally important APIs: diphenhydramine, rufinamide, nevirapine and atropine. Understanding reaction kinetics allows insight into synthesis performance under different design and operating conditions to inform reaction optimisation and plant vessel sizing. Reaction rate law elucidation via comparative evaluation of candidate rate laws and kinetic parameter estimation from analysis of published conversion/yield data for different flow reactions is used to facilitate flow reactor design as part of upstream CPM steady-state plant models. Comparison of different candidate rate laws are made where sufficient kinetic data is available and reasonable assumptions on plausible rate laws and/or attainable conversions are made where necessary. A summary of the relevant kinetic parameter estimations for each API performed are provided here.

10.1.1 Diphenhydramine

This work presents original reaction kinetic analysis, rate law elucidation and kinetic parameter estimation for the demonstrated continuous flow synthesis of diphenhydramine by Snead and Jamison (2013).[32] Diphenhydramine is a potent antihistamine and hypnotic with high global sales volumes, being used as part of several popular brand formulations. The cost-effective production of diphenhydramine via CPM has the potential for significant economic impact. The original flow synthesis of diphenhydramine features a single reaction between CDPM and DMAE with carrier solvent (NMP) and without (as a neat mixture). The availability of time-dependent conversion data allowed comparison of candidate rate law expressions to describe the kinetic behaviour of the API synthesis. Comparison of zero-, first-, and overall second-order (first order in both CDPM and DMAE) rate laws show first-order kinetics (in CDPM) for the synthesis in NMP but second-order behaviour (first-order in both reagents) in a neat mixture. Corroboration of the estimated kinetic

parameter values with larger reaction performance data sets will further clarify this hypothesis and rate law elucidation.

10.1.2 Rufinamide

This work performs reaction kinetic analysis and comparative evaluation of rate law assumption on upstream CPM plant design and technoeconomic performance for the demonstrated continuous flow synthesis of rufinamide by Zhang et al. (2014).[40] Rufinamide is an important API for the treatment of childhood epilepsy. The considered continuous flow synthesis of rufinamide features three reactions in flow towards the desired API. The first two reactions assume first-order kinetics due to them involving a large organic molecule reacting with a much smaller reagent in excess. For the third reaction, comparative evaluation of candidate rate laws for their effect on the upstream plant designs are considered. Corroboration of the estimated kinetic parameter values with larger reaction data sets will further clarify rate laws.

10.1.3 Nevirapine

This work performs the first-ever Arrhenius parameter regression for modelling the temperature-dependence for nevirapine production from published data of the considered API continuous flow synthesis by Verghese et al. (2017),[170] which considers a three step synthesis from advanced starting materials. The first two reactions in the synthesis are assumed to perform as per the demonstrated lab-scale synthesis. For the third reaction (between CYCLOR and NaH to form nevirapine), first-order kinetics in CYCLOR are assumed due to it reacting with a significant excess of NaH. Temperature-dependent reaction performance data available in the literature for this step is used for the regression of Arrhenius law parameters in order to be able to simulate reaction performance as a function of temperature in the nevirapine upstream CPM plant model.

10.1.4 Atropine

This work elucidates the plausible rate law and kinetic parameters for the continuous flow synthesis of atropine demonstrated by Bédard et al. (2016),[177] featuring two steps in series. The first reaction is very fast (99% conversion in 3.5 min residence time) and the reported lab-scale performances is assumed to apply to the study presented in this work. Kinetic parameter estimation for the second reaction is performed, comparing zero-, first- and overall second- order (first-order in both reagents) as candidate rate law expressions. An overall second-order rate law expression is shown as the most plausible. The literature does not contain sufficient data to model the effect of an undesired side reaction of API to apoatropine; however, it is assumed that a fixed portion of formed API converts to apoatropine, as described in the literature.[177] Corroboration of the

estimated kinetic parameter values with larger reaction performance datasets will clarify reaction kinetic rate law elucidation.

10.2 Upstream CPM Plant Design and Economic Evaluation

Original steady-state process simulation for comparative economic evaluation and design of different separation process alternatives for the upstream CPM of diphenhydramine (synthesis + LLE) and rufinamide (synthesis + antisolvent crystallisation) is performed. This work is also the first instance of rigorous process design screening for the greatest cost savings vs. demonstrated batch processes for both diphenhydramine and rufinamide.

10.2.1 Diphenhydramine: Continuous Synthesis + Liquid-Liquid Extraction

This study uses regressed reaction kinetics for PFR design and UNIFAC/NRTL modelling for the design and technoeconomic comparative evaluation of LLE process options for diphenhydramine.

Regressed reaction kinetics are used in order to conduct reactor sizing. Comparison of the effect of assumed reactor diameter on the resulting tube length shows that reasonable volumes and lengths result from the computed reaction kinetics, mass balances and assumed API plant capacity (Q_{API} = 100 kg API yr^{-1}). The potential for significant unit operation vessel size/dimension reductions is one of the many benefits attainable via CPM implementation. Reactor heating duty estimation shows sensible heating duties for the reactor sizes computed; group contribution methods are used to estimate standard enthalpies of formation and component specific heat capacities where values are not available in the literature.

The design of the continuous LLE process uses the UNIFAC and NRTL models for consideration of non-ideal multicomponent mixture behaviour for the prediction of liquid-liquid equilibria phase compositions and API solubilities and partitioning between resulting mixture phases. Candidate separation solvents are chosen on the basis of availability of phase compositions (either from available experimental data or the ability to model them via UNIFAC or NRTL). Comparison of the effect of LLE operating temperature (T_{LLE} = {20, 40, 60} °C) and the LLE solvent-to-feed ratio for different candidate LLE solvents are conducted for technoeconomic evaluation of the best continuous LLE design option.

It is shown that chloroform allows for the greatest CPM cost savings with respect to the plant with a batch separation, however its usage is undesirable due to the inherent toxicity issues with chlorinated solvent usage. Methylcyclohexane emerges as the next most promising LLE solvent with more suitable EHS characteristics while still attaining high API recoveries, good material efficiencies (quantified by green chemistry metrics) and significant cost savings. This study

illustrates the trade-off that often occurs between LLE solvent performance vs. EHS criteria, e.g., although chlorinated solvents are harmful, they often allow for the most rapid phase splitting, API recovery and material efficiency.

10.2.2 Rufinamide: Continuous Synthesis + Antisolvent Crystallisation

This study demonstrates the use of regressed reaction kinetics for PFR design and the design and technoeconomic comparative evaluation of antisolvent crystallisation process options for rufinamide CPM.

Regressed reaction kinetics for each synthetic step are used for the purposes of reactor design. Comparison of the effect of reaction rate law assumption and regressed kinetic parameter values shows that the assumed rate law does not significantly affect the technoeconomic performance of the upstream CPM plant. Due to the large fraction of water in the incoming mixture to the antisolvent (using water) crystallisation process, it is assumed that the mixture is mostly aqueous. The aqueous solubility of rufinamide is estimated via a published correlation using the API's octanol-water partition coefficient. This solubility is then used to estimate the crystallisation yield as a function of antisolvent (i.e., water) usage on the technoeconomic performance of the rufinamide CPM plant.

Examination of crystallisation performance as a function of antisolvent usage shows that beyond an antisolvent-to-feed ratio of 2 there are only incremental benefits to the attained crystallisation yield and resulting plant costs. All CPM processes show significant cost savings and material efficiency improvements over the published continuous flow synthesis with batch crystallisation.

10.3 Economic NLP Optimisation of Upstream CPM Plants

This work is the first demonstration of economic optimisation via NLP for warfarin (synthesis + LLE) and nevirapine (synthesis + pH crystallisation) upstream CPM and for MSMPR crystallisation for cyclosporine, paracetamol and aliskiren; in particular, it is the first utilisation of economic optimisation for MSMPR cascade design for any compound. The quantification of economic benefits of CPM processes is essential for elucidating the best designs to maximise its impact on pharmaceutical production.

10.3.1 Warfarin: Continuous Synthesis + Liquid-Liquid Extraction

This work illustrates the first NLP formulation for technoeconomic optimisation of the upstream CPM of warfarin, based on the published continuous flow synthesis,[166] as well as using UNIFAC

modelling to screen candidate continuous LLE process designs with explicit detailed mass transfer correlations to estimate continuous LLE efficiency.

Reactor design assumes the same conversion/API yield as per the published lab-scale demonstration. Candidate LLE solvents are shortlisted as per the same criteria as for diphenhydramine, i.e., formed a biphasic mixture between whose phases warfarin can partition favourably into the organic phase and presented no significant EHS concerns.

The formulated NLP optimisation problem is to minimise the upstream CPM plant total cost objective function subject to suitable constraints on LLE solvent usage and vessel residence time, both of which are considered as NLP decision variables. Separate problem instances of LLE operating temperature (T_{LLE} = {20, 40, 60} °C) and candidate LLE solvent are solved. The optimal operating temperature varies between different solvent choices due to the varying thermodynamic and mass transfer behaviours of solutes in different ternary solvent mixtures. It is also observed that solvents with similar properties and molecular structures (e.g., esters, alcohols) result in similar plantwide performances due to the similar phase splitting behaviour and API partitioning between phases. The optimal temperature choice varies across different LLE solvent choices due to differing thermodynamic behaviours between ternary solvent systems. The optimal LLE solvent (attaining the lowest total costs and having suitable EHS characteristics) is isobutyl acetate operating at 60 °C.

10.3.2 Nevirapine: Continuous Synthesis + pH Crystallisation

This study is the first use regressed reaction kinetics for reactor and pH crystallisation modelling and optimisation for the design and technoeconomic comparative evaluation of process options for nevirapine CPM. The study also demonstrates the first comparative evaluation of different CPM designs vs. published batch processes from both a plantwide total costs + API cost of goods perspective for nevirapine.

The regressed Arrhenius kinetic parameters for the final step in the continuous flow synthesis of nevirapine allow temperature-dependent reaction modelling. For the pH crystallisation, a published pH-dependent aqueous solubility model for nevirapine is used to predict the crystallisation yield as a function of pH. The NLP optimisation problem is formulated for plant total cost minimisation subject to constraints on the final reactor operating temperature and crystallisation pH, both of which are used as NLP decision variables in the optimisation problem. Separate problem instances of assumed plant API production capacity and attainable solvent recovery are considered.

The reactor operating temperature is driven to its upper bound whereas crystallisation pH is always lower than that of the batch process (pH = 7) to minimise material consumption associated with the pH change to crystallise the API and thus operating expenditure contributions which constitute a major component of plantwide total costs in all cases. Furthermore, CPM operation allows for significant reduction in the API cost of goods compared to the demonstrated continuous flow synthesis with a batch crystallisation.

10.3.3 Cyclosporine, Paracetamol + Aliskiren: MSMPR Cascades

This work demonstrates the first-ever economic optimisation via NLP for MSMPR cascade design. The published demonstration of the continuous MSMPR cooling crystallisation of cyclosporine, paracetamol and aliskiren with solubility behaviour as a function of temperature, nucleation and growth kinetic and population balance equation parameters are used to formulate a NLP optimisation problem for the total cost minimisation of a MSMPR cascade for API production, subject to constraints on crystalliser residence times and operating temperatures, which are used as decision variables for the NLP problem. Separate problem instances of assumed plant capacity and number of crystallisers are considered.

It is shown that for lower capacities that only one crystalliser is cost optimal whereas at higher capacities more vessels are optimal. Implementing multiple crystallisers also allows for higher operating temperatures (i.e., less crystalliser cooling and associated lower duties). The modelling and optimisation framework can easily consider different plant capacities, more crystallisers and can be expanded to other APIs given the availability of crystallisation kinetics and their amenability to cooling crystallisation.

10.4 MINLP Optimisation of Continuous Separation Cascades

This work presents the first-ever instance of MINLP optimisation for process synthesis of separation cascades for pharmaceutical applications. While MINLP optimisation for process synthesis has been implemented in literature for separation design in many different applications (see Table 2), the contributions towards LLE and MSMPR cascade syntheses made in this work are the first instances of MINLP for pharmaceutical separation process design. The contributions made towards atropine and melitracen production are described here.

10.4.1 Atropine: Optimal Process Synthesis of LLE Cascades

Dimensionless number analysis is conducted to ensure reaction mixture homogeneity as part of upstream CPM plant design. Following the kinetic parameter estimation implemented for the atropine synthesis, the analysis is performed to ensure the validity of the assumption of

homogeneous reaction mixtures (with respect to concentration, temperature and velocity gradients) holds true for all reactor designs. Quantification of Reynolds, Péclet and Damköhler numbers as a function of assumed reactor diameter is performed to ensure they are not out with critical value ranges that would contradict the assumption of homogenous reaction mixture behaviour. It is found that the Damköhler numbers dictated the maximum allowable PFR diameters for both reactions.

This study showcases the first demonstration of MINLP for LLE process synthesis for pharmaceutical applications in the literature. Candidate LLE solvents are screened as per diphenhydramine and warfarin CPM design methodologies. Liquid-liquid equilibria phase compositions are estimated using the UNIFAC model and the Skelland-Moeti correlation is used for the estimation of LLE efficiency for different options. The MINLP optimisation problem formulation for plant total cost minimisation considers LLE solvent feed rate and vessel volumes as continuous decision variables with LLE solvent allocation to vessels as binary decision variables. Separate problem instances of LLE solvent choice and number of vessels are considered.

It is demonstrated that synthesis equipment (reactors) is of significantly higher cost compared to the LLE vessels and thus implementing more LLE stages in the cascade does not have a detrimental effect on total costs within the range considered. It is shown that using toluene with four LLE vessels is cost optimal for the considered plant capacities. The MINLP optimisation framework presented for continuous flow synthesis + LLE can be used for other APIs given the availability of reaction kinetics and ternary phase equilibria acquired via experimental data or a group contribution method (e.g., UNIFAC, NRTL etc.) as implemented here.

10.4.2 Melitracen: Optimal Process Synthesis of MSMPR Cascades

This study is the first-ever instance of MINLP optimisation for optimal MSMPR cascade process synthesis. The demonstrated continuous MSMPR cooling crystallisation from the literature describes API solubility as a function of temperature and crystal nucleation and growth kinetic parameters and population balances to allow steady-state process modelling of MSMPR cascades for this API.[181] This work expands the process model to consider a solids recycling configuration previously examined in the literature, wherein the product magma of the final crystalliser in the cascade is fed to a gravitational separation column, removing mother liquor in order to produce a concentrated slurry from the bottom, part of which is recycled to the cascade and the remainder of which is withdrawn as product. This work formulates a MINLP optimisation problem for Net Present Value (NPV) maximisation of the MSMPR cascade with recycle, with crystalliser operating temperatures, vessel volumes, recycle stream flowrates and mother liquor removal extent as

continuous decision variables with recycle stream allocation as binary decision variables. Separate problem instances of number of vessels and plant capacity are solved.

It is found for both assumed plant capacities that the optimum cascade configuration is three crystallisers, beyond which the benefits of increasing number of units on crystallisation yield are incremental at best, with recycle allocation to the first and last crystalliser. The MINLP optimisation framework presented for continuous MSMPR crystallisation with solids recycle can be used for other APIs given the availability of crystallisation kinetics, solubility description as a function of temperature (either from experimental data or estimated via group contribution methods such as the activity coefficient models UNIFAC, NRTL or others) and the amenability of the API to cooling crystallisation.

Chapter 11

Thesis Conclusions

This PhD thesis presents a framework for steady-state modelling, simulation and optimisation of Continuous Pharmaceutical Manufacturing (CPM) upstream plants, focussing on reaction and separation processes, the latter of which presents a technically challenging obstacle with respect to end-to-end CPM process implementation. This work has been conducted with the aim to elucidate optimal technoeconomic benefits of CPM processes to maximise their potential for industrial adoption. Continuous process case studies on several Active Pharmaceutical Ingredients (APIs) have been conducted for the first time, including upstream CPM flowsheets (reaction + separation) for diphenhydramine (antihistamine), rufinamide (antiepileptic), warfarin (anticoagulant), nevirapine (HIV-1 treatment) and atropine (nerve agent effects) and continuous cooling crystallisation cascades in Mixed Suspension, Mixed Product Removal (MSMPR) vessels for cyclosporine (immunosuppressant), paracetamol (analgaesic), aliskiren (antihypertensive) and melitracen (antidepressant). Process simulation and NLP/MINLP optimisation have been implemented to various extents for different APIs for the best design and operation of CPM plants with respect to economic performance and environmental impact.

Reaction kinetic parameter estimation from published data for diphenhydramine, rufinamide, nevirapine and atropine have been conducted for flow reactor design. Separation process design predicts ternary phase compositions and API solubilities using popular activity coefficient models such as UNIFAC and NRTL and mass transfer correlations for biphasic mixtures in agitated tanks to estimate continuous separation efficiency (for Liquid-Liquid Extraction (LLE) design) and crystal nucleation and growth kinetics, population and mass balances for MSMPR cascade design.

Continuous flowsheet simulation for process design has been implemented for diphenhydramine and rufinamide, performing comparative evaluation of separation options on the respective merits of plant total costs, material efficiency and EHS criteria of solvents. Economic optimisation via Nonlinear Programming (NLP) has been conducted for upstream CPM plants (reaction + separation) for warfarin and nevirapine and for MSMPR cascades for cyclosporine, paracetamol and aliskiren; the latter presents the first instance of economic optimisation of MSMPR cascades.

Process synthesis for optimal separation design for pharmaceutical applications has been conducted for the first time in the literature. The case studies considered are the design of LLE cascades for upstream CPM (reaction + separation) of atropine and MSMPR cascades with solids recycle for the continuous cooling crystallisation of melitracen. Continuous decision variables

involve vessel volumes, operating temperatures and stream flowrates, while binary decision variables describe whether stream allocation to certain vessels occurs.

The results presented in this thesis are subject to various assumptions and limitations.

- Reaction kinetic parameter estimations for the continuous syntheses of diphenhydramine, rufinamide, nevirapine and atropine are subject to limited datasets (i.e., yields as a function of concentration and temperature). Parameter estimations from larger datasets (concentrations for many time, temperature, initial concentration, base and catalyst equivalents combinations etc.) will allow more robust regressions and consideration of more complex rate laws. These datasets should include details of side reactions towards undesired by-products whose presence in pharmaceuticals can drastically affect downstream processing and efficacy in patients.
- Phase equilibria involved in pharmaceutical separation processes involve non-ideal multicomponent mixtures for which experimental data (phase compositions, API solubilities, solute partitioning) is often not available, necessitating theoretical methods (e.g., UNIFAC + NRTL models) for prediction of the phase behaviour of these mixtures for separation process design. These models are best used as guides/indicators of promising process options, but not for accurate design; thus, the design options highlighted as best via the case studies presented in this thesis should be investigated further via experimental campaigns and pilot plant studies.
- The modelling of MSMPR cascades for continuous cooling crystallisation of cyclosporine, paracetamol, aliskiren (NLP studies) and melitracen (MINLP study) use nucleation and growth kinetics available in the literature; however, these do not consider agglomeration and breakage of crystallisation, nor do they decouple primary and secondary nucleation phenomena in their nucleation model equations. The optimisation cases in the MSMPR studies (Chapters 7 and 9) consider technoeconomic objective functions in comparison to other research groups that address optimisation from a product quality perspective (see Chapter 2). Product quality constraints (regarding size properties, purity and polymorph) can easily be incorporated into the modelling and optimisation methodologies presented here.
- The aims of the optimisation cases are from technoeconomic perspectives with comparison of material efficiencies of different process designs. Material efficiency can also be explicitly considered in the optimisation objective functions by formulation of multi-objective problems.
- The case studies presented highlight the immense value in systematic and rigorous model-based simulation and optimisation campaigns for CPM process systems, and the applicability of the methodologies outlined in this PhD thesis. The frameworks presented within can be extended to other APIs with similar processes.

PART VI

AUXILIARY CHAPTERS

Appendix A

Nomenclature and Acronyms

A.1 Acronyms

API	Active Pharmaceutical Ingredient
BONMIN	Basic Open Source Nonlinear Mixed Integer Programming
BX	Batch
CEPCI	Chemical Engineering Plant Cost Index
COBC	Continuous Oscillatory Baffled Crystalliser
CPM	Continuous Pharmaceutical Manufacturing
CSTR	Continuous Stirred Tank Reactor
DWC	Dividing Wall Column
EHS	Environment, Health and Safety
HEN	Heat Exchange Network
HX	Heat Exchanger
HIV	Human Immunodeficiency Virus
IPOPT	Interior-Point Nonlinear Optimiser
LCA	Life Cycle Assessment
LLE	Liquid-Liquid Extraction
MINLP	Mixed Integer Nonlinear Programming
MSMPR	Mixed Suspension, Mixed Product Removal
NLP	Nonlinear Programming
NRTL	Non-Random Two Liquid
ODE	Ordinary Differential Equation
OSN	Organic Solvent Nanofiltration
PAT	Process Analytical Technology
PDE	Partial Differential Equation
PFC	Plug Flow Crystalliser
PFR	Plug Flow Reactor
PR	Product
PSA	Pressure Swing Adsorption
PSE	Process Systems Engineering
R&D	Research and Development
SMB	Simulated Moving Bed
UNIFAC	UNIQUAC Functional group Activity Coefficient
UNIQUAC	Universal Quasichemical
WHO	World Health Organisation
WS	Waste

A.2 Molecules and Reagents

1-HxOH	1-Hexanol
1-PnOH	1-Pentanol
1-PrOH	1-Propanol
2-CAN	2-(Cyclopropylamino)nicotinic acid
AC	Activated carbon
Ac_2O	Acetic anhydride
AcOH	Acetic acid
Al_2O_3	Aluminium oxide
BuOAc	Butyl acetate
BuOH	1-Butanol
CAPIC	2-Chloro-3-amino-4-picoline
CAPIC-Na	CAPIC sodium salt
CDPM	Chlorodiphenylmethane
CH_2O	Formaldehyde
COMAD	2-Chloro-4-methylnicotinamide
CPA	Cyclopropylamine
CYCIC	2-Chloro-4-methylnicotinonitrile
CYCLOR	*N*-(2-chloro-4-methylpyridin-3-yl)-2-(cyclopropylamino)nicotinamide
CyHex	Cyclohexane
DCM	Dichloromethane
DMAE	Dimethylaminoethanol
DMF	Dimethylformamide
DMF-DMS	Dimethyl formamide-dimethyl sulphate
DMK	Dimethyl ketone
DMSO	Dimethyl sulfoxide
Et_2O	Diethyl ether
EtOAc	Ethyl acetate
H_2O	Water
H_2SO_4	Sulphuric acid
HepOH	Heptanol
HCl	Hydrogen chloride
iBuOH	Isobutanol
iPrOAc	Isopropyl acetate
iPrOH/IPA	Isopropanol
KOH	Potassium hydroxide
MeCAN	2-(Cyclopropylamino)nicotinate
MeCyHex	Methylcyclohexane
MEK	Methyl ethyl ketone
MeOH	Methanol

Mg_2SO_4	Magnesium sulphate
N_2	Nitrogen
NaBr	Sodium bromide
$NaCH_3O$	Sodium methoxide
NaCl	Sodium chloride
NaH	Sodium hydride
NaN_3	Sodium azide
NaOBr	Sodium hypobromite
NaOH	Sodium hydroxide
NH_3	Ammonia
nHep	*N*-Heptane
nHex	*N*-Hexane
NMP	*N*-Methylpyrrolidone
OcOH	Octanol
PhMe	Toluene
$SOCl_2$	Thionyl chloride
TCM	Chloroform / Trichloromethane
TEA	Triethylamine
TFA	Trifluoroacetic acid

A.3 Variables

A.3.1 Latin Letters and Symbols

A	Arrhenius pre-exponential factor (–)
a	Interfacial area between LLE phases ($m^2\ m^{-3}$)
a_i^s	Solid component activity
a_{ij}	Interaction energy between components i and j in the NRTL model ($J\ mol^{-1}$)
a_k	Parameter in eq. 12
$\boldsymbol{b}$	Right hand side of NLP/MINLP inequality constraint vector
B_i	Nucleation rate in MSMPR crystalliser i (# crystals m^{-3} suspension s^{-1})
b_k	Parameter in eq. 12
b_{MSMPR}	Nucleation rate exponent (–)
BLIC	Battery Limits Installed Costs (GBP)
$\boldsymbol{c}$	Right hand side of NLP/MINLP equality constraint vector
C_i	Concentration of species i (M or $kg\ m^{-3}$)
C_i^{sat}	Saturation concentration of i (M or $kg\ m^{-3}$)
C_j	Cost of equipment purchase at capacity j (GBP)
C_k	Group additivity coefficient for group k in estimation of total phase change entropy
c_k	Parameter in eq. 12
C_0	Initial / Feed concentration (M or $kg\ m^{-3}$)

$C_{p,m}$	Mixture specific heat capacity at constant pressure (J kg^{-1} K^{-1})
CapEx	Capital Expenditure (GBP)
CoG	Cost of goods (GBP kg API^{-1})
D	Diffusivity (m^2 s^{-1})
d_{32}	Sauter mean droplet diameter (m)
d_{imp}	LLE tank impeller diameter (m)
d_k	Parameter in eq. 12
d_{PFR}	Inner diameter of PFR (m)
$d_{PFR,MAX}$	Maximum PFR diameter (m)
d_t	LLE tank inner diameter (m)
Da	Damköhler number (–)
E	Environmental (*E*)-factor
E_a	Activation energy (J mol^{-1})
E_b	Energy barriers to crystal nucleation (J mol^{-1})
E_f	Solute extraction factor
E_g	Energy barrier to crystal growth (J mol^{-1})
E_{LLE}	LLE efficiency (%)
Eo	Eotvos number (–)
f	Correction factor in costing correlation (–)
F_i	Flowrate of stream leaving vessel i (varying units)
F_0	Flowrate of fresh feed entering process (varying units)
FOB	Free-on-Board Costs (GBP)
Fr	Froude number (–)
$\boldsymbol{g}$	NLP/MINLP inequality constraint function vector
g	Acceleration due to gravity (= 9.81 m s^{-2})
G_i	Crystal growth rate in MSMPR i (m API s^{-1})
G_{ij}	Coefficient of NRTL equation between components i and j in the NRTL model
G_k	Contribution of functional group k to total phase change entropy
g_{MSMPR}	Crystal growth rate exponent (–)
$\boldsymbol{h}$	NLP/MINLP equality constraint function vector
h_{1i}, h_{2j}	Group contribution of first-order group i, second-order group j in estimation of standard enthalpy of formation
h_{f0}	Constant in estimating the standard enthalpy of formation (= 10 kJ mol^{-1})
$\Delta^0 H_f$	Standard enthalpy of formation (J mol^{-1})
ΔH_{fus}	Enthalpy of fusion (J mol^{-1})
$\Delta^0 H_{rxn}$	Standard enthalpy of reaction (J mol^{-1})
ΔH_{rxn}	Enthalpy of reaction (J mol^{-1})
HD_i	Crystalliser API holdup in MSMPR i (kg API)
K	Overall mass transfer coefficient (m s^{-1})
k_b	Boltzmann constant (= 1.38064852×10^{-23} m^2 kg s^{-2} K^{-1})
k_{b0}	Pre-exponential factor for nucleation (# crystals m^{-3} suspension s^{-1})

k_{g0}	Pre-exponential factor for growth (m API s^{-1})
$k_{i,j}$	i^{th} order reaction rate constant in PFR j (varying units)
K_{OW}	API octanol-water partition coefficient (–)
k_p	Specific mass transfer coefficient of phase p (m s^{-1})
k_v	API volume shape factor (–)
L	Crystal length (m API)
L_i	UNIFAC compound parameter of r, q and z for molecule i
L_{PFR}	PFR length (m)
m	Solute partition coefficient
m_{API}	Mass of recovered API (kg yr^{-1})
M_i	Suspension density in MSMPR i (kg API m^{-3} suspension)
M_j	Number of second-order functional groups
m_{MSMPR}	MSMPR suspension density exponent (–)
$m_{process}$	Plant material throughput (kg yr^{-1})
m_{uAPI}	Mass of unrecovered API (kg yr^{-1})
m_{ur}	Mass of reagents remaining in waste streams (kg yr^{-1})
m_{us}	Mass of unrecovered solvent (kg yr^{-1})
m_{waste}	Mass of waste (kg yr^{-1})
MCS	Mean Crystal Size (m API)
MP	Mass Productivity (%)
n	Exponent in Eq. 41 (–)
N	Number of vessels (–)
n_{CH2}	Number of consecutive CH_2 groups
N_i	Number of first-order functional groups
n_i	Crystal population density function in MSMPR i (# crystals m^{-3} suspension m^{-1} API)
n_i^0	Nuclei population density function in MSMPR i (# crystals m^{-3} suspension m^{-1} API)
N_{imp}	Tank impeller rotation speed (rps)
n_k	Number of functional groups of type k
NPV	Net Present Value (GBP)
$OpEx$	Operating Expenditure (GBP)
p_{API}	API wholesale price (GBP kg API^{-1})
P_j	Equipment purchase cost at capacity j (GBP)
PBP	Payback Period (yr)
Pe	Péclet number (–)
pH_{CRYST}	Crystallisation pH
PMI	Process Mass Intensity (–)
Q_{API}	Plant API capacity (kg API yr^{-1})
q_i	UNIFAC parameter of molecule i, representing van der Waals molecular surface area

Q_k	UNIFAC surface area parameter for functional group k
R	Universal gas constant (= 8.314 J mol^{-1} K^{-1})
R^2	Coefficient of determination (–)
R_i	Volumetric flowrate of recycle stream entering vessel i (m^3 s^{-1})
r_i	Molecular radius of component i (m)
R_k	UNIFAC volume parameter for functional group k
r_{MIN}	Minimum LLE solvent-to-feed ratio (mass basis)
r_0	Initial value for LLE solvent-to-feed ratio (mass basis)
r_{TOT}	LLE solvent-to-feed ratio (mass basis) to LLE process (mass basis)
Re_{imp}	LLE tank impeller Reynolds' number (–)
Re_{PFR}	PFR Reynolds' number (–)
RR_{TOT}	Total solids recycle ratio (–)
S	LLE solvent feed rate (m^3 s^{-1})
S_{aq}	Aqueous API solubility (g L^{-1})
S_j	Capacity of equipment j (varying units)
S_0	Non-ionised aqueous API solubility (g L^{-1})
ΔS	Entropy of fusion (J mol^{-1} K^{-1})
$\Delta_0^{T_{fus}} S_{pc}$	Total phase change entropy (J mol^{-1}K^{-1})
Sc	Schmidt number (–)
Sh	Sherwood number (–)
t	Interest rate (%)
T	Temperature (°C)
T_{fus}	Melting point (K)
U_{mn}	UNIFAC energy of interaction between groups m and n
$U\&W$	Utilities and Waste (GBP or GBP yr^{-1})
u_{PFR}	Average fluid mixture velocity in PFR (m s^{-1})
V_i	Volume of vessel i (m^3)
V_m	API molar volume (cm^3 mol^{-1})
WCC	Working Capital and Contingency costs (GBP)
We	Weber number
WS	Waste (kg API hr^{-1})
x	Clear mother liquor removal ratio in solid-liquid separation column (–)
$\boldsymbol{x}$	Decision variable vector
X_A	Conversion of limiting reagent A (%)
$x_{i,p}^S$	Mole fraction of component i in phase p in solvent system S
x_i^{sat}	Component i saturation mole fraction
$\boldsymbol{x}_{LB}$, $\boldsymbol{x}_{UB}$	Lower, Upper bound on decision variable vector
x_m	UNIFAC mole fraction of group m
y_i	Binary decision variable deciding whether to allocate stream to vessel i (–)
Y_i	Yield in stage i (%)
z	UNIFAC coordination number (= 10)

A.3.2 Greek Letters and Symbols

α_{ij}	Non-randomness parameter between components *i* and *j* in the NRTL model
$\alpha_{i,p}^{S}$, $\beta_{i,p}^{S}$, $\gamma_{i,p}^{S}$	Quadratic, linear and constant coefficients in Eq. 97, respectively
β	Coefficient of thermal expansion (K^{-1})
γ_i	UNIFAC activity coefficient of molecule *i*
γ_i^{c}, γ_i^{R}	Combinatorial, Residual UNIFAC activity coefficient component of molecule *i*
γ_i^{sat}	UNIFAC activity coefficient of molecule *i* at saturation
η	Fugacity ratio
Θ	Molar ratio of excess reagent to limiting reagent
θ_i	UNIFAC molecular-weighted area fraction component for molecule *i*
θ_m	UNIFAC summation of area fraction of group *m* over all groups
λ_m	Mixture thermal conductivity (W m^{-1} K^{-1})
μ	Viscosity (kg m^{-1} s^{-1})
ν	Component stoichiometric coefficient (–)
ν_k^i	Number of occurrences of group *k* on molecule *i*
ρ	Density (kg m^{-3})
σ	Interphase surface tension (N m^{-1})
τ	Residence time (s)
τ_{ij}	Dimensionless interaction parameter between components *i* and *j* in the NRTL
ϕ	Dispersed phase volume fraction (–)
Γ_k	UNIFAC residual group activity coefficient for group *k*
Γ_k^i	UNIFAC residual group activity coefficient for group *k* in a solution of pure *i*
ϕ_i	UNIFAC molecular-weighted segment fractional component of molecule *i*
χ	Parameter in Eq. 46
ψ_{mn}	Interaction parameter between groups *m* and *n* in the UNIFAC model
ω	Parameter in Eq. 46

Appendix B

Peer-Reviewed Publications

The work in this PhD thesis has been published in various peer-reviewed publications.

B.1 Journal Articles

Diab, S.; Gerogiorgis, D.I., Design space identification and visualization for continuous pharmaceutical manufacturing, *Pharmaceutics* **2020**, *12*(3), 235–259.
DOI: 10.3390/pharmaceutics12030235

Diab, S.; Gerogiorgis, D.I., Technoeconomic mixed integer nonlinear programming (MINLP) optimisation for design of Liquid-Liquid Extraction (LLE) cascades in continuous pharmaceutical manufacturing of atropine, *AIChE J.*, **2019**, *65*(11), e16738. DOI: 10.1002/aic.16738

Diab, S.; McQuade, D.T.; Gupton, B.F.; Gerogiorgis, D.I. Process design and optimisation for the continuous manufacturing of nevirapine, an active pharmaceutical ingredient for H.I.V. treatment, *Org. Process Res. Dev.* **2019**, *23*(3), 320–333. DOI: 10.1021/acs.oprd.8b00381

Diab. S.; Mytis, N.; Boudouvis, A.G.; Gerogiorgis, D.I. Process modelling, design and technoeconomic Liquid-Liquid Extraction (LLE) optimisation for comparative evaluation of batch vs. continuous pharmaceutical manufacturing of atropine, *Comput. Chem. Eng.* **2019**, *124*, 28–42. DOI: 10.1016/j.compchemeng.2018.12.028

Diab, S.; Gerogiorgis, D.I. Technoeconomic optimisation of continuous crystallisation for three active pharmaceutical ingredients, (APIs): cyclosporine, paracetamol and aliskiren, *Ind. Eng. Chem. Res.* **2018**, *57*(29), 9489–9499. DOI: 10.1021/acs.iecr.8b00679

Diab, S.; Gerogiorgis, D.I. Technoeconomic evaluation of separation solvents and technologies for continuous pharmaceutical manufacturing of four key drug substances, *Chem. Today* **2018**, *36*(3), 16−19.

Diab, S.; Gerogiorgis, D.I. Process modelling, simulation and technoeconomic evaluation of crystallisation antisolvents for the continuous pharmaceutical manufacturing of rufinamide, *Comput. Chem. Eng.* **2018**, *111*, 102−114. DOI: 10.1016/j.compchemeng.2017.12.014

Diab, S.; Gerogiorgis, D.I. Process modelling, simulation and technoeconomic evaluation of separation solvents for the continuous pharmaceutical manufacturing (CPM) of diphenhydramine, *Org. Process Res. Dev.* **2017**, *21*(7): 924−946. DOI: 10.1021/acs.oprd.6b00386

Diab, S.; Gerogiorgis, D.I. Techno-economic analysis of separation processes for continuous pharmaceutical manufacturing: assessing process performance, material efficiency and economic viability, *Chem. Today* **2017**, *35*(2): 14−17.

B.2 Book Chapter Contributions

Diab, S.; Jolliffe, H.G; Gerogiorgis, D.I. Economic analysis of continuous crystallisation. In *The Handbook of Continuous Crystallisation*, Yazdanpanah, N., Nagy, Z.K., Eds.; Royal Society of Chemistry: 2020; 542–576. DOI: 10.1039/9781788013581-00542

Diab, S.; Jolliffe, H.G.; Gerogiorgis, D.I. Plantwide technoeconomic analysis and separation solvent selection for continuous pharmaceutical manufacturing. In *Process Systems Engineering for Pharmaceutical Manufacturing*, Singh, R., Yuan, Z. (Eds.); *Comput.-Aided Chem. Eng.*; Elsevier: 2018; 41, 85−120. DOI: 10.1016/B978-0-444-63963-9.00004-X

B.3 Conference Proceedings

Diab, S.; Gerogiorgis, D.I. Design space investigation for development of continuous flow syntheses of active pharmaceutical ingredients. In *30th European European Symposium on Computer Aided Process Engineering*; Pierucci, S., Bogle, D., Manenti, F.; *Comput.-Aided Chem. Eng.*; Elsevier: 2020. In press.

Diab. S.; Mytis, N.; Boudouvis, A.G.; Gerogiorgis, D.I. Technoeconomic MINLP optimisation of Liquid-Liquid Extraction (LLE) cascades for continuous pharmaceutical manufacturing of atropine. In *29th European Symposium on Computer Aided Process Engineering*; Kiss, A.A., Zondervan, E., Lakerveld, R., Özkan, L., Eds.; *Comput.-Aided Chem. Eng.*; Elsevier: 2019; 46, 211–216. DOI: 10.1016/B978-0-12-818634-3.50036-9.

Diab, S.; Gerogiorgis, D.I. Process modelling, simulation and technoeconomic optimisation for continuous pharmaceutical manufacturing of (*S*)-warfarin. In *28th European Symposium on Computer Aided Process Engineering*, Friedl, A., Klemeš, J.J., Radl, S., Varbanov, P.S., Wallek, T., Eds.; *Comput. Aided Chem. Eng.*; Elsevier: 2018; 43, 1643−1648. DOI: 10.1016/B978-0-444-64235-6.50286-2

B.4 Presentations & Symposia

Presenting author in **bold**. Where no author is highlighted in bold, Emmanuel I. Epelle presented on the authors' behalf.

Diab, S.; **Gerogiorgis, D.I.** Design space investigation for development of continuous flow syntheses of active pharmaceutical ingredients. Proceedings of the 30th Symposium on Computer Aided Process Engineering (ESCAPE-30), Milan, Italy, August 30 – Sep 3, 2020. Accepted for presentation.

Diab, S.; Gerogiorgis, D.I. Technoeconomic MINLP optimisation of MSMPR cascades for continuous crystallisation of melitracen hydrochloride, an antidepressant API. Proceedings of the 2019 AIChE Annual Meeting, Orlando (FL), USA, Nov 10–15, 2019.

Diab, S.; Mytis, N.; Boudouvis, A.G.; Gerogiorgis, D.I. Technoeconomic MINLP optimisation of Liquid-Liquid Extraction (LLE) cascades for continuous pharmaceutical manufacturing of atropine. Proceedings of the 29th European Symposium on Computer Aided Process Engineering (ESCAPE-29), Eindhoven, The Netherlands, June 16–19, 2019.

Diab, S.; McQuade, D.T.; Gerogiorgis, D.I. Optimal design of separation systems for the continuous manufacturing of nevirapine, an active pharmaceutical ingredient (API) for HIV treatment. Proceedings of the 2018 AIChE Annual Meeting, Pittsburgh (PA), USA, Oct 28–Nov 2, 2018.

Diab, S.; **Gerogiorgis, D.I.** Technoeconomic evaluation of cyclosporine crystallisation intensification using a cascade of MSMPR crystallisers. Proceedings of the 2017 AIChE Annual Meeting, Minneapolis (MN), USA, Oct 29–Nov 3, 2017.

Diab, S.; Gerogiorgis, D.I. Technoeconomic evaluation and antisolvent selection for crystallisation in continuous pharmaceutical manufacturing: ibuprofen and diphenhydramine. Proceedings of the 3rd EuCheMS Conference on Green and Sustainable Chemistry, York, UK, Sept 3–6, 2017.

Diab, S.; Gerogiorgis, D.I. Systematic antisolvent selection for diphenhydramine crystallisation in continuous pharmaceutical manufacturing. PSE@ResearchDayUK Imperial College, London, UK, June 27, 2017.

Diab, S.; Gerogiorgis, D.I. Systematic antisolvent selection for diphenhydramine crystallisation in continuous pharmaceutical manufacturing. Proceedings of the 2nd Green & Sustainable Chemistry Conference, Berlin, Germany, May 14–17, 2017.

Diab, S.; **Gerogiorgis, D.I.** Systematic technoeconomic comparison of separation solvents for green continuous pharmaceutical manufacturing of diphenhydramine. Proceedings of the 2016 AIChE Annual Meeting, San Francisco (CA), USA, Nov 13–18, 2016.

Gerogiorgis, D.I.; Jolliffe, H.G.; Diab, S. Systematic design and technoeconomic analysis of continuous pharmaceutical processes. Proceedings of the 2nd International Symposium of Continuous Manufacturing of Pharmaceuticals, Cambridge (MA), USA, Sep 26–27, 2016.

B.5 Research Collaborations

This PhD thesis project has featured collaborations with Virginia Commonwealth University (Richmond, VA, USA), for the work presented in Chapter 6, and the National Technical University of Athens (NTUA, Athens, Greece), for the work presented in Chapter 8.

Appendix C

Literature References

(1) Plumb, K. Continuous Processing in the Pharmaceutical Industry - Changing the Mind Set. *Chem. Eng. Res. Des.* **2005**, *83* (A6), 730–738.

(2) Gernaey, K. V; Cervera-Padrell, A. E.; Woodley, J. M. Development of Continuous Pharmaceutical Production Processes Supported by Process Systems Engineering Methods and Tools. *Future Med. Chem.* **2012**, *4* (11), 1371–1374.

(3) Iervolino, A. *Pharmaceutical Innovation in Europe New Pharmaceutical Breakthroughs Approaching-Is the System Set up to Fund Them All?* **2016**.

(4) UK Office for National Statistics. Business enterprise research and development, UK - Office for National Statistics. Available at: https://www.ons.gov.uk/economy/governmentpublicsectorandtaxes/researchanddevelopmentexpenditure/bulletins/businessenterpriseresearchanddevelopment/2016 (accessed Jul 27, 2018).

(5) EFPIA. The Pharmaceutical Industry in Figures. *Eur. Fed. Pharm. Ind. Assoc. Brussels Off.* **2018**.

(6) Tufts Center for the Study of Drug Development. Tufts CSDD Outlook 2013. Available at: http://csdd.tufts.edu/reports/outlook_reports (accessed Mar 5, 2016).

(7) Morgan, S.; Grootendorst, P.; Lexchin, J.; Cunningham, C.; Greyson, D. The Cost of Drug Development: A Systematic Review. *Health Policy.* **2011**, *100* (1), 4–17.

(8) EvaluatePharma. World Preview 2018. Available at: http://www.evaluategroup.com/public/Reports/EvaluatePharma-World-Preview-2018.aspx (accessed Jul 27, 2018).

(9) Behr, A.; Brehme, V. A.; Ewers, C. L. J.; Gron, H.; Kimmel, T.; Kuppers, S.; Symietz, I. New Developments in Chemical Engineering for the Production of Drug Substances. *Eng. Life Sci.* **2004**, *4* (1), 15–24.

(10) Baumann, M.; Baxendale, I. R. The Synthesis of Active Pharmaceutical Ingredients (APIs) Using Continuous Flow Chemistry. *Beilstein J. Org. Chem.* **2015**, *11*, 1194–1219.

(11) Eger, S.; Mahlich, J. C. Pharmaceutical Regulation in Europe and Its Impact on Corporate

R&D. *Geogr. Nat. Resour.* **2014**, *4* (1), 23.

(12) Henderson, R. K.; Jiménez-González, C.; Constable, D. J. C.; Alston, S. R.; Inglis, G. G. A.; Fisher, G.; Sherwood, J.; Binks, S. P.; Curzons, A. D. Expanding GSK's Solvent Selection Guide – Embedding Sustainability into Solvent Selection Starting at Medicinal Chemistry. *Green Chem.* **2011**, *13* (4), 854–862.

(13) Anderson, N. G. Using Continuous Processes to Increase Production. *Org. Process Res. Dev.* **2012**, *16* (5), 852–869.

(14) Gerogiorgis, D. I.; Jolliffe, H. G. Continuous Pharmaceutical Process Engineering and Economics Investigating Technical Efficiency, Environmental Impact and Economic Viability. *Chem. Today* **2015**, *33* (6), 29–32.

(15) Plouffe, P.; Macchi, A.; Roberge, D. M. From Batch to Continuous Chemical Synthesis — A Toolbox Approach. *Org. Process Res. Dev.* **2014**, *18* (11), 1286–1294.

(16) Yadav, V. G.; Stephanopoulos, G. Metabolic Engineering: The Ultimate Paradigm for Continuous Pharmaceutical Manufacturing. *ChemSusChem* **2014**, *7* (7), 1847–1853.

(17) Ashe, R. From Batch to Continuous Processing. *Chem. Eng.* **2012**, *119* (10), 34–40.

(18) Plutschack, M. B.; Pieber, B.; Gilmore, K.; Seeberger, P. H. The Hitchhiker's Guide to Flow Chemistry. *Chem. Rev.* **2017**, *117* (18), 11796–11893.

(19) Gérardy, R.; Emmanuel, N.; Toupy, T.; Kassin, V. E.; Tshibalonza, N. N.; Schmitz, M.; Monbaliu, J.-C. M. Continuous Flow Organic Chemistry: Successes and Pitfalls at the Interface with Current Societal Challenges. *European J. Org. Chem.* **2018**, *2018* (20–21), 2301–2351.

(20) de Souza, R. O. M. A.; Watts, P. Flow Processing as a Tool for API Production in Developing Economies. *J. Flow Chem.* **2017**, *7* (3–4), 146–150.

(21) Britton, J.; Raston, C. L. Multi-Step Continuous-Flow Synthesis. *Chem. Soc. Rev.* **2017**, *52* (5), 10159–10162.

(22) Yoshida, J.; Nagaki, A.; Yamada, D. Continuous Flow Synthesis. *Drug Discov. Today. Technol.* **2013**, *10* (1), e53–59.

(23) Porta, R.; Benaglia, M.; Puglisi, A. Flow Chemistry: Recent Developments in the Synthesis of Pharmaceutical Products. *Org. Process Res. Dev.* **2016**, *20* (1), 2–25.

(24) Malet-Sanz, L.; Susanne, F. Continuous Flow Synthesis. A Pharma Perspective. *J. Med.*

Chem. **2012**, *55* (9), 4062–4098.

(25) Mascia, S.; Heider, P. L.; Zhang, H.; Lakerveld, R.; Benyahia, B.; Barton, P. I.; Braatz, R. D.; Cooney, C. L.; Evans, J. M. B.; Jamison, T. F.; Jensen, K. F.; Myerson, A. S.; Trout, B. L. End-to-End Continuous Manufacturing of Pharmaceuticals: Integrated Synthesis, Purification, and Final Dosage Formation. *Angew. Chemie-International Ed.* **2013**, *52* (47), 12359–12363.

(26) Kupracz, L.; Kirschning, A. Multiple Organolithium Generation in the Continuous Flow Synthesis of Amitriptyline. *Adv. Synth. Catal.* **2013**, *355* (17), 3375–3380.

(27) Palmer, E. GSK commits to continuous processing. Available at: http://www.fiercepharmamanufacturing.com/story/gsk-commits-continuous-processing/2013-02-19?utm_medium=nl&utm_source=internal (accessed Mar 5, 2016).

(28) Kopetzki, D.; Lévesque, F.; Seeberger, P. H. A Continuous-Flow Process for the Synthesis of Artemisinin. *Chem. - A Eur. J.* **2013**, *19* (17), 5450–5456.

(29) Gustafsson, T.; Sörensen, H.; Pontén, F. Development of a Continuous Flow Scale-Up Approach of Reflux Inhibitor AZD6906. *Org. Process Res. Dev.* **2012**, *16* (5), 925–929.

(30) Kuehn, S. E. Janssen Embraces Continuous Manufacturing for Prezista. Available at:

http://www.pharmamanufacturing.com/articles/2015/janssen-embraces-continuous-manufacturing-for-prezista/ (accessed Oct 5, 2016).

(31) FDA Approves Tablet Production on Janssen Continuous Manufacturing Line. Available at: http://www.pharmtech.com/fda-approves-tablet-production-janssen-continuous-manufacturing-line (accessed Oct 7, 2016).

(32) Snead, D. R.; Jamison, T. F. End-to-End Continuous Flow Synthesis and Purification of Diphenhydramine Hydrochloride Featuring Atom Economy, In-Line Separation, and Flow of Molten Ammonium Salts. *Chem. Sci.* **2013**, *4* (7), 2822–2827.

(33) Adamo, A.; Beingessner, R. L.; Behnam, M.; Chen, J.; Jamison, T. F.; Jensen, K. F.; Monbaliu, J.-C. M.; Myerson, A. S.; Revalor, E. M.; Snead, D. R.; Stelzer, T.; Weeranoppanant, N.; Wong, S. Y.; Zhang, P. On-Demand Continuous-Flow Production of Pharmaceuticals in a Compact, Reconfigurable System. *Science* **2016**, *352* (6281), 61–67.

(34) Pastre, J. C.; Browne, D. L.; O'Brien, M.; Ley, S. V. Scaling Up of Continuous Flow Processes with Gases Using a Tube-in-Tube Reactor: Inline Titrations and Fanetizole

Synthesis with Ammonia. *Org. Process Res. Dev.* **2013**, *17* (9), 1183–1191.

(35) Ahmed-Omer, B.; Sanderson, A. J. Preparation of Fluoxetine by Multiple Flow Processing Steps. *Org. Biomol. Chem.* **2011**, *9* (10), 3854–3862.

(36) LaPorte, T. L.; Hamedi, M.; DePue, J. S.; Shen, L.; Watson, D.; Hsieh, D. Development and Scale-up of Three Consecutive Continuous Reactions for Production of 6-Hydroxybuspirone. *Org. Process Res. Dev.* **2008**, *12* (5), 956–966.

(37) Bogdan, A. R.; Poe, S. L.; Kubis, D. C.; Broadwater, S. J.; McQuade, D. T. The Continuous-Flow Synthesis of Ibuprofen. *Angew. Chemie-International Ed.* **2009**, *48* (45), 8547–8550.

(38) Snead, D. R.; Jamison, T. F. A Three-Minute Synthesis and Purification of Ibuprofen: Pushing the Limits of Continuous-Flow Processing. *Angew. Chemie-International Ed.* **2015**, *54* (3), 983–987.

(39) Hopkin, M. D.; Baxendale, I. R.; Ley, S. V.; Baxendale, I. R.; Ley, S. V.; Kirschning, A.; Monenschein, H.; Wittenberg, R.; Baxendale, I. R.; Hayward, J. J.; Ley, S. V.; Tranmer, G. K.; Griffiths-Jones, C. M. A Flow-Based Synthesis of Imatinib: The API of Gleevec. *Chem. Commun.* **2010**, *46* (14), 2450–2452.

(40) Zhang, P.; Russell, M. G.; Jamison, T. F. Continuous Flow Total Synthesis of Rufinamide. *Org. Process Res. Dev.* **2014**, *18* (11), 1567–1570.

(41) Murray, P. R. D.; Browne, D. L.; Pastre, J. C.; Butters, C.; Guthrie, D.; Ley, S. V. Continuous Flow-Processing of Organometallic Reagents Using an Advanced Peristaltic Pumping System and the Telescoped Flow Synthesis of (E/Z)-Tamoxifen. *Org. Process Res. Dev.* **2013**, *17* (9), 1192–1208.

(42) Martin, A. D.; Siamaki, A. R.; Belecki, K.; Gupton, B. F. A Flow-Based Synthesis of Telmisartan. *J. Flow Chem.* **2015**, *5* (3), 145–147.

(43) Fuse, S.; Mifune, Y.; Tanabe, N.; Takahashi, T. Continuous-Flow Synthesis of Activated Vitamin D3 and Its Analogues. *Org. Biomol. Chem.* **2012**, *10* (27), 5205.

(44) Federsel, H.-J. En Route to Full Implementation: Driving the Green Chemistry Agenda in the Pharmaceutical Industry. *Green Chem.* **2013**, *15* (11), 3105–3115.

(45) Lee, S. L.; O'Connor, T. F.; Yang, X.; Cruz, C. N.; Chatterjee, S.; Madurawe, R. D.; Moore, C. M. V.; Yu, L. X.; Woodcock, J. Modernizing Pharmaceutical Manufacturing: From Batch to Continuous Production. *J. Pharm. Innov.* **2015**, *10* (1), 191–199.

(46) Benedetti, A.; Khoo, J.; Sharma, S.; Facco, P.; Barolo, M.; Zomer, S. Data Analytics on Raw Material Properties to Accelerate Pharmaceutical Drug Development. *Int. J. Pharm.* **2019**, *563*, 122–134.

(47) Zhao, C.; Jain, A.; Hailemariam, L.; Suresh, P.; Akkisetty, P.; Joglekar, G.; Venkatasubramanian, V.; Reklaitis, G. V.; Morris, K.; Basu, P. Toward Intelligent Decision Support for Pharmaceutical Product Development. *J. Pharm. Innov.* **2006**, *1* (1), 23–35.

(48) Teoh, S. K.; Rathi, C.; Sharratt, P. Practical Assessment Methodology for Converting Fine Chemicals Processes from Batch to Continuous. *Org. Process Res. Dev.* **2015**, *20* (2), 414–431.

(49) Schaber, S. D.; Gerogiorgis, D. I.; Ramachandran, R.; Evans, J. M. B.; Barton, P. I.; Trout, B. L. Economic Analysis of Integrated Continuous and Batch Pharmaceutical Manufacturing: A Case Study. *Ind. Eng. Chem. Res.* **2011**, *50* (17), 10083–10092.

(50) Jolliffe, H. G.; Gerogiorgis, D. I. Process Modelling and Simulation for Continuous Pharmaceutical Manufacturing of Ibuprofen. *Chem. Eng. Res. Des.* **2015**, *97*, 175–191.

(51) Jolliffe, H. G.; Gerogiorgis, D. I. Process Modelling and Simulation for Continuous Pharmaceutical Manufacturing of Artemisinin. *Chem. Eng. Res. Des.* **2016**, *112*, 310–325.

(52) Bana, P.; Örkényi, R.; Lövei, K.; Lakó, Á.; Túrós, G. I.; Éles, J.; Faigl, F.; Greiner, I. The Route from Problem to Solution in Multistep Continuous Flow Synthesis of Pharmaceutical Compounds. *Bioorg. Med. Chem.* **2017**, *25* (23), 6180–6189.

(53) Jolliffe, H. G.; Diab, S.; Gerogiorgis, D. I. Nonlinear Optimisation via Explicit NRTL Model Solubility Prediction for Antisolvent Mixture Selection in Artemisinin Crystallisation. *Org. Process Res. Dev.* **2018**, *22* (1), 40–53.

(54) Grom, M.; Stavber, G.; Drnovšek, P.; Likozar, B. Modelling Chemical Kinetics of a Complex Reaction Network of Active Pharmaceutical Ingredient (API) Synthesis with Process Optimization for Benzazepine Heterocyclic Compound. *Chem. Eng. J.* **2016**, *283*, 703–716.

(55) Patel, M. P.; Shah, N.; Ashe, R. Robust Optimisation Methodology for the Process Synthesis of Continuous Technologies. *Comput. Aided Chem. Eng.* **2011**, *29*, 351–355.

(56) Ott, D.; Kralisch, D.; Denčić, I.; Hessel, V.; Laribi, Y.; Perrichon, P. D.; Berguerand, C.; Kiwi-Minsker, L.; Loeb, P. Life Cycle Analysis within Pharmaceutical Process Optimization and Intensification: Case Study of Active Pharmaceutical Ingredient Production. *ChemSusChem* **2014**, *7* (12), 3521–3533.

(57) Ott, D.; Borukhova, S.; Hessel, V. Life Cycle Assessment of Multi-Step Rufinamide Synthesis – from Isolated Reactions in Batch to Continuous Microreactor Networks. *Green Chem.* **2016**, *18* (4), 1096–1116.

(58) Drageset, A.; Bjørsvik, H.-R. Continuous Flow Synthesis Concatenated with Continuous Flow Liquid–Liquid Extraction for Work-up and Purification: Selective Mono- and Di-Iodination of the Imidazole Backbone. *React. Chem. Eng.* **2016**, *1* (4), 436–444.

(59) Monbaliu, J.-C. M.; Stelzer, T.; Revalor, E.; Weeranoppanant, N.; Jensen, K. F.; Myerson, A. S. Compact and Integrated Approach for Advanced End-to-End Production, Purification, and Aqueous Formulation of Lidocaine Hydrochloride. *Org. Process Res. Dev.* **2016**, *20* (7), 1347–1353.

(60) Weeranoppanant, N.; Adamo, A.; Saparbaiuly, G.; Rose, E.; Fleury, C.; Schenkel, B.; Jensen, K. F. Design of Multistage Counter-Current Liquid–Liquid Extraction for Small-Scale Applications. *Ind. Eng. Chem. Res.* **2017**, *56* (14), 4095–4103.

(61) Yang, Y.; Nagy, Z. K. Combined Cooling and Antisolvent Crystallization in Continuous Mixed Suspension, Mixed Product Removal Cascade Crystallizers: Steady-State and Startup Optimization. *Ind. Eng. Chem. Res.* **2015**, *54* (21), 5673–5682.

(62) Ridder, B. J.; Majumder, A.; Nagy, Z. K. Population Balance Model-Based Multiobjective Optimization of a Multisegment Multiaddition (MSMA) Continuous Plug-Flow Antisolvent Crystallizer. *Ind. Eng. Chem. Res.* **2014**, *53* (11), 4387–4397.

(63) Li, J.; Lai, T. C.; Trout, B. L.; Myerson, A. S. Continuous Crystallization of Cyclosporine: The Effect of Operating Conditions on Yield and Purity. *Cryst. Growth Des.* **2017**, *17* (3), 1000–1007.

(64) Acevedo, D.; Tandy, Y.; Nagy, Z. K. Multiobjective Optimization of an Unseeded Batch Cooling Crystallizer for Shape and Size Manipulation. *Ind. Eng. Chem. Res.* **2015**, *54* (7), 2156–2166.

(65) Ridder, B. J.; Majumder, A.; Nagy, Z. K. Parametric, Optimization-Based Study on the Feasibility of a Multisegment Antisolvent Crystallizer for in Situ Fines Removal and Matching of Target Size Distribution. *Ind. Eng. Chem. Res.* **2016**, *55* (8), 2371–2380.

(66) Park, K.; Kim, D. Y.; Yang, D. R. Operating Strategy for Continuous Multistage Mixed Suspension and Mixed Product Removal (MSMPR) Crystallization Processes Depending on Crystallization Kinetic Parameters. *Ind. Eng. Chem. Res.* **2016**, *55* (26), 7142–7153.

(67) Zhang, H.; Quon, J.; Alvarez, A. J.; Evans, J.; Myerson, A. S.; Trout, B. Development of Continuous Anti-Solvent/Cooling Crystallization Process Using Cascaded Mixed Suspension, Mixed Product Removal Crystallizers. *Org. Process Res. Dev.* **2012**, *16* (5), 915–924.

(68) Lee, J. W.; Horváth, Z.; O'Brien, A. G.; Seeberger, P. H.; Seidel-Morgenstern, A. Design and Optimization of Coupling a Continuously Operated Reactor with Simulated Moving Bed Chromatography. *Chem. Eng. J.* **2014**, *251*, 355–370.

(69) Jolliffe, H. G.; Gerogiorgis, D. I. Plantwide Design and Economic Evaluation of Two Continuous Pharmaceutical Manufacturing (CPM) Cases: Ibuprofen and Artemisinin. *Comput. Chem. Eng.* **2016**, *91*, 269–288.

(70) Dencic, I.; Ott, D.; Kralisch, D.; Noel, T.; Meuldijk, J.; de Croon, M.; Hessel, V.; Laribi, Y.; Perrichon, P. Eco-Efficiency Analysis for Intensified Production of an Active Pharmaceutical Ingredient: A Case Study. *Org. Process Res. Dev.* **2014**, *18* (11), 1326–1338.

(71) Hartman, R. L.; McMullen, J. P.; Jensen, K. F. Deciding Whether To Go with the Flow: Evaluating the Merits of Flow Reactors for Synthesis. *Angew. Chemie-International Ed.* **2011**, *50* (33), 7502–7519.

(72) Patrascu, M.; Barton, P. I. Optimal Campaigns in End-to-End Continuous Pharmaceuticals Manufacturing. Part 2: Dynamic Optimization. *Chem. Eng. Process. - Process Intensif.* **2018**, *125*, 124–132.

(73) Jolliffe, H. G.; Gerogiorgis, D. I. Technoeconomic Optimization of a Conceptual Flowsheet for Continuous Separation of an Analgaesic Active Pharmaceutical Ingredient (API). *Ind. Eng. Chem. Res.* **2017**, *56* (15), 4357–4376.

(74) Jolliffe, H. G.; Gerogiorgis, D. I. Technoeconomic Optimisation and Comparative Environmental Impact Evaluation of Continuous Crystallisation and Antisolvent Selection for Artemisinin Recovery. *Comput. Chem. Eng.* **2017**, *103*, 218–232.

(75) Diab, S.; Gerogiorgis, D. I. Process Modeling, Simulation, and Technoeconomic Evaluation of Separation Solvents for the Continuous Pharmaceutical Manufacturing (CPM) of Diphenhydramine. *Org. Process Res. Dev.* **2017**, *21* (7), 924–946.

(76) Diab, S.; Gerogiorgis, D. I. Process Modelling, Simulation and Technoeconomic Evaluation of Crystallisation Antisolvents for the Continuous Pharmaceutical Manufacturing of Rufinamide. *Comput. Chem. Eng.* **2018**, *111*, 102–114.

(77) Diab, S.; Gerogiorgis, D. I. Process Modelling, Simulation and Technoeconomic Optimisation for Continuous Pharmaceutical Manufacturing of (*S*)-Warfarin. *Comput. Aided Chem. Eng.* **2018**, *43*, 1643–1648.

(78) Wang, J.; Lakerveld, R. Continuous Membrane-Assisted Crystallization to Increase the Attainable Product Quality of Pharmaceuticals and Design Space for Operation. *Ind. Eng. Chem. Res.* **2017**, *56* (19), 5705–5714.

(79) Chen, J.; Sarma, B.; Evans, J. M. B.; Myerson, A. S. Pharmaceutical Crystallization. *Cryst. Growth Des.* **2011**, *11* (4), 887–895.

(80) Zhang, D.; Xu, S.; Du, S.; Wang, J.; Gong, J. Progress of Pharmaceutical Continuous Crystallization. *Engineering* **2017**, *3* (3), 354–364.

(81) Randolph, A. D.; Larson, M. A. *Theory of Particulate Processes: Analysis and Techniques of Continuous Crystallization*; Academic Press, 1988.

(82) Eder, R. J. P.; Schmitt, E. K.; Grill, J.; Radl, S.; Gruber-Woelfler, H.; Khinast, J. G. Seed Loading Effects on the Mean Crystal Size of Acetylsalicylic Acid in a Continuous-Flow Crystallization Device. *Cryst. Res. Technol.* **2011**, *46* (3), 227–237.

(83) McGlone, T.; Briggs, N. E. B.; Clark, C. A.; Brown, C. J.; Sefcik, J.; Florence, A. J. Oscillatory Flow Reactors (OFRs) for Continuous Manufacturing and Crystallization. *Org. Process Res. Dev.* **2015**, *19* (9), 1186–1202.

(84) Alvarez, A. J.; Myerson, A. S. Continuous Plug Flow Crystallization of Pharmaceutical Compounds. *Cryst. Growth Des.* **2010**, *10* (5), 2219–2228.

(85) Lawton, S.; Steele, G.; Shering, P.; Zhao, L.; Laird, I.; Ni, X.-W. Continuous Crystallization of Pharmaceuticals Using a Continuous Oscillatory Baffled Crystallizer. *Org. Process Res. Dev.* **2009**, *13* (6), 1357–1363.

(86) Eder, R. J. P.; Radl, S.; Schmitt, E.; Innerhofer, S.; Maier, M.; Gruber-Woelfler, H.; Khinast, J. G. Continuously Seeded, Continuously Operated Tubular Crystallizer for the Production of Active Pharmaceutical Ingredients. *Cryst. Growth Des.* **2010**, *10* (5), 2247–2257.

(87) Su, Q.; Benyahia, B.; Nagy, Z. K.; Rielly, C. D. Mathematical Modeling, Design, and Optimization of a Multisegment Multiaddition Plug-Flow Crystallizer for Antisolvent Crystallizations. *Org. Process Res. Dev.* **2015**, *19* (12), 1859–1870.

(88) Vetter, T.; Burcham, C. L.; Doherty, M. F. Regions of Attainable Particle Sizes in

Continuous and Batch Crystallization Processes. *Chem. Eng. Sci.* **2014**, *106*, 167–180.

(89) Rogers, A.; Ierapetritou, M. Challenges and Opportunities in Pharmaceutical Manufacturing Modelling and Optimization. *Comput. Aided Chem. Eng.* **2014**, *34*, 144–149.

(90) Alvarez, A. J.; Singh, A.; Myerson, A. S. Crystallization of Cyclosporine in a Multistage Continuous MSMPR Crystallizer. *Cryst. Growth Des.* **2011**, *11* (10), 4392–4400.

(91) Power, G.; Hou, G.; Kamaraju, V. K.; Morris, G.; Zhao, Y.; Glennon, B. Design and Optimization of a Multistage Continuous Cooling Mixed Suspension, Mixed Product Removal Crystallizer. *Chem. Eng. Sci.* **2015**, *133*, 125–139.

(92) Quon, J. L.; Zhang, H.; Alvarez, A.; Evans, J.; Myerson, A. S.; Trout, B. L. Continuous Crystallization of Aliskiren Hemifumarate. *Cryst. Growth Des.* **2012**, *12* (6), 3036–3044.

(93) Morris, G.; Power, G.; Ferguson, S.; Barrett, M.; Hou, G.; Glennon, B. Estimation of Nucleation and Growth Kinetics of Benzoic Acid by Population Balance Modeling of a Continuous Cooling Mixed Suspension, Mixed Product Removal Crystallizer. *Org. Process Res. Dev.* **2015**, *19* (12), 1891–1902.

(94) Acevedo, D.; Yang, Y.; Warnke, D. J.; Nagy, Z. K. Model-Based Evaluation of Direct Nucleation Control Approaches for the Continuous Cooling Crystallization of Paracetamol in a Mixed Suspension Mixed Product Removal System. *Cryst. Growth Des.* **2017**, *17* (10), 5377–5383.

(95) Yang, X.; Acevedo, D.; Mohammad, A.; Pavurala, N.; Wu, H.; Brayton, A. L.; Shaw, R. A.; Goldman, M. J.; He, F.; Li, S.; Fisher, R. J.; O'Connor, T. F.; Cruz, C. N. Risk Considerations on Developing a Continuous Crystallization System for Carbamazepine. *Org. Process Res. Dev.* **2017**, *21* (7), 1021–1033.

(96) Agnew, L. R.; McGlone, T.; Wheatcroft, H. P.; Robertson, A.; Parsons, A. R.; Wilson, C. C. Continuous Crystallization of Paracetamol (Acetaminophen) Form II: Selective Access to a Metastable Solid Form. *Cryst. Growth Des.* **2017**, *17* (5), 2418–2427.

(97) Ferguson, S.; Morris, G.; Hao, H.; Barrett, M.; Glennon, B. Characterization of the Anti-Solvent Batch, Plug Flow and MSMPR Crystallization of Benzoic Acid. *Chem. Eng. Sci.* **2013**, *104*, 44–54.

(98) Su, Q.; Nagy, Z. K.; Rielly, C. D. Pharmaceutical Crystallisation Processes from Batch to Continuous Operation Using MSMPR Stages: Modelling, Design, and Control. *Chem. Eng. Process. Process Intensif.* **2015**, *89*, 41–53.

(99) Li, J.; Trout, B. L.; Myerson, A. S. Multistage Continuous Mixed-Suspension, Mixed-Product Removal (MSMPR) Crystallization with Solids Recycle. *Org. Process Res. Dev.* **2016**, *20* (2), 510–516.

(100) Gruber-Woelfler, H.; Escribà-Gelonch, M.; Noël, T.; Maier, M. C.; Hessel, V. Effect of Acetonitrile-Based Crystallization Conditions on the Crystal Quality of Vitamin D3. *Chem. Eng. Technol.* **2017**, *40* (11), 2016–2024.

(101) Yang, Y.; Nagy, Z. K. Advanced Control Approaches for Combined Cooling/Antisolvent Crystallization in Continuous Mixed Suspension Mixed Product Removal Cascade Crystallizers. *Chem. Eng. Sci.* **2015**, *127*, 362–373.

(102) Vetter, T.; Burcham, C. L.; Doherty, M. F. Regions of Attainable Particle Sizes in Continuous and Batch Crystallization Processes. *Chem. Eng. Sci.* **2014**, *106*, 167–180.

(103) Wong, S. Y.; Tatusko, A. P.; Trout, B. L.; Myerson, A. S. Development of Continuous Crystallization Processes Using a Single-Stage Mixed-Suspension, Mixed-Product Removal Crystallizer with Recycle. *Cryst. Growth Des.* **2012**, *12* (11), 5701–5707.

(104) Su, Q.; Rielly, C. D.; Powell, K. A.; Nagy, Z. K. Mathematical Modelling and Experimental Validation of a Novel Periodic Flow Crystallization Using MSMPR Crystallizers. *AIChE J.* **2017**, *63* (4), 1313–1327.

(105) Powell, K. A.; Saleemi, A. N.; Rielly, C. D.; Nagy, Z. K. Periodic Steady-State Flow Crystallization of a Pharmaceutical Drug Using MSMPR Operation. *Chem. Eng. Process. Process Intensif.* **2015**, *97*, 195–212.

(106) Tahara, K.; O'Mahony, M.; Myerson, A. S. Continuous Spherical Crystallization of Albuterol Sulfate with Solvent Recycle System. *Cryst. Growth Des.* **2015**, *15* (10), 5155–5156.

(107) Ferguson, S.; Ortner, F.; Quon, J.; Peeva, L.; Livingston, A.; Trout, B. L.; Myerson, A. S. Use of Continuous MSMPR Crystallization with Integrated Nanofiltration Membrane Recycle for Enhanced Yield and Purity in API Crystallization. *Cryst. Growth Des.* **2014**, *14* (2), 617–627.

(108) Vartak, S.; Myerson, A. S. Continuous Crystallization with Impurity Complexation and Nanofiltration Recycle. *Org. Process Res. Dev.* **2017**, *21* (2), 253–261.

(109) Hou, G.; Power, G.; Barrett, M.; Glennon, B.; Morris, G.; Zhao, Y. Development and Characterization of a Single Stage Mixed-Suspension, Mixed-Product-Removal Crystallization Process with a Novel Transfer Unit. *Cryst. Growth Des.* **2014**, *14* (4), 1782–

1793.

(110) Acevedo, D.; Peña, R.; Yang, Y.; Barton, A.; Firth, P.; Nagy, Z. K. Evaluation of Mixed Suspension Mixed Product Removal Crystallization Processes Coupled with a Continuous Filtration System. *Chem. Eng. Process. Process Intensif.* **2016**, *108*, 212–219.

(111) Wang, J.; Lakerveld, R. Integrated Solvent and Process Design for Continuous Crystallization and Solvent Recycling Using PC-SAFT. *AIChE J.* **2018**, *64* (4), 1205–1216.

(112) Galan, K.; Eicke, M. J.; Elsner, M. P.; Lorenz, H.; Seidel-Morgenstern, A. Continuous Preferential Crystallization of Chiral Molecules in Single and Coupled Mixed-Suspension Mixed-Product-Removal Crystallizers. *Cryst. Growth Des.* **2015**, *15* (4), 1808–1818.

(113) Sang-Il Kwon, J.; Nayhouse, M.; Christofides, P. D.; Orkoulas, G. Modeling and Control of Crystal Shape in Continuous Protein Crystallization. *Chem. Eng. Sci.* **2014**, *107*, 47–57.

(114) Lai, T.-T. C.; Cornevin, J.; Ferguson, S.; Li, N.; Trout, B. L.; Myerson, A. S. Control of Polymorphism in Continuous Crystallization via Mixed Suspension Mixed Product Removal Systems Cascade Design. *Cryst. Growth Des.* **2015**, *15* (7), 3374–3382.

(115) Lai, T. T. C.; Ferguson, S.; Palmer, L.; Trout, B. L.; Myerson, A. S. Continuous Crystallization and Polymorph Dynamics in the L-Glutamic Acid System. *Org. Process Res. Dev.* **2014**, *18* (11), 1382–1390.

(116) Yang, Y.; Song, L.; Gao, T.; Nagy, Z. K. Integrated Upstream and Downstream Application of Wet Milling with Continuous Mixed Suspension Mixed Product Removal Crystallization. *Cryst. Growth Des.* **2015**, *15* (12), 5879–5885.

(117) Wood, B.; Girard, K. P.; Polster, C. S.; Croker, D. M. Progress to Date in the Design and Operation of Continuous Crystallization Processes for Pharmaceutical Applications. *Org. Process Res. Dev.* **2019**, *23* (2), 122–144.

(118) Diab, S.; Gerogiorgis, D. I. Technoeconomic Optimization of Continuous Crystallization for Three Active Pharmaceutical Ingredients (APIs): Cyclosporine, Paracetamol and Aliskiren. *Ind. Eng. Chem. Res.* **2018**, *57* (29), 9489–9499.

(119) Rooney, W. C.; Biegler, L. T. Multiperiod Reactor Network Synthesis. *Comput. Chem. Eng.* **2000**, *24* (9–10), 2055–2068.

(120) Kokossis, A. C.; Floudas, C. A. Synthesis of Isothermal Reactor—Separator—Recycle Systems. *Chem. Eng. Sci.* **1991**, *46* (5–6), 1361–1383.

(121) Smith, O. J.; Westerberg, A. W. The Optimal Design of Pressure Swing Adsorption Systems. *Chem. Eng. Sci.* **1991**, *46* (12), 2967–2976.

(122) Aggarwal, A.; Floudas, C. A. Synthesis of Heat Integrated Nonsharp Distillation Sequences. *Comput. Chem. Eng.* **1992**, *16* (2), 89–108.

(123) Paules, G. E.; Floudas, C. A. Stochastic Programming in Process Synthesis: A Two-Stage Model with MINLP Recourse for Multiperiod Heat-Integrated Distillation Sequences. *Comput. Chem. Eng.* **1992**, *16* (3), 189–210.

(124) Viswanathan, J.; Grossmann, I. E. Optimal Feed Locations and Number of Trays for Distillation Columns with Multiple Feeds. *Ind. Eng. Chem. Res.* **1993**, *32* (11), 2942–2949.

(125) Novak, Z.; Kravanja, Z.; Grossmann, I. E. Simultaneous Synthesis of Distillation Sequences in Overall Process Schemes Using an Improved MINLP Approach. *Comput. Chem. Eng.* **1996**, *20* (12), 1425–1440.

(126) Diaz, S.; Serrani, A.; Bandoni, A.; Brignole, E. A. A Study on the Capital and Operating Alternatives in an Ethane Extraction Plant. *Comput. Chem. Eng.* **1996**, *20*, S1499–S1504.

(127) Diaz, S.; Gros, H.; Brignole, E. . Thermodynamic Modeling, Synthesis and Optimization of Extraction — Dehydration Processes. *Comput. Chem. Eng.* **2000**, *24* (9–10), 2069–2080.

(128) Alonso, A. I.; Lassahn, A.; Gruhn, G. Optimal Design of Non-Dispersive Solvent Extraction Processes. *Comput. Chem. Eng.* **2001**, *25* (2–3), 267–285.

(129) Emet, S.; Westerlund, T. Solving an MINLP Problem Including Partial Differential Algebraic Constraints Using Branch and Bound and Cutting Plane Techniques. *Comput. Aided Chem. Eng.* **2003**, *14*, 107–112.

(130) Emet, S.; Westerlund, T. Comparisons of Solving a Chromatographic Separation Problem Using MINLP Methods. *Comput. Chem. Eng.* **2004**, *28* (5), 673–682.

(131) Lee, S.; Logsdon, J. S.; Foral, M. J.; Grossmann, I. E. Superstructure Optimization of the Olefin Separation Process. *Comput. Aided Chem. Eng.* **2003**, *14*, 191–196.

(132) Kookos, I. K. Optimal Design of Membrane/Distillation Column Hybrid Processes. *Ind. Eng. Chem. Res.* **2003**, *42* (8), 1731–1738.

(133) Tsiakis, P.; Papageorgiou, L. G. Optimal Design of an Electrodialysis Brackish Water Desalination Plant. *Desalination* **2005**, *173* (2), 173–186.

(134) Sirdeshpande, A. R.; Ierapetritou, M. G.; Andrecovich, M. J.; Naumovitz, J. P. Process

Synthesis Optimization and Flexibility Evaluation of Air Separation Cycles. *AIChE J.* **2005**, *51* (4), 1190–1200.

(135) Chen, C. L.; Hung, P. S. Retrofit of Mass-Exchange Networks with Superstructure-Based MINLP Formulation. *Ind. Eng. Chem. Res.* **2005**, *44* (18), 7189–7199.

(136) Chávez-Islas, L. M.; Vásquez-Medrano, R.; Flores-Tlacuahuac, A. Optimal Synthesis of a High Purity Bioethanol Distillation Column Using Ionic Liquids. *Ind. Eng. Chem. Res.* **2011**, *50* (9), 5175–5190.

(137) Khor, C. S.; Foo, D. C. Y.; El-Halwagi, M. M.; Tan, R. R.; Shah, N. A Superstructure Optimization Approach for Membrane Separation-Based Water Regeneration Network Synthesis with Detailed Nonlinear Mechanistic Reverse Osmosis Model. *Ind. Eng. Chem. Res.* **2011**, *50* (23), 13444–13456.

(138) Lu, Y.; Liao, A.; Hu, Y. The Design of Reverse Osmosis Systems with Multiple-Feed and Multiple-Product. *Desalination* **2012**, *307*, 42–50.

(139) Kanchanalai, P.; Lively, R. P.; Realff, M. J.; Kawajiri, Y. Cost and Energy Savings Using an Optimal Design of Reverse Osmosis Membrane Pretreatment for Dilute Bioethanol Purification. *Ind. Eng. Chem. Res.* **2013**, *52* (32), 11132–11141.

(140) Al Wahedi, Y.; Rabie, A. H.; Al Shaiba, A.; Geuzebroek, F.; Daoutidis, P. Optimization of Adsorption-Based Natural Gas Dryers. *Ind. Eng. Chem. Res.* **2016**, *55* (16), 4658–4667.

(141) Faruque Hasan, M. M.; First, E. L.; Floudas, C. A. Discovery of Novel Zeolites and Multi-Zeolite Processes for p-Xylene Separation Using Simulated Moving Bed (SMB) Chromatography. *Chem. Eng. Sci.* **2017**, *159*, 3–17.

(142) Franke, M. B. Design of Dividing-Wall Columns by Mixed-Integer Nonlinear Programming Optimization. *Chemie Ing. Tech.* **2017**, *89* (5), 582–597.

(143) Aliaga-Vicente, A.; Caballero, J. A.; Fernández-Torres, M. J. Synthesis and Optimization of Membrane Cascade for Gas Separation via Mixed-Integer Nonlinear Programming. *AIChE J.* **2017**, *63* (6), 1989–2006.

(144) Richardson, G. S.; Roehrs, T. A.; Rosenthal, L.; Koshorek, G.; Roth, T. Tolerance to Daytime Sedative Effects of H1 Antihistamines. *J. Clin. Psychopharmacol.* **2002**, *22* (5), 511–515.

(145) Ferraz, R.; Branco, L. C.; Prudencio, C.; Noronha, J. P.; Petrovski, Z. Ionic Liquids as Active

Pharmaceutical Ingredients. *ChemMedChem* **2011**, *6* (6), 975–985.

(146) Olivier-Bourbigou, H.; Magna, L.; Morvan, D. Ionic Liquids and Catalysis: Recent Progress from Knowledge to Applications. *Appl. Catal. a-General* **2010**, *373* (1–2), 1–56.

(147) Renken, A.; Hessel, V.; Loeb, P.; Miszczuk, R.; Uerdingen, M.; Kiwi-Minsker, L. Ionic Liquid Synthesis in a Microstructured Reactor for Process Intensification. *Chem. Eng. Process.* **2007**, *46* (9), 840–845.

(148) Waterkamp, D. A.; Heiland, M.; Schlueter, M.; Sauvageau, J. C.; Beyersdorff, T.; Thoeming, J. Synthesis of Ionic Liquids in Micro-Reactors - a Process Intensification Study. *Green Chem.* **2007**, *9* (10), 1084–1090.

(149) Statista. *OTC Pharmaceuticals - United States*; 2017.

(150) Aher, N. G.; Pore, V. S.; Mishra, N. N.; Kumar, A.; Shukla, P. K.; Sharma, A.; Bhat, M. K. Synthesis and Antifungal Activity of 1,2,3-Triazole Containing Fluconazole Analogues. *Bioorg. Med. Chem. Lett.* **2009**, *19* (3), 759–763.

(151) da Silva, F. de C.; de Souza, M. C. B. V.; Frugulhetti, I. I. P.; Castro, H. C.; Souza, S. L. de O.; de Souza, T. M. L.; Rodrigues, D. Q.; Souza, A. M. T.; Abreu, P. A.; Passamani, F. Synthesis, HIV-RT Inhibitory Activity and SAR of 1-Benzyl-1H-1,2,3-Triazole Derivatives of Carbohydrates. *Eur. J. Med. Chem.* **2009**, *44* (1), 373–383.

(152) Kamal, A.; Shankaraiah, N.; Devaiah, V.; Laxma Reddy, K.; Juvekar, A.; Sen, S.; Kurian, N.; Zingde, S. Synthesis of 1,2,3-Triazole-Linked Pyrrolobenzodiazepine Conjugates Employing 'Click' Chemistry: DNA-Binding Affinity and Anticancer Activity. *Bioorg. Med. Chem. Lett.* **2008**, *18* (4), 1468–1473.

(153) Wang, X.-L.; Wan, K.; Zhou, C.-H. Synthesis of Novel Sulfanilamide-Derived 1,2,3-Triazoles and Their Evaluation for Antibacterial and Antifungal Activities. *Eur. J. Med. Chem.* **2010**, *45* (10), 4631–4639.

(154) Costa, M. S.; Boechat, N.; Rangel, É. A.; da Silva, F. de C.; de Souza, A. M. T.; Rodrigues, C. R.; Castro, H. C.; Junior, I. N.; Lourenço, M. C. S.; Wardell, S. M. S. V.; Ferreira, V. F. Synthesis, Tuberculosis Inhibitory Activity, and SAR Study of N-Substituted-Phenyl-1,2,3-Triazole Derivatives. *Bioorganic Med. Chem.* **2006**, *14* (24), 8644–8653.

(155) Badgujar, D. M.; Talawar, M. B.; Asthana, S. N.; Mahulikar, P. P. Advances in Science and Technology of Modern Energetic Materials: An Overview. *J. Hazard. Mater.* **2008**, *151* (2–3), 289–305.

(156) Baumann, M.; Baxendale, I. R.; Ley, S. V. The Flow Synthesis of Heterocycles for Natural Product and Medicinal Chemistry Applications. *Mol. Divers.* **2011**, *15* (3), 613–630.

(157) Prevention, C. for D. C. and. About Underlying Cause of Death, 1999-2017. Available at: https://wonder.cdc.gov/ucd-icd10.html (accessed Jan 14, 2020).

(158) Movsisyan, M.; Delbeke, E. I. P.; Berton, J. K. E. T.; Battilocchio, C.; Ley, S. V.; Stevens, C. V. Taming Hazardous Chemistry by Continuous Flow Technology. *Chem. Soc. Rev.* **2016**, *45* (18), 4892–4928.

(159) Gutmann, B.; Cantillo, D.; Kappe, C. O. Continuous-Flow Technology: A Tool for the Safe Manufacturing of Active Pharmaceutical Ingredients. *Angew. Chemie-International Ed.* **2015**, *54* (23), 6688–6728.

(160) Mudd, W. H.; Stevens, E. P. An Efficient Synthesis of Rufinamide, an Antiepileptic Drug. *Tetrahedron Lett.* **2010**, *51* (24), 3229–3231.

(161) Borukhova, S.; Noël, T.; Metten, B.; de Vos, E.; Hessel, V. From Alcohol to 1,2,3-Triazole via a Multi-Step Continuous-Flow Synthesis of a Rufinamide Precursor. *Green Chem.* **2016**, *99*, 9–13.

(162) Borukhova, S.; Noël, T.; Metten, B.; de Vos, E.; Hessel, V. Solvent- and Catalyst-Free Huisgen Cycloaddition to Rufinamide in Flow with a Greener, Less Expensive Dipolarophile. *ChemSusChem* **2013**, *6* (12), 2220–2225.

(163) Bonacorso, H. G.; Moraes, M. C.; Luz, F. M.; Quintana, P. S.; Zanatta, N.; Martins, M. A. P. New Solventless and Metal-Free Synthesis of the Antiepileptic Drug 1-(2,6-Difluorobenzyl)-1H-1,2,3-Triazole-4-Carboxamide (Rufinamide) and Analogues. *Tetrahedron Lett.* **2015**, *56* (2), 441–444.

(164) Porter, W. R. Warfarin: History, Tautomerism and Activity. *J. Comput. Aided Mol. Des.* **2010**, *24*, 553–573.

(165) Barnes, G. D.; Lucas, E.; Alexander, G. C.; Goldberger, Z. D. National Trends in Ambulatory Oral Anticoagulant Use. *Am. J. Med.* **2015**, *128* (12), 1300–1305.

(166) Porta, R.; Benaglia, M.; Coccia, F.; Rossi, S.; Puglisi, A. Enantioselective Organocatalysis in Microreactors: Continuous Flow Synthesis of a (*S*)-Pregabalin Precursor and (*S*)-Warfarin. *Symmetry* **2015**, *7* (3), 1395–1409.

(167) Fortunak, J. M.; de Souza, R. O. M. A.; Kulkarni, A. A.; King, C. L.; Ellison, T.; Miranda,

L. S. M. Active Pharmaceutical Ingredients for Antiretroviral Treatment in Low- and Middle-Income Countries: A Survey. *Antivir. Ther.* **2014**, *19* (3), 15–29.

(168) UNAIDS. Data 2018.

(169) World Economic Forum. The Global Competitiveness Report 2017/2018.

(170) Verghese, J.; Kong, C. J.; Rivalti, D.; Yu, E. C.; Krack, R.; Alcázar, J.; Manley, J. B.; McQuade, D. T.; Ahmad, S.; Belecki, K.; Gupton, B. F. Increasing Global Access to the High-Volume HIV Drug Nevirapine through Process Intensification. *Green Chem.* **2017**, *19* (13), 2986–2991.

(171) Correia, C. A.; Gilmore, K.; McQuade, D. T.; Seeberger, P. H. A Concise Flow Synthesis of Efavirenz. *Angew. Chemie - Int. Ed.* **2015**, *54* (16), 4945–4948.

(172) Mandala, D.; Chada, S.; Watts, P. Semi-Continuous Multi-Step Synthesis of Lamivudine. *Org. Biomol. Chem.* **2017**, *15* (16), 3444–3454.

(173) Ziegler, R. E.; Desai, B. K.; Jee, J.-A.; Gupton, B. F.; Roper, T. D.; Jamison, T. F. Multistep Synthesis 7-Step Flow Synthesis of the HIV Integrase Inhibitor Dolutegravir. *Angew. Chemie - Int. Ed.* **2018**, *57*, 1–6.

(174) Hargrave, K. D.; Proudfoot, J. R.; Grozinger, K. G.; Cullen, E.; Kapadia, S. R.; Patel, U. R.; Fuchs, V. U.; Mauldin, S. C.; Vitous, J.; Behnke, M. L.; Klunder, J. M.; Pal, K.; Skiles, J. W.; McNeil, D. W.; Rose, J. M.; Chow, G. C.; Skoog, M. T.; Wu, J. C.; Schmidt, G.; Engel, W. W.; Eberlein, W. G.; Saboe, T. D.; Campbell, S. J.; Rosenthal, A. S.; Adams, J. Novel Non-Nucleoside Inhibitors of HIV-1 Reverse Transcriptase. 1. Tricyclic Pyridobenzo- and Dipyridodiazepinones. *J. Med. Chem.* **1991**, *34* (7), 2231–2241.

(175) Vale, A.; Marrs, T. C.; Rice, P. Chemical Terrorism and Nerve Agents. *Medicine* **2012**, *44* (2), 106–108.

(176) Field, J. M.; Hazinski, M. F.; Sayre, M. R.; Chameides, L.; Schexnayder, S. M.; Hemphill, R.; Samson, R. A.; Kattwinkel, J.; Berg, R. A.; Bhanji, F.; Cave, D. M.; Jauch, E. C.; Kudenchuk, P. J.; Neumar, R. W.; Peberdy, M. A.; Perlman, J. M.; Sinz, E.; Travers, A. H.; Berg, M. D.; Billi, J. E.; Eigel, B.; Hickey, R. W.; Kleinman, M. E.; Link, M. S.; Morrison, L. J.; O'Connor, R. E.; Shuster, M.; Callaway, C. W.; Cucchiara, B.; Ferguson, J. D.; Rea, T. D.; Vanden Hoek, T. L. Part 1: Executive Summary: 2010 American Heart Association Guidelines for Cardiopulmonary Resuscitation and Emergency Cardiovascular Care. *Circulation* **2010**, *122*, S640–S656.

(177) Bédard, A. C.; Longstreet, A. R.; Britton, J.; Wang, Y.; Moriguchi, H.; Hicklin, R. W.; Green, W. H.; Jamison, T. F. Minimizing E-Factor in the Continuous-Flow Synthesis of Diazepam and Atropine. *Bioorganic Med. Chem.* **2016**, *25* (23), 6233–6241.

(178) Dai, C.; Snead, D. R.; Zhang, P.; Jamison, T. F. Continuous-Flow Synthesis and Purification of Atropine with Sequential in-Line Separations of Structurally Similar Impurities. *J. Flow Chem.* **2015**, *5* (3), 133–138.

(179) Singhvi, N.; Koo, M.; Kyle, A. *Systemic Hypertension Market and Forecast Analyst to 2023*. 2017.

(180) *Antidepressants, Antipsychotics, Anxiolytics*; Buschmann, H., Díaz, J. L., Holenz, J., Párraga, A., Torrens, A., Vela, J. M., Eds.; Wiley, 2007.

(181) Capellades, G.; Joshi, P. U.; Dam-Johansen, K.; Mealy, M. J.; Christensen, T. V.; Kiil, S. Characterization of a Multistage Continuous MSMPR Crystallization Process Assisted by Image Analysis of Elongated Crystals. *Cryst. Growth Des.* **2018**, *18* (11), 6455–6469.

(182) Jolliffe, H. G.; Gerogiorgis, D. I. Process Modelling, Design and Technoeconomic Evaluation for Continuous Paracetamol Crystallisation. *Comput. Chem. Eng.* **2018**, *118*, 224–235.

(183) Nadeem, Z.; Mcintosh, A.; Lawrie, S. Mental Health Mental Health. *OurWorldInData* **2004**, April, 1500–1531.

(184) Organisation for Economic Co-operation and Development (OECD). Pharmaceutical Market. Available at: https://stats.oecd.org/Index.aspx?DataSetCode=HEALTH_PHMC# (accessed Jul 3, 2019).

(185) Tripathi, B. S.; Awasthi, A.; Pandey, P. K.; Awasthi, A. Thermal Expansion Coefficient of Ternary Liquid Mixture Using Hard Sphere Models and Flory's Statistical Theory. *Indian J. Phys.* **2010**, *84* (4), 449–458.

(186) Rihani, D. N.; Doraiswamy, L. K. Estimation of Heat Capacity of Organic Compounds from Group Contributions. *Ind. Eng. Chem. Fundam.* **1965**, *4* (1), 17–21.

(187) Constantinou, L.; Gani, R. New Group-Contribution Method for Estimating Properties of Pure Compounds. *AIChE J.* **1994**, *40* (10), 1697–1710.

(188) García, B.; Aparicio, S.; Alcalde, R.; Dávila, M. J.; Leal, J. M. Modeling the PVTx Behavior of the N-Methylpyrrolidinone/Water Mixed Solvent. *Ind. Eng. Chem. Res.* **2004**, *43* (12),

3205–3215.

(189) Marchidan, D. I.; Ciopec, M. Relative Enthalpies and Related Thermodynamic Functions of Some Organic Compounds by Drop Calorimetry. *J. Therm. Anal.* **1978**, *14* (1–2), 131–150.

(190) Gurvich, L. V; Bergman, G. A.; Gorokhov, L. N.; Iorish, V. S.; Leonidov, V. Y.; Yungman, V. S. Thermodynamic Properties of Alkali Metal Hydroxides .1. Lithium and Sodium Hydroxides. *J. Phys. Chem. Ref. Data* **1996**, *25* (4), 1211–1276.

(191) PubChem. Available at: https://pubchem.ncbi.nlm.nih.gov/ (accessed Apr 8, 2020).

(192) NIST Chemistry WebBook, NIST Standard Reference Database. Available at: http://webbook.nist.gov/cgi/cbook.cgi?ID=C7732185&Units=SI&Mask=4#Notes (accessed Apr 8, 2020). https://doi.org/10.18434/T4D303.

(193) Chickos, J. S.; Acree, W. E. Estimating Solid-Liquid Phase Change Enthalpies and Entropies. *J. Phys. Chem. Ref. Data* **1999**, *28* (6), 1535–1673.

(194) Fredenslund, A.; Jones, R. L.; Prausnitz, J. M. Group-Contribution Estimation of Activity-Coefficients in Nonideal Liquid-Mixtures. *AIChE J.* **1975**, *21* (6), 1086–1099.

(195) Abrams, D. S.; Prausnitz, J. M. Statistical Thermodynamics of Liquid-Mixtures - New Expression for Excess Gibbs Energy of Partly or Completely Miscible Systems. *AIChE J.* **1975**, *21* (1), 116–128.

(196) Mishra, D. S.; Yalkowsky, S. H. Ideal Solubility of a Solid Solute: Effect of Heat Capacity Assumptions. *Pharm. Res.* **1992**, *9* (7), 958–959.

(197) Neau, S. H.; Flynn, G. L.; Yalkowsky, S. H. The Influence of Heat Capacity Assumptions on the Estimation of Solubility Parameters from Solubility Data. *Int. J. Pharm.* **1989**, *49* (3), 223–229.

(198) Gracin, S.; Brinck, T.; Rasmuson, A. C. Prediction of Solubility of Solid Organic Compounds in Solvents by UNIFAC. *Ind. Eng. Chem. Res.* **2002**, *41* (20), 5114–5124.

(199) Magnussen, T.; Rasmussen, P.; Fredenslund, A. UNIFAC Parameter Table for Prediction of Liquid-Liquid Equilibria. *Ind. Eng. Chem. Process Des. Dev.* **1981**, *20* (2), 331–339.

(200) Renon, H.; Prausnitz, J. M. Local Compositions in Thermodynamic Excess Functions for Liquid Mixtures. *AIChE J.* **1968**, *14* (1), 135–144.

(201) Gebreyohannes, S.; Neely, B. J.; Gasem, K. A. M. Generalized Nonrandom Two-Liquid

(NRTL) Interaction Model Parameters for Predicting Liquid-Liquid Equilibrium Behavior.

(202) Alfonsi, K.; Colberg, J.; Dunn, P. J.; Fevig, T.; Jennings, S.; Johnson, T. A.; Kleine, H. P.; Knight, C.; Nagy, M. A.; Perry, D. A.; Stefaniak, M. Green Chemistry Tools to Influence a Medicinal Chemistry and Research Chemistry Based Organisation. *Green Chem.* **2008**, *10* (1), 31–36.

(203) FDA. Guidance for Industry Q3C - Tables and List. Available at: http://www.fda.gov/downloads/drugs/guidancecomplianceregulatoryinformation/guidances/ucm073395.pdf (accessed Apr 25, 2016).

(204) Maczynski, A.; Shaw, D. G.; Goral, M.; Wisniewska-Goclowska, B.; Skrzecz, A.; Owczarek, I.; Blazej, K.; Haulait-Pirson, M. C.; Hefter, G. T.; Kapuku, F.; Maczynska, Z.; Szafranski, A.; Young, C. L. IUPAC-NIST Solubility Data Series. 81. Hydrocarbons with Water and Seawater-Revised and Updated. Part 5. C-7 Hydrocarbons with Water and Heavy Water. *J. Phys. Chem. Ref. Data* **2005**, *34* (3), 1399–1487.

(205) Du, S.; Wang, Y.; Li, J.; Wu, S.; Dun, W.; Song, X.; Wang, J.; Gong, J. Correlation and Thermodynamic Analysis of Solubility of Diphenhydramine Hydrochloride in Pure and Binary Solvents. *J. Chem. Thermodyn.* **2015**, *93*, 132–142.

(206) Chen, J.-T.; Chen, M.-C. Liquid–Liquid Equilibria for the Quaternary Systems of Sater + N -Methyl-2-Pyrrolidone + 1-Hexanol + NaCl, + KCl, or + KAc. *J. Chem. Eng. Data* **2008**, *53* (1), 217–222.

(207) Constable, D. J. C.; Curzons, A. D.; Cunningham, V. L. Metrics to Green Chemistry - Which Are the Best? *Green Chem.* **2002**, *4* (6), 521–527.

(208) Sheldon, R. A. Fundamentals of Green Chemistry: Efficiency in Reaction Design. *Chem. Soc. Rev.* **2012**, *41* (4), 1437–1451.

(209) Ritter, S. K. Reducing Environmental Impact of Organic Synthesis. *Chem. Eng. News* **2013**, *91* (15), 22–23.

(210) Sheldon, R. A. The: E Factor 25 Years on: The Rise of Green Chemistry and Sustainability. *Green Chem.* **2017**, *19* (1), 18–43.

(211) Curzons, A. D.; Mortimer, D. N.; Constable, D. J. C.; Cunningham, V. L. So You Think Your Process Is Green, How Do You Know? Using Principles of Sustainability to Determine What Is Green – a Corporate Perspective. *Green Chem.* **2001**, *3* (1), 1–6.

(212) Woods, D. R. *Rules of Thumb in Engineering Practice*; Wiley, 2007.

(213) Couper, J. R. *Process Engineering Economics*; CRC Press, 2003.

(214) Corning. Corning Advanced-Flow G1 SiC Reactor. Available at: http://www.corning.com/media/worldwide/global/documents/G1_SiC_leaflet_FINAL_6.1.15.pdf (accessed Mar 8, 2016).

(215) Cole-Parmer. Cole Parmer Polystat Advanced 15L Heat Cool Bath 35 to 200C 115VAC from Cole-Parmer United Kingdom. Available at: http://www.coleparmer.co.uk/Product/Cole_Parmer_Polystat_Advanced_15L_Heat_Cool_Bath_35_to_200C_115VAC/WZ-12122-56 (accessed Mar 8, 2016).

(216) ProMinent. Solenoid Driven Metering Pumps. Available at: https://www.prominent.co.uk/en/Products/Products/Metering-Pumps/Solenoid-Driven-Metering-Pumps/pg-solenoid-driven-metering-pumps.html (accessed Mar 8, 2016).

(217) Adamo, A.; Heider, P. L.; Weeranoppanant, N.; Jensen, K. F. Membrane-Based, Liquid-Liquid Separator with Integrated Pressure Control. *Ind. Eng. Chem. Res.* **2013**, *52* (31), 10802–10808.

(218) Chemical Database Service. Accelrys Available Chemicals Directory. Available at: http://cds.rsc.org/accelrys.asp (accessed Mar 14, 2019).

(219) Roberge, D. M.; Ducry, L.; Bieler, N.; Cretton, P.; Zimmermann, B. Microreactor Technology: A Revolution for the Fine Chemical and Pharmaceutical Industries? *Chem. Eng. Technol.* **2005**, *28* (3), 318–323.

(220) Bouillot, B.; Teychene, S.; Biscans, B. An Evaluation of Thermodynamic Models for the Prediction of Drug and Drug-like Molecule Solubility in Organic Solvents. *Fluid Phase Equilib.* **2011**, *309* (1), 36–52.

(221) Miller, M. M.; Wasik, S. P.; Huang, G. L.; Shiu, W. Y.; Mackay, D. Relationships between Octanol-Water Partition Coefficient and Aqueous Solubility. *Environ. Sci. Technol.* **1985**, *19* (6), 522–529.

(222) Onyemelukwe, I. I.; Parsons, A. R.; Wheatcroft, H. P.; Robertson, A.; Nagy, Z. K.; Rielly, C. D. The Role of Residence Time Distribution in the Continuous Steady-State Mixed Suspension Mixed Product Removal Crystallization of Glycine. *Cryst. Growth Des.* **2019**, *19* (1), 60–80.

(223) Alder, C. M.; Hayler, J. D.; Henderson, R. K.; Redman, A. M.; Shukla, L.; Shuster, L. E.; Sneddon, H. F. Updating and Further Expanding GSK's Solvent Sustainability Guide. *Green Chem.* **2016**, *18* (13), 3879–3890.

(224) Skelland, A. H. P.; Moeti, L. T. Mechanism of Continuous-Phase Mass Transfer in Agitated Liquid-Liquid Systems. *Ind. Eng. Chem. Res.* **1990**, *29* (11), 2258–2267.

(225) Roschangar, F.; Sheldon, R. A.; Senanayake, C. H. Overcoming Barriers to Green Chemistry in the Pharmaceutical Industry – the Green Aspiration Level™ Concept. *Green Chem.* **2015**, *17* (2), 752–768.

(226) Kuminek, G.; Rodríguez-Hornedo, N.; Siedler, S.; Rocha, H. V. A.; Cuffini, S. L.; Cardoso, S. G. How Cocrystals of Weakly Basic Drugs and Acidic Coformers Might Modulate Solubility and Stability. *Chem. Commun.* **2016**, *52* (34), 5832–5835.

(227) Macha, S.; Yong, C. L.; Darrington, T.; Davis, M. S.; MacGregor, T. R.; Castles, M.; Krill, S. L. In Vitro-In Vivo Correlation or Nevirapine Extended Release Tablets. *Biopharm. Drug Dispos.* **2009**, *30* (9), 542–550.

(228) Cheeseman, S. H.; Hattox, S. E.; McLaughlin, M. M.; Koup, R. A.; Andrews, C.; Bova, C. A.; Pav, J. W.; Roy, T.; Sullivan, J. L.; Keirns, J. J. Pharmacokinetics of Nevirapine: Initial Single-Rising-Dose Study in Humans. *Antimicrob. Agents Chemother.* **1993**, *37* (2), 178–182.

(229) Hill, A. M.; Barber, M. J.; Gotham, D. Estimated Costs of Production and Potential Prices for the WHO Essential Medicines List. *BMJ Glob. Heal.* **2018**, *3* (1), 1–7.

(230) Diab, S.; Gerogiorgis, D. I. Technoeconomic Evaluation of Multiple Mixed Suspension-Mixed Product Removal (MSMPR) Crystallizer Configurations for Continuous Cyclosporine Crystallization. *Org. Process Res. Dev.* **2017**, *21* (10), 1571–1587.

(231) Myerson, A. S.; Ginde, R. Crystals, Crystal Growth, and Nucleation. In *Handbook of Industrial Crystallization*; Butterworth-Heinemann, 2002; 33–65.

(232) Wu, H.; Dong, Z.; Li, H.; Khan, M. An Integrated Process Analytical Technology (PAT) Approach for Pharmaceutical Crystallization Process Understanding to Ensure Product Quality and Safety: FDA Scientist's Perspective. *Org. Process Res. Dev.* **2015**, *19* (1), 89–101.

(233) Gillespie, D. T. Stochastic Simulation of Chemical Kinetics. *Annu. Rev. Phys. Chem.* **2007**, *58* (1), 35–55.

(234) Hartman, R. L.; Jensen, K. F. Microchemical Systems for Continuous-Flow Synthesis. *Lab*

Chip **2009**, *9* (17), 2495–2507.

(235) Nagy, K. D.; Shen, B.; Jamison, T. F.; Jensen, K. F. Mixing and Dispersion in Small-Scale Flow Systems. *Org. Process Res. Dev.* **2012**, *16* (5), 976–981.

(236) Choi, H. C.; Shin, J. S.; Qasim, F.; Park, S. J. Liquid–Liquid Equilibrium Data for the Ternary Systems of Water, Isopropyl Alcohol, and Selected Entrainers. *J. Chem. Eng. Data* **2016**, *61* (4), 1403–1411.

(237) Bonami, P.; Biegler, L. T.; Conn, A. R.; Cornuéjols, G.; Grossmann, I. E.; Laird, C. D.; Lee, J.; Lodi, A.; Margot, F.; Sawaya, N.; Wächter, A. An Algorithmic Framework for Convex Mixed Integer Nonlinear Programs. *Discret. Optim.* **2008**, *5* (2), 186–204.

(238) Caballero, J. A.; Grossmann, I. E. Rigorous Design of Complex Liquid-Liquid Multi-Staged Extractors Combining Mathematical Programming and Process Simulators. *Comput. Aided Chem. Eng.* **2009**, *27*, 981–986.

(239) Dafnomilis, A.; Diab, S.; Rodman, A. D.; Boudouvis, A. G.; Gerogiorgis, D. I. Multi-Objective Dynamic Optimization of Ampicillin Batch Crystallization: Sensitivity Analysis of Attainable Performance vs. Product Quality Constraints. *Ind. Eng. Chem. Res.* **2019**, *58* (40), 18756–18771.

(240) Capellades, G.; Wiemeyer, H.; Myerson, A. S. Mixed-Suspension, Mixed-Product Removal Studies of Ciprofloxacin from Pure and Crude Active Pharmaceutical Ingredients: The Role of Impurities on Solubility and Kinetics. *Cryst. Growth Des.* **2019**, *19* (7), 4008–4018.

(241) Pal, K.; Yang, Y.; Nagy, Z. K. Model-Based Optimization of Cooling Crystallization of Active Pharmaceutical Ingredients Undergoing Thermal Degradation. *Cryst. Growth Des.* **2019**, *19* (6), 3417–3429.

(242) Schall, J. M.; Mandur, J. S.; Braatz, R. D.; Myerson, A. S. Nucleation and Growth Kinetics for Combined Cooling and Antisolvent Crystallization in a Mixed-Suspension, Mixed-Product Removal System: Estimating Solvent Dependency. *Cryst. Growth Des.* **2018**, *18* (3), 1560–1570.